Diverse firing patterns of neurons of the medial septum and their hippocampal targets

Michael G. Crump

Brasenose College, University of Oxford

Thesis submitted for the degree of Doctor of Philosophy,

Trinity term, 2014.

Supervisors: Prof. Peter Somogyi

Dr. Damien Lapray

Dr. Tim Viney

Abstract

Diverse firing patterns of neurons of the medial septum and their hippocampal targets

Michael G. Crump

Brasenose College, University of Oxford. Thesis submitted for the degree of Doctor of Philosophy, Trinity term, 2014.

The medial septum has a profound influence on the activity of the hippocampus, through cholinergic and GABAergic innervation. During exploration and paradoxical sleep, the hippocampus produces a prominent voltage oscillation of theta frequency (4-12 Hz), which represents the synchronous activity of hippocampal neurons. This organisation includes the temporal redistribution of inhibition throughout the subcellular domains of pyramidal neurons, via the theta phase locked activity of diverse interneuron populations. GABAergic septo-hippocampal neurons fire rhythmic, phase locked action potentials during theta oscillatory epochs. Within the hippocampus they project exclusively to interneurons; stimulation of the septum disinhibits pyramidal neurons. If the septo-hippocampal projection is inactivated, theta oscillation no longer occurs and animals demonstrate behavioural deficits in episodic memory. This evidence led to the hypothesis that septal rhythmic inhibition of interneurons is a crucial step in the pacing of the hippocampal theta oscillation *in vivo*.

I used extracellular recording and the juxtacellular labelling method of neurons under anaesthesia *in vivo* to investigate how the electrophysiological activity of septal neurons correlated with the identity of the cell, its axonal arbour and synaptic targets in the hippocampus. I tested the hypothesis that septal neurons display a selective and non-uniform innervation of interneurons and the firing phase and/or spike timing of septal neurons is correlated with that predicted of the innervated hippocampal interneuron(s).

I found a diversity of medial septal neurons, which was partially predicted by the firing frequency change during sharp wave associated ripple oscillations. Septal neurons which display significantly different firing patterns and axonal arbours may share molecular markers detected by immunohistochemistry. The axonal arbours of septal neurons were limited to a relatively small area within the hippocampus. Within those regions I defined some of the synaptic targets of three neurons and suggest that septal GABAergic neurons selectively innervate hippocampal interneuron types. Furthermore, the preferred theta phase of septal neurons was out of phase with that predicted for their identified target cells, indicating that septal GABAergic neurons may suppress the firing of interneurons rhythmically during theta.

Acknowledgements

I want to thank Prof. Peter Somogyi for allowing me this opportunity and funding to develop scientifically and professionally. I hoped for the chance to answer genuinely interesting questions, and that was what Peter gave me. Many lessons have been taught and many lessons have been learnt; some of these were even the same lessons. You have been the greatest force in shaping the experience I have had for the last few years.

Throughout this time I would not have succeeded without the help and support of Dr. Damien Lapray. Throughout immensely difficult times he put up with me and we got through it eventually. He gave me the confidence to do this and is an inspiration to me as I hopefully begin my own career as a postdoc. My thanks also go to Dr. Tim Viney who continued the difficult work of co-supervision. His criticism and patience with my work has been incredibly valuable, and my thesis is all the better for it. I can't thank you both enough for your input to my time in Oxford, not just professionally but personally. Me finishing is testament to the job done by both of you.

The lab would not function at all without Mary and the help she provides every day without fail. Thank you so much. I would like to also thank Jenny, Agnieszka and Jo for always being helpful and providing support to the unit. Thank you to Liz for her crucial support of our work. Throughout my studies I have received expert input from Thomas Klausberger, Bálint Lasztóczi, Zsolt Borhegyi, Ray Guillery, Pete Magill, David Dupret, Paul Bolam, Jozsef Somogyi and David Roberts. All of you have improved my work and understanding and I would like to thank you for your advice, discussion and teaching. I hope I get the chance to interact with so many outstanding scientists in a single environment again.

The lab, and my time in it, wouldn't be the same without the people whom surrounded me every day and whom deserve special mention. Thank you all: Kristina, Linda, Daniel, Ben, Tim, Damien, Lema, Rob, Szabi and Eszter. Thank you for putting up with me. I'm sorry about that! It's been interesting… I certainly will be leaving with a lot of good memories of the chats, lab meetings, Vienna trips, late nights, early mornings, trips to the club, rants, raves, trials and successes of being part of the group. No one else will ever understand the reaction that can be induced by the sound of a metal medal hitting a glass door like you can. You all made the day-to-day time here more enjoyable. Although it was brief: Timea, Kristie, Tugrul, Abhilasha, and Gunes, thank you too.

There are numerous others who have helped to add positivity to this experience through friendship. All the guys downstairs in the Magill and Bolam labs, but particularly: Megan, Paul, Andy, and Eleftheria. And let's not forget Chad, our 4pm conference calls and joint love of

caffeinated beverages got me through many days, and the less said about our trips to Hi Lo the better. My Brasenose crew who helped me escape when I needed. More so than anyone: Chris and Chelsea who are awesome.

Many thanks to Prof Trevor Sharp and Prof Francesco Ferraguti for their comments and corrections.

It is a sad feature of the scientific and academic life that you meet such great people and then have to leave soon after. I won't forget this time, that's for sure.

Contents

Abstract 1

Acknowledgements 2

List of Abbreviations 8

Chapter 1 – Introduction 12

1.1 The organisation of the septo-hippocampal network 13

1.2 The septum is highly interconnected with a diverse group of brain regions 14

1.3 Intrinsic connectivity within and between septal nuclei 18

1.4 Hippocampal neuron theta-related firing patterns 19

1.5 Pyramidal neurons can display place fields 20

1.6 Sharp-wave associated ripple oscillations and place cell ensembles 20

1.7 Interneuron phase-locking and relationship to pyramidal neuron firing in both theta and SWR oscillations 22

1.8 The medial septum is a frequency pacemaker for the hippocampal theta oscillation 23

1.9 Frequency integrators for hippocampal theta oscillation 25

1.10 The septum in disease 28

Aim 29

Chapter 2 - Methods 31

2.1 Animals 32

2.2 Anterograde tracing using PHAL 32

2.3 Juxtacellular recording and labelling 34

2.4 Analysis of electrophysiological data 37

2.4.1 Theta phase analysis 37

2.4.2 Sharp-wave ripple analysis 38

2.5 Juxtacellular labelling with recovery 39

2.6 Tissue processing for light microscopy 39

2.7 Imaging 41

2.7.1 Imaging of horseradish peroxidase visualised tissue 42

2.7.2 Reconstruction and quantification of neurons 42

2.8 Hierarchical clustering 43

Chapter 3 – Anatomical analysis of confirmed septo-hippocampal neurons and their targets ... 60

3.1 Introduction 62

3.2 Results 65

3.2.1 Glutamatergic septo-hippocampal projections 68

3.2.2 Innervation of NOS-expressing ivy and neurogliaform neurons 68

3.2.3 Innervation of PV-expressing, SATB1 negative axo-axonic neurons 69

3.2.4 Innervation of M2R-expressing neurons including the mGluR8a-decorated trilaminar cell type. 69

3.2.5 Anatomical analysis of single medial septal and septo-hippocampal neurons 75

3.2.6 Axonal location of septo-hippocampal neurons within the hippocampus 82

3.2.7 Immunohistochemical analysis of the hippocampal targets of single septo-hippocampal neurons 91

3.3 Discussion 100

Chapter 4 – *In vivo* firing patterns of theta rhythmic septal neurons which are inhibited or did not change their firing pattern during hippocampal sharp-wave ripple oscillations 108

4.1 Introduction 109

4.2 Results 111

4.2.1 The theta oscillation (3-6 Hz) 112

4.2.2 The sharp wave associated ripple oscillation (90-200 Hz) 116

4.2.3 Theta rhythmic neurons, both those inhibited and not changed by SWRs, are septo-hippocampal projection neurons. 120

4.2.4 Septo-hippocampal neurons which display similar theta phase preference do not share an axonal distribution within the hippocampus. 120

4.3 Discussion 125

Chapter 5 - Characterisation of sharp-wave ripple active neurons of the medial septum 133

5.1 Introduction 134

5.2 Results 136

5.2.2 The theta oscillation (3-6 Hz) 140

5.2.3 Anatomical characterisation of SWR active neurons of the medial septum 144

5.3 Discussion 149

Chapter 6 - Diverse firing patterns of medial septal neurons 155

6.1 Introduction 156

6.2 Results 159

6.2.1 Hierarchical clustering 168

6.3 Discussion 175

Chapter 7 - Discussion 181

7.1 The glutamatergic septo-hippocampal projection is sparse and unlikely to be a major excitatory projection to CA3 pyramidal neurons 182

7.2 NOS-expressing neurons receive GABAergic septal input 184

7.3 Parvalbumin-immunopositive, SATB1-immunonegative putative axo-axonic neurons receive GABAergic septo-hippocampal input 187

7.4 Expression of presynaptic mGluR8a on some medial septal terminal in the hippocampus and an input to trilaminar neurons 188

7.5 Novel immunohistochemical markers in theta rhythmic neurons did not correlate with difference in SWR-dependent firing patterns or axonal location 189

7.6 Possible relevance of transcription factor SATB1 to connectivity 191

7.7 Axonal location and distribution of septo-hippocampal neurons 192

7.8 Limitations of confocal microscopy and synaptic markers 196

7.9 Caveats of immunohistochemical identification of interneuron targets 197

7.10 Future quantification of single septo-hippocampal neurons 200

7.11 Septo-hippocampal neurons during theta oscillation. 202

7.12 Septo-hippocampal neurons during SWR 205

7.13 Clustering of septal neurons 208

Concluding remarks 211

References 212

List of Abbreviations

5-HT	5-hydroxytryptamine
5-HT2a	5-hydroxytryptamine receptor 2a
AAC	Axo-axonic cell
AC	Anterior commissure
ACh	Acetylcholine
AChE	Acetylcholine esterase
AD	Alzheimer's disease
AI	Agranular insular cortex
AO	Anterior olfactory nucleus
APs	Action potentials
BDA	Biotinylated dextran amine
BL	Basolateral amygdaloid nucleus
CA1-3	Cornu ammonis 1-3
CB	Calbindin
CB1	Cannabinoid 1 type receptor
CC	Corpus callosum
CCK	Cholecystokinin
Cg	Cingulate cortex
Ch	Chicken
ChAT	Choline acetyltransferase
COUP TFII	Chicken ovalbumin upstream promoter transcription factor II
Cpu	Caudate putamen
CR	Calretinin
DAB	3,3’-diamino-benzidine
dcw	Deep cerebral white matter
dF	Dorsal fornix
DG	Dentate gyrus
EEG	Electroencephalogram
ENT	Entorhinal cortex
f/t	Freeze thaw permeabilisation
FFT	Fast Fourier transform

GABA	Gamma-aminobutyric acid
GABAaR-α1	GABAa receptor alpha-1 subunit
GAD	Glutamate decarboxylase
Gp	Guinea pig
Gran	Granular cell layer
Gt	Goat
HCl	Hydrogen chloride
HCN1/4	Hyperpolarisation activated cyclic nucleotide gated non-selective cation channel 1/4
HCRT2	Hypocretin (orexin) receptor type 2
HDB	Horizontal limb of the diagonal band
i.p.	Intraperitoneal
IINI	Infrequent intensely NOS-immunopositive
IL	Infralimbic cortex
Kv1.1	Potassium voltage-gated channel member A, subunit 1
L	Lateral amygdaloid nucleus
LC	Locus coeruleus
LFP	Local field potential
LSD/I/V	Lateral septum dorsal/intermediate/ventral
M	Motor cortex
M1/2	Motor cortex area 1/2
M2R	Acetylcholine muscarinic receptor subunit 2
MBNa/i/p	Magnocellular basal nucleus anterior/intermediate/posterior
mGluR1α	Metabotropic glutamate receptor subunit 1 alpha
mGluR8a	Metabotropic glutamate receptor subunit 8a
M-L	Medio-lateral
Mo	Mouse
Mol	Molecular layer
MS	Medial septum
NaCl	Sodium chloride
NaPBS	Saline phosphate buffered saline
NB	Neurobiotin
NECAB1	Neuronal calcium binding protein 1

NI	Nucleus incertus
NOS	Nitric oxide synthase
NPY	Neuropeptide Y
NRT	Nucleus reuniens thalami
OB	Olfactory bulb
OC	Occipital cortex
PaS	Parasubiculum
PB	Phosphate buffer
PCl/m	Lateral/medial precentral cortex
PFA	Paraformaldehyde
PHAL	Phaseolus vulgaris leucoagglutinin
PIR	Piriform cortex
PL	Prelimbic cortex
PnO	Pontine nucleus oralis
PR	Perirhinal cortex
Proj/BiStr	Projection/Bistratified interneuron
PrS	Presubiculum
PV	Parvalbumin
PVBC	Parvalbumin-expressing basket cell
Rb	Rabbit
R-C	Rostro-caudal
RS	Retrosplenial cortex
s.c.	Subcutaneous
SATB1/2	Special AT binding protein 1/2
SOM	Somatostatin
SS1/2	Somatosensory cortex area 1/2
sst2a	Somatostatin receptor subunit 2a
STr	Subicular transition area
str. Pyr/ori/luc/rad /lac-mol	Stratum pyramidale/oriens/lucidum/radiatum/lacunosum-moleculare
SuM	Supramammillary nucleus
SWR	Sharp wave associated ripple oscillation

TBS/T	Tris-buffered saline/containing triton
TE	Temporal cortex
TH	Tyrasine hydroxylase
TMR	Tetramethyl-rhodamine dextran amine
TTX	Tetrodotoxin
VAChT	Vesicular acetylcholine transporter
VDB	Vertical limb of the diagonal band
VGAT	Vesicular GABA transporter
VGluT1/2	Vesicular glutamate transporter 1/2
VIP	Vasoactive intestinal peptide
VTA	Ventral tegmental area

Chapter 1 – Introduction

The Symbol of all Art is the Prism.

The goal is unrealism. The method destructive.

To break up the white light of objective realism into the secret glories which it contains.

e.e. cummings

1.1 The organisation of the septo-hippocampal network

The septal nuclei are a complex group of basal forebrain regions implicated in numerous behaviours and functions. The septal nuclei are highly evolutionarily conserved and found in animals from lizards and birds to mammals, including humans (Risold and Swanson 1997; Montagnese et al. 2008; Carvalho Pimentel et al. 2011; Iannetti et al. 2011; Kuenzel et al. 2011). The septum, or septal nuclei, is linked to diverse behaviours including: drug addiction (Sartor and Aston-Jones 2012), mating and pair bonding (Kollack-Walker and Newman 1995), aggression (Trent and Menard 2013), gustation (Gong et al. 2013), memory (Lecourtier et al. 2011; Yousefi et al. 2012), navigation and spatial representation (Lecourtier et al. 2011), and alertness and arousal (Green and Arduini 1954; Wu et al. 2002). It forms the most anterior tip of a basal forebrain neuronal grouping, which runs from the most anterior point, the medial septum, ventrally and posteriorly through the forebrain to the most posterior region, the magnocellular basal nucleus (Luiten et al. 1987); Figure 1.1). In rodents this system is composed of the medial septum and diagonal band of Broca, nucleus basalis magnocellularis, median preoptic nucleus, substantia innominata and ventral pallidum (Luiten et al. 1987). They are the main source of acetylcholine-releasing neurons which supply the cortex (Rye et al. 1984). The medial septum, the midline nucleus of the septum, is reciprocally connected with the hippocampus (Takács et al. 2008). It is necessary for proper hippocampal functions and the formation of memory (Green and Arduini 1954). Pathology of the septum, as seen in Alzheimer's disease, correlates with a decrease in both septal and hippocampal synchrony as well as a dramatic decrease in memory formation (Whitehouse et al. 1982; Jyoti et al. 2010; Villette et al. 2010; Fonseca et al. 2011; Kim et al. 2012). Hippocampal synchrony is observed as a large amplitude voltage oscillation of 4 – 12 Hz, known as the theta frequency oscillation (Buzsáki et al. 1983). Theta oscillation occurs during movement, exploratory behaviour and paradoxical sleep (Buzsáki et al. 1983; Lapray et al. 2012). When the septo-hippocampal pathway is lesioned, theta oscillation is lost and the hippocampus does not function properly; theta oscillation is ablated and animals no longer

perform memory-dependent spatial learning tasks (Lecourtier et al. 2011; Green and Arduini 1954; Apartis et al. 1998).

1.2 The septum is highly interconnected with a diverse group of brain regions

Given the diverse behavioural correlates in which the septum has been implicated, it is not surprising that it is extensively connected with ascending brainstem and diencephalon regions, such as the nucleus incertus, ventral tegmental area, hypothalamus, and the locus coeruleus, as well as receiving descending cortical inputs from the entorhinal cortex, the subiculum and the hippocampus.

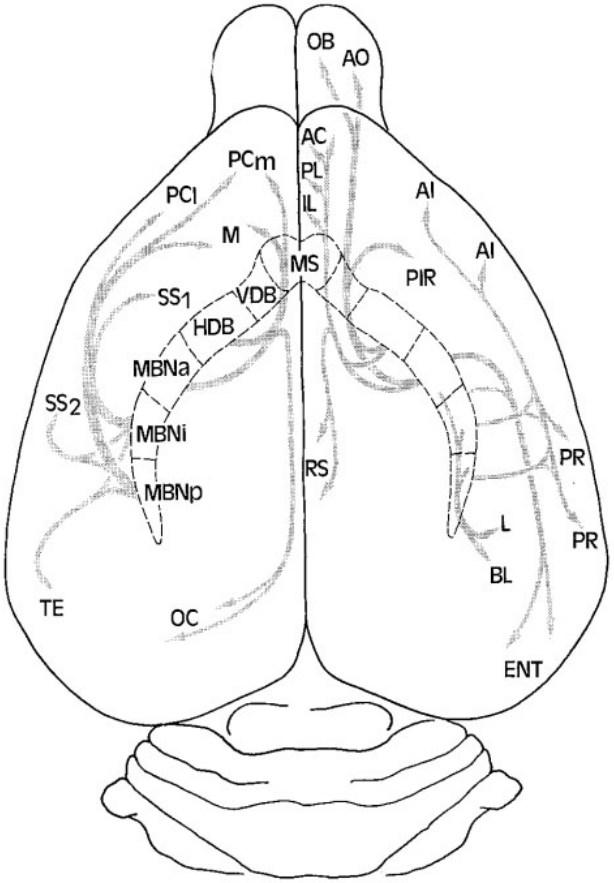


Figure 1.1 – Major connections from the basal forebrain to the neocortex, olfactory bulb, amygdaloid complex, and allocortex. Projections occur throughout the brain to multiple regions; the majority of cholinergic input to the rest of the brain has its origin from the basal forebrain (adapted from Luiten et al., 1987; for full list of abbreviations see List of Abbreviations).

Ascending connections contribute to homeostatic regulation via the lateral septum by the diencephalon, whereas arousal and alertness signals are received by the medial septum. The lateral septal nuclei are complex. Input to these regions form distinct dense bands of presynaptic axons which connect to distinct lateral septal nuclei (for review see (Risold and Swanson 1997)). The ventral tegmental area (VTA), a midbrain region, provides a dense dopaminergic (tyrosine hydroxylase (TH)-containing) input to neurons of the dorsointermediate lateral septum (Onténiente et al. 1987). The function of dopamine release from the VTA to lateral septum neurons is not known, but may relate to the effects of chronic cocaine use, as well as neuronal changes which occur during drug addiction (Sotomayor-Zárate et al. 2013). The lateral septum is necessary for cocaine-dependent place preference likely via its projection to orexin-expressing neurons in the lateral hypothalamus (Sartor and Aston-Jones 2012).

Ascending input to the medial septum forms part of the ascending activating system which synchronises the cortex (Fuller et al. 2011). Both noradrenergic afferent inputs from locus coeruleus and histaminergic inputs from the tuberomammillary nucleus directly stimulate medial septal neurons and promote wakefulness (Berridge and Foote 1996; Xu et al. 2004; Bergado et al. 2007).

The nucleus pontis oralis (PnO) and the nucleus incertus (NI) provide a disynaptic pathway to the medial septum together with the septo-hippocampal projection form the brainstem-diencephalon-septo-hippocampal system (Cervera-Ferri et al. 2012; Teruel-Martí et al. 2008). The PnO projects to the NI, but not the septum itself, and both are capable of generating theta oscillation (4-12 Hz) via the medial septum when stimulated *in vivo* (Faris and Sainsbury 1990; Nuñez et al. 2006). Neurons of the nucleus incertus projects directly to GABAergic rhythmic septo-hippocampal neurons and may fire rhythmically phase locked to the theta oscillation; these neurons also express relaxin-3 (Olucha-Bordonau et al. 2012). Neurons of the supramammillary nucleus (SuM) also

project to medial septum, as well as to septal calretinin neurons, and fire rhythmically (Vertes 1992; Vertes and McKenna 2000; Cui et al. 2013; Kocsis and Vertes, 1994).

The brainstem provides a large serotonergic input to the forebrain from the dorsal raphe nucleus, which is functionally opposed to that of the medial septum; whilst the medial septum synchronises, the raphe nucleus desynchronises this system (Kitchigina et al. 1999). The median raphe provides 5-HT input to both the medial septum/diagonal band and the hippocampus (Leranth and Vertes 1999). Like the GABAergic septo-hippocampal pathway, the raphe input to the hippocampus provides cell type specific innervation (Miettinen and Freund 1992; Acsady et al. 1993; Papp et al. 1999). The neurons of the median raphe are involved in the promotion of waking and actively desynchronise the hippocampus, reducing theta power (Kitchigina et al. 1999). Stimulation of the median raphe reduces the power of theta within the hippocampus whereas pharmacological inactivation of the median raphe causes persistent theta oscillation which is dependent on the medial septum (Crooks et al. 2012). The median raphe provides an excitatory projection to PV-expressing GABAergic neurons of the medial septum/diagonal band via activation of metabotropic 5-HT2a receptors (Alreja 1996; Lüttgen et al. 2004). As a result, a locally generated inhibitory circuit may inhibit septo-hippocampal neurons and acts to ablate the synchronising septal projection to the hippocampus.

A major descending input to both medial and lateral septum is from the hippocampus. Hippocampal pyramidal neurons from all regions (CA1, CA2, CA3 as well as subicular pyramids) project to, and form excitatory synapses with, GABAergic somato-spiny lateral septum neurons in a topographical manner (Risold and Swanson 1997; Risold and Swanson 1997). Pyramidal neurons of dorsal CA1 and the dorsal subiculum project to the rostral region of the lateral septum, CA3 pyramidal neurons projects further to the caudal lateral septum, and ventral hippocampal subicular and CA1 neurons project to the ventral lateral septum (Risold and Swanson 1997). The hippocampal input has a profound effect on the firing of lateral septum neurons. Lateral septum neurons fire

during hippocampal sharp-wave associated ripple (SWR) events (Dragoi et al. 1999), have place fields (Takamura et al. 2006), and show hippocampus-dependent plasticity (Garcia and Jaffard 1992; Garcia and Jaffard 1993; Jaffard et al. 1996).

The hippocampal projection to the medial septum is commonly considered to be exclusively from GABAergic hippocampo-septal interneurons, also known as double projection interneurons as these neurons also project to the subiculum (Jinno et al. 2007; Takács et al. 2008). These interneurons express the peptide somatostatin, and less frequently calbindin or parvalbumin (Jinno and Kosaka 2002; Jinno et al. 2007), and synaptically target other interneurons within the hippocampus (Gulyás et al. 2003). These neurons form reciprocal connections with GABAergic medial septum neurons and this may be necessary for both proper hippocampal and septal functioning and development (Takács et al. 2008; Quilichini et al. 2012). The GABAergic input from the hippocampus is likely to be responsible for the inhibition of medial septal neurons during hippocampal SWR as hippocampo-septal neurons increase their firing during these epochs (Jinno et al. 2007).

The connectivity between the septum and other temporal lobe regions such as the subiculum and entorhinal cortices has been less investigated. The subiculum projects to both the ventral region of the lateral septum – likely from excitatory pyramidal cells – and potentially to the medial septum also (Gaykema et al. 1990). Calretinin-expressing neurons located at the border of the medial and lateral septum receive excitatory, probably glutamatergic, input from neurons located within the entorhinal cortex which also express calretinin (Leranth et al. 1999). Furthermore, the calretinin-positive GABAergic neurons in the septum project to calretinin-containing neurons in the SuM which are known to innervate both the septal calretinin neurons, and hippocampal dentate gyrus and CA2/CA3a regions (Vertes 1992; Leranth and Kiss 1996; Leranth et al. 1999; Vertes and McKenna 2000).

The functional connectivity reviewed above has been used for a hypothesis whereby the brainstem-diencephalo-septo-hippocampal circuit acts in a behaviourally-dependent manner to synchronise the hippocampal circuit. A product of this synchrony is the hippocampal theta frequency oscillation.

1.3 Intrinsic connectivity within and between septal nuclei

Investigation of connectivity between neurons within the septum is limited. One group of medially located parvalbumin-expressing (PV) neurons in the medial septum receives synaptic inhibition from PV-expressing boutons hypothesised to be of local origin (Henderson et al. 2004). Some of these boutons may originate from infrequent PV-expressing hippocampo-septal projection neurons (Jinno and Kosaka 2002). Other PV-containing neurons in the medial septum located laterally to those which have dense PV-input, do not have observable PV-containing boutons decorating their soma. Analysis of the *in vivo* firing patterns of medial septal neurons has led to a hypothesis that there are two mutually inhibiting populations of GABAergic septo-hippocampal neurons (Borhegyi et al. 2004). The same study also demonstrated that PV-expressing medial septal neurons received cholinergic innervation suggested to originate from local cholinergic neurons to their somatic domain (Henderson et al. 2004). Cholinergic neurons, although they receive input from other cholinergic neurons, do not receive PV-containing input somatically.

A dense PV-positive axonal plexus is formed at the border of the medial and lateral septum by ascending axons from the diagonal band. The synaptic partners of this ascending projection are calbindin-expressing lateral septum neurons (Kiss et al. 1997). The diagonal band may be reciprocally connected with the medial septum, with some putative septo-hippocampal neurons sending multiple descending bouton-bearing axons to the diagonal band (Gaykema et al. 1990; Borhegyi et al. 2004). Other cell populations, such as those which express calretinin, NECAB-1, NOS, and VGluT2 (the glutamatergic neurons) within the medial septum have not had their local synaptic partners defined, to my knowledge.

Neuronal populations within the lateral septum include a number of GABAergic cell types which express calbindin in principal neurons (somato-spiny neurons), putative interneurons containing PV and calretinin, and non-GABAergic cholinergic neurons (Doutrelant et al. 1993; Zhao et al. 2013). Neurons containing PV and calretinin are likely to be local interneurons, which primarily target the principal neurons of the lateral septum, the somato-spiny neurons. It is not known whether all lateral septum domains are uniformly organised, or interconnected, or contain similar cell types, but their inputs differ (Risold and Swanson 1997).

The connection between the medial and lateral septum has been debated, because of difficulties in using traditional tracing methods relying on large injections of a molecule into regions which are continuous and next to each other. Whilst a number of studies have failed to find a latero-medial connection (Leranth et al. 1992), a single study reported a large connection between the rostro-ventromedial lateral septum and the medial septum (Risold and Swanson 1997). This provides a potential synaptic loop from the medial septum to the hippocampus, then to the lateral septum and back to the medial septum. As the lateral septal principal neurons receive direct hippocampal pyramidal input, a projection from these neurons to medial septal neurons would be functionally important, providing feedback from the hippocampus. No observable projection from the medial to the lateral septum has been found to my knowledge.

1.4 Hippocampal neuron theta-related firing patterns

The extracellular voltage oscillation, the theta oscillation, has been used as a reference to investigate cell type-dependent firing patterns and the role of different cell types in hippocampal network activity (Klausberger and Somogyi 2008). A prominent feature of neurons throughout the brainstem-diencephalo-septo-hippocampal system is the phase locking of single neurons to the theta oscillation (Petsche et al. 1962; Kocsis and Vertes 1994; Kocsis et al. 2006; Ma et al. 2013). Within the hippocampus numerous identified cell types demonstrate phase locking, including

pyramidal neurons, granule cells, and interneurons (West et al. 1981; Klausberger and Somogyi 2008).

1.5 Pyramidal neurons can display place fields

Pyramidal neurons can display place fields (O'Keefe and Dostrovsky 1971; Lapray et al. 2012). They have a dynamic firing frequency which correlates with the animal's location in space, and this has been observed in numerous species including humans (Ekstrom et al. 2003). The firing frequency of place cells increases as the animal enters the place field; it is maximal as the animal moves to the centre of the place field, and decreases as the animal leaves the place field. Place cells display a complex relationship to theta phase referred to as phase precession (O'Keefe and Recce 1993). The theta phase of action potentials of place cells occurs earlier with every subsequent theta cycle during the animal's transition across the place field. This translates to firing at the peak of the theta local field potential in the pyramidal layer as the animals enters the field, subsequent action potentials occurring earlier in each cycle so the maximal firing is at the trough of a theta cycle and up to a full 360° phase shift may occur as the animal leaves the place field. The mechanism by which place fields are generated and maintained has not been agreed upon, but there are several models which may explain both place fields and phase precession (Burgess and O'Keefe 2011).

1.6 Sharp-wave associated ripple oscillations and place cell ensembles

As an animal moves through an environment, a number of place fields will be traversed in sequence, represented by the corresponding place cells firing in the appropriate sequence. This is called a place cell ensemble (Eichenbaum et al. 1989). In periods of consummatory behaviour and sleep, another prominent oscillation is present in the hippocampus known as the sharp-wave ripple oscillation (SWR) (O'Keefe and Nadel 1978; Buzsáki et al. 1983; Buzsáki 1986). The sharp-wave is large field potential event of 100 – 150 ms duration associated with an oscillation of 90 – 250 Hz, the ripple occurring concurrently with highest amplitude in the pyramidal layer. In the CA1 region the sharp-wave is positively deflected in stratum oriens/pyramidale reversing polarity at the border

with stratum radiatum where it has the largest amplitude (Buzsáki et al. 1983). Sharp-waves are local events with approximately 10 – 15 % of all pyramids participating in each event (Csicsvari et al. 2000). The initiation of SWRs is hypothesised to occur in CA3, propagated by the recurrent connectivity of CA3 pyramidal neuron axons (Csicsvari et al. 2000). Excitation from CA3 SWRs is communicated via the Schaffer collateral/commissural pathways to CA1 pyramidal neurons, which then participate in an independent SWR event.

Hippocampal pyramidal neurons display remarkable organisation and synchrony during SWR events. Pyramidal cell ensembles which have been recently active in wakefulness, display replay during SWRs. That is, sequences of place cells which fired in a defined order as they occurred in space, are replayed in the same order, or reverse order, in a temporally compressed manner (Wilson and McNaughton 1994; Gupta et al. 2012). The highly coherent firing of pyramidal neurons in monosynaptically connected regions during ripples is hypothesised to lead to plasticity of synaptic connections between CA3 and CA1, and CA1 and the cortical regions (Chrobak and Buzsáki 1996; Chrobak and Buzsáki 1998; Csicsvari et al. 2000; Wierzynski et al. 2009). It has been suggested that this is the mechanism by which hippocampus-dependent memory is transferred to other cortical structures and produce long term potentiation of synapses (Bliss and Lømo 1973).

Recently a novel phenomenon of “preplay” has been described which may illustrate another firing pattern correlate of SWRs. During preplay, pyramidal neuron firing sequences which have not yet occurred during waking experience, assemble in SWR events (Dragoi and Tonegawa 2011; Dragoi and Tonegawa 2013). It is probable that these sequences are seen in novel waking experiences as place fields are coded and then consolidated. Preplayed pyramidal cell ensembles are therefore likely to self-arrange in preparation of coding of novel place sequences in the future.

Pyramidal neurons of CA1, unlike that of CA3, are only rarely (~1%) connected synaptically and lack strong recurrent connectivity (Deuchars and Thomson 1996). Complex behaviours, such as those

described during theta and SWR oscillations, arise from the organisation of complex excitatory inputs as well as the actions of numerous interneuron types.

1.7 Interneuron phase-locking and relationship to pyramidal neuron firing in both theta and SWR oscillations

There are at least 21 identified types of interneuron within the CA1 of the rat hippocampus (Klausberger and Somogyi 2008; Somogyi 2010). GABAergic interneurons innervate distinct subcellular domains of pyramidal neurons. The soma, dendrites and axon initial segment receive specialised input from distinct interneuron types. Distinct interneuron axonal domains overlap with known excitatory pathways and inputs such as the perforant path and Schaffer collaterals (Klausberger et al. 2004; Leao et al. 2012). The timing of GABA release by each interneuron type onto respective pyramidal neurons is highly organised and phase modulated to the theta oscillation, often in a behaviourally-dependent manner (Lapray et al. 2012; Varga et al. 2012; Viney et al. 2013). This has led to the concept of a temporal redistribution of inhibition to different subcellular domains of pyramidal neurons by distinct interneurons, organised over a single theta cycle (Somogyi et al. 2014).

Distinct interneuron populations can be identified by the presence or lack of molecular markers. Particular molecular markers present in hippocampal interneurons correlate with the domain which is targeted by the interneuron, as well as the timing of GABA release relative to the theta cycle (Somogyi and Klausberger 2005).

Inhibition is a dynamic process, with GABA release throughout the theta cycle to all domains of pyramidal neurons (Klausberger and Somogyi 2008; Varga et al. 2012). Bistratified interneurons, a PV-, SOM-, NPY-expressing neuron type, fire maximally during the trough of the theta oscillation *in vivo* (Klausberger et al. 2004). This is when pyramidal neurons, as a population, fire maximally (Mizuseki *et al*. 2012). This means that the pyramidal dendritic branches, which are the synaptic targets of bistratified neurons, are maximally inhibited during pyramidal cell firing, illustrating that

GABAergic interneuron inhibition is not necessarily functioning to prevent action potential generation in principal cells. However, GABA released to the axon initial segment by axo-axonic neurons may be able to dictate the firing pattern of pyramidal neurons (Klausberger et al. 2003; Viney et al. 2013). Axo-axonic neurons have maximal firing probability close to the peak of theta, when the majority of pyramidal neurons display minimal firing probability. Axo-axonic neuron silencing is hypothesised to be a necessary condition for the initiation of SWR oscillations and synchronisation of pyramidal cell firing at the start of these events (Klausberger et al. 2003; Viney et al. 2013). Axo-axonic cells, but not bistratified and PV-expressing basket cells, are silent during SWR; both of the latter types of neuron fire strongly during SWR events (Klausberger et al. 2004; Lapray et al. 2012; Varga et al. 2012). Hippocampal interneurons release GABA to diverse pyramidal cell domains throughout the theta oscillation, as well as the SWR, in a behaviour-dependent manner.

Interneuron spike-timing within the hippocampus, i.e. the temporally organised redistribution of GABA release to pyramidal cell domains from interneurons, is important for pyramidal neuron coding (Lovett-Barron et al. 2012; Royer et al. 2012). The septum is likely to be a significant causal input in defining the spike timing of interneurons relative to the theta oscillation (Freund and Antal 1988; Hangya et al. 2009).

1.8 The medial septum is a frequency pacemaker for the hippocampal theta oscillation

Lesion of the medial septum in awake rabbits abolished the generation and propagation of the theta oscillation within the hippocampus (Green and Arduini 1954). This was the first evidence linking the septum to the hippocampal oscillation. Pharmacological lesioning and silencing of the medial septum also produce silencing or alteration of the hippocampal theta oscillation, including the atropine-sensitive and insensitive components (Kramis et al. 1975; Lamprea et al. 2010; Orzeł-

Gryglewska et al. 2012; Pilly and Grossberg 2013). These pharmacological manipulations, unlike electrolytic lesions, prove that the medial septum and not axons of passage is the site of this effect.

The firing of some medial septal neurons is phase-locked to the hippocampal theta oscillation *in vivo*; a given population of neurons in the medial septum fire action potentials at the same time relative to each theta cycle in the hippocampus (Petsche et al. 1962). These neurons are GABAergic and express PV (Freund 1989; Borhegyi et al. 2004) and the hyperpolarisation-activated cyclic nucleotide-gated non-selective cation channel 1 (HCN1) (Varga et al. 2008). Neurons with this molecular phenotype project to the hippocampus and exclusively innervate interneurons (Freund and Antal 1988). The firing of this population of neurons may lead the hippocampal theta oscillation; changes in their burst frequency correlates with a change in theta frequency, and is causative of that change, rather than following it (Hangya et al. 2009).

GABAergic rhythmic septo-hippocampal neurons are often referred to as "pace-maker" neurons of the hippocampal theta for the behaviour described above. However, they display behaviour, which is not that of true intrinsic pacemaker neurons, such as those of the suprachiasmatic nucleus. *In vitro*, medial septal neurons do not fire spontaneously in a rhythmic fashion without pharmacological induction (Jones et al. 1999; Morris et al. 1999; Wen et al. 2013). However, using nicotinic acetylcholine receptor activation in slice, both rhythmic firing and theta frequency oscillation can be induced (Wen et al. 2013). *In vivo* recording of neurons in regions which project to the medial septum, such as the supramammillary nucleus and nucleus incertus, have shown that potentially excitatory input to medial septal neurons may be rhythmic, and phase-locked to the hippocampal theta oscillation (Kocsis and Vertes 1994; Ma et al. 2013). Anaesthetic injection within the medial septum produces a dose-dependent decrease in the amplitude of concurrent hippocampal theta, without changing the frequency (Kirk and McNaughton 1993). Conversely, anaesthetic inactivation of parts of the supramammillary nucleus alter the frequency as well as the amplitude (Kirk and McNaughton 1993; Figure 1.2). This suggests that the medial septum is not the

point at which tonic excitatory information is transduced into phasic/frequency information, but is the point at which phasic, and other information is integrated and imposed via interneuron inhibition, onto the hippocampal network. In summary, the medial septum modulates theta oscillations generated downstream and implements theta in the hippocampus.

1.9 Frequency integrators for hippocampal theta oscillation

Stimulation of the nucleus pontis oralis is known to be the most efficient means to generate hippocampal theta oscillation (Faris and Sainsbury 1990) in a septum-dependent manner (Kirk and McNaughton 1993). Non-rhythmic stimulation produces rhythmic firing of septal neurons (Kitchigina et al. 1999), the frequency of which positively correlates with the frequency of the resultant oscillation (Faris and Sainsbury 1990). The transduction of this intensity signal to a frequency signal is likely to be earlier in the circuit than the medial septum. The septo-hippocampal pathway, integrating rhythmic and non-rhythmic signals, synchronises the hippocampus via rhythmic inhibition of interneurons, and disinhibition of pyramidal neurons. This rhythmic synchrony results in the theta oscillation within these areas.

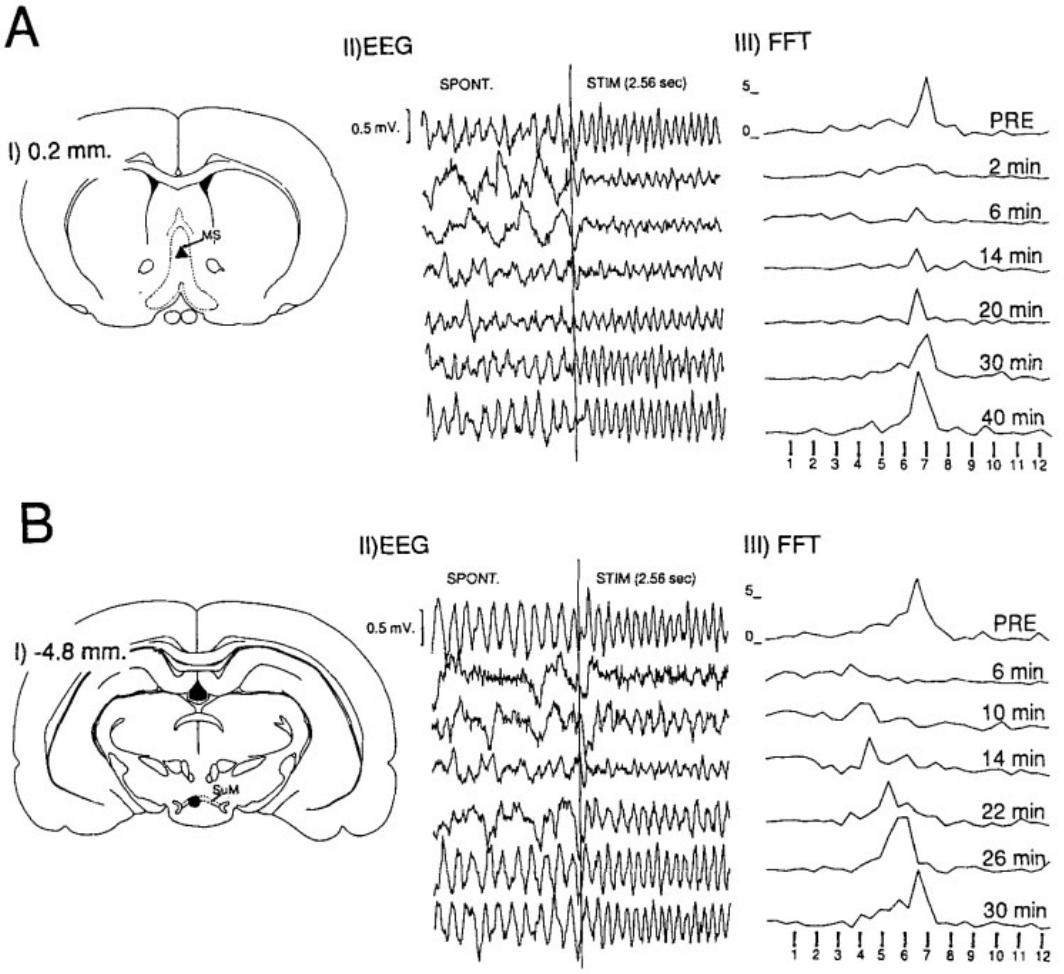


Figure 1.2 – Relative contribution of the medial septum and supramammillary nuclei to power and frequency of stimulation evoked theta oscillation within the hippocampus. Procaine was injected into **Ai)** the medial septum and **Bi)** the supramammillary nucleus. The local field potential was recorded from hippocampus at varying time intervals shown in **ii** under both spontaneous activation (left) and reticular stimulation evoked activation (right). The FFTs shown in **iii** demonstrating the clear decrease in power produced by medial septum inactivation **Aiii)** and decreasing frequency and power from supramammillary inactivation **Biii)**. (Adapted from Kirk and McNaughton 1993).

Anaesthesia, lesion, or pharmacological blockade of parts of the supramammillary nucleus, reduce the frequency of theta in the hippocampus even during noxious stimuli or PnO stimulation (Kirk and McNaughton 1993). However, in drug free animals even extensive ablation of the supramammillary nucleus does not have a significant effect on hippocampal theta oscillation frequency (Thinschmidt et al. 1995), although the lesion reduces the frequency of PnO stimulation induced theta (McNaughton et al. 1995; Thinschmidt et al. 1995). This indicates that other regions must also be capable of acting as a frequency integrator in behaving animals. The entorhinal cortex is a region known to project to the hippocampus and septum (Hjorth-Simonsen 1972; Hjorth-Simonsen and Jeune 1972; Leranth et al. 1999) and it is involved in the coding of space (Hafting al. 2005). Locally generated theta in the entorhinal cortex is coherent with that in the hippocampus (Dickson et al. 1994; Chrobak and Buzsáki 1998), thus it may be a candidate for frequency integration. Lesions of the entorhinal cortex produce a reduction in hippocampus-dependent behaviours and reduce the power of theta rather than its frequency in behaving animals (Nachkebiya et al. 1987; Hagan et al. 1992).

The nucleus incertus is a brainstem region which projects to the septo-hippocampal system, including a glutamatergic projection to PV-expressing septo-hippocampal neurons (Cervera-Ferri et al. 2012). Stimulation of the nucleus incertus induces hippocampal theta oscillation (Nuñez et al. 2006). Under anaesthesia, nucleus incertus produces a theta frequency oscillation which is coherent with that of the hippocampus (Cervera-Ferri et al. 2011). Relaxin-3-expressing neurons in the nucleus incertus project to septo-hippocampal GABAergic neurons and fire rhythmic bursts of action potentials which are phase locked to hippocampal theta (Ma et al. 2009; Olucha-Bordonau et al. 2012). To my knowledge, no studies have shown a decrease in frequency by pharmacological dose-dependent inactivation of the nucleus incertus, but its lesions ablate PnO induced theta completely (Teruel-Martí et al. 2008).

The existence of multiple frequency integrators may be relevant to the contrasting effects seen during various brain lesions in different behavioural contexts (McNaughton et al. 1995).

1.10 The septum in disease

Dysfunction of the septum and basal forebrain is found in numerous pathologies, most prominently in Alzheimer's disease (AD) (Whitehouse et al. 1982; Henke and Lang 1983). During AD, degeneration of the cholinergic as well as the GABAergic projection from the septum occurs (Villette et al. 2010; Rubio et al. 2012). Markers of cholinergic axonal arbour are significantly reduced throughout the hippocampus with severity of decrease correlated with disease progression (Perry et al. 1978; Kuhl et al. 1996).

A hallmark symptom of AD which relates to the septo-hippocampal pathology is memory loss and a lack of memory formation (Hart et al. 1988). Alzheimer's disease has several genetic components which relate to the early-onset of the disease, as well as sporadic AD, and have been used to replicate many of the symptoms of the disease, both pathological and symptomatic, in transgenic animal models (Wang et al. 2002; Robertson et al. 2009; Belbin et al. 2011; Wang et al. 2012; Lambert et al. 2013). Using electrophysiological techniques in transgenic animal models, changes in septal neuron firing and hippocampal field potential oscillations have been reported (Wang et al. 2002; Villette et al. 2010; Rubio et al. 2012). These changes include decreases in the GABAergic component of the septo-hippocampal pathway and a resultant decrease in hippocampal theta and gamma oscillations. This effect was not dependent on GABAergic cell loss but on a potential decrease in the number and extent of GABAergic septal axons within the hippocampus (Rubio et al. 2012). Disruption in cortical oscillations is observed in humans and correlates with disease progression (Moretti et al. 2007; Babiloni et al. 2009; Fonseca et al. 2011; Wang et al. 2012).

Epilepsy may involve the uncontrolled and excessive synchronisation of neuronal populations. Temporal lobe epilepsy, which often manifests within the hippocampus, has been linked to reciprocal GABAergic pathways between the septum and hippocampus (García-Hernández et al.

2010; Quilichini et al. 2012). The septo-hippocampal pathway undergoes changes in excitability and inhibitory control in an epileptic guinea pig model. Neurons within the septum of epileptic animals are more sensitive to exogenous application of GABA. This increase in septal inhibition is concomitant with an increase in neuronal bursting (Malkov and Popova 2011). Increased septal bursting may result in additional pathological inhibition of hippocampal interneurons. Rhythmically firing medial septal neurons, whilst firing phase locked to hippocampal theta, do not increase firing during interictal (epileptic) events (García-Hernández et al. 2010). Whilst pyramidal neurons increase activity during epileptic activity, GABAergic lateral septum neurons have a decreased firing rate in epileptic animals (García-Hernández et al. 2010). Lateral septal neurons receive a significant input from hippocampal pyramidal cells (Alonso and Frotscher 1989). A subset of lateral septum neurons increase their firing rate before and during interictal events, as would be expected from their increased firing during SWRs (García-Hernández et al. 2010).

Decreased GABA release by interneurons due to increased medial septal inhibition may produce the uncontrolled excitability within pyramidal cells and is likely to evoke epileptiform activity. This is then transmitted to the lateral septum producing excessive firing in a similar manner to SWR (Dragoi et al. 1999; García-Hernández et al. 2010). The hippocampus alone is also capable of generating theta frequency oscillations, as has been demonstrated *in vitro* (Goutagny et al. 2009). Therefore dysfunction of a major input that has an effect on temporal organisation, such as the septum, could provoke physiologically irrelevant synchronous firing which may include epilepsy.

Aim

I will test the hypothesis that single GABAergic, septal neurons, which fire phase locked to the hippocampal theta oscillation, innervate specific interneuron types within the hippocampus. The septum is a basal forebrain region which forms a part of the brainstem-diencephalo-septo-hippocampal system. Septal connectivity with the hippocampus is necessary for frequency oscillation and pyramidal cell theta-related firing. A portion of this connection is GABAergic and

provides rhythmic, phase-locked inhibition exclusively to GABAergic interneurons. Stimulation of this pathway is capable of disinhibiting pyramidal cells. This study aims to investigate the specificity of the septo-hippocampal pathway using population and single cell anatomical techniques. Extracellular recording followed by juxtacellular labelling will be used to electrophysiologically investigate septal neurons testing their activity relative to the hippocampal field potential. In parallel, the recorded neurons will be analysed anatomically together with their hippocampal targets using immunohistochemistry. I will attempt to define neuron groups by firing pattern parameters. I will test if firing pattern parameters and molecular phenotypes are correlated with the location of the axonal arbour and the specific interneuron targets of septal neurons within the hippocampus.

Chapter 2 - Methods

2.1 Animals

All experiments were carried out under the Animals (Scientific procedures) act 1986 in accordance with the Home Office. Adult male Sprague-Dawley rats (Charles River) between 200-375g were used for all experiments. Animals were kept on a 7 hour light-dark cycle with food and water *ad libitum* in cages with up to six rats in total. Temperature and humidity were kept constant at 21 ± 2 °C and 50 ± 10 % respectively.

2.2 Anterograde tracing using PHAL

Rats were induced with 4% isoflurane (Abbott) in pure oxygen (BOC Medical) using an anaesthetic vapourisor (Vet Tech Solutions). Animals were then placed in a stereotaxic frame (Kopf) with variable concentrations of isoflurane delivered through a face mask. The scalp was shaved with clippers (Wella) and the rat was placed on a heating pad with feedback from a rectal probe (Harvard Apparatus). The skull was fixed in place using blunt ear bars (Kopf) and the mouth was opened with the tongue pulled out to promote breathing. Exhaled isoflurane was removed and processed with a scavenger (Fluovac) throughout the experiment through a co-axial tube. Lignocaine gel (5 %; AstraZeneca) was applied to all contact points between the animal and the frame; ocular lubricant (Allergan) was applied to the eyes. The analgesic buprenorphine (0.03 mg/kg; Vetagesic) was injected intraperitoneal. The scalp was then washed three times with chlorhexidine (Animal Care) and sterile water (Hameln Pharmaceuticals). Isoflurane concentration was maintained at the lowest level which maintained no response to pinch and no blinking reflex. A sterile drape was placed over the animal during surgery.

Marcaine (AstraZeneca) was injected subcutaneously along the midline of the scalp. After 10 minutes, using a disposable sterile scalpel (Swann-Moston), a single cut was made at the midline from the level just posterior to the eyes, to the neck muscles. Excess blood was removed using sterile cotton swabs (Johnson's) soaked in sterile saline. The skin flaps were parted and held in place using four loops of suture (Ethicon) weighted with haemostats (Fine Science Tools); one

placed in each corner of the wound. Underlying tissue and periosteum was removed from the skull using cotton swabs and a surgical bone scraper (Fine Science Tools). Bleeding from the skull was stopped by light scraping with a bone scraper. Special attention was paid to cleaning the tissue associated with the bregma for accurate stereotaxic measurements.

Using an operating microscope with light blue filter (Zeiss), a glass electrode fitted to a micromanipulator was used to measure the medio-lateral (M-L) and rostro-caudal (R-C) distances from bregma. An small ink dot marked the skull location for drilling. A craniotomy was performed at the marked location with a bone drill (Harvard Apparatus), and forceps (Fine Science Tools) for removing bone fragments. Saline and cotton swabs were also used to remove all excess bone pieces. For the duratomy, a cut was made at the edge of the craniotomy site using a needle tip attached to a small syringe. The remaining dura was carefully pulled from the site using forceps to preserve the vasculature above the brain. Throughout the experiment the brain surface was kept moist using sterile saline.

A glass electrode with a tip diameter of ~10 µm was filled with *Phaseolus vulgaris* leucoagglutinin (PHAL; Vector Laboratories) 2.5 % in 10 mM NaPBS (AnalaR) solution. The electrode was placed relative to bregma in the M-L and R-C axis and depth was measured from the surface of the brain. It was then lowered slowly by hand over ~ 1 minute to the deepest dorso-ventral co-ordinate before being left to equilibrate for 15 minutes. Standard iontophoretic protocol for PHAL was used (Gerfen and Sawchenko 1984). Briefly, 5 nA positive current pulses were applied with a 7 second duty cycle for the time required using a custom made iontophoresis unit (University of Oxford). After each injection, the electrode was left in place for >10 minutes before being moved either to the next depth, after which it was left in place for another 10 minutes before injection, or being removed from the brain. After the injection protocol, the wound was sutured closed, a small amount of suture glue (3M) was occasionally used for further support of the wound.

Post-surgery, 2 ml glucose-saline (5 % / 0.9 %; Dechra) and carprofen (5 mg/kg; Pfizer) were injected subcutaneously. Animals were recovered on a heating blanket in single cages with free access to food and water. Supplementary high energy food mix was given to promote weight gain. Animals were weighed and scored for signs of suffering or infection daily (Figure 2.1). The oral analgesic meloxicam (4 mg/kg; Boehringer Ingelheim) was given daily until animals demonstrated minimal signs of stress. After three days recovery, animals were occasionally housed in pairs. Between 4 – 18 days post-surgery animals were terminally anaesthetised with 2ml pentobarbitone (20 % w/v; Animal Care) and perfused transcardially with 0.05 % glutaraldehyde (TAAB) 4 % paraformaldehyde (TAAB), 15 % picric acid (as saturated solution in dH_2O v/v; Sigma), 0.1 M phosphate buffer containing fixative using a pump.

2.3 Juxtacellular recording and labelling

Induction of anaesthesia was as above, followed by a single dose of urethane (1.25 g/kg; i.p.; Sigma). After animals lost their blink reflex and no longer responded to a noxious foot pinch, a large dose of ketamine/xylazine was given (0.1ml injection of 20 and 2 mg/kg respectively; i.p.), the scalp was prepared as above and the animal placed into invasive ear bars (Kopf). The stereotaxic frame was mounted on an air table (Scientifica). Supplementary doses of ketamine/xylazine (0.01 – 0.05 ml; 20/2 mg/kg respectively; i.p.) were given throughout the experiment to maintain anaesthetic level and manipulate network states, as well as 2 ml glucose - saline solution (5 % / 0.9% w/v; s.c.) every 2-3 hours. Locating and marking of each craniotomy was performed as above. An oval wall of dental cement (Biomet) ~5 mm in height was constructed around the perimeter of the exposed skull so as to not be in contact with the vascular tissue. Another diagonal wall was made separating the craniotomy sites from each other but not covering bregma to allow for measurements later. The overall shape of the wall is similar to a “Ɵ” with a diagonal central line. Both craniotomy and duratomy were as described above, with a drop of sterile saline applied to each site after duratomy. For increased accuracy a third partial craniotomy was made anterior to the septal craniotomy, this

was a long ~ 1 cm horizontal line, the width of a large drill bit, centred on the midline central sinus. The purpose of this site was to be able to visualise the width of the central sinus and use it to measure the medio-lateral co-ordinates; this was found to be a more consistent measure of medio-lateral relative position than bregma. The skull was drilled to a depth whereby the sinus can be clearly seen to each lateral edge through the skull; a drop of saline was used to aid the visualisation.

Both septal unit and hippocampal reference electrodes were acquired in the same manner. Signals were acquired using silver wires treated with HCl bleach for >4 h. This was sent to a preamplifier (npi) attached to the micromanipulator stepper motors (Scientifica) via a male gold pin soldered to the wire. Signal was carried to an amplifier (npi) for 1000x total amplification gain, (10x from the preamplifier, 100x from the main amplifier). All connections from this point are by BNC cable (Farnell) unless stated. Signals were sent to a 50 Hz noise reducing Humbug (Quest Scientific) and the output split using a splitter to form two channels into the amplifier. One, the “units” channel containing the action potentials, was band-pass filtered between 0.8 – 5 KHz (20 kHz sampling rate), the other, the local field potential channel was band-pass filtered between 0.3 – 300 Hz (1 kHz sampling rate). For the septal electrode only, in addition to, or instead of, the field potential channel, a “wideband” 0.3 – 5000 Hz (20 kHz sampling rate) channel was also used. Signals were digitised using an analogue to digital converter (Cambridge Electronic Design) and sent to a PC for recording and online visualisation in Spike2 v7 (Cambridge Electronic Design). For the juxtacellular labelling protocol, an external timing unit (npi) was used to apply 250 ms square pulses of current to the unit electrode (Pinault 1996). Signal from the septal unit’s channels was visualised on an oscilloscope (Tektronix) for juxtacellular labelling, as well as made audible using speakers.

For septal juxtacellular recording and labelling glass electrodes, made from filamented borosilicate capillaries tubes (Harvard Apparatus) pulled and broken to a tip diameter of ~1.5 µm; these electrodes were filled using Microfil tips (World Precision Instruments, inc). Electrodes were pulled on a vertical electrode puller (Narishige) and manually broken under a microscope against a flat

glass probe. Initially, a small volume of the tracing molecule to be used (usually 3 % neurobiotin (Vector Laboratories) in 0.5 M NaCl (AnalaR) was placed into the top of the electrode and it was held tip side down for a couple of minutes to allow the very thin tip to fill by capillary action. The electrode filler was then advanced into the electrode to below the level of liquid and carefully filled the majority of the way up to prevent bubbles. For reference electrodes, the same process occurred with tip diameters of > 1.5 µm, and using either neurobiotin, or sterile saline. Sterile saline is preferred so as not to produce accidental delivery of neurobiotin into the hippocampus.

Saline was removed from the recording sites and electrodes were lowered using micromanipulators (npi) at ~25 µm/s; depth was zeroed at the point the electrode touched the brain. At ~300 µm depth the electrode's impedance was tested, electrodes between 17-30 mΩ were kept, those outside this range were discarded and another electrode used. Brief current pulses were used to clear electrodes which had an impedance larger than required (known as "buzzing"). Saline was again applied to the surface and electrodes were advanced again. The septal electrode was advanced to 4000 µm, approximately the corpus callosum or cortex, and buzzed again before being advanced more slowly at <5 µm/s into the septum. The hippocampal reference was advanced to a depth of 2800, usually the stratum radiatum, additional ketamine/xylazine was given to induce negative-going sharp-wave ripple oscillations, and the electrode depth altered until sharp-waves were positively deflected with no units seen in the signal.

When the septal recording electrode was deeper than 5200 µm, it was advanced at 2 µm/s until units were seen which corresponded with a cell type of interest. The electrode was then advanced into the juxtacellular position until the recorded unit was > 1 mV in amplitude. Recordings were attempted during all network states: theta, sharp-wave ripple, and slow oscillations before labelling was attempted. A labelling was considered successful when: the modulation of a cell was greater than 4 minutes, a large increase in firing frequency occurred throughout, and a firing pattern which does not show significant injury (increased wave width, high firing rate without current injection,

spontaneous increase and decrease of spike amplitude). After a successful labelling animals were maintained for 2-24 hours until transcardial perfusion with the standard fixative described above. Reference electrode position, depth of each neuron recorded, time and amount of anaesthesia given and other details of each experiment were recorded in a data sheet (Figure 2.2).

2.4 Analysis of electrophysiological data

All electrophysiological data was acquired using Spike2 (Cambridge Electronic Design). Spike sorting was performed using a standard Spike2 waveform function. All spikes were manually inspected before being transposed as single time points which correspond to the peak amplitude of the action potential waveform.

Recordings were segregated into distinct brain states of hippocampal theta and sharp-wave ripple oscillations. Delineation was performed using a custom script (John Tukker) using the following parameters: hippocampal theta oscillatory epochs were defined as periods with a 3-6 Hz / 1-3 Hz (theta/delta band) power ratio greater than 4. Septal delta oscillation (1-3 Hz) reliably occurred during hippocampal theta epochs and therefore theta epoch timings were used as defined periods of delta oscillation within the septum. Ripple events were defined as periods with a 90-200 Hz power greater than 6 SD of the baseline. Start and end of the SWR was defined as when the 90-200 Hz band exceeded or diminished past 2 SD of the base line. All epochs were visually inspected and manually corrected.

2.4.1 Theta phase analysis

All analysis of spike-LFP phases was performed using a custom MATLAB script (Balint Lasztoczi). The hippocampal LFP was band pass filtered between 3-6 Hz, and the troughs of each cycle were detected. The time between each trough was then separated into 18 bins of 20° and a sine wave was extrapolated. The timing of each spike which occurred during a theta epoch was compared to the phase at which it occurred relative to the theta oscillation. Mean firing phase was calculated.

For testing of significant phase modulation of a neuron to the theta oscillation, Rayleigh's test of circular uniformity was performed with mean vector length used to describe coupling strength.

2.4.2 Sharp-wave ripple analysis

The analysis of the phase of action potentials occurring during SWRs was performed as for the theta oscillation; ripple oscillation (90-200 Hz) troughs were detected in a band pass filtered channel and phases were extrapolated. Action potentials were binned by phase and Rayleigh's test of uniformity was performed to detect strength of modulation.

To test for significant differences in firing frequency between intra- and peri- SWR periods a custom script was used (Linda Katona). Time windows which corresponded to the timings of SWRs within a recording were randomly shuffled 100 times within ±10 s around each ripple (excluding other SWR epochs) and the distribution of spike timings within these shuffled periods was compared by Mann-Whitney-U test to intra-SWR action potential distributions. Septal neurons could decrease, increase, or not change their firing pattern.

To describe the temporal relationship of SWR active and inhibited neurons to the SWR in absolute time, the timing of each SWR peak was taken as time 0 and a histogram of spike timings ±1 s, in 10 ms bins, to all SWR events was generated. Each neuron was then normalised to 0-1. For SWR active neurons, the largest bin for each of the neurons was taken as the peak timing and these were averaged to produce the maximal spike timing of SWR active neurons relative to the SWR peak timing in CA1. For SWR inhibited neurons, each time bins were averaged for all neurons. Paired Student's t-test was then performed comparing each bin to the baseline time of -150 ms from the peak.

Average action potential per cycle histogram was calculated using a custom script in Spike2 (Jon Tukker). As for the theta phase calculations above, spikes were binned according to the phase they occurred at in the phase of theta produced by linear iteration of the detected troughs. Number of action potentials for each bin was averaged to produce the action potentials per cycle for each

phase bin. The maximal firing phase was taken as the bin which had the highest action potentials per cycle.

2.5 Juxtacellular labelling with recovery

Experiments were performed as for PHAL experiments above for all anaesthesia and post-operative care. Methods are identical to the PHAL experiments in preparation of craniotomy and duratomy. Recording and labelling were as for the electrophysiology experiments above, excluding the use of neurobiotin from the labelling electrode. Electrodes were filled with 10 % biotinylated dextran amine in 0.5 M potassium acetate (Sigma) solution. Isoflurane produces activity which is unlike that seen in drug free or urethane anaesthetised animals and was therefore not analysed further. Neurons seen deeper than 5400 µm were labelled; after a successful labelling animals were recovered as for PHAL experiments for between 3-4 days before transcardial perfusion with the standard fixative.

2.6 Tissue processing for light microscopy

All brains were washed in 0.1 M phosphate buffer for 1-48 h before coronal sectioning at 70 µm using a vibrating microtome (Leica) and stainless steel razorblades (Wilkinson Sword). Coronal sections were stored sequentially in 24 well plates in 0.1 M phosphate buffer with 0.05 % sodium azide. For storage, plates were wrapped along the edges with parafilm to prevent evaporation and stored at 4 °C.

For permeabilising fixed brain tissue for either fluorescent or permanent visualisation one of two methods were used: washing in tris-buffered saline (TBS) with 0.1 % Triton-X100 (TBST; Sigma) or the freeze-thaw of sucrose-cryoprotected tissue over liquid nitrogen (f/t method).

For the method using TBST, sections were washed 3 times for ≥ 30 minutes total in TBST. All processing after this point, for both fluorescence and permanent horse-radish peroxidase

visualisation, was performed in TBST-based solutions unless otherwise stated, including all blocking and antibody incubations.

To permeabilise using the f/t method, sections are never incubated in triton-X100-containing solution. The use of f/t method maintains the ultrastructure of the lipid membranes and organelles and is appropriate for further processing for electron microscopy. Fixed brain tissue was briefly washed in 0.1 M phosphate buffer before incubation in 20 % sucrose solution in 0.1 M PB for >4 h at room temperature; incubation occurred until the freely suspended sections no longer floated in sucrose. An open reservoir was filled with liquid nitrogen (BOC Medical), individual sucrose-cyroprotected sections were layed flat in a plastic 6 well plate (processed one at a time), sucrose solution was removed and the tray was gently put on the surface of the liquid nitrogen until the section freezes and visibly white. The tray was retracted from the solution and warm sucrose solution applied to the section to thaw it quickly. This was repeated a second time but was thawed in 0.1 M PB and further washed 3 times for ≥ 30 minutes in total. For antibody and/or avidin incubations after f/t permeabilisation TBS without triton-X100 was used.

For the visualisation of biotinylated molecules (BDA or neurobiotin), permeabilised sections were incubated in TBS/T containing 0.1 % v/v streptavidin-conjugated Alexa Fluor 488 (Invitrogen) for 4 – 24 h (between 4-12 h incubations were at room temperature, greater than that incubations were done overnight at 4 °C).

For immunohistochemistry, sections were initially blocked to prevent non-specific antibody binding by incubation of permeabilised sections in 20 % normal horse serum (Vector Laboratories) (or for TMR 5 % cold water fish skin gelatine (Sigma) was used) for > 1 h at room temperature. Blocked sections were incubated for 1 – 3 nights at 4 °C in TBS/T including primary antibodies (Table 2.1). Sections were then washed in TBS/T 3 times for ≥ 30 minutes total and incubated in TBS/T containing secondary antibodies raised in donkey (except with use of TMR where the secondary was raised in goat) and against the species in which the primary antibodies were raised. Secondary

antibodies were preabsorped against other species if possible. If streptavidin-dependent fluorescence was needed, it was incubated concurrently with the secondary antibodies.

For the production of a permanent nickel intensified diamino-benzidine (DAB; Sigma) end-product for visualisation of biotinylated molecules (BDA or neurobiotin), a horse-radish peroxidase enzyme conjugated to avidin (Vector Laboratories) was used. Processing of permeabilised sections which had previously been visualised with streptavidin conjugated to Alexa Fluor 488 were washed and incubated for 4 – 24 h in 1 % biotin v/v in TBS/T. After this point all processing is the same as for sections which have not been visualised previously. Sections were then incubated in 1 % avidin and 1 % biotin v/v in TBS/T for 1 – 3 nights at 4 °C.

Sections were incubated in a pre-reaction solution for 15 minutes containing a varying concentration of DAB depending on the intensity of the reaction to be produced and the previous quality of the tissue (Table 2.2).The reaction was initiated by the addition of glucose oxidase enzyme (1000 U/ml solution) and mixed. Reactions continued until sections were moderately dark. Reactions were stopped by the liberal washing of the sections with 0.1 M PB over 30 minutes. Sections were incubated in 0.1 – 1 % osmium tetraoxide solution (TAAB) in 0.1 M PB for 30 – 45 minutes depending on the darkness of the tissue. To end the deposit of osmium, sections were washed 3 times with 0.1 M PB over 30 minutes, dehydration in a series of increasing concentrations of alcohol and propylene oxide (VMR Chemicals) was performed. Sections were then immersed in Durcupan resin (Sigma) overnight before mounting on slides. The resin mounted slides were polymerised overnight in an oven at 60 °C.

2.7 Imaging

Confocal images were acquired using an LSM710 confocal microscope (Axio ImagerZ1, Carl Zeiss) with Zen 2008 software v5.0 (Zeiss) used to acquire multichannel fluorescent images. Lens used were: EC Plan-NeoFluar 10x/0.3, Plan-Apochromat 20x/0.8, DIC Plan-Apochromat 40x/1.3 oil immersion, DIC M27 Plan-Apochromat 63x/1.4 n.a. oil immersion, and alpha Plan-Apochromtat

100x/1.46 n.a. oil immersion. For immersion lenses, Immersol 518 (Zeiss) oil was used. Imaging channels were as follows (laser and excitation wavelength, fluorophores, beam splitters, emission spectral filter): 405-30 solid state 405 nm with attenuation filter ND04, DyLight405, MBS-405, 409-499 nm; argon 488 nm, AlexaFluor 488, MBS-488, 493-542 nm; HeNe 543 nm, Cy3, MBS-458/543, 552-639 nm; HeNe 633 nm, Cy5/DyLight 649/Alexa Fluor 647, MBS 488/543/633, 637-757 nm. Channels were scanned sequentially to minimise excitation cross-talk with an eight-bit dynamic range. For each channel the pin hole was set to 1 Airy unit. Pixel number was optimised by Nyquist sampling for the channel with the smallest wavelength. Routinely a line averaging was used of ≥4. The majority of images were taken using the 63x lens and a zoom of 1-2. Image manipulation was most often performed in Zen 2008 software or less frequently using ImageJ. Images were mean filtered before further manipulation such as deconvolution (Zen 2008) or intensity projections.

2.7.1 Imaging of horseradish peroxidase visualised tissue

Sections were imaged using an Axio ImagerZ1 microscope (Zeiss) and Axiovision (Zeiss) software with the lens described above. The image exposure was altered manually at the middle depth of a Z-stack. Optical slice number was optimised by Nyquist sampling. Contrast and balances were manually altered and processing, such as maximum intensity projection, was calculated in ImageJ.

2.7.2 Reconstruction and quantification of neurons

The full dendritic and partial axonal reconstruction of the septo-hippocampal neuron presented was produced using a drawing tube attached to a Dialux 22 (Leitz) with NPL Fluotar 40x/0.7 lens (Leitz). Reconstruction was made using sequential sections of 70 µm thick coronal brain visualised by DAB (as above). Sections were drawn onto separate sheets of tracing paper (Goldline) and for each point of the neuron which formed a cut end at the top or bottom of the section, blood vessels and other “landmarks” were also reconstructed to allow for correct alignment between sections. For final construction of all the individual slide drawings, drawings were enlarged to that of a near to the soma section treated by freeze-thaw to account for shrinkage during TBST-treatment. A scale

bar was drawn using a graticule (Graticules LTD) and each section, adjusted for shrinkage and aligned, was drawn onto a single paper in ink. The resultant reconstruction was photographed using a digital SLR camera (Canon) and digitally manipulated in Photoshop CS3 (Adobe) and Illustrator CS3 (Adobe).

For the full 3 dimensional somato-dendritic and axonal reconstruction of a septo-hippocampal neuron sections were traced using Neurolucida v.9 (MBF Bioscience) at 63x under oil immersion. Contours were added for all major boundaries, which includes the midline and the outline of the whole brain for at least every 3rd section. Hippocampal boundaries which were added to all sections were: the fimbria and alveus border for the whole hemisphere, alveus/stratum oriens, stratum oriens/stratum pyramidale, stratum pyramidale/stratum radiatum, stratum pyramidale/stratum lucidum (in CA3 only), stratum lucidum/stratum radiatum (in CA3 only), and the granule cell layer of the dentate gyrus. Boundaries were based on visible differences in cell density and neuropil in peroxidase visualised tissue. To correct for the shrinkage induced by tissue processing, sections treated by TBST were uniformly scaled manually to fit the x-y dimensions of the closest freeze-thaw section. For z-axis correction, each section was measured visually from the top to the bottom of the section on the acquisition microscope and adjusted to 70 µm. Reconstruction was performed on all sections which had visible neuron processes; the neuron was considered complete because all branches ended in natural boutons rather than fading which would be indicative of incomplete filling.

2.8 Hierarchical clustering

To characterise statistically, the differences in firing patterns between confirmed and putative septo-hippocampal neurons, as well as to compare theta rhythmic septal neurons to other cell types, hierarchical clustering was employed. Data was extracted for all parameters as described above. Diversity within theta rhythmic neurons, putative GABAergic septo-hippocampal neurons, was the focus of this study. These were defined as theta phase locked neurons, with a high mean

vector length (usually >0.4) and a high percentage of active theta cycles (usually >95 %). For quality control, two non-theta rhythmic populations were included which shared some, but not all firing properties of theta rhythmic neurons and were identified as distinct from theta rhythmic neurons in labelled examples. These were: lateral septum neurons, and delta-coupled neurons. Lateral septum neurons were phase locked to theta oscillation, typically had a high mean vector length (>0.3), but fired during a lower percentage of theta cycles than theta rhythmic neurons (<70 %). Where non-labelled examples were included they were recorded superficially to any theta rhythmic neurons and can be assumed therefore to be within the lateral and not medial septum. Delta-coupled neurons located within or close to the medial septum, had a spike timing which was related more strongly to the local septal oscillation than the hippocampal oscillation; some of which were only phase-locked to the septal and not the hippocampal oscillation. Examples of these neurons were found within the medial septum. For inclusion into the clustering neurons must have at least 1 theta epoch (defined above) of greater than 6 s, as well as having >5 SWR epochs, and be phase locked to the theta and/or delta oscillation and be of a high recording quality. All other firing patterns were excluded from the clustering analysis even if they met the quality criteria. This is to remove excess redundancy within the feature space and for better clustering quality of the theta rhythmic neurons.

Hierarchical clustering using Euclidean distances was performed using a custom MATLAB script (Robert Stewart). Pre-processing of parameters was performed in SPSS 19 (IBM). Normality of distribution was tested using Shapiro-Wilk; only non-normally distributed parameters were included for analysis. For clustering analysis, non-normality suggests the presence of more than a single group which could be described as a uniform distribution. All parameters were tested for correlation by Spearmann's Rank test. Correlated parameters were not included if they were direct measures of the same property (e.g. firing frequency and action potentials per theta cycle). Including correlated, and uniformly distributed features increases redundancy and decreases

quality of clustering. In Euclidean space, redundancy brings all points closer together and therefore reduces distances between clusters and reduces clustering quality.

For the inclusion of theta phase data into the clustering space, measurements of Euclidean pairwise distances in circular space was performed using the circular statistics package for MATLAB (Berens 2009).

Two parameter sets: hippocampal theta and septal delta mean vector lengths, and intra- and peri-SWR frequencies were made into an index for inclusion. This produced a single metric which represents the preference for the hippocampal or septal LFP, and the change in firing frequency between intra- and peri- SWR epochs. The method was as follows:

(a-b)/(a+b)

Where *a* is the hippocampal theta mean vector length/intra-SWR firing frequency, and *b* is septal delta mean vector length/peri-SWR firing frequency.

Before clustering all parameters were normalised to a similar feature space by Z-score:

(x-parameter mean)/SD

Where x is each single data point in a parameter.

From the final parameters used: theta phase, percentage of active theta cycles, vector length index and SWR index, Ward's method (Ward 1963) of clustering was used. Each neuron to be clustered is plotted in n-dimensional space with each axis being a single parameter z-score normalised. Pair-wise Euclidean distances are measured between each point and cluster amalgamation occurs resulting in centroid clusters with minimised summed Euclidean distances.

Cluster number was calculated as the mean of two measures: L-method estimation of the knee of an evaluation graph (Salvador and Chan 2004), and evaluation by silhouette method (Rousseeuw 1987) using custom (Robert Stewart) and standard MATLAB functions respectively. For L-method

estimation, a total merge distance versus cluster number graph is generated. The L-method is a function which finds the “knee” of this graph by plotting two linear lines to the curve. The knee is defined as the x-axis value corresponding to the intercept between the two lines when they have minimal error. The evaluation graph as three ‘stages’: the initial stage where large very different clusters are being merged and produces large differences between points, the knee regions, and the tail which represents when many single points close together are being merged. The knee region contains a number of points which are produced when distinct or valid clusters are being merged. It is a transition from clusters which are too small being merged (the tail region), to the merging of what are likely to be multiple grouped clusters being merged (the initial region).

For evaluation by silhouette method, clustering was run with forced cluster numbers from 3 upwards and mean silhouette value was taken. Cluster number was deemed optimal when the silhouette value was maximal without the introduction of more than one cluster which contained only a single neuron. Post-clustering, validity was investigated using the silhouette method for each cluster (Rousseeuw 1987). The silhouette method evaluates the similarity between a point and its intra-cluster neighbours from points in other clusters. When a point is more similar to its own cluster neighbours the silhouette value is high (>0.5), when a point is more similar to points in another cluster the value is low (<0). A low value can occur when a suboptimal number of clusters is used, or if clusters do not form very distinct groups. In this study only clusters with a mean internal silhouette value ≥0.5 but <1 were taken forward for analysis (a value of 1 suggests a cluster with a single member). Table 2.3 summarises the data sets used in each experimental condition.

Appendix 6: Distress Scoring Table I 24h Telephone

Name of Investigator: ..... **PIL:** ..... **PPL:** ..... **contact number**.....

Animal Identification: ..... **Starting weight:** ..... **Species:** ..... **Strain:** ..... **Source:** ..... **Start Date**.....

	Score	Day after Treatment								
		0	1st	2nd	3rd	4th	5th	6th	7th	8th
GENERAL APPEARANCE	Date									
Normal	0									
General lack of grooming	1									
Piloerection	2									
Coat staring, ocular/ nasal discharges or hunched	3									
APPEARANCE OF HEAD WOUND										
Normal	0									
Slight irritation/inflammation at wound margins	1									
Excessive bleeding, local infection or torn sutures	2									
SPONTANEOUS BEHAVIOUR										
Normal	0									
Minor changes	1									
Less mobile and alert, isolated	2									
Restless, very still or no activity	3									
PROVOKED BEHAVIOUR										
Normal	0									
Minor depression or exaggerated response	1									
Moderate change in expected behaviour	2									
Reacts violently, or very weak.	3									
WEIGHT (note: take implants into account)										
<-5% starting weight	0									
-5% to -10% of starting weight	1									
-10% to -15% of starting weight	2									
SCORE ADJUSTMENT										
+1 point for each maximum score after first	1-4									
TOTAL SCORE	0-17									

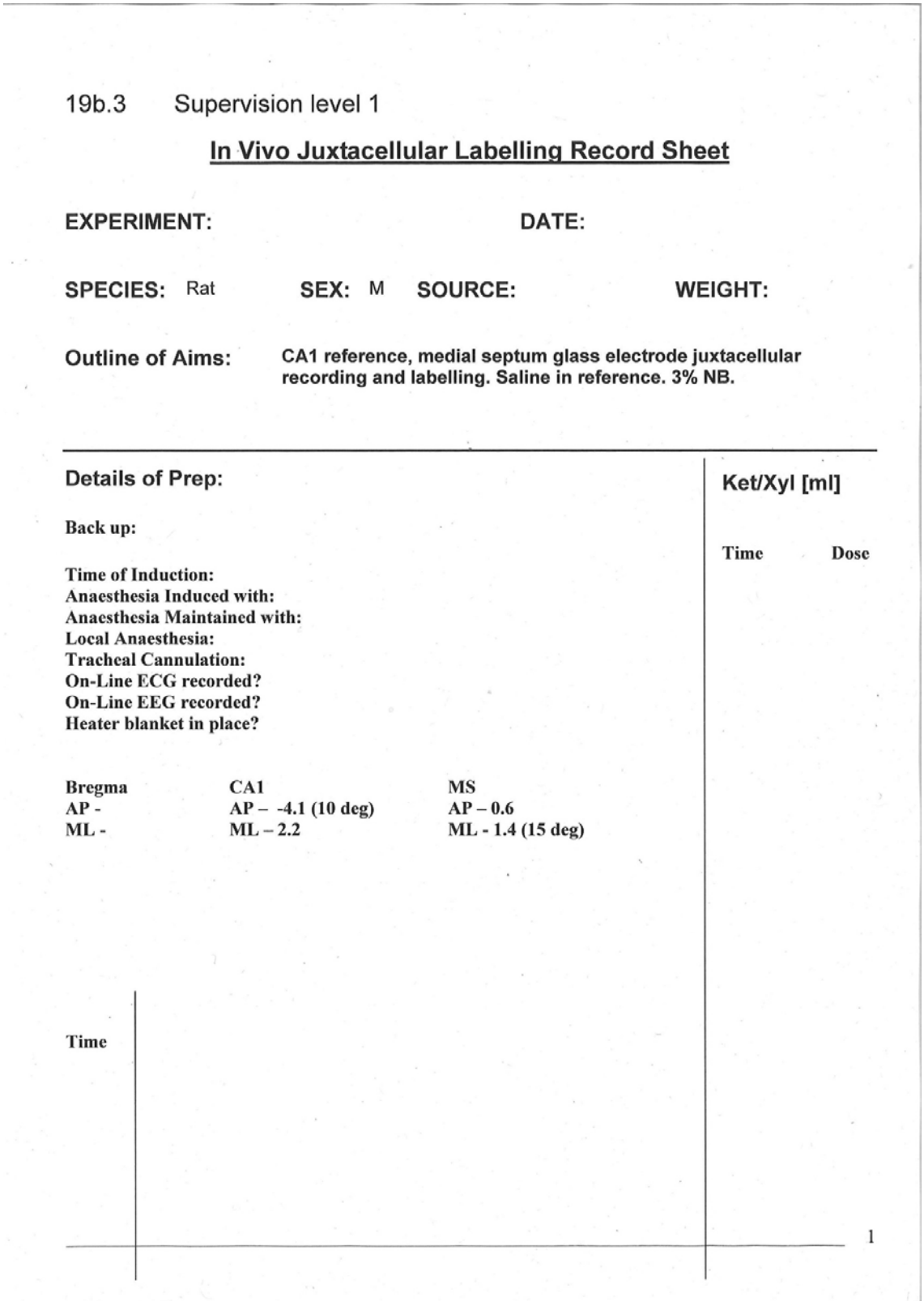
0-4: *'Normal'* **5-9:** *'Mild distress'*: Monitor carefully; consider analgesics and fluid/energy replacement therapy; seek advice as to possibility of infection.

10-13: *'Distress'*: Immediately provide relief. Observe regularly and often over next 24h; if no improvement then humanely kill. **14-17** *'Suffering'*: Kill humanely.

Humane End Points

1. If the weight is less than 85% of starting weight for 48 hours
2. If, after anaesthesia, there is no faecal output and signs of a bloated abdomen for 48 hours.
3. If the animal exhibits spontaneous vocalisation or self-mutilation.
4. If a score of 10-13 persists for 24 hour without improvement
5. If a score of 13 is exceeded.

Figure 2.1 – Example of the post-operative animal surveillance record. Every day post-surgery until the animal had recovered it was scored by these parameters whilst peri-operative drugs were given.



19b.3 Supervision level 1

In Vivo Juxtacellular Labelling Record Sheet

EXPERIMENT: **DATE:**

SPECIES: Rat **SEX:** M **SOURCE:** **WEIGHT:**

Outline of Aims: **CA1 reference, medial septum glass electrode juxtacellular recording and labelling. Saline in reference. 3% NB.**

Details of Prep:

Back up:

Time of Induction:
Anaesthesia Induced with:
Anaesthesia Maintained with:
Local Anaesthesia:
Tracheal Cannulation:
On-Line ECG recorded?
On-Line EEG recorded?
Heater blanket in place?

Bregma	CA1	MS
AP -	AP – -4.1 (10 deg)	AP – 0.6
ML -	ML – 2.2	ML - 1.4 (15 deg)

Ket/Xyl [ml]

Time **Dose**

Time

1

Figure 2.2 – Example of the record sheet used during juxtacellular recording and labelling protocol.

Table 2.1 – Identification and specificity data for primary antibodies used for all immunohistochemistry described in this study. Rb rabbit, Mo mouse, Gt goat, Ch chicken, Gp Guiana pig.

Molecule	Host animal	Internal ref number	Dilution (x)	Source	Source code	Epitope, amino acid residues	Stock protein concentration	Specificity reference
Calbindin (CB)	Rb	989	500, 5000	Swant, Bellinzona, Switzerland	CB-38	Raised against recombinant rat calbindin D-28k.	Unknown	Airaksinen et al., 1997 - KO test
	Mo	707	1k	Swant, Bellinzona, Switzerland	300	Raised against purified calbindin from chicken gut	Unknown	Airaksinen et al., 1997 - KO test
Cannabinoid receptor 1 (CB1)	GP	1274	1k	Prof. M. Watanabe, FRONTIER INSTITUTE Co. Ltd, Hokkaido, Japan	Af530	Raised against mouse CB1, C-terminus aa 443-473	Unknown	Fukudome et al., 2004 - Western blot, preabsorption test
Cholecystokinin (CCK)	Rb	1090	500	Dr. M. Watanabe, Hokkaido University, Japan	pro-CCK	Cysteine-tagged C-terminal 9 aa of pro-CCK (CSAEDYEYPS) coupled to keyhole limpet hemocyanin	Affinity purfied 350µg/ml	Labelling pattern as published with other antibodies
	Gp	1306	1k	Dr. M. Watanabe, Hokkaido University, Japan	CCK-8	Cysteine-tagged CCK-8 (CDYMGWMDF) coupled to keyhole limpet hemocyanin	Affinity purfied 380µg/ml	Labelling pattern as published with other antibodies
Choline acetyl transferase (ChAT)	Gt	1200	500	Chemicon international (Millipore)	AB144P	C-terminus	Unknown	Gautron et al., 2013 - Western blot

COUP-TF2	Mo	1096	250	Perseus proteomics	PP-H7147-00	34-64 aa	1mg/ml	Qin et al., 2007 - KO animal
Calretinin (CR)	Gt	1116	500, 1k	Swant, Bellinzona, Switzerland	CG1	Produced against human recombinant calretinin	Unknown	Schiffman et al., 1999 - KO animal and western blot, cross reactivity with CB-28k in cerebellum only
	Rb	1305	1k	SYSY, Synaptic systems	214 102	Recombinant full length mouse calretinin	Unknown	Labelling pattern as published with other antibodies
erbB-4	Mo	1353	500	Thermo Scientific	MS-270-P0	Extracellular fragment of recombinant human c-erbB-4/HER-4 oncoprotein	200µg/ml	Neddens et al., 2011; Vullhorst et al., 2009; Chen et al., 1996 - KO test
$GABA_A$-α1	Rb	946	1k	Prof. W. Sieghart, Brain Res. Inst., Vienna, Austria	P16	Rat sequence, N-terminus	406µg/ml	Zezula et al., 1991; Baude et al., 2007, KO test
	Rb	947	1k	Prof. W. Sieghart, Brain Res. Inst., Vienna, Austria		Rat sequence, loop sequence	0.59mg/ml	Baude et al., 2007. Tretter et al., 1997 - Western blot
Glutamic acid decarboxylase (GAD)	Gt	1229	250	Dr. M. Watanabe, Hokkaido University, Japan	Af240	Mouse GAD 67, aa 268-593	Unknown	Yamada et al., 2001 - Western blot

	Rb	1228	100	Dr. M. Watanabe, Hokkaido University, Japan	Af260	Mouse GAD 67, aa 268-593	Unknown	Yamada et al., 2001 - Western blot
Gephyrin	Mo	1311	500	SYSY Synaptic Systems	147 021/ mAb7a	Recombinant protein, n-terminus, surrounding aa 268-270 phosphoserine region	Unknown	Kuhse et al., 2012. - recombinant expression in HEK293T cells, western blot
	Gp	1291	500	SYSY Synaptic Systems	147 004	Recombinant protein, c-terminus, aa 294-736	Unknown	Labelling pattern as published with other antibodies
Hyperpolarisation activated cyclic nucleotide-gated non-specific cation channel 1 (HCN1)	Rb	963	100	Alcomone	APC-056	Raised against peptide corresponding to aa 6-24 of rat HCN1, N-terminus	Unknown	Fenske et al., 2013 - KO animal, western blot and IHC
Hyperpolarisation activated cyclic nucleotide-gated non-specific cation channel 4 (HCN4)	Mo	1398	1k	Neuro Mab	N114/10	Fusion-protein aa 1019-1108, C-terminus of rat HCN4.	Unknown	Hughes et al., 2013. - labelling pattern as published with other antibodies. Stillitano et al., 2013 - western blot

Kv1.1	Mo	1443	1k	Neuro Mab	K36-15 / 75-105	Synthetic peptide aa 191-208 (extracellular domain) of rat Kv1.1	1mg/ml	Sosanya et al., 2013 - Western blot. Lorincz and Nusser, 2008 - KO animal
Muscarinic acetylcholine receptor 2 (M2R)	Rt	981	250	Chemicon International (Millipore)	MAB367	M2 receptor fusion protein aa 225-359, fused to Glutathione S-transferase	1mg/ml	Maison et al., 2010 - KO animal IHC
mGluR1α	Gp	1267	500	Prof. M. Watanabe, FRONTIER INSTITUTE Co. Ltd, Hokkaido, Japan	Af660	Raised from rat mGluR1α, aa 945-1127	0.6mg/ml	Nakamura et al., 2004, Tanaka et al., 2000
	Gt	1266	1k	Prof. M. Watanabe, FRONTIER INSTITUTE Co. Ltd, Hokkaido, Japan	Af1220	Raised from rat mGluR1α, aa 945-1127	1.2mg/ml	Personal communication with Prof. M. Watanabe
mGluR8a	Gp	879	500	R. Shigemoto, Division of Cerebral Structure, National Institute for Physiological Sciences, Okazaki, Japan.	Gift	Raised against C-terminus peptide, aa 886-908	Unknown	Kinoshita et al., 1996 - Western blot

Neuronal calcium-binding protein 1 (NECAB1)	Mo	1367	500	Abnova, Taipei City, Taiwan	H00064168-B01P	Raised against full length human NECAB1	0.5mg/ml	Sugita et al., 2002 - Western blot.
Neuronal nitric oxide synthase (NOS)	Rb	1150	1k	Millipore	AB5380	Raised against recombinant human NOS	Unknown	Aguilar-Melero et al., 2012 - Western blot in heterologous cell line expression
	Mo	1167	2k	Sigma	N2280 Lot 081K4815	Raised to recombinant rat nNOS residues 1-181.	ascites, 35.9 mg/ml	Labelling pattern as published with other antibodies
Neuropeptide Y (NPY)	Rb	1011	5k	Diasorin (Immunostar)	Cat No:-22940	NPY coupled to bovine thyroglobulin (with glutaraldehyde)	Unknown	Labelling pattern as published with other antibodies; absorption tested by manufacturer to 6 other peptides, leaving reactivity intact.
p75	Rb	1376	1k	Promega	G3231	Recombinant human p75 produced in E. *coli.*	1mg/ml	Labelling pattern as published with other antibodies
Phaseolus vulgaris leucoagglutinin (PHAL)	Gt	1092	5k	Vector Laboratories	AS-2224	Raised to pure lectins in hyperimmunised goat	2mg/ml	Reacts to both *Phaseolus vulgaris erythroagglutinin* and *leucoaggluitinin*

	Rb	1091	500	Vector Laboratories	AS-2300	Raised to pure lectins in hyperimmunised rabbit	2mg/ml	Reacts to both *Phaseolus vulgaris erythroagglutinin* and *leucoaggluitinin*
PHAL-biotinylated	Gt	N/A	1k	Vector Laboratories	BA-0224	Raised to pure lectins in hyperimmunised goat	1mg/ml	Reacts to both *Phaseolus vulgaris erythroagglutinin* and *leucoaggluitinin*
Parvalbumin (PV)	Gt	1258	1k	Swant, Bellinzona, Switzerland	PVG-214 Lot 3.6	Purified rat PV	Unknown	No signal in KO animal (Swant), similar labelling as previously published antibodies.
	Gp	1310	5k	SYSY Synaptic Systems	195 004	Recombinant full length rat parvalbumin	Unknown	Labelling pattern as published with previous antibodies.
	Rb	835	500	Swant, Bellinzona, Switzerland	PV-28 Lot 5.5	Purified rat PV	Unknown	Kagi et al., 1987; Schwaller et al., 1999 - KO test
	Mo	922	5k	Swant, Bellinzona, Switzerland	PV-235	Purified carp muscle parvalbumin	Unknown	Schwaller et al., 1999 - KO animal

Special AT-rich binding protein-1 (SATB1)	Rb	1393	1k	Abcam	ab70004	18 aa peptide, N-terminus of human SATB1	1mg/ml	Labelling pattern as published with previous antibodies – Huang *et al.*, 2011.
	Gt	1394	400	Santa cruz	sc-5989	N-terminus of human SATB1	0.2mg/ml	Labelling pattern as published with previous antibodies – Huang *et al.*, 2011.
Special AT-rich binding protein-1/2 (SATB1/2)	Mo	1341	100	Abcam	ab51502	recombinant fragment C-terminal (human)	0.1mg/ml	Britanova et al., 2008; Britanova et al., 2005; Nielsen et al., 2010.
Somatostatin (SOM)	Mo	1276	200	GeneTex Incorporate	GTX71935 cloneSOM-018	Monoclonal, somatostatin conjugated to protein carrier	0.14mg/ml	Labelling pattern as published with previous antibodies (Kubota et al., 2011)
	Rt	815	500	Chemicon	MAB354	Monoclonal, synthetic 1-14 cyclic somatostatin conjugated to bovine thyroglobulin using carbodiimide	1mg/ml	Labelling pattern as published with previous antibodies (Kubota et al., 2011)
	Mo	1241	200	GeneTex, Inc. Irvine, CA, USA	gtx71935, clone SOM-018	Monoclonal, human somatostatin conjugated to protein carier	1.4mg/ml	Labelling pattern as published with previous antibodies (Kubota et al., 2011)

Tyrosine hydroxylase (TH)	Rb	1354	500	Sigma	T 8700	Produced in rabbits from SDS-denatured rat tyrosine hydroxylase purified from pheochromocytoma	Unknown	Labelling pattern as published with other antibodies
	Ch	1344	500	Abcam	ab76442	Two synthetic peptides conjugated to keyhole limpet hemocyanin	0.2mg/ml	Manufacturer's technical information - Western blot, abolished IHC signal with TH peptide.
Tetramethylrhodamine conjugated dextran (TMR)	Rb	1354	500, 1000, 5000	Invitrogen (Molecular Probes)	A-6397	Raised against the dye molecule	1mg/ml	Cross-reactive with texas red dye - Invitrogen
Vesciular acetylcholine transporter (VAChT)	Rb	1390	10k	Sigma	V5387 (discontinued)	Raised against synthetic peptide corresponding to C-terminus aa 512-530	Unknown	Rodriguez-Diaz et al., 2011 - western blot of mouse brain and human islet lysates
Vesicular GABA transporter (VGAT)	Gp	1321	500	SYSY Synaptic Systems	131 004	Strep-tagged fusion protein, aa 2-115 of rat VGAT, cytoplasmic domain	Unknown	Labelling pattern as published with other antibodies

	Rb	1314	500	SYSY Synaptic Systems	131 003	Polyclonal, synthetic peptide of aa 75-87 of rat VGAT conjugated to keyhole limpet hemocyanin	1mg/ml	Same epitope and production as the specific VGAT antibody by Takamori et al., 2000
Vesicular glutamate transporter 2 (VGLUT2)	Gt	1270	500	Dr. M. Watanabe, Hokkaido University, Japan	Af310	C-terminus peptide conjugated to Gutathione-S-transferase, aa 519-582	Unknown	Miyazaki et al., 2003 - Western blot. Labelling pattern as published with other antibodies
	Gp	1271	500	Dr. M. Watanabe, Hokkaido University, Japan	Kind gift	C-terminus peptide conjugated to Gutathione-S-transferase, aa 519-582	Unknown	Miyazaki et al., 2003 - Western blot. Labelling pattern as published with other antibodies
	Rb	1263	500	SYSY Synaptic Systems	135 402	Strep-tagged fusion protein of rat VGluT2 (aa 510-582)	Unknown	Zhang et al., 2013 - Western blot, labelling pattern as published. Herzog et al., 2006 - same labelling pattern as mouse
Vasoactive intestinal peptide (VIP)	Mo	1053	50k	Dr. G. Ohning, Cure, UCLA, USA	55	Monoclonal, raised in mouse against VIP	Unknown	Wong et al., 1996

Table 2.2 – Reaction constituents for peroxidase reactions using Ni-enhanced DAB

Stock Solutions:

1 % Nickel ammonium sulphate (BDH)

0.4 % ammonium chloride (Sigma) in distilled water

20 % D-Glucose (BDH) in distilled water

1000 U/ml Glucose oxidase (Sigma)

0.2 M PB

2 ml DAB (1.14 mg/ml) in distilled water

	Pre-incubation solution						
Ni proportion	**Ni solution**	**Ammonium chloride**	**Glucose**	**PB**	**DAB**	**Distilled water**	**Glucose Oxidase**
No Ni	0	100 µl	100 µl	5 ml	1 ml	3.8 ml	1-3 µl/ml
Quarter Ni	100 µl	100 µl	100 µl	5 ml	1 ml	3.7 ml	1-3 µl/ml
Half Ni	200 µl	100 µl	100 µl	5 ml	1 ml	3.6 ml	1-3 µl/ml
Full Ni	400 µl	100 µl	100 µl	5 ml	1 ml	3.4 ml	1-3 µl/ml

Table 2.3 – Summary of data sets used in each experimental condition. The total number of experiments conducted was 82.

Anterograde tracing = 9	**Experiments**		**Chapter**
PHAL	7		
BDA	2		3
Juxtacellular experiments = 73	**Recorded**	**Labelled**	
Total number of neurons	190	65	
Rhythmic neurons with defined SWR response	**37**	15	
Rhythmic neurons used for immunohistochemical analysis	22	**24**	3
Rhythmic neurons inhibited or which did not change firing frequency during SWRs	24	10	3,4
Rhythmic SWR active neurons	13	5	3,5
Rhythmic neurons labelled but **without defined SWR response**	N/A	7	3
Neurons labelled **without defined physiology** displaying immunohistochemical markers correlated with rhythmic firing neurons	N/A	2	3
Neurons used in clustering	**51**		6
Rhythmic SWR inhibited	17		
Rhythmic SWR no change	7		
Rhythmic SWR active	13		
Lateral septum	8		
Delta coupled	6		

Chapter 3 – Anatomical analysis of confirmed septo-hippocampal neurons and their targets

3.1 Introduction

Behaviourally relevant network activity emerges from neuronal circuits. It is well established that physiological hippocampal network activity is dependent on reciprocal connectivity with the medial septum. The first study to demonstrate this was by Green and Arduini, 1954, however it was not until the study of Freund and Antal, 1988 that a monosynaptic connection was demonstrated between the GABAergic medial septal projection and the hippocampus. The cholinergic projection was described earlier (Woolf et al., 1984, Clarke, 1985, Frotscher and Léránth, 1985). The GABAergic septo-hippocampal neurons innervate interneurons selectively; they do not make synapses directly to pyramidal neurons (Freund and Antal, 1988, Gulyás et al., 1991). Septo-hippocampal neurons, as a population, innervate all interneuron population markers tested for: PV-, CCK-, CB-, CR-, VIP-, SOM-, NPY-immunoreactivity, and these neurons all receive GABAergic synaptic inhibition from medial septal neurons (Nyakas et al., 1987, Gulyas et al., 1990, Gulyás et al., 1991, Miettinen and Freund, 1992a, Miettinen and Freund, 1992b, Acsady et al., 1993, Lübke et al., 1997, Takács et al., 2008).

The inhibition of inhibitory interneurons can drive pyramidal neuron firing via disinhibition (Toth et al., 1997). By electrical stimulation, lesion, and single cell recording, it was shown that the frequency of septal firing directly relates to both the frequency of hippocampal theta (Lecourtier et al., 2011, Apartis et al., 1998, Kitchigina et al., 1999, Borhegyi et al., 2004, Varga et al., 2008, Orzeł-Gryglewska et al., 2012) and the performance of animals during learning tasks (Lecourtier et al., 2011, Lamprea et al., 2010, Hamlin et al., 2013).

In the hippocampal circuit, it is known that particular interneurons innervate pyramidal neurons at distinct subcellular domains (Somogyi and Klausberger, 2005). The function of this diversity is only partially understood but it relates to the temporal redistribution of inhibition to distinct subcellular domains of pyramidal neurons. The temporal and spatial relationship between neuron types defines the output and function. Population stimulation (discussed above) represents an artificially

synchronous environment of maximal interneuron inhibition and pyramidal cell disinhibition. *In vivo* recording demonstrated that medial septal neurons fire with diverse timing relative to hippocampal local field potential oscillations (Borhegyi et al., 2004, Varga et al., 2008), but does this correlate with disinhibition of different functional domains of the pyramidal neurons via distinct interneuron type innervation?

The synaptic relationship between individual septal and hippocampal neurons is not known. The current hypothesis is that rhythmic medial septal neurons, the so called pace maker neurons, with a particular firing phase, will innervate specific and distinct interneuron types in the hippocampus which fire at opposing theta phases, and innervate distinct pyramidal neuron domains. The hypothesised model acts like a see-saw, with two distinct medial septal groups mutually inhibiting each other whilst innervating peri-somatic and dendritic terminating interneurons selectively (Borhegyi et al., 2004).

Post-synaptically, GABAergic septal neurons produce fast synaptic inhibition in target neurons within the septum (DuBois et al., 2013), and the hippocampus (Toth et al., 1997). Synapses from septal neurons are present in all domains of the hippocampal GABAergic neurons including the dendrites, soma, and axon initial segment (Nyakas et al., 1987, Takács et al., 2008), although it is not known if single neurons innervate target neurons at all subcellular compartments, or if – as is the case for hippocampal interneurons synapsing on pyramidal neurons – inhibition by different neurons of the same postsynaptic cell is spatially segregated. Input to different subcellular compartments has different effects on signal integration within the innervated neurons (Harnett et al., 2013, Lee et al., 2013). For example, bistratified neurons, which, on average, inhibit pyramidal neurons during the theta phase when they are maximally active, may have a role in modulating spike timing of pyramidal neurons during theta and SWR oscillation (Klausberger et al., 2004). In contrast, axo-axonic neurons, which are active in both theta oscillation and SWRs when pyramidal neurons are fire minimally, may gate pyramidal output via inhibition of the axon initial segment

(Klausberger et al., 2003, Klausberger et al., 2004, Viney et al., 2013). To my knowledge, no hypotheses have been made about the subcellular distribution of septal synapses onto distinct interneuron types, although it does not appear to be uniform or obviously sequestered to a particular domain. The location of synapses onto interneuron types by single septal neurons may provide evidence for the mechanism by which the septum influences the firing of each interneuron type, and the resultant theta pacing effect.

The relatively recently discovered glutamatergic septo-hippocampal projecting neuronal population has not been characterised in depth (Sotty et al., 2003, Henderson et al., 2010, Huh et al., 2010). A recent study using whole septo-hippocampal preparation demonstrated that glutamatergic neurons may be capable of eliciting excitatory post synaptic potentials in CA3 pyramidal neurons and suggested that the glutamatergic septo-hippocampal projection was able to "drive" pyramidal neuron firing (Huh et al., 2010). This study, along with others which rely on genetically tagged VGluT2-expressing neurons to be visualised, has demonstrated a remarkable diversity in *in vitro* firing patterns, which could have wide ranging roles in the septo-hippocampal network. This method is confounded by the dynamic and transient expression of VGluT2, as well as VGluT1, in septal neurons which in maturity are GABAergic or cholinergic only (Danik et al., 2005). To my knowledge no *in vivo* firing patterns for glutamatergic neurons have been published, nor has any direct evidence of a hippocampal projection by glutamatergic neurons is available.

This study will focus on synaptic innervation by the septum of hippocampal interneuron classes not previously investigated: the nitric-oxide synthase expressing neurons, the axo-axonic neurons and the M2R expressing interneurons including the trilaminar interneurons. Understanding how the timing of GABA released synaptically to pyramidal cell domains is of key importance to understanding how coding occurs. The NOS-expressing interneurons, such as the ivy and neurogliaform neurons, fire slowly and have an axonal domain which overlaps with, and may gate, excitatory inputs from the Schaffer collaterals and performant pathway (Fuentealba et al., 2008;

Capogna 2010). Understanding factors, such as a septal synaptic input, which influence the spike timing of these neurons is important.

Similarly, axo-axonic interneuron synaptic inhibition is opportunely located at the axon initial segment to dictate when pyramidal neurons can fire; silencing during SWRs is hypothesised to be a necessary event in the propogation of pyramidal excitation (Viney et al., 2013). Synaptic input which influences axo-axonic action potential timing will have a direct influence on pyramidal cell firing and therefore hippocampal coding.

The trilaminar neurons, which project locally within the hippocampus as well as to the subiculum (Ferraguti et al., 2005), may be a source of synchronous inhibition between regions and involved in producing coherent activity in CA1 and the subiculum. Rhythmic septal inhibition acting on trilaminar neurons may therefore influence binding of multiple regions to a similar timing.

The aim of this chapter is to test key features of the above hypothesis of GABAergic septo-hippocampal synaptic selectivity using both large scale anterograde tracing, and single cell recording and labelling by the juxtacellular technique. These assumptions are: 1) single septo-hippocampal neurons demonstrate a uniform axonal distribution within the hippocampus; 2) they display target interneuron selectivity within the hippocampus; 3) septo-hippocampal neurons which display differences in axonal arbours will differ in the molecular markers that they express. I will also test the distribution of VGluT2-expressing septal fibres, and if distinct interneuron types which have thus far been unreported, such as axo-axonic, trilaminar, and NOS-expressing neurons, receive septal innervation.

3.2 Results

Using a combination of juxtacellular recording and labelling of neurons, and PHAL and BDA anterograde tracing, I have investigated the relationship between medial septal neurons (electrophysiology can be found in Chapters 4 and 5) and their hippocampal target neurons.

In 9 injections of anterograde tracers (7 using PHAL and 2 using BDA), 4 were predominantly within the medial septum (3 PHAL, 1 BDA; Table 3.1). Visual inspection of injection sites (Figure 3.1A) and position of resultant axons in respective brains was consistent with published data (Nyakas et al., 1987, Freund, 1989, Risold and Swanson, 1997). I investigated the septal innervation of three types of interneuron whose septal input has previously been undescribed: NOS-expressing ivy and neurogliaform, PV-immunopositive SATB1-immunonegative axo-axonic, and M2R-immunopositive mGLUR8a-innervated trilaminar neurons. These neurons were either not discovered at the time of previous investigation, or only recently able to be distinguished by immunohistochemistry.

Injections within the medial septum produced dense axons projecting ventrally into the diagonal band and basal forebrain. Axons were present throughout the whole fimbria-fornix formation and projecting into all regions of the hippocampus, particularly CA3 and the dentate gyrus. The dorsal fornix had numerous axons, perpendicular to the coronal plane, in all medial septum injected experiments. In the hippocampus, both thin (type II) and thicker (type I) axons were observed making both *en passant* boutons and boutons on a branching stalk (Nyakas et al., 1987). Thick axons made numerous basket-like structures around putative interneurons in all strata and regions of the hippocampus. Qualitatively, septal axons appeared densest in dentate gyrus and CA3 hilus and stratum oriens respectively, but this may have been due to the location of the injection sites. In CA1, axons were densest in stratum oriens and alveus with relatively fewer axons seen in other strata. Caudal structures to the dorsal hippocampus (e.g. subiculum, medial entorhinal cortex) were also labelled, but not analysed in this study.

Experiment identification	Tracing molecule	Intended injection depth/s (µm)	Injection durations (mins)	Days survival post injection	Location of injections
M09	PHAL	6000	30	3	Medial septum
		5500	20		
		5000	10		
M10	PHAL	6000	20	13	Cingulate cortex
M14	PHAL	6000	20	7	Lateral septum
M28	BDA 3k	6000	10	7	Medial septum
M29	BDA 3k	6000	20	7	Lateral septum
M49	PHAL	6200	10	4	Lateral/medial septum
		5800	10		
		5500	10		
M50	PHAL	6200	10	4	Lateral septum/fornix
		5800	10		
		5500	10		
M54	PHAL	6200	20	4	Medial septum
		5800	20		
		5500	20		
M55	PHAL	6200	20	4	Medial septum
		5800	20		
		5500	20		

PHAL 2.5 % in 10 µM NaPBS

BDA 3k 10 % in 0.1 M potassium acetate

Table 3.1 – Summary of anterograde tracing injection experiments performed. *PHAL phaseolus vulgaris leucoagglutinin, BDA biotinylated dextran amine 3000 dalton.*

3.2.1 Glutamatergic septo-hippocampal projections

In hippocampal sections of tissue from PHAL injected animals, septo-hippocampal axons were immunohistochemically tested for VGluT2, a synaptic protein found in glutamatergic synapse. Axons expressing VGluT2 were only observed in CA3. Axons were relatively thick; comparable to large calibre type I axons. Both *en passant* boutons and bouton-bearing branches were observed (Figure 3.1B). Glutamatergic septo-hippocampal axons were never observed making baskets around putative soma. The majority of VGluT2 immunostaining within the hippocampus was not accounted for by PHAL-labelled axons, suggesting it is extra-septal in origin, as reported previously from the supramammillary nuclei and nucleus reuniens thalami (Halasy et al., 2004).

3.2.2 Innervation of NOS-expressing ivy and neurogliaform neurons

Interneurons expressing NOS (Förstermann et al., 1990, Leigh et al., 1990, Fuentealba et al., 2008a) were relatively recently delineated in the hippocampus (Price et al., 2005, Fuentealba et al., 2008). Using anterograde tracing I demonstrated that NOS-expressing neurons present in all regions of the hippocampus receive septal innervation.

Immunohistochemical labelling of NOS was seen throughout the hippocampus and cortex (Figure 3.2). Within the hippocampus neurons were located in all regions (i.e. CA1, CA2, CA3 and dentate gyrus) and in all strata. Labelling was consistent with published data (Fuentealba et al., 2008a). In three sections from three PHAL medial septum injected animals I observed large boutons (from type I axons) in apparent contact with NOS-expressing soma and dendrites (Figure 3.1C). Single axons were observed innervating both ivy (strata pyramidale and radiatum-located) and neurogliaform (stratum lacunosum-moleculare-located) neurons. Axons with putative synaptic contacts onto NOS-expressing neurons had other boutons not in observable contact with NOS-

immunopositive structures. Based on the location of NOS-positive cell bodies and the intensity of labelling, I observed two types of NOS-expressing interneuron which frequently receive septal innervation in the hippocampus: ivy (n = 6 neurons from 3 animals) and neurogliaform neurons (n = 3 neurons from 3 animals). Infrequent intensely NOS-immunopositive (IINI) neurons, which are often found in the white matter, were only once observed in putative synaptic contact with PHAL-labelled axons (n =1). Within the white matter, IINI appear to have much fewer gephyrin puncta along their soma then other types of NOS-expressing cell.

3.2.3 Innervation of PV-expressing, SATB1 negative axo-axonic neurons

Previous work has described medial septal innervation of PV-expressing interneurons within the hippocampus (Freund and Antal, 1988), however the means to distinguishing different PV-expressing interneuron types using immunohistochemistry was lacking until recently (Viney et al., 2013). In three sections from three animals with PHAL injections within the medial septum, I observed GABAergic putative synaptic contacts onto PV-expressing neurons which expressed SATB1 (PV-expressing basket and bistratified cells), and others which did not express SATB1 (axo-axonic cells; figure 3.1D). Axo-axonic neurons (PV immunopositive / SATB1 immunonegative) were innervated in all regions of the hippocampus tested: CA1, CA3, and dentate gyrus (Figure 3.1D).

3.2.4 Innervation of M2R-expressing neurons including the mGluR8a-decorated trilaminar cell type.

Interneurons expressing the M2 receptor (M2R) were located primarily at the border of stratum oriens and the alveus in CA1. Neurons often had long horizontally positioned dendrites in CA1, with more variability in dendrite orientation in CA3 (Figure 3.2). The location and anatomical features of M2R-immunopositive cells observed in this study are similar to those previously published (Hájos et al., 1997, Jinno et al., 2007). Using medial septal axons labelled with PHAL, I observed that M2R-positive neurons received potential synaptic contacts along their soma and horizontal dendrites (n = 10 from 1 animal; Figure 3.1E1). Small calibre type II axons were observed making *en passant*

boutons along dendrites of M2R-immunopositive neurons (n = 3) which may also receive somato-dendritic boutons from type I axons (Figure 3.1E1 inset). Immunoreactivity of M2R was weaker at the site of the putative synaptic contact with PHAL-labelled boutons.

A subset of M2R-expressing neurons, the trilaminar neurons, are decorated with mGluR8a receptor positive presynaptic nerve terminals (Ferraguti et al., 2005). I found septal boutons juxtaposed to immunohistochemically identified trilaminar cell membranes (n = 6/7 M2R-expressing cells tested) in CA1 and CA3 (Figure 3.1E2). Numerous boutons were present for each trilaminar cell seen innervated perisomatically. Septal neurons express the mGluR8a, and in numerous cases septal boutons which were in apposition to trilaminar cell membranes had visible mGluR8a (Figure 3.1E2). This was in both type I and type II axon boutons. Septal boutons accounted for only a small proportion of mGluR8a puncta suggesting that there are other sources of mGluR8a-containing inputs to trilaminar neurons (Ferraguti et al., 2005). Septal boutons in the same field of view which did not innervate trilaminar neurons did not express visible mGluR8a suggesting it is not in all septal boutons, but may be specific to a subset.

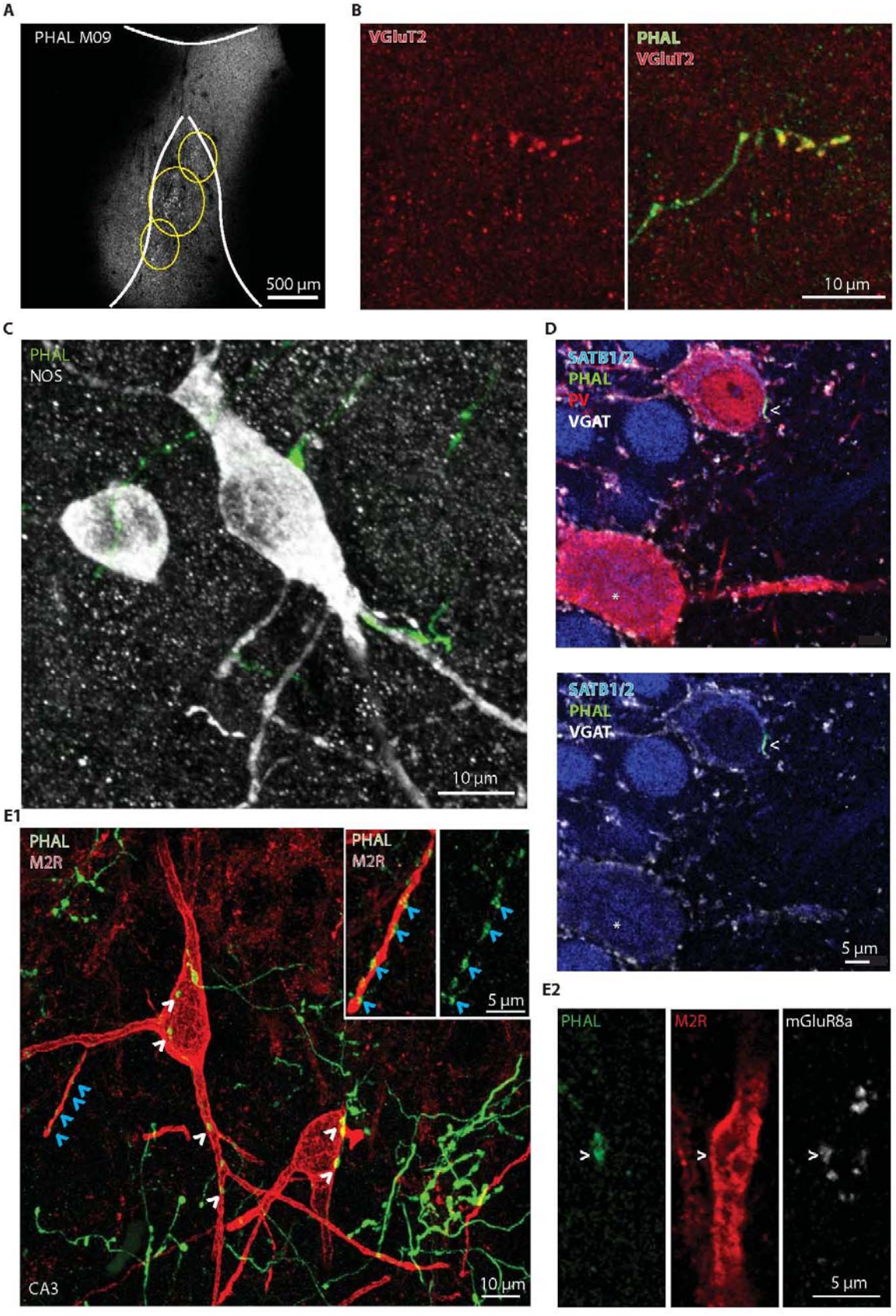
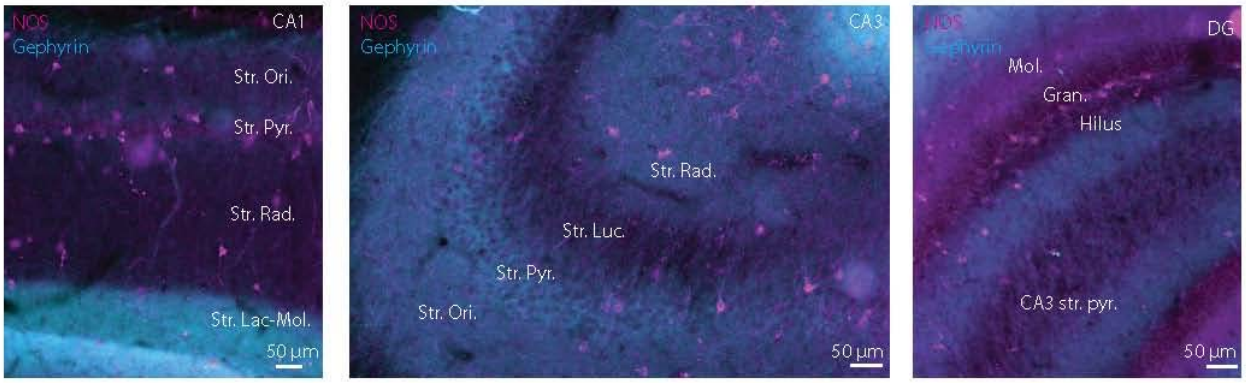

A
PHAL M09
500 µm
B
VGluT2
PHAL
VGluT2
10 µm
C
PHAL
NOS
10 µm
D
SATB1/2
PHAL
PV
VGAT
SATB1/2
PHAL
VGAT
5 µm
E1
PHAL
M2R
PHAL
M2R
5 µm
CA3
10 µm
E2
PHAL
M2R
mGluR8a
5 µm

Figure 3.1 – Characterisation of medial septal PHAL-labelled axons in the hippocampus and some of their interneuron targets All images are from experiment M09. **A)** Representative section of the iontophoretic injection sites of PHAL within the medial septum (yellow circles). Some labelling of cell bodies was observed in the lateral septum. **B)** A small number of septal axons (PHAL; green) in CA3 were immunopositive for VGluT2 (red). **C)** Large terminals (PHAL; green) made putative synaptic contacts with NOS-expressing (white) ivy neuron within CA1 stratum pyramidale. **D)** Axo-axonic neurons receive septal innervation from VGAT immunpositive boutons. **D)** A PV-expressing neuron (red) with a VGAT-immunopositive (white puncta) containing septal bouton (PHAL; green) in putative synaptic contact (white arrow head). Below, the innervated neuron does not express SATB1 (nucleus; blue) unlike the PV-expressing neuron below (asterisk). Adjacent pyramidal cell nuclei are immunopositive for SATB2 (blue). **E)** Muscarinic type 2 receptor-expressing neurons, both mGluR8a immunopositive and negative, are targets of putative septal synaptic input. **E1)** Two M2R immunofluorescent neurons (red) with numerous large (type 1; white arrow head) as well as fewer thinner axons and boutons (type 2; blue arrow head) in apparent synaptic contact. Insert shows the same branch as in E1 marked by blue arrows; a string of *en passant* small boutons of a thin axon along a dendritic branch. **E2)** Soma septal boutons (PHAL; green) contain mGluR8a puncta (white; arrow) enriched onto M2R immunoreactive trilaminar neuron membranes (red). Confocal z-stacks, number of optical sections (thickness in µm) / projection mode: **B**, 23(8.05)/maximum; **C**, 21(8.63)/maximum; **D**, 23(7.10)/single section; **E1**, 58(20.85)/maximum; **E2**, 48(17.19)/single section.

A


NOS
Gephyrin
CA1
Str. Ori.
Str. Pyr.
Str. Rad.
Str. Lac-Mol.
50 µm
NOS
Gephyrin
CA3
Str. Rad.
Str. Luc.
Str. Pyr.
Str. Ori.
50 µm
NOS
Gephyrin
DG
Mol.
Gran.
Hilus
CA3 str. pyr.
50 µm

B

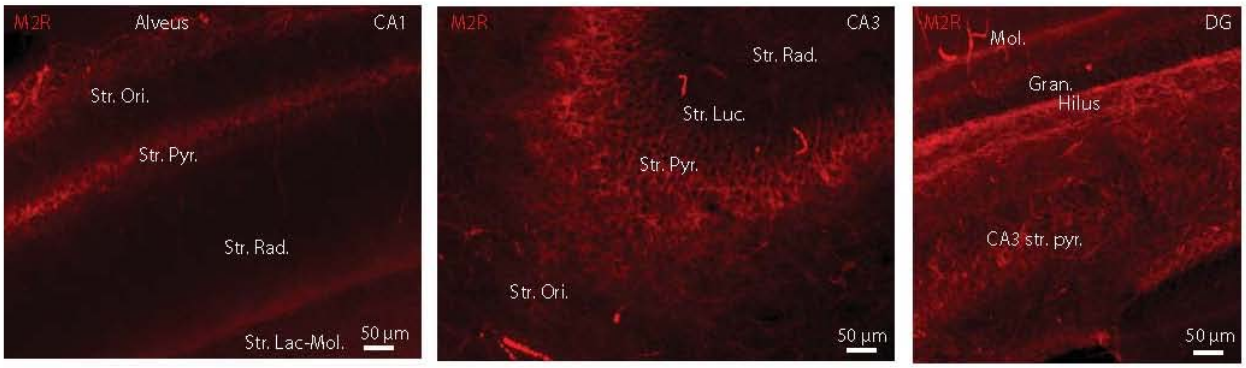

M2R
Alveus
CA1
Str. Ori.
Str. Pyr.
Str. Rad.
Str. Lac-Mol.
50 µm
M2R
CA3
Str. Rad.
Str. Luc.
Str. Pyr.
Str. Ori.
50 µm
M2R
DG
Mol.
Gran.
Hilus
CA3 str. pyr.
50 µm

Figure 3.2 – Distribution of immunohistochemically labelled interneurons within the hippocampus. A) Immunoreactivity for nitric oxide synthase (NOS) and the post-synaptic GABAergic scaffolding protein gephyrin within CA1, CA3, and dentate gyrus (from left to right). Within CA1, NOS-expressing neurons are most numerous around stratum pyramidale; in CA3 they appear throughout the strata; they are enriched within the subgranular zone of the dentate gyrus. **B)** Hippocampal distribution of the M2 receptor in CA1, CA3, and dentate gyrus (from left to right). In CA1 neurons are frequent in the border between alveus and stratum oriens, with horizontally running dendrites. In CA3, the dendrites of M2R-expressing neurons penetrate all layers, with fewer neurons located at the alveus/oriens border. Again, like the NOS-expressing neurons, M2R-immunopositive neurons are most densely found at the subgranular zone within the dentate gyrus.

3.2.5 Anatomical analysis of single medial septal and septo-hippocampal neurons

Neuron types differ in axon location, dendritic parameters, firing patterns, and protein compositions (Somogyi and Klausberger, 2005). I used immunohistochemistry on recorded and labelled medial septal neurons (electrophysiology can be found in Chapters 4 and 5) in an attempt to identify different populations of neuron, potentially different neuron types, which may have different roles in the system.

Of the 65 neurons which were labelled, 22 also had a rhythmic firing pattern strongly phase locked to hippocampal theta oscillations and a soma within the medial septum (Table 3.2; Chapters 4 and 5). I tested a fraction of these rhythmic neurons for published molecular markers (PV, CR and VGAT), and novel markers which I have found in PV-expressing medial septal neurons (Kv1.1, SATB1, HCN4 and NECAB1). Rhythmic neurons were largely homogenous in the expression of these proteins (Table 3.2; Figure 3.3). Of those tested, 8 / 8 expressed HCN4; 12 / 13 expressed SATB1; 6 / 9 expressed Kv1.1 (Figure 3.2A); 13 / 16 expressed PV (Figure 3.2B); none of 9 tested expressed CR or NECAB1 (Figure 3.2C) and 6 / 6 expressed VGAT. The latter test proves that these are GABAergic neurons.

The somatodendritic anatomic features of rhythmic neurons were similar with some dependence on somatic location (example M80d; Figure 3.2D). Neurons located at the dorsal tip of the medial septum where it is most narrow, tend to have dorso-ventrally oriented dendrites, whereas more ventrally located neurons, where the medial septum is wider, have more radial dendrites, some of them oriented dorso-ventrally. Dendrites of all rhythmically firing neurons tended to extend within the medial septum, often bilaterally, and rarely were located in the lateral septum. Dendritic spines were rarely observed but the distal ends of the dendrites could form extensive branches with filipodia-like structures.

Main axons emanated either from a proximal dendrite (3 / 5) or the soma (2 / 5) of rhythmic medial septum neurons. Typically, proximal axons were “hooked”, projecting ventral and anterior from the soma, before turning and running dorsal and posterior towards the fimbria-fornix and hippocampus (8 / 8 tested; Figure 3.3D). Frequent local axon collaterals were present in some well-labelled neurons. In a number of neurons, axon collaterals were observed in the triangular septal nucleus (3 / 8 tested) as well as in the hippocampus. In a single case (M63c) the sole target observed was the triangular septal nucleus, and no main axon could be identified more posterior. The majority of neurons had a main axon within the fimbria (n = 11 / 13). In two cases (M75a and M80d) an axon was identified only within the dorsal fornix (Table 3.3).

During this study I also labelled 12 confirmed lateral septal neurons (electrophysiological description in Chapter 6). Of note is M64c which projected to the medial hypothalamus with numerous boutons in this region.

I conclude that in my sample of rhythmic septal neurons, no molecular diversity is found using known (PV, VGAT and CR) and novel (HCN4, Kv1.1, SATB1, NECAB1) molecular markers. Septal neurons display distinct morphological features such as ramified distal dendrites and a “hooked” main axon.

Table 3.2 – Summary of immunoreaction performed on juxtacellularly labelled neurons in this study (theta rhythmic; refer to Chapter 4 and 5).

Name	Location	Labelling method	Type	PV	SATB1	CR	CB	HCN1	HCN4	KV1.1	ChAT	VGAT	VAChT	VGluT1	VGluT2	P75	NECAB1	NOS	CB1	TH dense innervation
M40f	Medial septum	NB	**SWRact**	+	+	-														
M65b	Medial septum	NB	**SWRact**	+	+	-			+	+							-			
M75a	Medial septum	NB	**SWRact**	+	+				+	-		+					-			
M80d	Medial septum	NB	**SWRact**	+	+	-	-		+	+		+					-			
M82f	Medial septum	NB	**SWRact**	+		-			+			+					-			
D55c	Medial septum	NB	**Theta rhythmic**	+	+				+	-		+	-		-					
M12 ZsB33	Medial septum	NB	**Theta rhythmic**																	
M21c	Medial septum	NB	**Theta rhythmic**	-	+		-	+	+			+					-			
M22a	Medial septum	NB	**Theta rhythmic**																	
M25a	Medial septum	NB	**Theta rhythmic**	-						-										
M26a	Medial septum	NB	**Theta rhythmic**																	
M35h	Medial septum	TMR	**Theta rhythmic**																	
M37h	Medial septum	NB	**Theta rhythmic**	+	+	-			+	+							-			
M40g	Medial septum	NB	**Theta rhythmic**	+		-		+									-			
M41e	Medial septum	NB	**Theta rhythmic**	+	+					-							-			
M60a	Medial septum	NB	**Theta rhythmic**	+	+	-			+	+										
M67a	Medial septum	NB	**Theta rhythmic**	+					+											
M73a	Medial septum	NB	**Theta rhythmic**	-	-	-				-										
M73b	Medial septum	NB	**Theta rhythmic**	+	+				+											
M76a	Medial septum	NB	**Theta rhythmic**	+	+				+			+					-			
M77c	Medial septum	NB	**Theta rhythmic**	+	+	-				+		+					-			
M78a	Medial septum	NB	**Theta rhythmic**	+	+	-				+							-			
M05c	Medial septum	NB	**Theta rhythmic (putative)**	-	+	-			+	-							-			
M44	Medial septum	BDA recovery	**Theta rhythmic (putative)**	+					+			+	-		-		-			

Table 3.2 continued – Summary of immunoreaction performed on juxtacellularly labelled neurons in this study (non-theta rhythmic).

Name	Location	Labelling method	Type	PV	SATB1	CR	CB	HCN1	HCN4	KV1.1	ChAT	VGAT	VAChT	VGluT1	VGluT2	P75	NECAB1	NOS	CB1	TH dense innervation
M20f	Cortex	TMR	Cortical pyramid																	
M08b	Septum	NB	CR-expressing			+					-	+			-					
M26d	Septum	TMR	CR-expressing			+														
M34b	Septum	BDA	CR-expressing	-		+					-									
M38e	Medial septum	NB	Delta-coupled	-		-														
M62a	Medial septum	NB	Delta-coupled	-		-					-									
M05b	Dentate gyrus	NB	Dentrate cell																	
M04d	Dentate gyrus	NB	Dentrate granule cell																	
M03d	CA1	NB	Hippocampal pyramid																	
M07m	Lateral septum	NB	Lateral septum																	-
M07n	Lateral septum	NB	Lateral septum																	-
M07o	Lateral septum	NB	Lateral septum																	-
M20b	Lateral septum	TMR	Lateral septum																	
M24f	Lateral septum	NB	Lateral septum																	-
M24g	Lateral septum	NB	Lateral septum																	-
M64c	Lateral septum	NB	Lateral septum																	-
M67b	Lateral septum	NB	Lateral septum				-													-
M72e	Lateral septum	NB	Lateral septum																	-
M78b	Lateral septum	NB	Lateral septum			-														-
M01b	CA1	NB	PV-expressing basket cell	+	+															
M22b	Medial septum	NB	Unknown																	
M30b	Medial septum	NB	Unknown								-									
M25d	Medial septum	NB	Unknown																	
M08c	Septum	NB	Unknown			-					-	+			-					
M21f	Medial septum	NB	Unknown																	
M27a or d	Lateral septum	NB	Unknown																	
M31c	Medial septum	NB	Unknown																	
M31j	Medial septum	TMR	Unknown																	
M34d	Medial septum	BDA	Unknown																	
M42	Medial septum	NB	Unknown			-										-				
M43	Medial septum	BDA recovery	Unknown																	
M45	Medial septum	BDA recovery	Unknown																	
M60 (buzzed)	Medial septum	NB	unknown																	
M61a	Medial septum	NB	Unknown																	
M71c	Septum	NB	Unknown	-		-					-							-		
M82b	Medial septum	NB	Unknown																	
M82c	Medial septum	NB	Unknown																	
M06a	BNST?	NB	Unknown																	
M62b	Medial septum	NB	Unknown	-		-					-									
M63	Medial septum	NB	Unknown	-		-					-									
M71b	Medial septum	NB	Unknown								-							-		

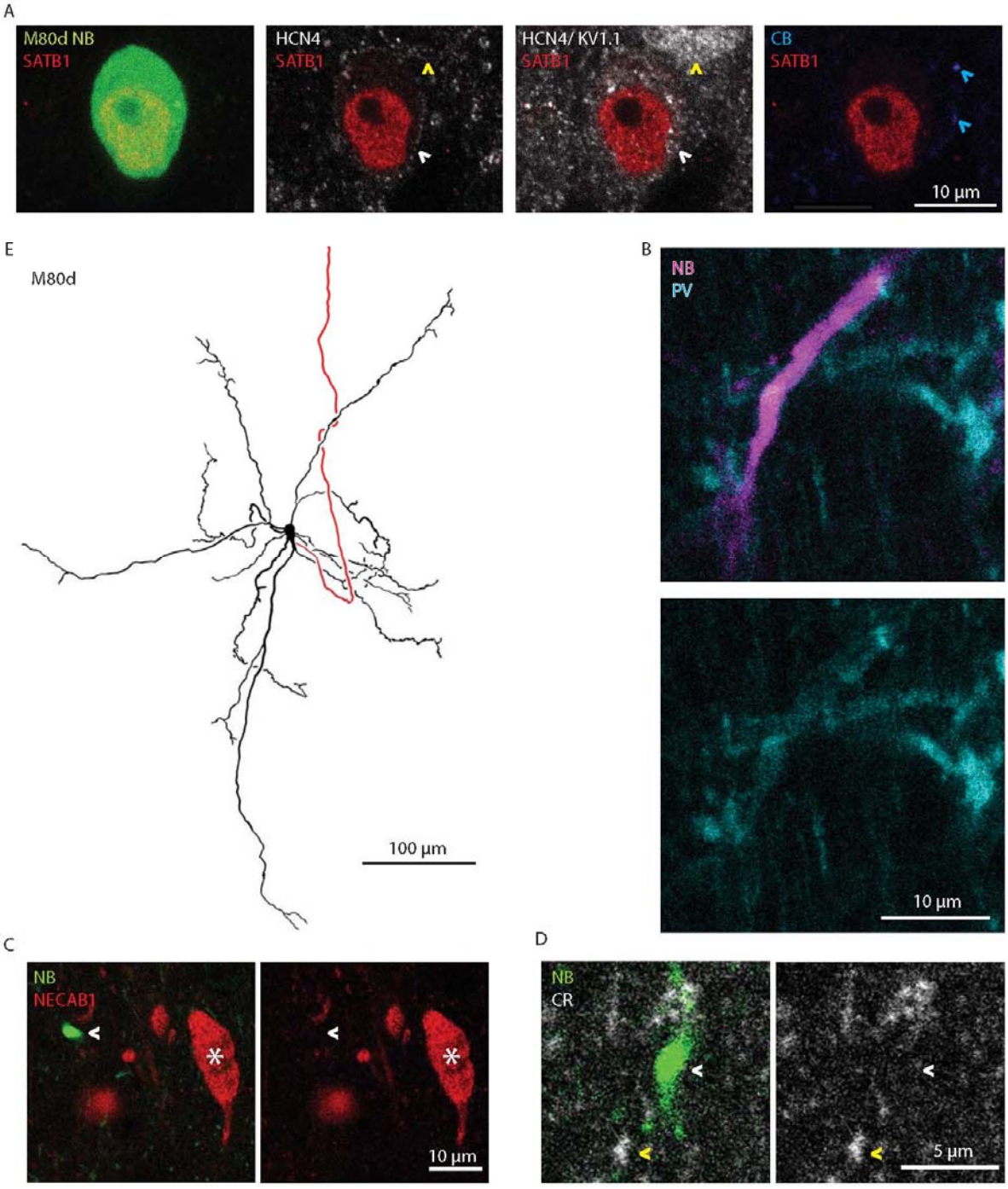

A
M80d NB
SATB1
HCN4
SATB1
HCN4/ KV1.1
SATB1
CB
SATB1
10 µm
E
M80d
100 µm
B
NB
PV
10 µm
C
NB
NECAB1
10 µm
D
NB
CR
5 µm

Figure 3.3 – Visualisation and immunohistochemical analysis of rhythmic firing medial septal neurons. A) The immunohistochemical profile of a typical rhythmic firing medial septal neuron M80d. The top row illustrates immunopositive nuclear signal for the transcription factor SATB1 (red). Immunofluorescent signal for HCN4 delineates the cell membrane (white; arrow head). A subsequent reaction for Kv1.1 was done in the same fluorescent channel as the previous HCN4 reaction (cy5) and Kv1.1-dependent signal, was demonstrated throughout the medial septum; M80d was immunopositive in the cytoplasm. Another neuron also expressing HCN4 and Kv1.1 is marked by yellow arrow head. The calcium-binding protein calbindin was not observed in rhythmic medial septum neurons tested, although immunopositive dendrites (blue; blue arrow heads) and cell bodies were observed. **B)** Septo-hippocampal neurons express PV. A dendritic segment with weak PV immunoreactive signal. **C)** Rhythmic neurons (green; white arrow head) were immunonegative for a novel calcium-binding protein, NECAB1, known to be expressed in septum (red). The asterisk marks a NECAB1 immunopositive soma. **D)** Neurons were immunonegative for CR in dendrites (green; white arrow head). Nearby immunopositive dendrites were present (white; yellow arrow head). **E)** Reconstruction of septo-hippocampal neuron M80d. Electrophysiological analysis of this neuron is found in Chapter 5. Dendrites and soma are represented in black; the main projecting axon is present in red. Notice the initially "hook" in the axon representative of septo-hippocampal neurons. Confocal z-stacks, number of optical sections (thickness in µm) / projection mode: **A** (panels 3,4), 71(21.6)/single optical section; **B**, 48(18.77)/maximum.

Table 3.3 – Summary of features of septo-hippocampal neurons and other significant septal projections. TSN triangular septal nucleus, DL Damien Lapray, TS Timea Szabadi, SB Szabolcs Biro, TO Tugrul Ozdemir, EM Eszter Kormann, DS Daniel Swiejkowski, AIS axon initial segment. * Putatively fully labelled, # Non-rhythmic neuron, ʔ No observable branches in hippocampus; exclusively dorsal fornix, § >50 bouton targets analysed, Ⱬ Lateral septum neuron.

Cell ID	Physiology	Extent of labelling	Location of branches and/or boutons	TSN innervation observed?	Origin of AIS	"Hooked" axon?	IHC characterisation of targets	Significant contribution from others
D55c	Y	Full*	Anterior CA3 and CA1	N		Y	Y§	DL, TS
M21c	Y	Partial	Ventral hippocampus	N			N	TO
M44	N	Full*	CA3a	N	Dendritic	Y	Y§	
M60a	Y	Partial	Midline CA1/2	Y	Somatic	Y	Y	
M62a	Y#	Partial	Intermediate hippocampus				N	
M62b	Y#	Partial	Midline CA1/2				N	
M63c	Y	Full*	Triangular septal nucleus	Y			N	
M65b	Y	Partial	CA3				N	
M75a	Y	Partialʔ	Dorsal fornix			Y	N	
M76a	Y	Full*	Dentate gyrus and CA3d	Y		Y	Y§	
M78a	Y	Partial	CA3		Dendritic	Y	N	
M80d	Y	Partial	Midline CA1/2 and subiculum	N	Dendritic	Y	Y	EM
M82f	Y	Partial	Ventral CA3	N	Somatic	Y	Y	EK
DS36	Y	Partial	Intermediate/ventral hippocampus	N			N	DS
M64c	Yⱬ	Partial	Hypothalamus				N	

3.2.6 Axonal location of septo-hippocampal neurons within the hippocampus

Twelve neurons were sufficiently labelled that they had observable boutons or thin branches within the hippocampus proper. These were considered as confirmed septo-hippocampal neurons. The partial or complete axonal distributions of this population spanned all regions of the hippocampus. One neuron, M80d, had boutons within the dorsal subiculum, and this is to my knowledge the first septo-subicular identified neuron (M80d, partial processing by Endre Marrosi). Several (n = 4; M21c, M62a, M82f, DS36) axons were observed projecting into intermediate or ventral hippocampus, including the non-rhythmic cell, M62a. The extent of these projections correlates with the distributions of axons seen in the PHAL anterograde labelling experiments described above (Figure 3.1). Two other septo-hippocampal neurons were recorded and labelled by other group members: D55c by Dr Damien Lapray and DS36 which was produced by Dr Daniel Swiejkowski.

Single axons varied dramatically in location within the fimbria and in the resultant hippocampal distribution. Generally, those which were positioned medially and dorsally within the fornix/fimbria innervated the dorsal hippocampus, neurons with axons ventrally and laterally in the fornix/fimbria projected to the intermediate or ventral hippocampus. Three well filled neurons (M44, M76a and D55c) were sufficiently complete to delineate their gross distribution relative to the hippocampal circuit.

Septo-hippocampal neuron M44 (physiological activity not recorded) projected in the fimbria to dorsal CA3. (This neuron was labelled under isoflurane anaesthesia with 10 % BDA). The animal recovered after the labelling and was maintained for 4 days before perfusion and fixation. Perpendicular branches were observed radiating from the main axon within the white matter and entering all strata; the majority of axons seen however were in stratum oriens (17.6 mm; 45.2 % total axon length) with less axon length in strata pyramidale (0.4 mm; 1.1 %), lucidum (1.4 mm; 3.7 %) and radiatum (0.6 mm; 1.4 %). The remaining axon in the fimbria/alveus made up 18.1 mm (46.6 %) this included the main axon and bouton-bearing branches (Figure 3.4A; reconstructed neuron).

All values refer to shrinkage uncorrected fixed brain, as recorded in F/T sections. The locations of the 1134 boutons observed were: alveus/fimbria (242; 21.3 %), stratum oriens (766; 67.5 %), stratum pyramidale (20; 1.8 %), stratum lucidum (77; 6.8 %) and stratum radiatum (29; 2.6 %).

The axon of M76a, a rhythmically firing neuron described in Chapter 4, was labelled with 3 % neurobiotin under urethane anaesthesia, displayed a different and non-overlapping hippocampal distribution to that of M44. The main axon projected within the fimbria posteriorly, the axon was located medially in the white matter close to the dentate gyrus and CA3. A common feature with all neurons is the perpendicular branches from the main axons within the white matter leading to bouton-bearing branches in the grey matter (Figure 3.5). The axonal arbour occupied primarily the dentate gyrus and CA3c. Unlike M44, axon branches were also observed, although much less frequently, in CA1 and more distally in CA3b stratum radiatum. Axonal branches and boutons were most densely found in the hilus positioned horizontally below the granule cells. Frequent but less dense axon was observed in CA3c strata pyramidale and radiatum. A relatively small amount of axon occurred in the molecular and granule cell layers of the dentate as well as in CA1.

Another fully labelled axon, D55c (recorded and labelled by Dr. Damien Lapray under urethane anaesthesia; partial processing performed by Dr. Timea Szabadi) was again minimally overlapping with the axonal arbours of M44 and M76a. The axon of this neuron, in common with the previous two neurons, was positioned in the fimbria, but had relatively few branches emerging whilst it was within the white matter surrounding the hippocampus. Branches were observed innervating the anterior pole of the CA3 region of the hippocampus. The main axon continued posteriorly into the dorsal CA1 strata radiatum and lacunosum-moleculare where numerous boutons and branches were visible (Figure 3.6). Branches are also present in CA1 stratum oriens and close to the midline in CA1/2 strata radiatum and pyramidale.

I conclude that single septo-hippocampal neurons have a relatively small and localised hippocampal axonal arbour. The axonal arbour of septo-hippocampal neurons may occupy a specific region or

regions of the hippocampus in a non-uniform manner. Within the regions innervated by single septal neurons, axons may demonstrate a preference for specific layers or strata.

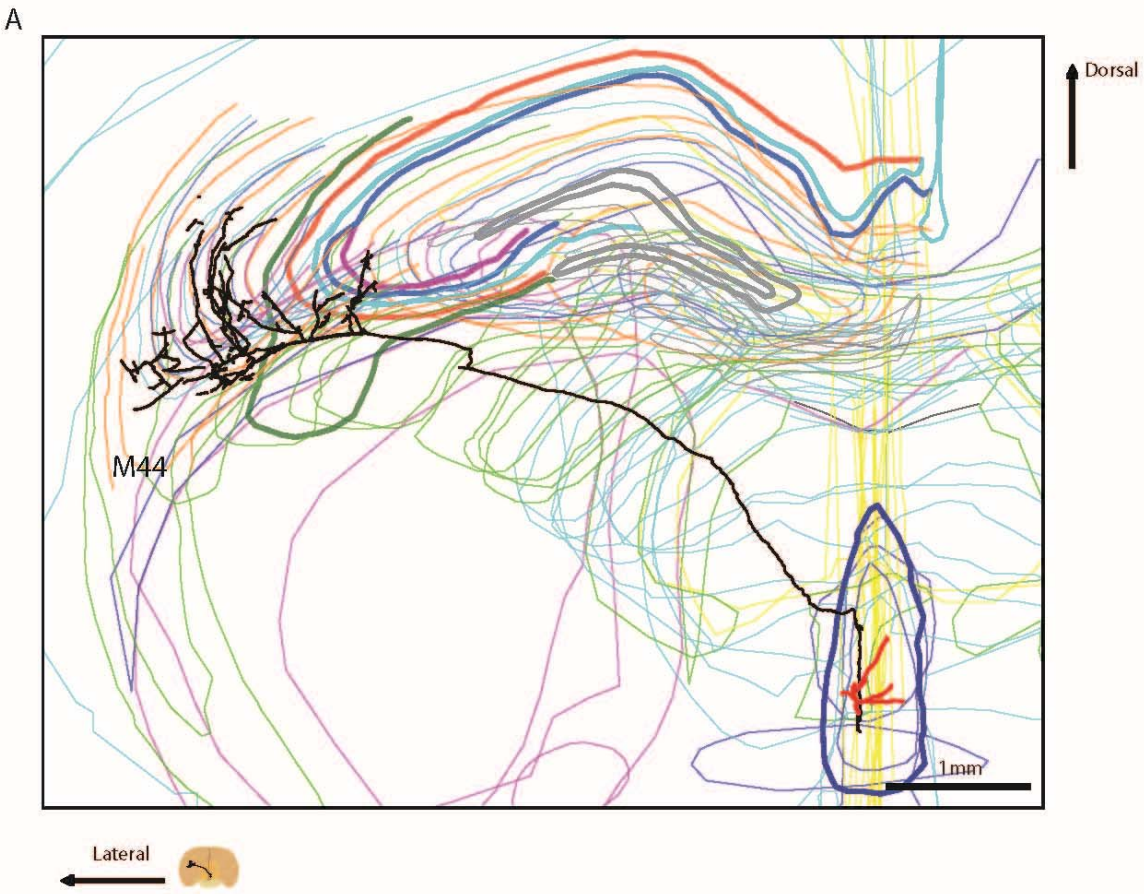

A
Dorsal
M44
1mm
Lateral
B
500 µm
Alveus/fimbria
Str. Ori.
Str. Pyr.
Str. Luc.
Str. Rad.
dorsal
medial
1%
4%
1%
48%
46%
Length per layer
3%
2%
7%
21%
67%
Varcosities per layer
(Total 1134)

Figure 3.4 - Distribution of single labelled septo-hippocampal axon, neuron M44, and quantification. A) Neurolucida reconstruction of neuron M44 in 3D coronal plane. Partial contours are included: soma and dendrites within the medial septum (red), axon projecting in the fimbria-fornix and innervated primarily CA3b of dorsal hippocampus (black). **B)** Illustration of the axon colour-coded by stratum: fimbria/alveus (red), oriens (green), pyramidale (light blue), lucidum (dark blue), radiatum (purple) illustrated in the coronal plane. Below, pie charts of relative percentages of the axon location by layer, and number of varicosities by layer.

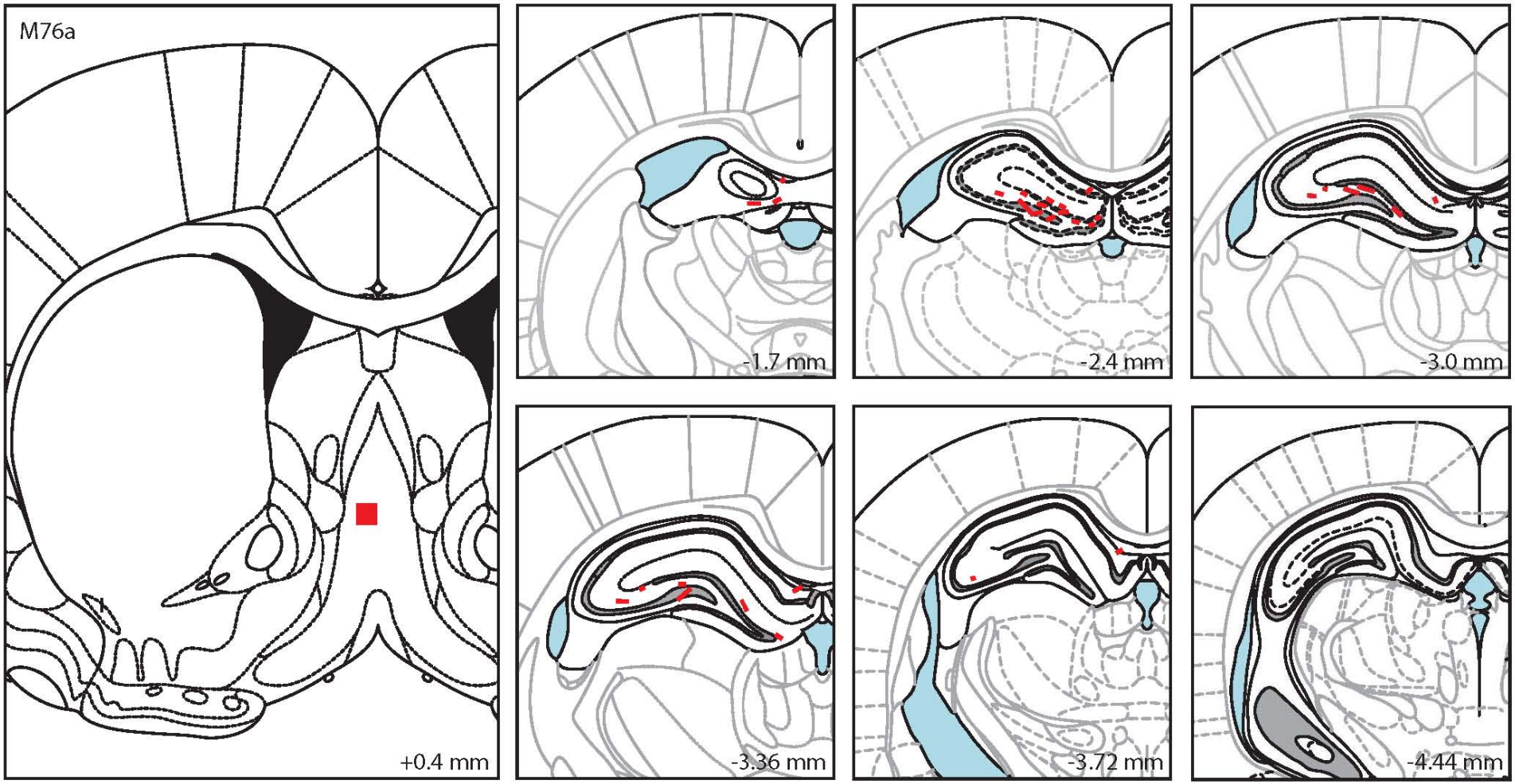

M76a
+0.4 mm
-1.7 mm
-2.4 mm
-3.0 mm
-3.36 mm
-3.72 mm
-4.44 mm
(Relative to Bregma)

Figure 3.5 - Observed distribution of single labelled septo-hippocampal axon from neuron M76a. Approximate locations of the neuron in the septum and hippocampus. Soma location (red square) approximately 0.4 mm anterior to bregma located in the medial septum. Axon (red lines) taken from single sections are the approximate coronal plane described in each box. Axon was located primarily within the blades of the dentate gyrus, including CA3, hilus, granule and molecular layers. Fewer branches were observed within CA1 in stratum oriens. (Images adapted from Paxinos and Watson 6th edition). Electrophysiological analysis of M76a is presented in Chapter 4.

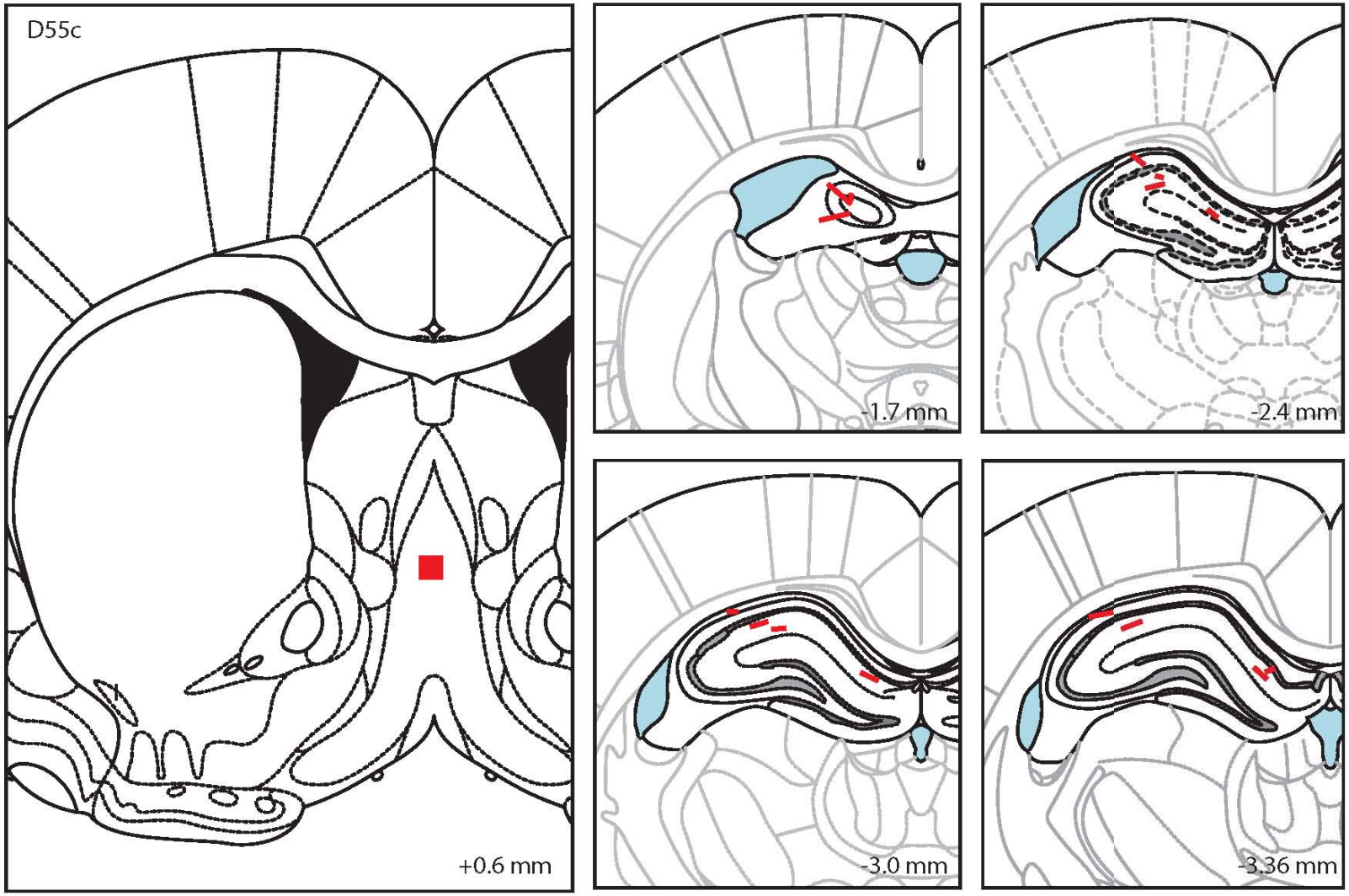

D55c
+0.6 mm
-1.7 mm
-2.4 mm
-3.0 mm
-3.36 mm
(Relative to Bregma)

Figure 3.6 - Observed distribution of single labelled septo-hippocampal axon from neuron D55c. Approximate locations of the neuron in the septum and hippocampus. Soma location (red square) approximately 0.6 mm anterior to bregma located in the medial septum. Axon (red lines) taken from single sections are the approximate coronal plane described in each box. Due to processing difficulties, the axon has not been reliably located posterior beyond the position shown. Axon located at the anterior pole of the hippocampus was within CA3 strata oriens and pyramidale. The majority of the axon was found in CA1 strata oriens and radiatum. (Images adapted from Paxinos and Watson 6th edition).

3.2.7 Immunohistochemical analysis of the hippocampal targets of single septo-hippocampal neurons

To date, the connectivity of the septo-hippocampal GABAergic projection has only been investigated at the population level using anterograde tracing techniques. I used juxtacellular recording and labelling of single medial septum neurons and immunohistochemistry to identify the potential synaptic targets of single neurons in the hippocampus. Electrophysiology for juxtacellular recorded neurons can be found in Chapters 4 and 5. My null hypothesis was that single septo-hippocampal neurons make synapses with most or all interneuron types and do not display specificity.

From the 73 juxtacellular labelling experiments in anaesthetised rats, and an additional 3 performed by my supervisor Dr. Damien Lapray, 3 axons were labelled sufficiently to allow for immunohistochemical analysis of their hippocampal targets, i.e. > 30 hippocampal putative boutons visible in fluorescence. As stated, 11 neurons had > 1 identified hippocampal bouton visible in the hippocampus under epifluorescence conditions.

In all three septo-hippocampal neurons characterised, both *en passant* and basket like axonal arrangements were seen (Figure 3.7); with axonal branches often making *en passant* boutons along dendrites in the region of interest. Figure 3.7 illustrates an example of how pre- and post- synaptic markers were used to define putative synaptic contact.

Septo-hippocampal boutons within the hippocampus were tested for numerous immunohistochemical molecular markers for interneuron populations. The first neuron fully labelled and characterised was M44, with a total of 99 boutons characterised. The boutons of the axonal arbour were within CA3 (Figure 3.4A), and were tested for potential synaptic contact with somata and dendrites expressing a total of 9 molecular markers. 70 % (69 / 99) of boutons appositions were tested with one or more synaptic marker: the presynaptic marker VGAT (n = 26 appositions) and / or the post synaptic marker gephyrin (n = 45 appositions; Figure 3.6).

The most frequently observed marker for the targets of M44 was PV, expressed by 84.9 % of structures opposed to septo-hippocampal boutons (n = 84 / 99 tested). Boutons were never observed in apposition with CR (0 / 4 tested), CB (0 / 21 tested), NPY (0 / 24 tested) or CCK (0 / 5 tested) immunohistochemically identified structures. Only one soma apposed to a bouton expressed NOS (7.1 %; 1 / 14 tested). Fourteen per cent of targets are thus far unknown (Figure 3.8).

Parvalbumin-expressing post-synaptic structures were further tested for markers known to be co-expressed by specific PV-expressing interneuron types. Nineteen PV-immunopositive structures were tested for mGluR1α, 26.3 % (5 / 19 tested) were also immune-positive for mGluR1α (Figure 3.8).

The majority of structures innervated were dendrites (74.1 %; 63 / 85), and 22 boutons innervated 11 neurons at a peri-somatic position. Neurons which were innervated somatically, as well as neurons which were innervated close to the soma could be further identified using somatically located molecular markers. Thirteen target interneuron somata could be identified, twelve of which were PV-expressing neurons and a single NOS-expressing putative ivy cell (Table 3.4). Of the PV-expressing interneurons, molecular phenotype was as follows: PV+, SATB1+, NPY- (n = 5 cells; 3 ± 0.9 boutons); PV+, CCK-, SOM-, CB- (n = 3 cells; 3 ± 1 boutons); PV+, mGluR1α- (n = 3 cells; 1.7 ± 0.6 boutons); PV+, mGluR1α+, SOM+, NPY- (n = 1 cell; 2 boutons). The immunohistochemical phenotype of innervated interneuron targets of the septo-hippocampal neuron M44 were consistent with PV-expressing basket cells (n = 11) and a putative double projection neuron (n = 1).

The septo-CA1 projection cell D55c had a different target distribution from M44. The immunohistochemistry, microscopy, and target quantification experiments were mainly carried out by Timea Szabadi, a visiting student whom I supervised. The majority of appositions were in the presence of GABAergic synaptic markers: VGAT on 14.5 % (n = 24 / 165) and gephyrin on 57.0 (94 / 165) appositions. Another 15 boutons were tested and immunonegative for the cholinergic

synaptic marker VAChT (n = 0 / 5 tested) and the glutamatergic marker VGluT2 (n = 0 / 15 tested). Parvalbumin immunoreactivity was found in 67.2 % of structures apposed to septal boutons (n = 84 / 125 boutons tested). Another prominent marker of post-synaptic structures was mGluR1α immunoreactivity in 34.1 % of cases (n = 45 / 132 boutons tested). These markers can be present together in single neurons; in 94 tests which included both PV and mGluR1α coexpression was found in 11.7 % of cases (n = 11 / 94 boutons tested); PV alone in 58 .5 % (n = 55 / 94 boutons tested); mGluR1α alone in 10.6 % (n = 10 / 94 boutons tested); and neither in 19.1 % (n = 18 / 94 boutons tested) (Figure 3.8). Metabotropic glutamate receptor mGluR1α expression differentiates PV-expressing targets of D55c.

A relatively small number of markers which are mutually exclusive with PV were found in apposition to boutons of axon D55c. Two boutons (of 32 tested; 6.3 %) were opposed to CB-positive dendrites; 2 boutons (of 49 tested; 4.1 %) were opposed to CR-positive dendrites, and 1 bouton (of 32 tested; 3.1 %) was opposed to an M2R-positive dendrite. No boutons were apposed to NOS-expressing structures (n = 0 / 61 boutons tested).

Four somatically innervated targets of D55c could be identified and immunohistochemically tested. All neurons tested were immunoreactive for PV (n = 4 / 4) and SOM (n = 4 / 4); 3 neurons were tested and immunopositive for $GABA_A$ α1 subunit (n = 3 / 3); two neurons were tested and immunopositive for NPY (n = 2 / 2). Diversity was found in the expression of mGluR1α in target neurons with 1 / 3 testing positive (Table 3.4). Numbers of boutons per somatic target were: 6, 16, 1, and 9; the two mGluR1α negative neurons having fewer boutons than the two mGluR1α positive neurons.

Lastly, the septo-dentate gyrus/CA3 projecting neuron M76a also had a unique profile of interneuron targets. A total of 279 boutons were tested for apposed putative postsynaptic targets, with 97.5 % in the presence of a synaptic marker (VGAT n = 138; gephyrin n = 134). Similar to the previous neurons, the majority (71.9 %; n = 69 / 96 tested) of structures were PV-immunopositive

and a small percentage were positive for NOS (8 %, n = 4 / 50 boutons tested). Boutons were never observed apposed to: CB- (n = 0 / 56 boutons tested), CR- (0 / 36 boutons tested), VIP- (0 / 7 boutons tested) or CCK-immunopositive (0 / 34 boutons tested) structures. The somata of fourteen interneuron targets were located and investigated. Of the 7 tested, 6 were PV-expressing neurons, and these were immunonegative for SATB1 (n = 7 / 7 tested), which had 5.3 ± 1.7 boutons per target visible. Innervated PV+/SATB1- soma were located within the hilus and sub granular layer of dentate gyrus, CA3d pyramidal layer as well as the midline CA1 region in both strata pyramidale and oriens. The dendritic distribution of dendrites of targeted PV+/SATB1- interneurons was dependent on the region it was located. Neurons within the subgranular zone often displayed horizontally oriented dendrites. Contrastingly, hilar neurons were observed to have radial dendrites towards both the granule layer and towards the CA3 pyramidal layer. The CA1 stratum oriens-located neuron had dendrites oriented radially towards both the alveus and ventrally towards the stratum pyramidale. Due to sectioning, I was not able to investigate the dendrites of the neurons located within the stratum pyramidale of CA1.

Two tested somata were immunonegative for CCK, one was immunonegative for CB and one was immunonegative for CR. These neurons were not tested for PV. Three interneuron somata were immunohistochemically tested for NOS, and one was immunopositive (n = 1 / 3; Table 3.4) with 3 visible boutons in apposition. All immunonegative neurons were in regions which contained other neurons immunopositive for the epitope tested. If immunoreactivity was not reliable in the area tested, the test was inconclusive and not used for further analysis.

Immunohistochemical analysis of the putative targets of three visualised septo-hippocampal neurons with extensive bouton bearing axonal branches in the hippocampus has demonstrated that single neurons are likely to target specific types of interneuron preferentially within the hippocampus, even when innervation is in multiple hippocampal laminae or regions.

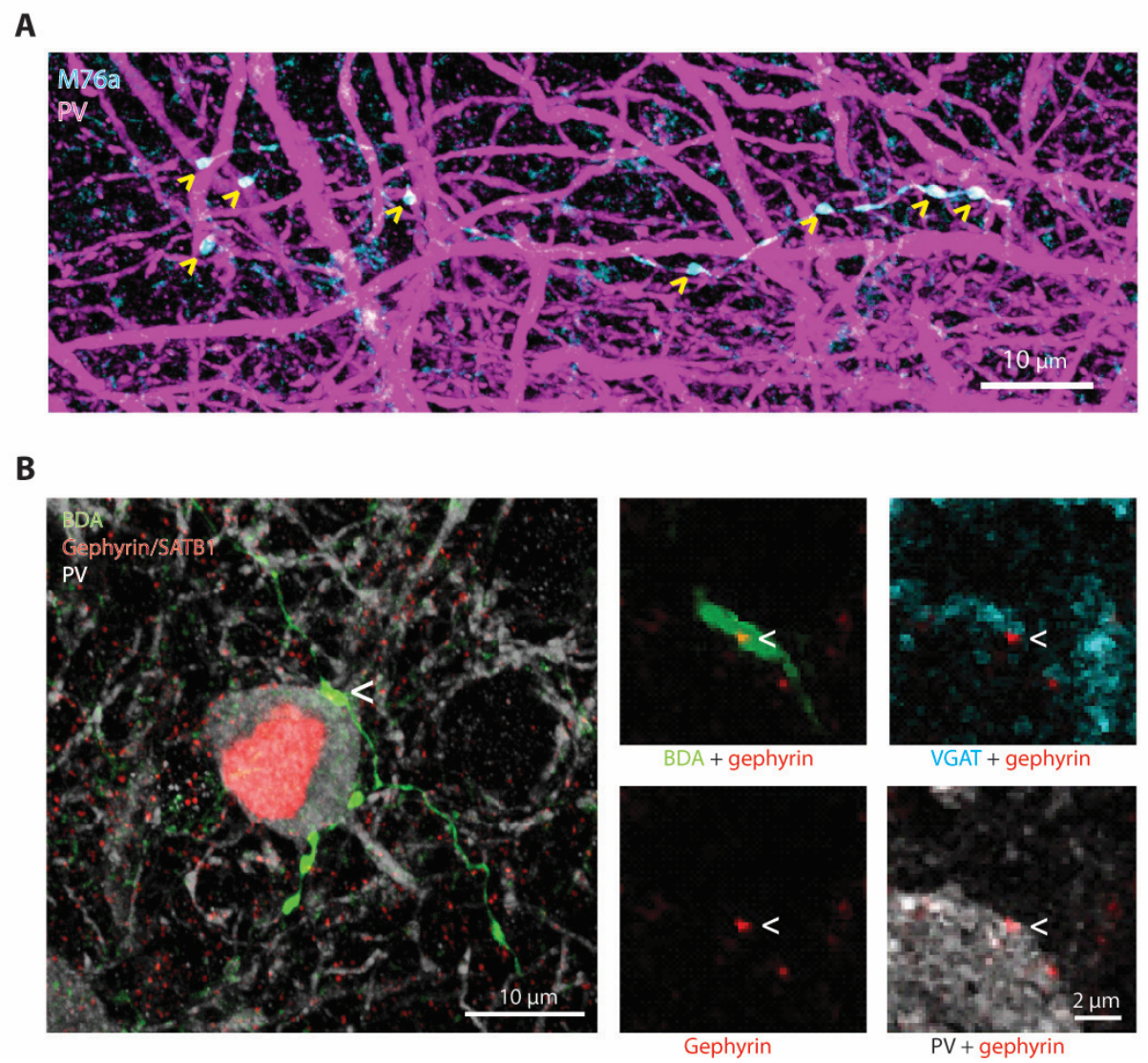
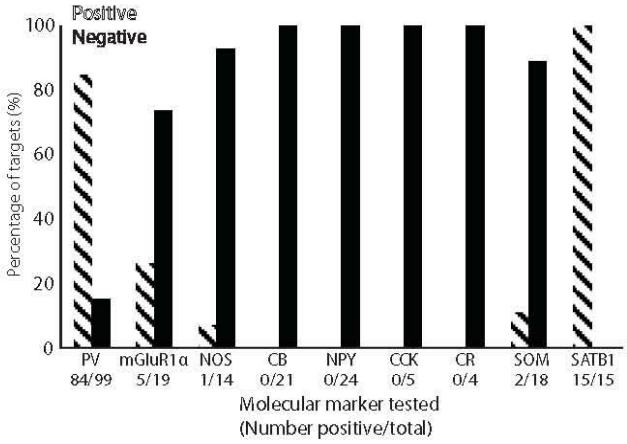
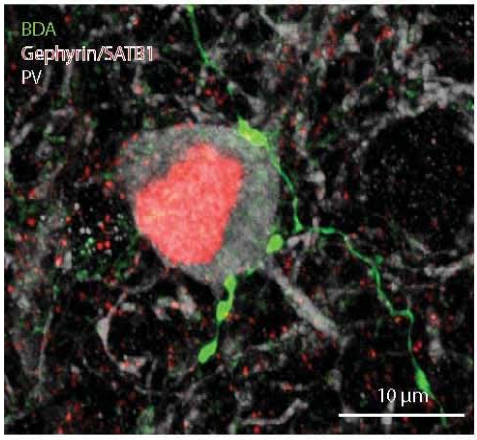

A
M76a
PV
10 µm
B
BDA
Gephyrin/SATB1
PV
10 µm
BDA + gephyrin
VGAT + gephyrin
Gephyrin
PV + gephyrin
2 µm

Figure 3.7 – Single GABAergic septo-hippocampal axons form both *en passant* and basket-like axon structures. A) A representative example of a single axon branch making *en passant* boutons with PV positive dendrites in the molecular layer of the dentate gyrus (M76a). Yellow arrows indicate boutons. **B)** An illustration of pre- and post- synaptic (VGAT and gephyrin respectively) immunohistochemistry in a basket-like axonal formation around a PV positive (white), SATB1 positive (red nucleus) interneuron in CA3 (M44). The bouton (BDA; green) is seen in apposition to a gephyrin puncta (red) and containing VGAT (cyan). None of the elements are resolvable from each other suggesting a synaptic contact. Confocal z-stacks, number of optical sections (thickness in µm) / projection mode: **A,** 104(37.7)/maximum**; B,** (main)**,** 26(8.22)/maximum.

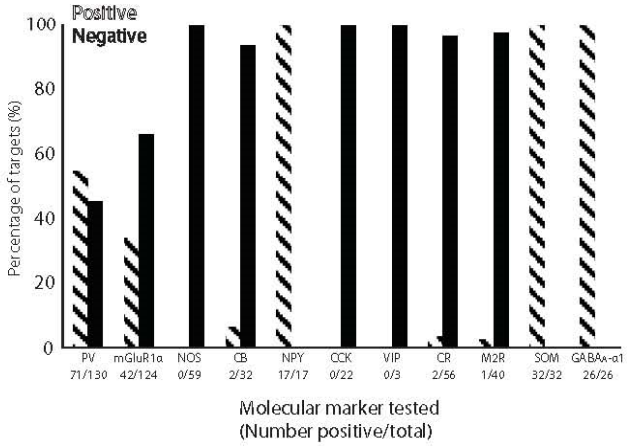
A1



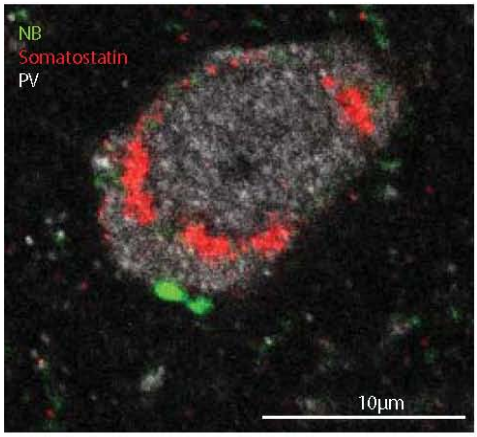
A2



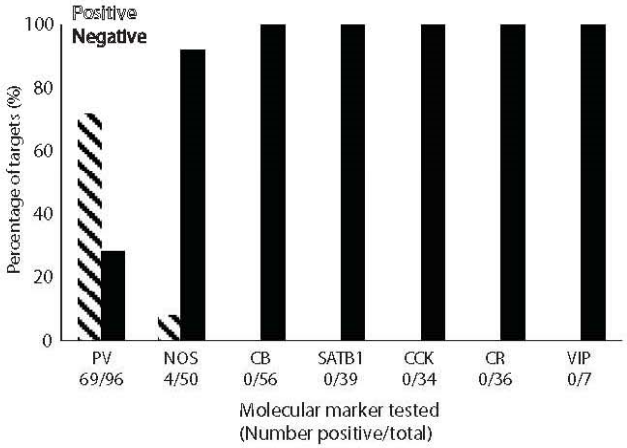
B1



B2



C1



C2

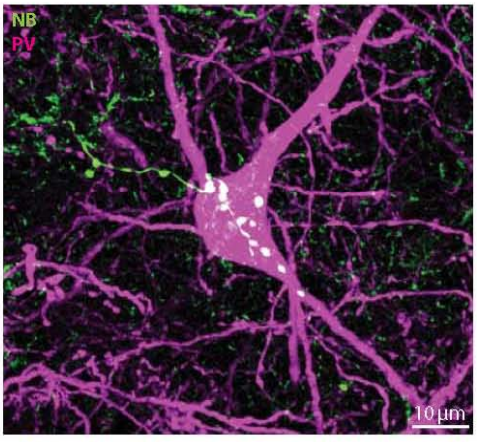


Figure 3.8 - Immunohistochemically identified hippocampal interneuron targets of single septal neurons. A) Interneuron targets of M44 in the CA3b area. **A1)** A bar chart of the tested phenotypes of post-synaptic targets of M44. **A2)** A maximum intensity projection of a confocal micrograph Z-stack, of an identified PV-expressing (white; cytoplasmic) SATB1-positive (red; nucleus) somatically innervated neuron by M44. The axon of M44 (green; BDA) is in synaptic apposition observed by gephyrin puncta (yellow; punctate) postsynaptically to each bouton within the PV cell (white cytoplasmic). The transcription factor SATB1 (red; nuclear) is found in basket and bistratified cells, amongst others, but not in axo-axonic neurons. **B)** Interneuron targets of D55c, a CA1 innervating septal neuron. **B1)** A bar chart of the tested phenotypes of post-synaptic targets of D55c **B2)** A confocal micrograph of an identified bistratified interneuron, somatically innervated by D55c. The boutons of D55c (green; neurobiotin) are apposed to a PV (white; cytoplasmic) positive neuron which also expresses SOM (red; golgi apparatus) found in bistratified and double projection neurons. **C)** Interneuron targets of M76a, a CA3/dentate gyrus innervating septal neuron. **C1)** A bar chart of the tested phenotypes of post-synaptic targets of M76a **C2)** The septal neuron M76a makes a basket-like innervation (white/green; neurobiotin) around a CA3 PV-expressing (magenta) neuron. Confocal z-stacks, number of optical sections (thickness in µm) / projection mode: **A2**, 26(8.22)/maximum; **B2**, 37(4.3)/single optical section; **C2**, 60(10.97)/maximum.

Table 3.4 – Summary of immunoreactions performed on innervated neurons by single septo-hippocampal neurons.

Afferent cell	Target name	Putative target identity	PV	NPY	SATB1	NOS	SOM	mGluR1α	GABAaR-α1	CB	CCK	CR
M44	A	PVBC	+	-	+							
	B	PVBC	+	-	+							
	C	Ivy	-			+						
	D	PVBC	+	-	+							
	E	PVBC	+	-	+	-						
	F	PVBC	+				-					
	G	PVBC	+				-					
	H	Proj/BiStr	+	-			+	+				
	I	PVBC	+	-	+							
	J		+				-					
	K		+					-				
	L		+					-				
	M		+					-				
D55c	A	Proj/BiStr	+				+	+				
	B	Proj/BiStr	+				+	+	+			
	C	BiStr	+	+			+	-	+			
	D	Proj/BiStr	+				+	-				
M76a	A	AAC	+		-							
	B	AAC	+		-							
	C	AAC	+		-							
	D	AAC	+		-							
	E		-		-							
	F					-						
	G	Ivy				+						
	H					-						
	I	AAC	+		-							
	J										-	
	K										-	
	L											-
	M									-		
	N	AAC	+		-							

PVBC	PV-expressing basket cell
Ivy	Ivy cell
Proj/BiStr	Double projection or bistratified cell
AAC	Axo-axonic cell

3.3 Discussion

In this study I used a combination of anterograde tracing and single neuron labelling *in vivo* by the juxtacellular method to study the connectivity of the septo-hippocampal pathway in rats. It was found that the septo-hippocampal projection includes a putative synaptic contact NOS-expressing, axo-axonic and M2R-epressing interneurons, including the trilaminar cells. Septal axons which were in appoisition to trilaminar neurons expressed the presynaptic protein mGluR8a. Single recorded and labelled septal neurons expressed similar immunohistochemical markers which did not differentiate them based on anatomical parameters, including novel markers SATB1, HCN4, and Kv1.1. The axons of septo-hippocampal neurons was varied in hippocampal location, however the immunohistochemically defined targets of 3 neurons may be selective based on interneuron type.

I demonstrated the GABAergic septal innervation of a number of previously untested interneuron types, which have not been tested previously, namely, the NOS-expressing neurons, trilaminar neurons, and the axo-axonic neurons. The current hypothesis is that theta-frequency GABAergic medial septal synaptic input to interneurons is responsible for the theta phase-related synchronous firing of interneuron types. Two of the NOS-expressing neuron types - the ivy and neurogliaform neurons - are known to fire action potentials phase-locked to the theta oscillation (Fuentealba et al., 2008a, Fuentealba et al., 2010). This may be due to the GABAergic input described in this study. The third type of NOS-expressing neuron, the infrequent, intensely NOS-immunopositive neurons, received very little, if any, observable input from septum. The role of this cell may be less related to theta-dependent processes in the hippocampus. This cell type in the cortex is known to increase its activity during slow wave sleep (Gerashchenko et al., 2008), supporting a network state-dependent role for this cell type independent of the theta oscillation.

Similarly to the NOS-expressing neurons, both trilaminar and axo-axonic neurons display phase-locked activity during hippocampal theta oscillation *in vivo* (Ferraguti et al., 2005, Viney et al.,

2013). As expected these cell types also received GABAergic septal input, as well as putative cholinergic input. This may provide a mechanism of theta phasing of these neurons *in vivo*.

I have also demonstrated that the septo-hippocampal pathway is a possible source of mGluR8a-containing input to the hippocampus and to trilaminar neurons. So far, only presumed VIP-expressing interneuron axons have been demonstrated as a source (Ferraguti et al., 2005). The receptor mGluR8a was present in both large type I and thin type II axons; it is assumed that they correspond to GABAergic and cholinergic inputs, respectively. Type three metabotropic glutamate receptors, which include mGluR8a, are presynaptic to trilaminar neurons (Kogo et al., 2004, Ferraguti et al., 2005) and function to inhibit synaptic release from the afferent terminals (Kogo et al., 2004) potentially via inhibition of N-type calcium channels (Guo and Ikeda, 2005). The sources of endogenous ligands, which likely includes synaptically released glutamate, are unknown; nor are the physiological context by which presynaptic mGluR8a activation might occur. Reduction of GABA (and acetylcholine) release to trilaminar neurons may act to uncouple these neurons from the hippocampal theta-synchronous behaviour, which is otherwise governed in frequency by the septum. High glutamate release will occur during periods of maximal pyramidal neuron firing, both from local cells and pyramidal neurons projecting to the hippocampus. Maximal pyramidal neuron synchrony occurs during SWR events when 10 – 15 % of pyramids may fire within ~100 ms (Csicsvari et al., 2000). In such events, the release of glutamate may act directly on the post-synaptic trilaminar neurons and also juxta-synaptically to modulate the release of other neurotransmitters to the cell to prevent any release to the cells. A significant proportion of medial septal neurons fire action potentials during SWR events, not only the SWR active neurons described in chapter 5, but also SWR-inhibited neurons at a low level. Modulation by mGluR8a activation may prevent GABA release specifically at these boutons, regardless of somatic action potentials to other axon branches or to other neuron types innervated by the same septal neuron. Trilaminar neurons fire at a high rate during SWR (Ferraguti et al., 2005) which may be supported by the reduction of synaptic GABA

release from septal afferents. This prevents the septum from modulating trilaminar neurons during network states which involve high pyramidal neuron synchrony.

Another possibility is that high firing pyramidal neurons, such as place cells coding the location of the animal in space, entrain trilaminar neurons by shutting off the septal modulation via mGluR8a activation. The firing of some interneurons have been demonstrated to phase precess along with that of pyramidal neurons (Maurer et al., 2006, Ego-Stengel and Wilson, 2007). I hypothesise that trilaminar neurons may account for a portion of observed phase precessing interneurons, as do other mGluR8a decorated neurons such as those which express mGluR1α. Mechanistically, entrainment of certain interneurons during phase precession may in part be dependent on the reduction of septal theta-frequency GABAergic inhibition via mGluR8a activation in individual boutons. In this manner, single branches or small areas of a septal axonal arbour can be regulated independent of other areas. This could be tested using virally-mediated calcium imaging of septal axons *in vivo* and the application of mGluR8a agonists (Kaifosh et al., 2013).

Interestingly, neuron types which fire at a higher frequency during theta oscillations, such as the PV-expressing basket and axo-axonic cells (Tukker et al., 2013, Viney et al., 2013), appear to receive denser peri-somatic synaptic input than low frequency firing neurons such as the ivy neuron (Fuentealba et al., 2008a). The size of pre-synaptic boutons, as well as post-synaptic structures, is correlated with the size of inhibitory post-synaptic currents (Kay et al., 2011). A greater number of GABAergic synapses are likely to result in greater somatic inhibition. It can be assumed that interneuron types firing at higher rates which are innervated by greater numbers of boutons, receive greater somatic phase-locked inhibition as a result of septal neuronal firing. Such cell types may have a greater level of excitability, whether intrinsic or from synaptic sources, requiring higher level of septal inhibition to produce the resultant phase-locking to theta oscillations. The methodology of the present study is biased towards identification and investigation of peri-somatic input to interneurons. Molecular markers which identify distinct cell types from larger groups of

interneurons have most often been immunohistochemical markers of the somatic region, such as SATB1 or somatostatin. Because of this, somatically innervated interneurons were analysed with immunohistochemistry in more detail than the majority of the inputs, which were dendritic. These results may be biased towards the over-representation of somatically innervated interneuron types. Both NOS and PV are expressed throughout the somato-dendritic arbour meaning that if an unusually dense dendritic innervation of either population did occur I would be able to detect it. In all three neurons characterised, the majority of boutons were found on the dendritic domains, however the dendrites account for the majority of the surface area of a neuron. Stereological investigation of labelled septal boutons, by PHAL or genetic means, onto hippocampal interneurons would answer whether the density of input is uniform or not along interneuron subcellular domains. The axonal location of different septo-hippocampal neurons within this study does suggest, however, that a non-uniform distribution may be present. M44 for example, has the majority of axonal length and number of boutons within the alveus, a region which is almost devoid of soma but which interneurons extend their dendrites. Likewise, D55c is located largely within the strata radiatum and lacunosum-moleculare, regions which contain few PV-expressing neuron somas.

From the labelling and immunohistochemical characterisation of single septo-hippocampal neurons I was unable to differentiate rhythmic septal neurons with different preferred theta phases or projections; the tested molecules include 4 calcium binding proteins (PV, CR, CB, NECAB1) and two ion channels (HCN4 and Kv1.1). This may suggest that medial septum (septo-hippocampal) neurons are more uniform than hippocampal interneurons and GABAergic projection neurons in terms of molecular composition. Both calcium-binding proteins and ion channels are known to be intrinsic regulators of neuronal firing properties (Aponte et al., 2008, Dodson et al., 2011, Bischop et al., 2012). Whilst some firing parameters of rhythmic medial septum neurons do vary (firing frequency, preferred theta phase, SWR response), these neurons fire with little variability from theta cycle to cycle (see chapter 5). Network behaviour, such as theta phase coupling and SWR

response may be explained by differences in connectivity, both internally within the septum and input from extrinsic sources such as the hippocampus. Evidence from *in vitro* recordings from these neurons shows that they are not intrinsically pace-makers, nor do they fire rhythmic bursts (Morris et al., 1999, Knapp et al., 2000, Sotty et al., 2003, Henderson et al., 2010). However they can fire theta frequency spikes (Wen et al., 2013). This suggests that the *in vivo* firing patterns of these neurons are likely to be largely shaped by synaptic connectivity. I propose that rhythmic GABAergic medial septum neurons with the molecular profile demonstrated in this study are intrinsically of the same cell type if devoid of inputs. Further, I suggest a mechanism by which, during developmental mechanisms, may cause differences in gene regulation by transcription factors within these neurons leading to differences in axonal signalling molecules (adhesion molecules, guidance cues etc.) between cells. Such mechanisms could result in both differences in intra-septal connectivity which dictates the final preferred theta phase, as well as differences in axonal projection properties to the hippocampus. The transcriptional-dependent differences in connectivity due to differences in adhesion molecule profiles may result in network-dependent firing pattern differences seen *in vivo*. These biochemical differences may or may not be maintained into adulthood. Neurons of the same type assemble within the septum to form an internal connectivity which may partially dictate the resultant theta phase of firing. This internal connectivity may correlate with the interneuron type/s innervated within the hippocampus.

My results have implication for the optogenetic study of this pathway. Currently only one study is published using optogenetic manipulation of the septo-hippocampal pathway; namely the cholinergic projection *in vitro* (Bell et al., 2013). Diversity of the cholinergic projection to the hippocampus has previously been demonstrated in the NOS-expressing cholinergic projection (Sugaya and McKinney, 1994). The results presented here demonstrate that neurons which project to different hippocampal regions, and fire at different times during the theta cycle, express similar molecular markers. These markers are commonly used for genetic means to label subsets of neurons for optogenetic manipulation. Optogenetics causes synchronous excitation or depression

of all neurons manipulated. Given the *in vivo* firing patterns of septo-hippocampal neurons, this would lead to a state of artificial synchrony, where neurons which do not usually fire within the same theta phase are entrained to. Conclusions based on this hyper-synchronous state should be treated with caution as it may not give biologically meaningful data. The meaningful manipulation of the GABAergic septo-hippocampal project will require the isolation of only similar neurons, similar in their theta phase spike timing and hippocampal targets; the PV-expressing or GABAergic cell types within the medial septum cannot be treated as similar for optogenetic manipulation just because they express similar molecular markers.

The anatomical analysis of the axonal arbour of single medial septal neurons has revealed they are surprisingly small and localised within the hippocampus, with each fully labelled axon occupying only a portion of the hippocampus and showing a preference to a subregion (e.g. M44 innervates dorsal CA3, mostly within stratum oriens). Axons were frequently observed travelling to posterior parts of the hippocampus and hippocampal formation without sending observable innervation to the dorsal hippocampus. Single neurons of the septo-hippocampal projection do not provide a uniform input to the hippocampus but have distinct regional specificity. Because of the large size of these neurons and relative difficulties combining the immunohistochemical analysis with producing high quality visualisation for reconstruction, the reconstruction of the axonal arbours was incredibly time consuming and prohibited me from reconstruction all three neurons myself. Both neurons are being reconstructed by other members of the group.

Recently it was demonstrated that hippocampal theta oscillation behaves as a travelling wave, originating from the dorso-medial hippocampus, and terminating in the ventral hippocampus (Lubenov and Siapas, 2009, Patel et al., 2012). As a dynamic wave, all phases of theta are represented at any time, separated in space. Interneurons are phased-locked to the locally generated theta oscillation. In a travelling wave model, at a given reference point, phase is constantly changing as each wave front moves through it. This means that all phases are

represented at a single time point throughout the hippocampus. This suggests that interneurons of a given type are not synchronous throughout the whole hippocampus, as would be expected in a standing wave model. Segregation of septal inputs into relatively small regions allows for interneurons of the same type in different locations, to receive the same inhibition relative to the local theta whilst differing in absolute time. This maintains synchrony within regions whilst providing the necessary diversity of inhibitory input timing needed for a traveling wave. I propose that the network basis of the travelling theta wave is the hippocampal region specific restricted axonal projection by septo-hippocampal neurons revealed in this project.

There is evidence to suggest that cortical oscillations share properties with other types of waves, such as water waves, such as the ability to form spiral singularities (Harris-White et al., 1998, Huang et al., 2010). The observation of the theta wave being a propagating wave is potentially important clinically. It will be important to understand how theta propagation is affected by focal disruption, such as stroke or epilepsy induced damage. The theta wave is directional so it will be important to know if the wave continues unimpeded "skipping" the foci, or if like a gravity wave interacting with a coast line, it dissipates. The former suggests that the theta wave, directed by the septum is propagated and produced throughout the hippocampus actively at each point and independently of earlier hippocampal regions; the later suggests that the wave is generated and then theta "downstream" is dependent on "upstream", like an action potential propagating along an axon. Modulation of any point of the hippocampus within it or through the septal afferents directing it would have either local only or also downstream effects.

One of the core pathological events which occur during Alzheimer's disease is the degeneration of the medial septum and the hippocampus (Rossor et al., 1982, Whitehouse et al., 1982); this correlates with the symptomatic loss of hippocampal function and memory (Wang et al., 2002, Jyoti et al., 2010). The relatively region specific innervation made by septal neurons and their scarcity suggest that little redundancy may exist in this system. Does loss of specific GABAergic septo-

hippocampal neurons result in a significant deficit in inhibitory input to specific classes of interneurons in a region of the hippocampus? Qualitative comparison of the number of boutons received by interneurons in PHAL-labelled experiments versus the number received by single neurons suggests that multiple neurons innervate a single interneuron type. It is not yet known if all inputs to a single neuron have similar theta- and SWR- related firing patterns to provide apparent redundancy.

Specificity by septal afferents was not only regional but also interneuron type specific. This was suggested because in all three cases tested, a higher than expected number of synapses were made onto interneurons with similar immunohistochemical markers, for example PV. In the identified interneurons which were found, a high level of homogeneity was found with relatively uncommon interneuron types, such as the axo-axonic cell, being found with a disproportionately occurance. The most common molecular marker expressed by interneurons, NOS, was rarely found to be in synaptic contact with these neurons, which would be likely if the innervation was non-selective. Interneuron type specificity was hypothesised as the model of septo-hippocampal connectivity previously, based on firing patterns *in vivo* (Borhegyi et al., 2004). This may explain the synchronous firing of hippocampal interneurons during particular theta phases – theta phase modulation – as multiple neurons of the same type, within the same region, receive GABAergic synaptic inhibition synchronously from single medial septum neurons. The ability of single medial septum neurons to innervated and probably inhibits many interneurons of a few types' acts as a signal amplification within the hippocampus. Activation of the septo-hippocampal fibres results in disinhibition of pyramidal neurons *in vitro* (Toth et al., 1997). However on a single neuron level, as septal axons innervate single or few interneuron types, one can think of the product of individual septal neuron's firing as pyramidal cell domain-specific disinhibition at theta frequency via specific interneuron inhibition.

Chapter 4 – *In vivo* firing patterns of theta rhythmic septal neurons which are inhibited or did not change their firing pattern during hippocampal sharp-wave ripple oscillations

4.1 Introduction

The medial septum is necessary for the generation of hippocampal theta oscillation, whether this is generated by brainstem stimulation or behaviour-driven activity (Green and Arduini, 1954). Rhythmic activity of GABAergic septo-hippocampal neurons within the medial septum project to hippocampal interneurons and is hypothesised to pace the frequency of the theta oscillation by rhythmic inhibition (Freund and Antal, 1988, Freund, 1989, Borhegyi et al., 2004, Varga et al., 2008).

One proposed mechanism for the emergence of rhythmicity within these neurons is that these GABAergic cell groups mutually innervate each other, causing a feedback inhibition and a "see-saw" like firing between the neurons (Borhegyi et al., 2004). Synaptic innervation between septal PV-expressing neurons has been suggested as a population of these neurons has dense PV-immunopositive somatic synaptic contacts (Henderson et al., 2004). The origin of this input is unknown but is suggested to be local. Parvalbumin-expressing neurons may have a large local axon (Borhegyi et al., 2004, Henderson et al., 2004), and cholinergic neurons are not the synaptic targets of these neurons (Henderson et al., 2004). Contrasting to the mutual inhibition hypothesis presented by Borhegyi et al. (2004) which suggest two populations of PV-expressing rhythmic neurons innervate each other, this suggests rhythmogenesis may occur by a one-way input between cell types.

Other inputs and circuits may contribute to the rhythmic firing pattern of GABAergic septo-hippocampal neurons. The medial septum and hippocampus are reciprocally connected by GABAergic long-range projection neurons from each region (Takács et al., 2008). Hippocampo-septal neurons have a firing pattern which is highly modulated to the hippocampal theta oscillation; single neurons have a highly rhythmic firing pattern (Jinno et al., 2007). GABAergic projection cells from both regions are synaptically connected with each other. This may be the anatomical correlate of the mutual inhibition which acts to produce highly rhythmic, theta-phased, neuron firing in these regions. Although septal neurons are often referred to as "pace-makers" see Introduction for

discussion of the septum in this context. Rhythmic GABAergic septo-hippocampal neurons are necessary for the generation of theta oscillation within the hippocampus. The firing patterns of these neurons correlates with the frequency of the resultant theta oscillation and leads the oscillation (Hangya et al., 2009). However the medial septum is not a *frequency integrator*, that is, a region which functions to transduce a frequency from tonic signals. These are not mutually exclusive but in this context of the medial septum's role in the hippocampus, the medial septum may act as a pace-maker, but is not a frequency integrator.

Lesion of the medial septum or the fimbria, the white matter tract between these regions, ablates the generation of hippocampal theta by pontine stimulation (Green and Arduini, 1954, Faris and Sainsbury, 1990, McNaughton et al., 1995, Nuñez et al., 2006). Under behavioural conditions which correlate with a hippocampal theta oscillation occurring, medial septal or fimbrial lesion prevent the emergence of the hippocampal oscillation (McNaughton et al., 2006). Behaviourally, this correlates with a decreased performance during memory and learning paradigms (McNaughton et al., 2006, Lecourtier et al., 2011). The medial septum is necessary for theta oscillation to occur *in vivo*. The medial septum is unlikely to be the site of frequency generation (a frequency integrator) because progressive inactivation by anaesthetic causes a reduction in amplitude, but not frequency, of the theta oscillation (McNaughton et al., 1995). Together, this data suggests that the connectivity within the medial septum does not itself produce a rhythmic signal, but integrate ascending theta rhythmic signals with other modulatory signals before enforcing it upon the hippocampus via rhythmic inhibition of interneurons.

During another network state distinct from the theta oscillation, the sharp-wave ripple oscillation (SWR), the most frequently reported firing pattern of PV-expressing and putative septo-hippocampal neurons is suppression of firing *in vivo* (Dragoi et al., 1999, Borhegyi et al., 2004), although a minority of HCN1-expressing neurons were suppressed (Varga et al., 2008). This firing suppression is hypothesised to come from hippocampo-septal GABAergic neurons which are

reciprocally synaptically connected with septo-hippocampal neurons (Takács et al., 2008); these neurons increase their firing frequency during SWR events *in vivo* which may result in synaptic inhibition of the efferent septal neuron (Jinno et al., 2007). The neuropeptide somatostatin is expressed by hippocampo-septal neurons (Jinno et al., 2007). Septal neurons express various somatostatin receptors and likely receive synaptic somatostatin released from hippocampal projection neurons (Bassant et al., 2005). The action of somatostatin is inhibitory when exogenously applied to septal neurons (Bassant et al., 2005); during SWRs somatostatin synaptically released from inhibitory hippocampo-septal neurons may contribute to the suppression of firing in septal neurons during this time. (For a description and analysis of septal neurons which increased firing frequency during SWR see Chapter 5)

I will investigate the firing pattern of septo-hippocampal neurons *in vivo* during both hippocampal theta oscillation and SWR events. Specifically I will describe the firing patterns of SWR inhibited septal neurons and the temporal relationship between action potential firing and SWR events.

4.2 Results

Using the juxtacellular recording and labelling method I have investigated the GABAergic septo-hippocampal population, of which I recorded a total of 37 theta rhythmic neurons during both the theta oscillation and SWR hippocampal network states. Of these, 17 neurons displayed a firing pattern most commonly reported; that is, firing frequency suppression during SWR epochs. I have included here 7 other rhythmic neurons which did not significantly change their firing pattern during SWR epochs as also they on average fired action potentials during less than half of SWR epochs (43.2 % ± 12.1; n = 7). Theta rhythmic neurons which were significantly more active during SWR epochs are described in Chapter 5 and the anatomical description of these neurons in found in Chapter 3.

I was able to label 17 of these theta rhythmic neurons of which 10 had recordings which allowed for analysis in both theta and SWR states (7 inhibited and 3 not changing during SWR epochs). A

total of 5 neurons which were inhibited or non-changing had projecting axons (M21c, M60a, M76a were inhibited and M63c and D55c did not change their firing frequency). Because M63c did not project to the hippocampus (but to the triangular septal nucleus) and D55c was recorded by Dr. Damien Lapray (anatomically characterised in Chapter 3) I did not use these neurons in this electrophysiological analysis.

4.2.1 The theta oscillation (3-6 Hz)

During hippocampal theta oscillation, neurons display a rhythmic firing pattern of bursts of action potentials phase locked to the hippocampal theta oscillation; characteristic of previously described "pace-making" neurons (Figure 4.1A). All neurons were significantly phase locked to theta oscillation recorded in CA1 stratum pyramidale ($p < 0.05$; Rayleigh's test; 24/24), firing a mean 5.3 ± 0.66 (ranging between 1.7 and 15.3) action potentials per cycle (n = 24 neurons) with a variance of 10.5 action potentials per cycle. The mean firing frequency during theta of rhythmic neurons was 20.4 ± 2.6 Hz (n = 24). Characteristic of these neurons is the high degree of phase locking, the mean r value being 0.55 ± 0.03 (n = 24; ranging between 0.22 and 0.82), combined with a high percentage of active cycles, the mean being 94.8 ± 1.5 % (ranging between 71.8 and 99.7 %). The high degree of phase locking, high percentage of active cycles produces the stereotypical rhythmic firing pattern previously published (Borhegyi et al., 2004) and shown in Figure 4.1A. The rhythmic firing pattern of these neurons is illustrated by the distinctive waves shown in the autocorrelogram (Figure 4.1C); each peak representing the next and previous theta cycle ~200 ms apart.

Rhythmic septal neurons are phase locked to a particular timing of the theta cycle (Figure 4.1B,E; also see chapter 5). Septal neurons which decreased, or did not change, their firing frequency during SWRs has mean firing phases non-uniformly distributed throughout the theta cycle (Rayleigh's test; $p < 0.05$; n = 24). The majority of neurons had a mean firing phase of between 262.5 and 330.3° (n = 15) with the remaining 9 neurons distributed throughout the rest of the theta cycle (Figure 4.1B). No significant correlation was found between maximal firing phase and maximal

number of action potentials per cycle (circular linear correlation; $r = 0.4$; $p > 0.05$; $n = 24$; Figure 4.1D).

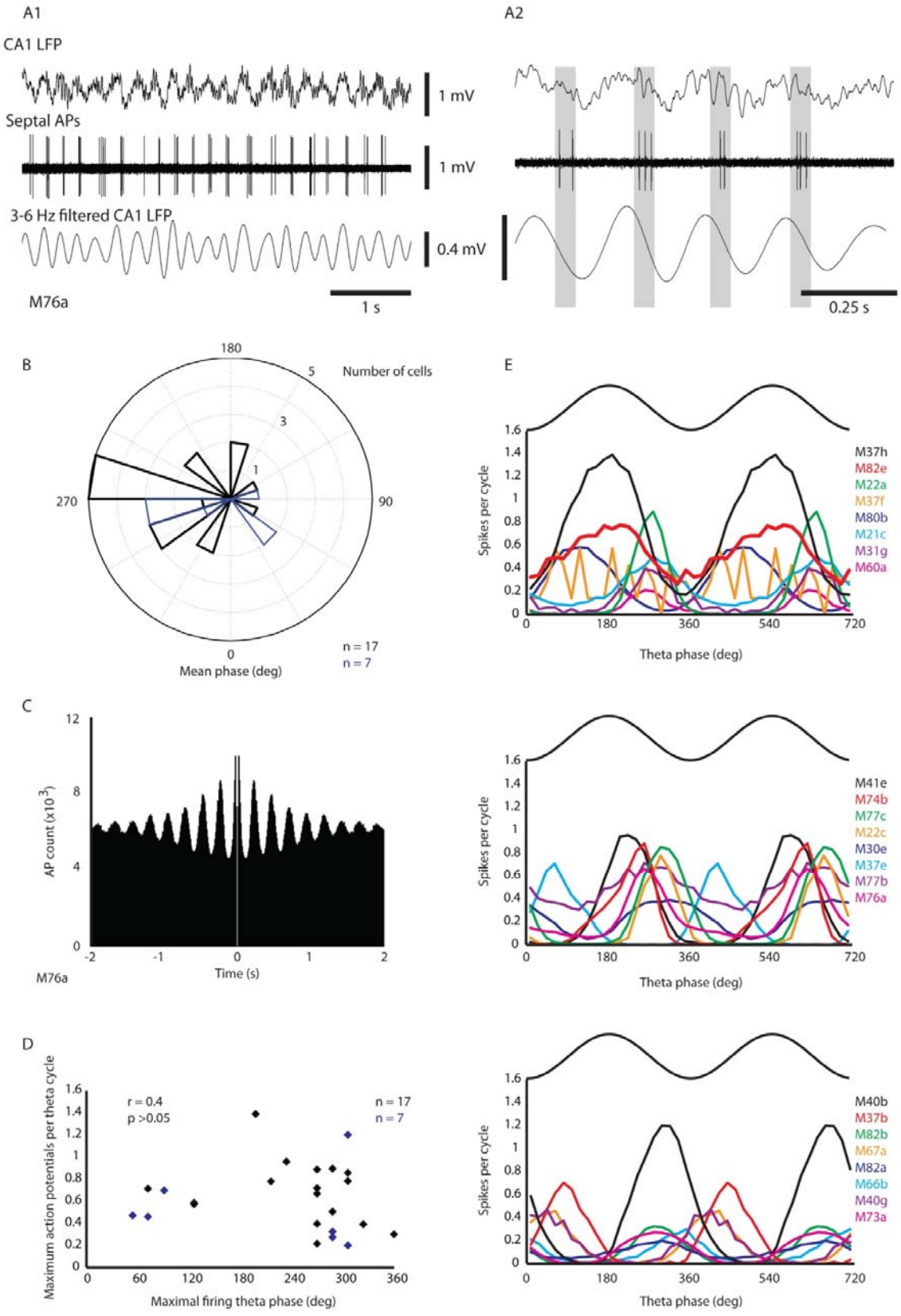

A1
CA1 LFP
1 mV
Septal APs
1 mV
3-6 Hz filtered CA1 LFP
0.4 mV
M76a
1 s
A2
0.25 s
B
180
5
Number of cells
3
1
270
90
0
Mean phase (deg)
n = 17
n = 7
C
AP count (x10^3)
12
8
4
0
-2
-1
0
1
2
Time (s)
M76a
D
Maximum action potentials per theta cycle
r = 0.4
p >0.05
n = 17
n = 7
0
60
120
180
240
300
360
Maximal firing theta phase (deg)
E
Spikes per cycle
M37h
M82e
M22a
M37f
M80b
M21c
M31g
M60a
0
180
360
540
720
Theta phase (deg)
M41e
M74b
M77c
M22c
M30e
M37e
M77b
M76a
M40b
M37b
M82b
M67a
M82a
M66b
M40g
M73a

Figure 4.1 – Theta related firing patterns of SWR inhibited and non-changing medial septal neurons. A1) A representative 5 second epoch of septal neuron (M76a) action potential firing during detected theta oscillation. CA1 local field potential (top) with regular ~4 Hz. Action potential firing (middle) occurring rhythmically and correlating with the hippocampal oscillation. The 3-6 Hz filtered trace (bottom). **A2)** One second firing epoch demonstrating the correlation between neuronal firing and theta oscillation. **B)** Rose plot histogram illustrating the mean firing phase of SWR inhibited neurons (black bars) and neurons which did not change their firing frequency during detected SWRs (blue bars). Zero equals the trough of the theta cycle; radial axis corresponds to number of cells. **C)** An autocorrelogram of firing during theta epochs (same neurons as shown in A). **D)** Scatter plot demonstrating the lack of correlation between mean firing frequency and maximal firing theta angle for SWR inhibited neurons (black), and neurons which did not change their firing frequency during SWRs (blue). Correlation coefficient and p value are shown for the circular correlation. **E)** Action potentials per theta cycle versus theta phase for each neuron in three separate graphs. For each: top, model sine wave shown in black. Two cycles are shown by duplicating data to avoid edge effects.

4.2.2 The sharp wave associated ripple oscillation (90-200 Hz)

As stated previously, the majority of the 34 rhythmic septal neurons recorded either suppressed their firing frequency (Figure 4.2A) or did not change their firing pattern significantly, when using a random shuffling method which compares the actual number of intra-SWR action potentials to that of random peri-SWR periods (script written by Linda Katona and Balint Lasztoczi; see Methods). I observed 17 neurons which fired significantly fewer action potentials than expected from a random firing probability during this time, and 7 which did not have a firing pattern significantly different from random firing probability (Mann-Whitney U; $p < 0.05$ and $p > 0.05$ respectively; $n = 17$ and 7) during periods defined as SWRs in CA1 stratum pyramidale (Figure 4.2B). The mean number of SWRs detected per recording was 37.1 ± 5.2; ranging from 8 to 116 detected SWR epochs. The mean firing frequency peri-SWR for supressed neurons was 19.9 ± 2.8 Hz significantly decreasing to 4.6 ± 1.4 Hz (Student's t test; $p < 0.05$; $n = 17$). I found that for neurons which did not significantly change their firing frequency, no significant change occurred as a population (Student's t test; $p > 0.05$; $n = 7$). The response for all neurons peri-SWR compared to intra-SWR can be seen in the normalised histogram (Figure 4.2C). A decrease can be seen throughout the SWR (black bars); three examples demonstrate single cell responses M40g (blue), M60a (red), and M82e (black). The neuron M40g demonstrates a firing pattern not related to, or not changing during, SWRs; M60a illustrates a neuron which decreases its firing during SWRs and has a relatively slow firing frequency; M82e is a neuron with a high firing frequency and also decreases firing frequency during SWRs. As a population the extent of suppression varied, the mean percentage change between peri-SWR firing frequency and intra-SWR was 77.6 ± 4.9 % for inhibited neurons ($n = 17$). I observed only 2 neurons which were completely suppressed (M31g and M73a) during SWRs.

I was interested in the time scale of by which these neurons alter their firing during SWRs, both in the initial decrease in firing, but also in the return to baseline firing frequency. For this I looked at the spike timing relative to the peak of SWRs in real time for all neurons, to define an average normalised response during these epochs. By normalising the spike number for each neuron in 10

ms bins centring on the peak of the SWR I could look at the timing of the response (Figure 4.2D). I compared each 10 ms bin to an arbitrary baseline of -150 ms from the peak of SWRs. Spike counts significantly different from baseline occurred -50 to +80 ms after the peak of SWRs (Paired Student's t test; $p < 0.05$; $n = 17$), after this spike count was not different from baseline ($p>0.05$). In normalised spike count, from 0 being the bin with the least spikes to 1 being the bin with the greatest spike count, baseline (- 150 ms) was 0.5 ± 0.06. At the SWR peak normalised spike count was 0.09 ± 0.04 ($p > 0.05$), and reach a minimal value of 0.07 ± 0.02 10 ms after the peak of the SWR ($p < 0.05$; Figure 4.2D). Spike count returned to baseline 90 ms after the peak of SWRs at 0.34 ± 0.05 ($p>0.05$). I conclude that the inhibition of firing seen in SWR inhibited septal neurons closely follows the timing of the peak of the SWR recorded from CA1; firing suppression rapidly occurs before the peak (~50 ms) of the SWR event and is sustained for ~80 ms.

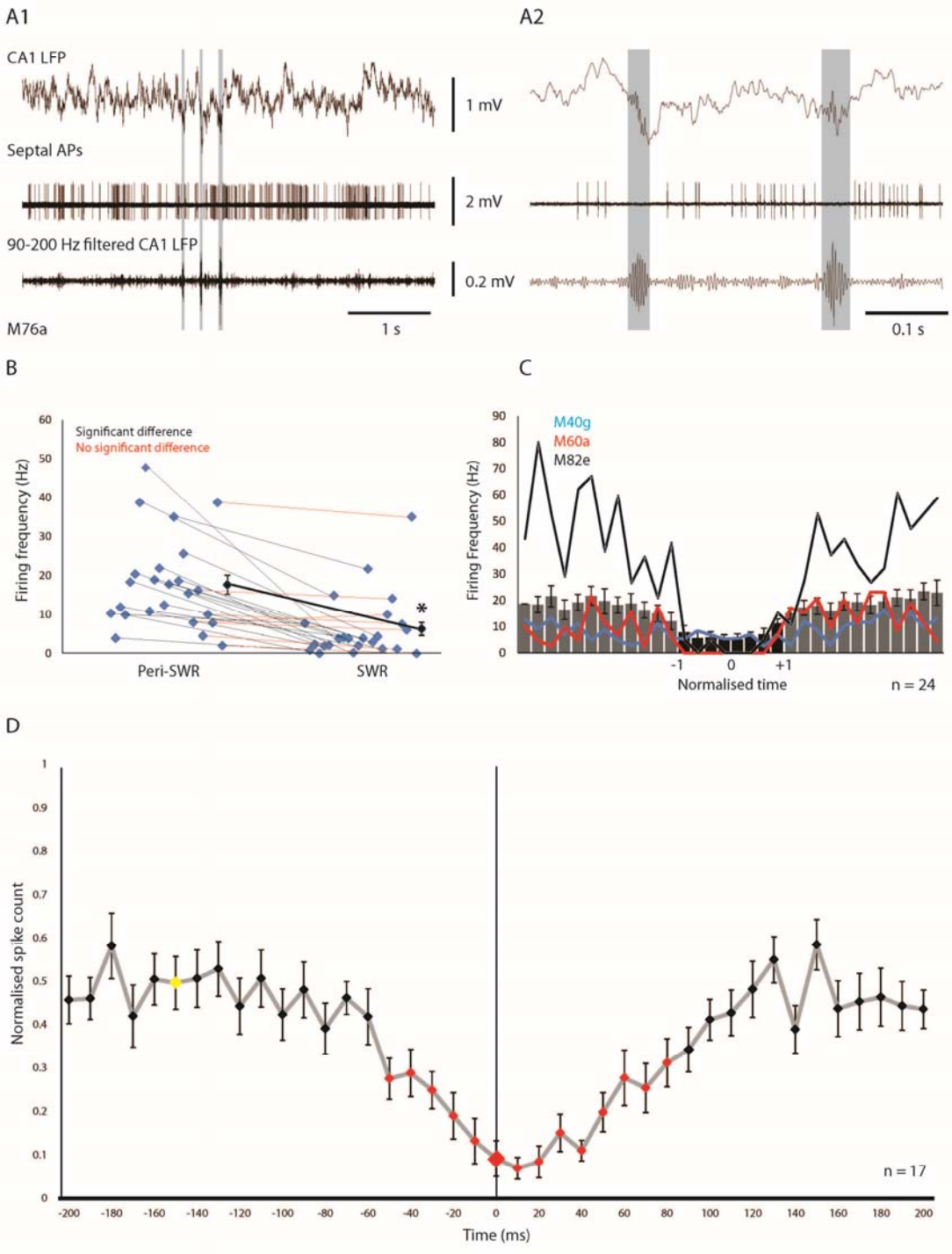

A1
CA1 LFP
1 mV
Septal APs
2 mV
90-200 Hz filtered CA1 LFP
0.2 mV
M76a
1 s
A2
0.1 s
B
Significant difference
No significant difference
Firing frequency (Hz)
Peri-SWR
SWR
*
C
M40g
M60a
M82e
Firing Frequency (Hz)
-1
0
+1
Normalised time
n = 24
D
Normalised spike count
Time (ms)
n = 17

Figure 4.2 – Sharp-wave ripple dependent activity of medial septal neurons. A1) A 5 second representative epoch of the activity of a SWR inhibited neuron (M76a) are SWR events recorded in CA1 (highlighted in grey). Sharp-waves are visible in the CA1 local field potential (top). Action potential firing of the neuron (middle) occurred around, but not during the SWR events (grey bars). Irregular activity can be seen in the non-theta, non-slow oscillation period flanking the detected SWRs. Filtered 90-200 Hz trace (bottom) showing the relatively large amplitude events corresponding to the ripple oscillations. **A2)** A 1 second period containing SWR events present in A1). Action potentials occurred before and after each event, but not during the detected SWR periods. **B)** Peri-SWR and SWR firing frequencies for each neuron. Mean ± SEM is shown by the black diamond (asterisk: $p<0.05$ paired Student's t-test; n = 24) **C)** Normalise time histogram showing firing frequency for the population (black bars are the defined SWR period, the peak at 0; -1 and +1 represent start and end of SWRs respectively. Grey bars signify peri-SWR period). Three individual neurons are included as examples of firing pattern during SWR. **D)** Line graph of normalised spike count ± SEM in real time relative to the peak ± 200 ms of SWRs for neurons which were inhibited during SWRs. Zero represents the peak of the ripple oscillation power. Around the SWR peak spike count significantly decreased (red) compared to 150 ms before the SWR (yellow; paired Student's t test; $p< 0.05$; n = 17**)**.

4.2.3 Theta rhythmic neurons, both those inhibited and not changed by SWRs, are septo-hippocampal projection neurons.

Of the electrophysiologically defined neurons presented in this chapter, 4 which were labelled and recorded by myself, as well as D55c (by Damien Lapray) represent the first anatomically confirmed, *in vivo* electrophysiologically characterised, septo-hippocampal neurons to date; including the first electrophysiologically defined septo-triangular nucleus neuron (M63c). Detailed anatomical descriptions, including immunohistochemical characterisation of the hippocampal targets of M76a and D55c can be seen in Chapter 3.

Of the 4 neurons with firing patterns described in this chapter and which projected to the hippocampus, 3 were inhibited during SWRs and 1 neuron did not change its firing frequency. The SWR inhibited neurons (including M76a described anatomically in chapter 3) had mean theta phases around the descending region of the theta cycle, as do the majority (262.5, 270.6, and 264.8°; Figure 4.3A). The single neuron (D55c) which did not change its firing frequency during SWRs had a mean theta phase of 150.8°. As discussed in Chapter 3, all neurons displayed a similar immunohistochemical profile with the notable exception of M21c lacking detectable PV immunoreactivity (Table 4.1).

4.2.4 Septo-hippocampal neurons which display similar theta phase preference do not share an axonal distribution within the hippocampus.

A key aim of this study is to address whether network-dependent firing patterns are predictive of the hippocampal axon of single septo-hippocampal neurons. Although having similar mean theta phase (Figure 4.3C-E1) the axonal arbour of the three SWR inhibited neurons was dramatically different, occupying primarily non-overlapping regions. The neuron M21c, although only partially filled, was observed projecting a main axon into the ventral hippocampus in the lateral alveus surrounding CA3 (Figure 4.3C2); whereas M60a projected into the midline region of CA1 with a small number of visible boutons present in stratum pyramidale (Figure 4.3D2). The neuron M76a

(fully described in chapter 3) innervated primarily the dentate gyrus of dorsal hippocampus (Figure 4.3D2). This is highly suggestive that the mean theta phase of a single septo-hippocampal neuron is not predictive of the axonal arbour location. Both neurons M21c and M60a were only partially filled and apart from a small number of boutons, only the main axon could be seen with light microscopy; therefore it is possible that the full extent of the axonal field is not represented by the main axon location, with branches throughout the hippocampus. With only the main axon visible however, they are still distinct in location from the two putatively fully labelled neurons M76a and D55c.

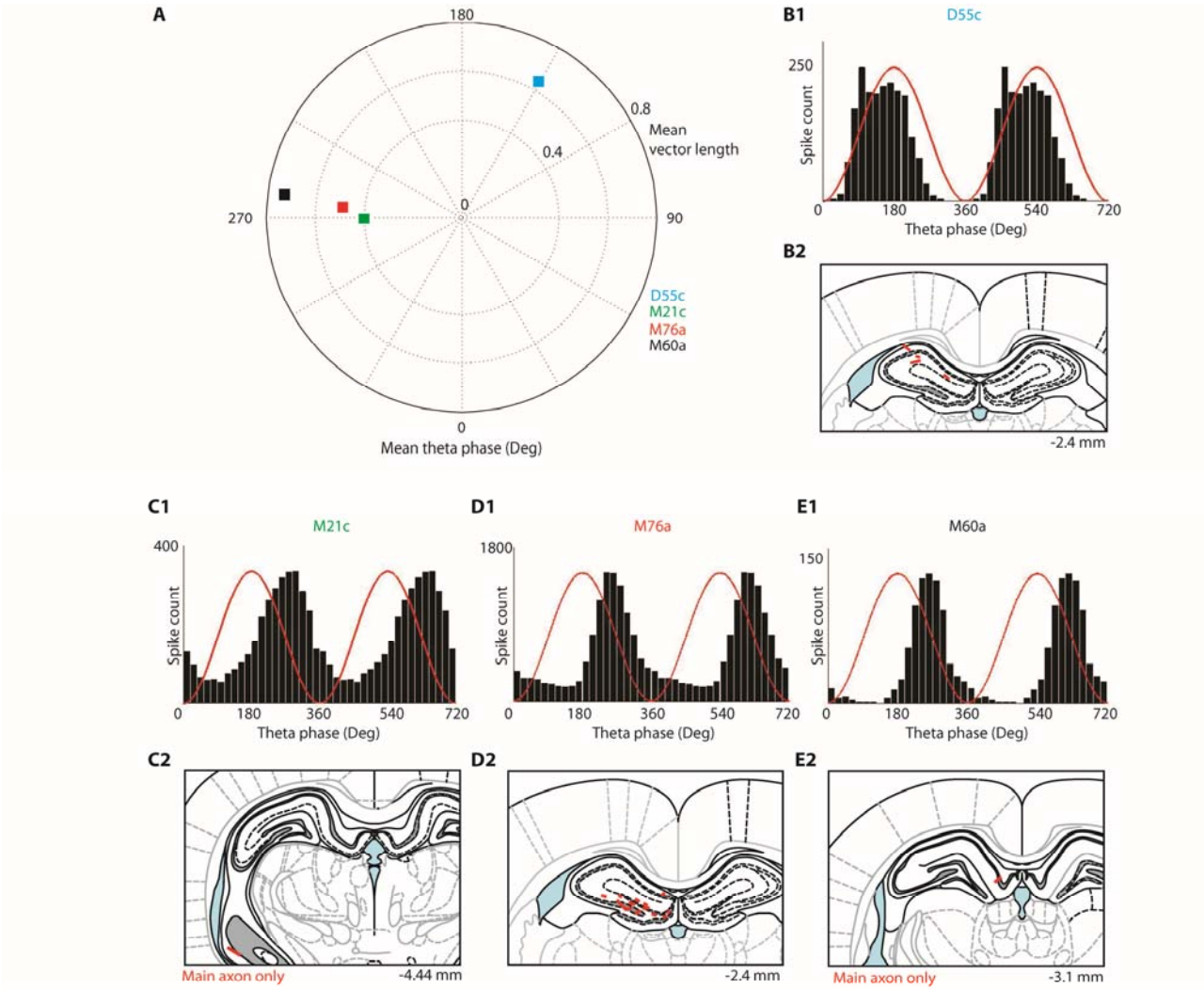

A
180
0.8
0.4
Mean
vector length
0
270
90
0
Mean theta phase (Deg)
D55c
M21c
M76a
M60a
B1
D55c
250
Spike count
0
180
360
540
720
Theta phase (Deg)
B2
-2.4 mm
C1
M21c
400
Spike count
0
180
360
540
720
Theta phase (Deg)
D1
M76a
1800
Spike count
0
180
360
540
720
Theta phase (Deg)
E1
M60a
150
Spike count
0
180
360
540
720
Theta phase (Deg)
C2
Main axon only
-4.44 mm
D2
-2.4 mm
E2
Main axon only
-3.1 mm

Figure 4.3 – relationship between mean theta phase and axonal location for septo-hippocampal neurons. A) Polar plot of the mean theta phase of 4 anatomically confirmed septo-hippocampal neurons with the radial axis being mean vector length. The SWR inhibited neurons group around the middle of the descending region of the theta cycle. Neurons are colour coded. **B-E1)** Theta phase histogram for each neuron. Sine wave shown in red; two cycles included for clarity. **B-E2)** Schematic of main axonal location observed within the hippocampus. The red bands represent regions with axon and distances are approximate relative to bregma. For neurons M60a and M21c, the red bar indicates only the approximate location of the main axon; the full antero-posterior extent of all cells is not represented here (adapted from Paxinos and Watson, 6th edition).

Table 4.1 – Summary of immunohistochemical tests performed on anatomically confirmed septo-hippocampal neurons which were either SWR inhibited, or did not change their firing frequency.

For a full description of the anatomical analysis of septal neurons see Chapter 3.

Name	Type	PV	SATB1	CR	CB	HCN4	KV1.1	VGAT	VAChT	VGluT2	Necab1
D55c	SWR N.C.	+	+			+	-	+	-	-	
M21c	SWR inhibited	-	+		-	+		+			
M60a	SWR inhibited	+	+	-		+	+				
M76a	SWR inhibited	+	+			+		+			-

4.3 Discussion

Using the juxtacellular recording and labelling technique I have described the most commonly sampled firing pattern of rhythmically firing medial septal neurons; that is theta rhythmic, phase-locked, which is supressed during sharp-wave ripples. A number of neurons which displayed a similar firing pattern during theta oscillation did not significantly change their firing pattern during SWRs. Importantly, the mean phase of action potentials occurring during theta oscillation did not correlate with the axonal location within the hippocampus.

During CA1 hippocampal theta oscillation a large proportion of septal neurons displayed a firing pattern similar to that previously published (Dragoi et al., 1999, Borhegyi et al., 2004, Simon et al., 2006, Varga et al., 2008). The firing pattern displayed by these neurons, theta phase locked and rhythmic firing correlates with a GABAergic, PV-expressing, septo-hippocampal phenotype published by others (Borhegyi et al., 2004, Simon et al., 2006, Varga et al., 2008, Villette et al., 2010), and demonstrated in this chapter and Chapter 3.

Previous recordings of both single and multiple rhythmic septal neurons have demonstrated that as a population they display a wide range of preferred theta phases to which any given neuron may display phase locking (Borhegyi et al., 2004, Varga et al., 2008). However, a recent study found that GABAergic septal neurons which express HCN1 may group into one of two preferred phases of theta, approximately the ascending phase and the trough (Varga et al., 2008). All rhythmic neurons, both HCN1- expressing and not, display phase preferences which occur throughout the whole theta cycle. Here, I have grouped neurons by the response during SWR oscillations. Neurons which are suppressed during SWRs or do not change their firing frequency, most frequently displayed a theta oscillation phase prefers during the descending phase; this contrasts with the groupings found in Varga et al., (2008) which did not find a distribution of rhythmic neurons which fired preferentially during this time. Although the fundamental firing properties of these neurons are similar, the

difference in phase relationship between this study and the published work may be due to methodological differences.

Two fundamental differences may explain the differences in phase distribution: a difference in medial septal neurons sampled, or a difference in the reference phase information (i.e. hippocampal theta phase) sampled. The neurons presented by Varga et al., (2008) display differences in axonal structure from the neurons which I have observed. Namely, the neurons presented in the published study have descending axons, as well as a dorsally projecting putative hippocampal axon, whereas the neurons I labelled and observed did not often display this axonal feature. In only a single case was this observed and the neuron was located more ventral than most (neuron M35h). From personal correspondence with Dr. Zsolt Borhegyi, an author of this study, they sampled and analysed septal neurons only after having observing a rhythmic neuron which was then disgarded. This suggests they may have sampled a different group of deeper neurons than I did, possibly within the vertical diagonal band. In my study, all rhythmic neurons were recorded and sampled irrespective of depth. This suggests that deeper neurons those sampled by Varga et al., (2008), display a different distribution of preferred theta phases than more superficial neurons sampled in my study.

The hippocampal theta oscillation is not a uniform wave and has been demonstrated to act as a travelling wave, changing in phase across the dorso-ventral axis (Lubenov and Siapas, 2009, Patel et al., 2012). In this study I have used a consistently placed reference electrode within dorsal CA1 stratum pyramidale from which all phase preference data for each single medial septal neuron is the calculated. Over the septo-temporal axis the phase of theta shifts ~180 degrees. A difference in reference electrode position relative to the theta travelling wave could result in a phase shift which could account for the differences seen between this study and the published study. Theta phase shift occurs with depth through the strata of hippocampal regions also; theta recorded in stratum alveus/oriens is phase coherent with stratum pyramidale, however deeper than this a

gradual phase shift results in 180 degree shift in mid stratum radiatum (Buzsáki et al., 1983). A consistent reference placement within stratum pyramidale means that phase information can be compared between recordings and studies. Both studies which reported the bimodal distribution of phase preference, state a reference electrode placement within dorsal CA1 stratum pyramidale although no medio-lateral or antero-posterior co-ordinates are given. The difference in exact location of reference electrode could explain the discrepancy in phase.

As suggested in the previous chapter medial septal neurons may innervate relatively small regions of the hippocampus. Future studies could sample multiple regions of the hippocampus, by using a tetrode array or silicon probe for example (Montgomery et al., 2009), to find the region which most couples to the septal neuron. The best reference which could provide the most informative local field potential is that which comes from the region directly innervated and influenced by the efferent neuron. Further, using electrodes at multiple depths to sample large groups of medial septal neurons at the same time, the effect of depth on preferred theta phase could test the hypothesis that the dorso-ventral axis of the septum and vertical diagonal band produces a shift in phase preference of the neurons which may account for the results found in previous studies (Borhegyi et al., 2004, Varga et al., 2008).

Grouping was also found in the group of neurons which did not significantly change their firing pattern during SWRs. The majority of these neurons also displayed a preferred firing phase during the descending phase. Previous studies have not to my knowledge investigated the SWR response of neurons with a defined theta preferred phase, although neurons which do not change their firing pattern have been previously described (Dragoi et al., 1999, Borhegyi et al., 2004, Varga et al., 2008). These neurons may release GABA to their synaptic targets in a SWR-independent fashion, or alternatively, are coupled to SWRs not detected by the reference electrode in CA1 but that occur elsewhere in the hippocampus. There is a high level of co-occurrence between SWRs in different areas of the hippocampus however, as well as those which occur in the subiculum and entorhinal

cortex (Chrobak et al., 2000, Csicsvari et al., 2000, Patel et al., 2013). These events are not static within the hippocampus at least. The event is initiated in a small region and may stay local, may occur synchronously throughout large regions, may travel directionally after initiation and may split into multiple travelling events (Patel et al., 2013).

The role of these two septal firing patterns in theta oscillation rhythmogenesis may be comparable: providing GABAergic inhibition to hippocampal interneurons during the descending phase of the theta oscillation, but their roles during SWRs differ. This may correlate with the interneuron target of these two types given that interneurons, which differ in spatial distribution of their axon in relationship to pyramidal neurons and have firing patterns which differ during these two network states (Somogyi, 2010). As described in Chapter 3, a fraction of the interneuron targets of two neurons in this study are known, that is: M76a (264.8° mean theta phase; SWR inhibited) which innervated putative axo-axonic neurons, and D55c (150.8° mean theta phase; SWR not changed) which innervated bistratified and/or double projection neurons. In both cases, the septo-hippocampal neurons fire maximally at the time when the interneuron target is decreasing its firing frequency. Axo-axonic neurons are maximally active at the peak of theta oscillation (Klausberger et al., 2005, Viney et al., 2013) and receive GABAergic inhibition maximally from the neuron M76a at 264.8°, during the descending phase. Likewise bistratified and double projection neurons fire maximally during the trough of the theta cycle (Klausberger et al., 2004, Jinno et al., 2007) and receive GABAergic inhibition maximally during the peak from D55c at 150.8°. This provides the first evidence that theta phase information may be predictive of interneuron target in septo-hippocampal neurons; but as described not hippocampal axonal location. When synchronously stimulated septo-hippocampal GABAergic neurons reduce the firing frequency of hippocampal targets and disinhibit pyramidal neurons (Toth et al., 1997). This represents an abnormal synchronous condition with inhibition removed from all pyramidal cell domains at once; *in vivo*, interneurons fire at different phases of theta with inhibition dynamically redistributing at different pyramid cell domains at different times during the theta cycle (Somogyi et al., 2014). Here I present

a substrate for this dynamic redistribution, with single septo-hippocampal neurons, by inhibiting preferred interneuron types act to disinhibit a pyramidal cell domain. The sequential firing of septal neurons throughout the theta cycle may inhibit different interneurons and providing the sequence of firing seen *in vivo* (Somogyi, 2010).

During theta oscillation the firing frequency of rhythmic septo-hippocampal neurons varied remarkably by between 5 and 55.5 Hz. An increased firing frequency likely correlates with an increased release of GABA to the post-synaptic target, pre-synaptic activity magnitude correlates with post-synaptic activity magnitude (Kay et al., 2011). High firing neurons may produce a stronger phase locking in the hippocampal interneuron target due to a greater summed GABA-dependent inhibitory potential. Integration of inhibitory signals in interneuron cellular domains has not been studied extensively to my knowledge, and as is described in the previous chapter, the distribution of synapses throughout interneuron cellular domains may not be uniform. Some interneuron types have a high degree of phase locking to hippocampal theta oscillation. Interneurons, which have a high firing rate during theta epochs and a high degree of phase locking such as axo-axonic neurons, may receive an input from septal neurons which have a higher firing frequency and are capable of producing strong phase locking of highly excitable neurons. Interneurons with a high firing rate may receive larger amounts of network state-dependent tonic excitation, or are more highly intrinsically excitable as has been seen *in vitro* with fast spiking neurons for example (Goldberg et al., 2008). This in turn may require greater phase locked inhibition to entrain the neuron to the on-going theta frequency, than neurons which are less excitable.

The majority of rhythmic septo-hippocampal neurons decrease their firing frequency during SWR epochs relative to peri-SWR periods. It is hypothesised that this suppression of firing allows for the post-synaptic interneuron target to have a corresponding increase in firing frequency during SWR, as is observed in PV-expressing bistratified and basket neurons (Klausberger et al., 2004, Klausberger et al., 2005, Lapray et al., 2012). A reduction of inhibition from the septum, alone or in

combination with an increase in SWR-dependent excitation from pyramidal neurons may result in an increase in interneuron firing frequency, for example the increase in bistratified and PV-basket cell firing which occurs during SWRs (Cutsuridis and Taxidis, 2013).

Borhegyi et al., (2004) demonstrate that inhibition of medial septal cells during SWRs was longer than the detected SWRs; this is supported by the average length of inhibition found in this study of 130 ms compared to the reported durations of 40-120 ms (Kudrimoti et al., 1999; Ylinen et al., 1995; Csicsvari et al., 2000). The SWR may be a travelling event, capable of propagating across regions of the hippocampus (Patel et al., 2013). Technically it is difficult to confidently detect the beginning or end of a SWR, given that a SWR occurring far from your electrode will be of a smaller amplitude and may only surpass the detection threshold after the actual initiation which cannot be detected by volume conductance. The movement of a SWR away from the reference site (where it is detected) may lead to the artificial detection of the SWR end point. A SWR, like all LFP events, is a product of a sequence of cellular electrical events. It can be assumed then that as the SWR moves new groups of pyramidal neurons and interneurons are recruited to produce the oscillation; this includes GABAergic projections neurons to the septum. The prolongation of septal inhibition may represent a sequence of inhibitory input from GABAergic projections neurons as a travelling SWR recruits them and maintains SWR-dependent inhibition to septal neurons. The combination of large scale electrophysiological measurement of LFP with calcium imaging of identified GABAergic projection neurons would identify if travelling SWRs recruit neurons in this manner.

The degree of firing frequency suppression during SWR varied from complete inhibition to no significant change in firing pattern, although most neurons in this study did not reach firing probability of zero during SWRs. The decreased (or maintained) firing frequency during SWR may result in the reduced inhibition to allow for increased firing of the interneuron targets, but may still provide modulatory inhibitory activity during the SWR in a manner independent of the ripple oscillation, although not the extent of SWR active neurons described in Chapter 5; (Dragoi et al.,

1999; Borhegyi et al., 2004). It is an important caveat that using a single reference electrode only a proportion of the SWRs are sampled. Inhibition, both somatic and dendritic, plays an active role during SWRs (Cutsuridis and Taxidis 2013). Septal neurons, in this chapter were rarely completely suppressed and were not observed to be phase coupled to the ripple oscillation suggesting they do not play a role in modulating the phase of the post-synaptic neurons. A temporally undefined inhibition during SWRs could act to shunt excitation which is found at the domains innervated by the medial septum, producing a higher relative excitation of inputs from synapses at distinct locations from the septal inhibitory inputs.

The current model of SWR-dependent inhibition of septo-hippocampal neurons is via the GABAergic double projection somatostatin-expressing neurons which project to both the medial septum, and the subiculum (Jinno et al., 2007; Fuentealba et al., 2008). Double projection neurons increase their firing during SWRs and locally target interneurons (Jinno et al., 2007), they are reciprocally connected to GABAergic septo-hippocampal neurons (Takacs et al., 2008). This study demonstrates that septo-hippocampal neurons reduce their firing frequency 50 ms before the peak of the ripple oscillation and continue to be suppressed for ~130 ms. This correlates with the increase in firing frequency of hippocampo-septal neurons, suggesting a role with the SWR resulting in the inhibition of septal neurons. However, because of the reciprocal nature of the connectivity, directionality of the SWR-dependent firing effects, i.e. suppression of septal and excitation of hippocampal neurons, is correlative. The genetic tagging of hippocampo-septal neurons alone combined with the optogenetic activation *in vivo* would allow a better understanding of the time scale of inhibition produced by these neurons onto septal neurons. Likewise the optogenetic inactivation of septo-hippocampal neurons would allow one to test the directionality to this pathway: is septo-hippocampal inactivation of this group of neurons sufficient to increase the firing frequency of hippocampo-septal neurons? I hypothesise that the increased SWR-dependent pyramidal cell excitation of hippocampo-septal neurons, combined with the suppression of septal inhibition, is required to produce the firing behaviour seen *in vivo*.

Two of the 3 fully characterised neurons innervated projection neurons, as well as another type (M44 innervated PV-expressing basket cells, and D55c innervated bistratified cells). The proposed feedforward inhibition of the reciprocal connected septo-hippocampal neurons by hippocampo-septal neurons would produce a disinhibition of any other neuron also innervated by the septo-hippocampal neurons. Both PV-expressing basket cells and bistratified cells display SWR-dependent firing frequency increases (Klausberger et al., 2004; Lapray et al., 2012).

In this chapter I have described populations of septal projection neurons which are rhythmic firing during theta oscillation, and may either decrease their firing frequency, or not change their firing frequency during hippocampal SWR epochs; this includes the first examples of anatomically defined septo-hippocampal neurons. Neurons suppressed during SWRs tend to display a mean firing phase during the descending phase of the theta oscillation which is not predictive of axonal location within the hippocampus. This is suggestive of diversity within septal neurons which was previously unknown and requires more study to understand the implications of how neurons with a similar firing pattern can innervate distinct hippocampal regions.

Chapter 5 - Characterisation of sharp-wave ripple active neurons of the medial septum.

A portion of this chapter has been published in:

Viney TJ*, Lasztoczi B*, Katona L*, Crump MG*, Tukker JJ, Klausberger T, Somogyi P (2013) Network state-dependent inhibition of identified hippocampal CA3 axo-axonic cells *in vivo*. Nat Neurosci 16:1802-1811.

5.1 Introduction

Previous studies have demonstrated the influence of the medial septum on the activity of the hippocampal network during theta oscillations (Green and Arduini, 1954, Petsche et al., 1962) which occur during movement and paradoxical sleep. I examined how the same septo-hippocampal circuit behaves during another behaviourally-relevant network state: sharp-wave associated ripple activity (SWR). As the septo-hippocampal pathway is a dominant input to hippocampal interneurons and hence able to define and temporally coordinate their firing during theta epochs, it may influence them in other network states.

During quiet wakefulness, consummatory behaviour and slow wave sleep as well as during awake behaviour (Buzsáki et al., 1983, Csicsvari et al., 2000, Foster and Wilson, 2006, O'Neill et al., 2006), large amplitude voltage events accompanied by a high frequency nested oscillatory component occur in the hippocampus (Buzsaki et al., 1992). These events, are collectively termed the sharp-wave associated ripple oscillations (SWR; for further description see Chapter 1).

Sharp-wave associated ripple oscillations rely on the precise temporal and spatial organisation of the hippocampal circuit. Like theta generation, high frequency oscillations involve the interneuron-dependent local release of GABA to spatially distinct domains of the pyramidal neurons (Nimmrich et al., 2005, Ellender et al., 2010, Lapray et al., 2012, Varga et al., 2012). Interneurons of different types have different firing patterns during the SWR event depending on both intrinsic conductances and synaptic inputs, as shown *in vitro* and *in vivo*. Bistratified, PV-expressing basket, or hippocampo-septal projection cells respond with depolarisation and increased spiking activity. Other interneurons, such as the axo-axonic cells appear to be inhibited (Klausberger et al., 2004, Fuentealba et al., 2008b, Lapray et al., 2012, Varga et al., 2012). The roles of these interneurons during a SWR is likely to be different. One would predict that the spike timing of GABAergic septal inputs to active or inactive cell populations would be different if the firing of septal neurons during the SWR was relevant to the network. Indeed, differences in SWR firing of septal neurons have

been observed. The canonical response of medial septal GABAergic rhythmic neurons is a decreasing spike occurrence and frequency during SWRs as demonstrated in previous studies *in vivo* (Dragoi et al., 1999, Borhegyi et al., 2004). GABAergic somatostatin-expressing projection neurons of the hippocampus, the hippocampo-septal neurons, densely innervate the medial septal neurons and increase their firing frequency in response to SWRs (Toth et al., 1993, Takács et al., 2008). *In vivo* these neurons fire bursts of action potentials during SWRs and are a potential source of the inhibition to medial septal GABAergic neurons (Jinno et al., 2007). Fewer neurons do not respond to the SWR events as their firing does not change significantly (Dragoi et al., 1999). Interestingly a small number of medial septum neurons increased their firing by >50% compared to the 250 ms peri-ripple periods. It was not demonstrated these cells were septo-hippocampal neurons or GABAergic (Borhegyi et al., 2004, Varga et al., 2008). The activation of medial septal neurons during SWRs is unexpected as there are no known excitatory inputs from the hippocampus to the medial septum. It is unknown where these SWR active neurons project to and if they are septo-hippocampal. I sought to determine if SWR active rhythmic firing septal neurons are GABAergic and septo-hippocampal projection cells, and if so which neurons are innervated by these cells. Is the inhibition of axo-axonic neurons, which may allow the disinhibition of pyramidal neurons during SWRs partially dependent on the septum? (Although Hajos N. has demonstrated that in slice axo-axonic neurons still receive inhibition during SWR; unpublished). I tested the hypothesis that SWR active septal cells differ from the septo-hippocampal neurons which are inhibited during these events; in protein composition, and/or through a distinct input or anatomical feature.

Here, I describe a relatively sparse population of medial septum neurons which are activated during the SWR event. I demonstrate that: their rhythmic firing of action potentials cluster around the trough of the theta oscillation, have firing parameters which are indistinguishable during theta epochs from SWR inhibited neurons, and project to the hippocampus. I will also describe a new medial septal neuronal type with an ascending/peak theta phase firing preference, which is

activated during SWRs and projects outside of the hippocampus via the dorsal fornix-dorsal cerebral white matter.

5.2 Results

Using the juxtacellular recording and labelling technique to investigate putative GABAergic septo-hippocampal neurons I found a small population of neurons (n=11) in my data set, which fired during SWR under anaesthesia. I was able to label 5 of these neurons, 4 of which were sufficiently labelled for the identification of a projecting axon.

5.2.1 The sharp wave associated ripple oscillation (90-200 Hz)

Eleven out of 37 recorded rhythmic medial septum neurons were verified as SWR active cells using a random shuffling method which compares the actual amount of intra-SWR firing to that of random peri-ripple periods (script written by Linda Katona and Balint Lasztoczi). I showed that these neurons fire significantly more action potentials than would be expected from a random firing probability (Mann-Whitney U; $p<0.05$) during periods of CA1 LFP defined as SWRs. The average number of SWRs detected for each neuron was 46.36 ± 4.13 and SWR active neurons fired action potentials in 78.15 ± 3.65 % of these SWRs. Figure 5.1 illustrates the firing patterns of these neurons in the context of the SWR network state. For many of these neurons the increase in firing frequency and action potential number was clearly visible compared to the peri-SWR periods (Figure 5.1 A1, A2). The firing frequency during the SWR periods compared to the 10 s peri-ripple periods is significantly higher, with neurons firing at 11.84 ± 3.12 Hz peri-ripple and rising to 28.3 ± 5.16 Hz during the SWR periods (paired Student's t-test; $p<0.05$; n = 11; Figure 5.1 B). This demonstrates that under anaesthesia, a subset of medial septal neurons significantly increases their firing frequency during CA1-detected SWR periods.

Next I examined the firing patterns associated with the SWR events for each of these SWR active neurons. Both peri- and intra- SWR firing frequency is variable in these cells (coefficient of variation 0.87 and 0.58 % respectively). Action potential timing relative to the SWR varied for each of the

cells. As a population the maximal firing relative to the SWR period is after the peak, during the detected SWR periods (Figure 5.1 C). In real time, maximal firing of the population is -6.4 ± 12.5 ms after the peak amplitude of the SWR in CA1, but could be as early as – 50 ms from the peak, or as late as 100 ms after. Peri-ripple levels returned in < 200 ms. In two cases (2/10 neurons; cells M65b and M75a) the action potentials of these neurons were significantly phase-modulated to the ripple oscillation with mean phase preference of 220.4 ± 69.9 and 132.2 ± 64.5 degrees respectively (Rayleigh's test; $p<0.05$; $r= 0.26$ and 0.37 respectively; Figure 5.1 D1, D2).

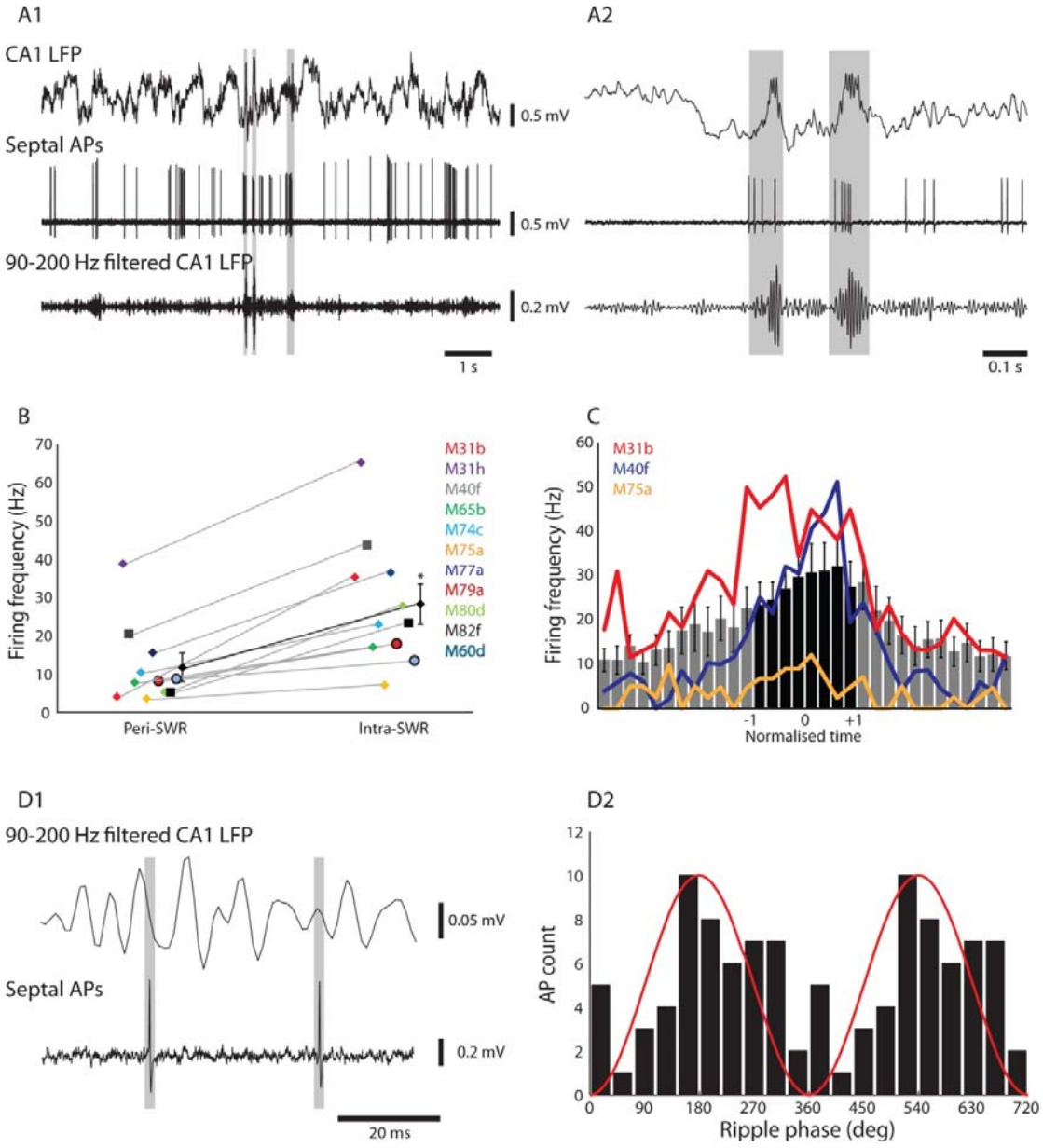

A1
CA1 LFP
0.5 mV
Septal APs
0.5 mV
90-200 Hz filtered CA1 LFP
0.2 mV
1 s
A2
0.1 s
B
Firing frequency (Hz)
M31b
M31h
M40f
M65b
M74c
M75a
M77a
M79a
M80d
M82f
M60d
Peri-SWR
Intra-SWR
C
Firing frequency (Hz)
M31b
M40f
M75a
-1
0
+1
Normalised time
D1
90-200 Hz filtered CA1 LFP
0.05 mV
Septal APs
0.2 mV
20 ms
D2
AP count
0
90
180
270
360
450
540
630
720
Ripple phase (deg)

Figure 5.1 – Sharp-wave ripple dependent activity of a subset of medial septal neurons. A1) A 10 second representative epoch of the activity of a SWR active neuron (M82f) around SWR events recorded in CA1 (highlighted in grey). Positively deflected sharp-waves are visible in the CA1 local field potential (top). Action potential firing of the neuron (middle) occurred both within SWR events (grey bars) and during slow oscillation network state. Filtered 90-200 Hz trace (bottom) shows large amplitude events corresponding to the ripple oscillation. **A2)** A one second period containing SWR events in A1. Action potentials occurred from the start of the detected SWRs. **B)** Peri-SWR and SWR firing frequencies for each of the SWR activate neurons. Each neuron is colour coded and mean ± SEM is shown by the black diamond (asterisk: $p<0.05$ paired Student's t-test; $n = 11$). **C)** Normalised time histogram showing firing frequency for the population (black bars are the defined SWR period, the peak at 0; -1 and +1 represent start and end of SWRs respectively. Grey bars signify peri-SWR period). Three individual neurons are included as examples of firing pattern during SWR. **D1)** A 0.1 s SWR epoch of neuron M65b showing action potentials occurring relative of the ripple oscillation. **D2)** Action potential histogram of neuron M65b during the ripple oscillation showing significant phase locking (Rayleigh's test; $p<0.05$; $r = 0.26$).

5.2.2 The theta oscillation (3-6 Hz)

During theta oscillations in CA1, SWR active neurons display characteristic rhythmic activity at theta frequency (Figure 5.2 A1, A2; similar to those presented earlier (Borhegyi et al., 2004)). Neurons were significantly phase-locked to the CA1 hippocampal LFP (Rayleigh's test; $p<0.001$; n=11/11). The degree of phase locking was also strong, the mean r value being 0.64 ± 0.03 (between 0.46 and 0.76; n=11/11). During theta oscillation the mean ± SD firing frequency was 23.3 ± 13.6 Hz. Another characteristic feature of these neurons is the high proportion of active cycles, the mean being 97 ± 0.97 % (range, 90.6 to 99.8 %). This strongly phase locked, and very consistent firing pattern identifies these cells as rhythmic neurons (Figure 5.2 B). The rhythmic firing of these neurons occurred at a preferred phase of the theta oscillation in a cell-dependent manner. An interesting feature of these neurons is the apparent relationship between firing rate and phase (Figure 5.2 C1). A circular-linear correlation was performed using the circular statistics toolbox for MATLAB (Berens, 2009) between mean firing frequency and mean firing phase and showed a significant correlation (Figure 5.2 C2; circular linear correlation; $r = 0.84$; $p <0.05$; $n = 11$). The highest firing frequency was observed at the descending phase, with frequency decreasing as phase progressing to the ascending phase and peak. Seven of the ten neurons had a mean firing phase which is ± 90 degrees from the trough (Figure 5.2 D). Firing parameters are summarised in Table 4.1. During theta oscillations, SWR active neurons display the rhythmic firing of identified septo-hippocampal neurons (see Chapter 4).

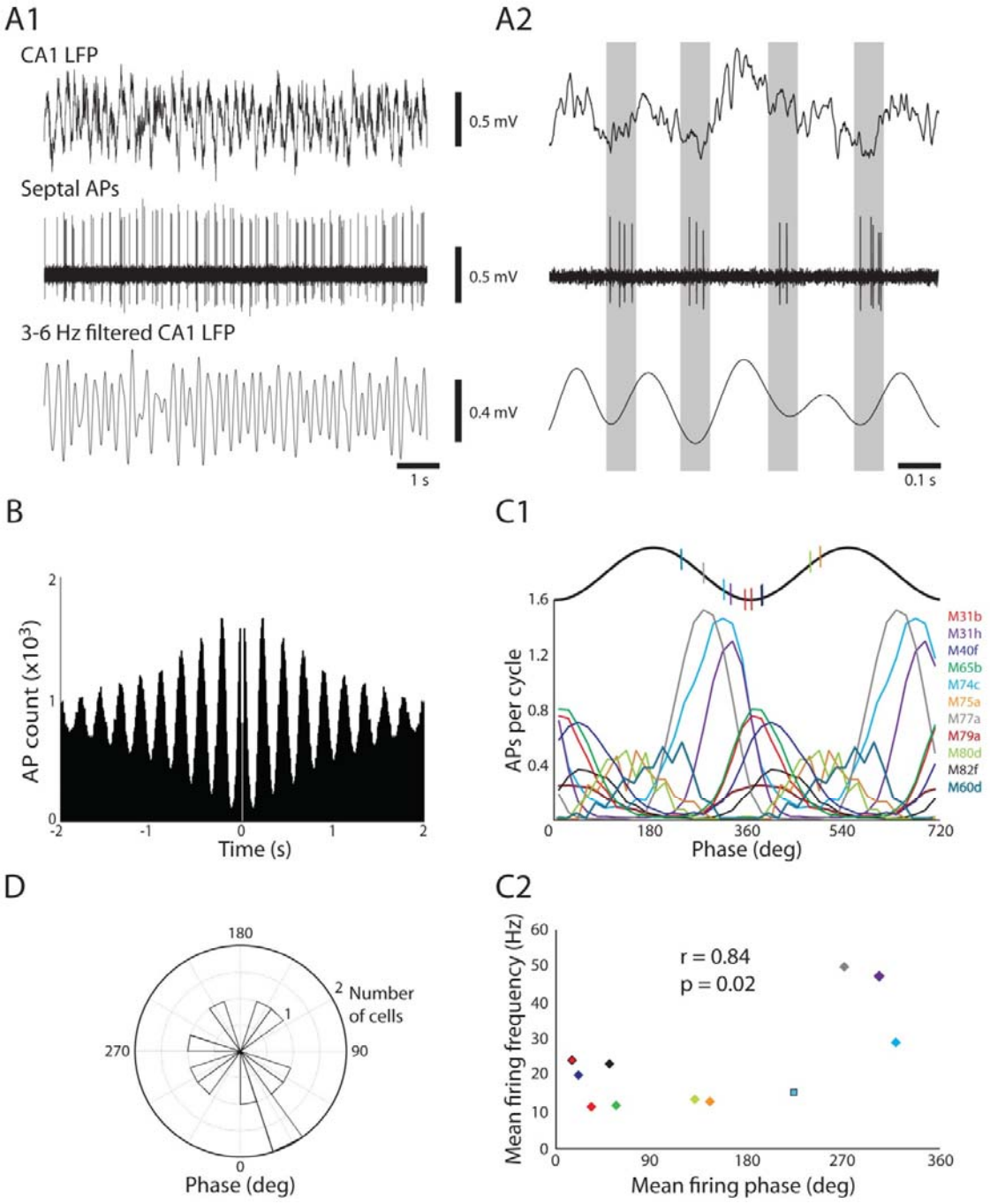

A1
CA1 LFP
0.5 mV
Septal APs
0.5 mV
3-6 Hz filtered CA1 LFP
0.4 mV
1 s
A2
0.1 s
B
AP count (x10³)
Time (s)
C1
APs per cycle
Phase (deg)
M31b
M31h
M40f
M65b
M74c
M75a
M77a
M79a
M80d
M82f
M60d
D
Number of cells
Phase (deg)
C2
r = 0.84
p = 0.02
Mean firing frequency (Hz)
Mean firing phase (deg)

Figure 5.2 – Theta-related firing properties of SWR activated neurons. A1) A representative 10 second epoch of a SWR activate neuron (M65b) during hippocampal theta oscillation. CA1 local field potential (top) with ~4 Hz oscillation. Action potential firing (M65b; middle) occurring rhythmically and correlated with the hippocampal field potential oscillation. The 3-6 Hz filtered trace (bottom). **A2)** One second firing epoch demonstrating the correlation between neuron firing and theta oscillation phase. **B)** An autocorrelogram of firing during theta epochs (Same neuron as shown in A). **C1)** Action potentials per theta cycle versus theta phase for each SWR activate neuron. Top, model sine wave shown in black with approximate maximal firing illustrated with colour-coded bars. Two cycles are shown by duplicating data to avoid edge effects. **C2)** Scatter plot demonstrating the correlation between mean firing frequency and maximal firing angle for all neurons. Correlation coefficient and p values are shown for circular correlation. **D)** Rose plot of mean phase (degrees) for each neuron. Zero degrees represents the theta trough.

Table 5.1 – Summary of *in vivo* firing patterns and immunohistochemistry for SWR active neurons described in this chapter.

Identified medial septal neuron			**M31b**	**M31h**	**M40f**	**M65b**	**M74c**	**M75a**	**M77a**	**M79a**	**M80d**	**M82f**	**M60d**
Immunohistochemical test	Parvalbumin				+s	+sd		+d			+da	+s	
	SATB1				+s	+s		+s			+s	n.t.	
	HCN4				n.t.	+sd		+s			+sd	+sd	
	CB				n.t.	n.t.		n.t.			-sd	n.t.	
	CR				-s	-da		-da			-da	-da	
	Kv 1.1				n.t.	+a		-s			+s		
	VGAT				n.t.	n.t.		+b			+b	+b	
	NECAB1				n.t.	-da		-da			-da	-da	
	Axon location				unknown	CA3 str. ori.		dF*			dF*	CA3 str. ori/pyr/luc	
***In vivo* firing patterns**	CA1 SWRs	Rate during SWRs (Hz)	35.33	65.25	43.89	17.17	23.02	7.3	36.5	18	27.9	23.40	13.70
		Rate peri-SWR (Hz)	4.27	39.04	20.56	7.96	10.6	3.8	15.7	8.4	5.5	5.50	8.90
		% active ripples (n)	84.4 (45)	100 (31)	89.5 (57)	82.3 (34)	69.4 (49)	54.5 (33)	71 (59)	75 (60)	85.3 (68)	77.8 (27)	70.2(33)
	Theta firing rate (Hz)		11.4	46.9	20	11.74	28.9	12.8	49.48	24.05	13.39	23.05	14.20
	Theta coupling	Mean phase CA1 (°)	32.9	302.7	20.8	56.2	318.3	144.1	269.9	14.8	129.9	49.80	207.30
		Mean vector length CA1	0.46	0.56	0.69	0.67	0.76	0.58	0.73	0.68	0.68	0.55	0.65
		Mean action potentials per cycle	3.4	12.4	5.2	2.7	7.3	3.5	10	5.4	3.5	6.00	3.80
		Percentage of active cycles	90.6	99	98.7	96.5	99.1	93.1	99.8	99.6	94.4	99.10	96.80
* Dorsal fornix to extrahippocampal regions													

5.2.3 Anatomical characterisation of SWR active neurons of the medial septum

Using the juxtacellular labelling method, five of ten SWR active neurons recorded were labelled and analysed anatomically. All 5 were found to have their soma within the medial septum (Figure 5.3 A) with dendrites extending within, and not further than the border of the medial and lateral septum (4 with visualised dendrites). I investigated if these neurons displayed similar immunohistochemical characteristics to other, SWR inhibited, medial septum neurons. All tested neurons (5/5) were positive for PV (Figure 5.3 B1), HCN4 (4/4; Figure 5.3 B1, B2), SATB1 (4/4; Figure 5.3 B2); immunonegative for NECAB1 (3/3; data not shown); and their boutons were immunopositive for VGAT (3/3; Figure 5.3 B3). Sharp-wave ripple active neurons display molecular markers that are also found in SWR inhibited septo-hippocampal neurons (see Chapter 3). Thus, from the known (PV and VGAT) and novel markers (SATB1, HCN4 and NECAB1) of rhythmic, putative and confirmed septo-hippocampal neurons, it is not possible to differentiate SWR active and inhibited neurons.

Although these neurons display the same immunohistochemical profile as septo-hippocampal neurons (see Chapter 3), they display a different firing pattern and it is therefore important to establish if they are also septo-hippocampal. Four of the five labelled neurons were sufficiently filled as to allow for observation of the axonal projection. The cell M40f was weakly labelled and did not have an observable axon leaving the septum. Two neurons (M65b, M82f) projected a main axon within the fimbria-fornix pathway posteriorly towards the hippocampus. Both neurons displayed branches from the main axon within the fimbria into dorsal CA3 (Figure 5.3 C). This branching was taken as evidence of hippocampal innervation and confirmation of these as GABAergic septo-hippocampal neurons.

Septo-hippocampal GABAergic neurons are known to innervate only interneurons (Freund and Antal, 1988). One of these interneuron types, the axo-axonic cell, is inhibited during SWRs in CA1 (Klausberger et al., 2003) and CA3 (Viney et al., 2013). This may be a key contribution in SWR

generation. Given that some of the SWR active neurons are septo-hippocampal, they are candidates for SWR-dependent inhibition to interneurons. Observable axonal boutons were identified in one example (M82f; Figure 5.3 E). Boutons were present in the dorsal and intermediate CA3, in strata oriens, pyramidale and lucidum. The main axon was present in all strata including str. radiatum. Unique amongst all labelled septo-hippocampal neurons I have observed, M82f had a second large main axon which projected within the dorsal fimbria, crossed the corpus callosum and entered the retrosplenial cortex where bouton-bearing branches were observed (data not shown). Immunohistochemical analysis of the interneurons targeted by M82f SWR active neuron demonstrated that one targeted soma was immunonegative for PV, calretinin and SATB1 immunoreactivity; these molecules being used in the identification of several types of interneuron including the axo-axonic cells (Viney et al., 2013).

Interestingly, 2 of 4 other SWR active neurons did not target the hippocampus (Figure 5.3 D; M75a, M80d). The main axon of both neurons was located in the dorsal fornix-dorsal hippocampal commissure-deep cerebral white matter and produced no observed branches into the hippocampus. Likewise, the subiculum did not receive observable branches. A single axon (M80d) was observed further posterior within the deep cerebral white matter although the terminal field has not been observed. It will be important to establish which extra-hippocampal regions receive the GABAergic input that has been described above. These two neurons are the first directly identified medial septal GABAergic cell neurons to my knowledge which expresses PV and HCN4, fire with the characteristic theta-dependent rhythmicity and increase firing frequency during CA1 detected SWRs but do not project to the hippocampus.

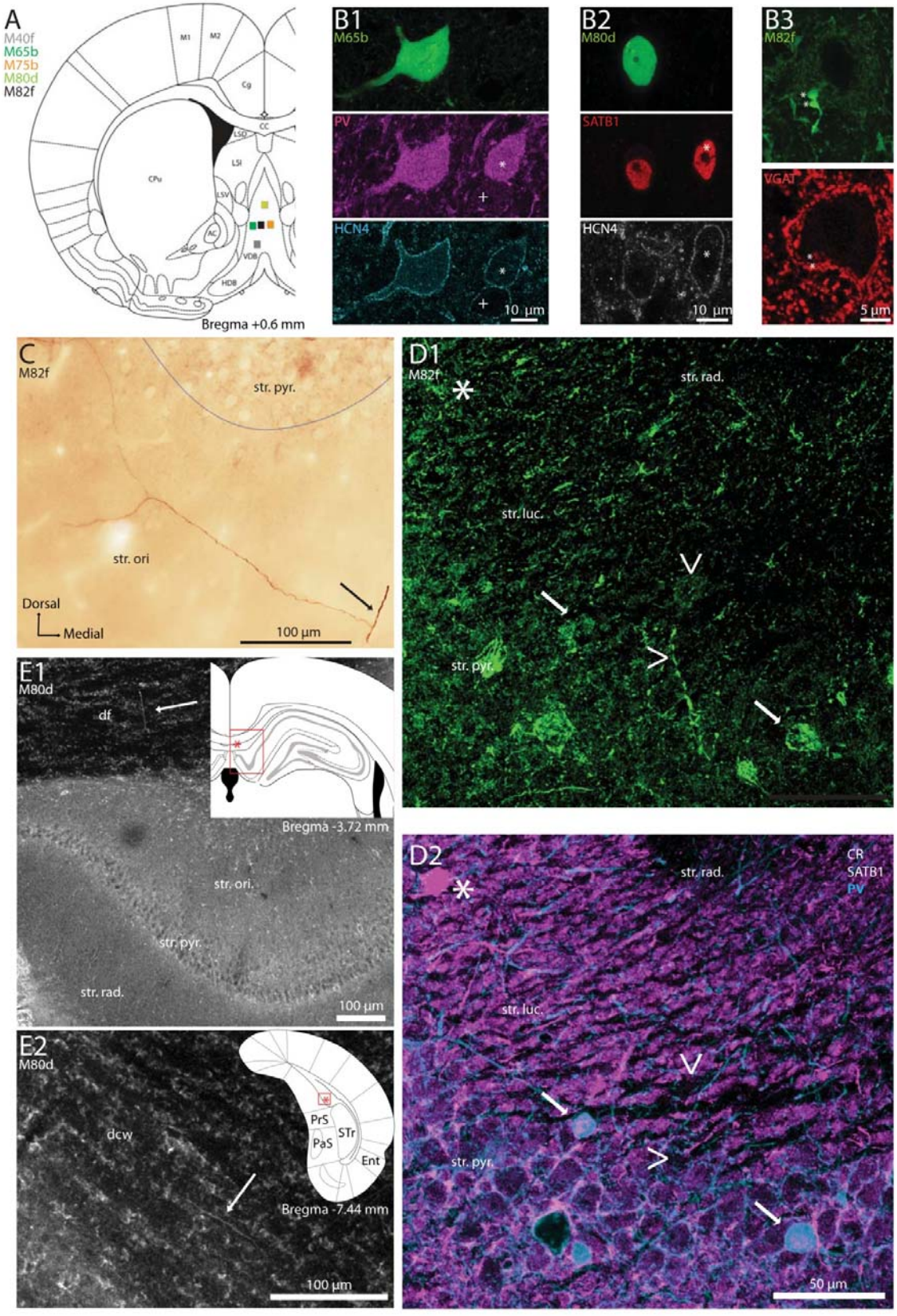

A
M40f
M65b
M75b
M80d
M82f
M1
M2
Cg
CC
LSD
LSI
LSV
CPu
AC
VDB
HDB
Bregma +0.6 mm
B1
M65b
PV
HCN4
10 µm
B2
M80d
SATB1
HCN4
10 µm
B3
M82f
VGAT
5 µm
C
M82f
str. pyr.
str. ori
Dorsal
Medial
100 µm
D1
M82f
str. rad.
str. luc.
str. pyr.
D2
CR
SATB1
PV
str. rad.
str. luc.
str. pyr.
50 µm
E1
M80d
df
Bregma -3.72 mm
str. ori.
str. pyr.
str. rad.
100 µm
E2
M80d
dcw
PrS
STr
PaS
Ent
Bregma -7.44 mm
100 µm

Figure 5.3 – Anatomical characterisation of SWR active neurons. A) Somatic location of SWR active neurons within the medial septum (adapted from Paxinos and Watson, 6th edition, 2007). **B1)** Single optical section of confocal micrograph of a SWR active neuron (M65b; neurobiotin, green; top), demonstrating positive immunoreactivity for both PV (cytoplasmic signal, magenta; middle) and HCN4 (membranous signal cyan; bottom). Note a second double immunopositive PV and HCN4 positive cell nearby (asterisk), and a PV immunonegative, HCN4 immunopositive neuron (cross). **B2)** SATB1 immunoreactivity of a SWR active neuron (M80d, green; top). The signal for SATB1 is localised to the nucleus sparing the nucleolus (red; middle). Also found in the membrane is HCN4 (white; bottom). Note another SATB1 and HCN4 positive neuron (asterisk). **B3)** Septal axonal boutons are VGAT immunoreactive (M82f; top). The boutons are in direct opposition to a soma which is densely innervated by other VGAT-containing boutons. **C)** Photographic Z-stack reconstruction of axonal branches within CA3 stratum oriens (Ni-enhanced DAB, M82f). The main axon within the fimbria (arrow) has a perpendicular branch which enters the hippocampus and ramifies further. Stratum pyramidale is delineated by the blue line. **D)** Boutons within the hippocampus are in strata pyramidale and lucidum of CA3 (D1; M82f; neurobiotin, green, horizontal arrow head) which closely oppose an interneuron soma and dendrites (vertical arrow head). The target cell of the boutons was not positive for CR or SATB1 (D2; magenta), or PV (D2; cyan). Immunoreactivity for PV and SATB1 (arrows) and CR (asterisk) is observed. The magenta signal within str. luc. is non-specific background. **E1,2)** Extra-hippocampal projection of a SWR active neuron (M80d). **E1)** The axon (neurobiotin, white arrow; bregma -3.72 mm) is in the dorsal fornix close to the midline (insert). **E2)** The axon posterior to the hippocampus (neurobiotin, white arrow; bregma -7.44 mm). The dorsal cerebral white matter. Inserts adapted from Paxinos and Watson (6th edition, 2007); red box is the approximate location of confocal micrographs, asterisk is the location of the axon. Images: **B3** Confocal Z-stack standard deviation projection, 12 optical sections/ 4.4 µm thickness; **D** Confocal Z-stack maximum intensity projection, 47 optical sections/ 19.84 µm

thickness; **E1** and **E2** Confocal maximum intensity projections, 6 and 7 optical sections/ 31.19 and 37.42 µm thickness, respectively.

Abbreviations: AC anterior commissure, CC corpus callosum, Cg cingulate cortex, CR calretinin, CPu caudate putamen, dcw dorsal cerebral white matter, df Dorsal fornix, Ent entorhinal cortex, HCN4 hyperpolarisation-activated cyclic nucleotide-gated cation channel 4, HDB horizontal diagonal band, LSD lateral septum dorsal, LSI lateral septum intermediate, LSV lateral septum ventral, M1 motor cortex 1, M2 motor cortex 2, PaS parasubiculum, PrS presubiculum, PV PV, SATB1 special AT-rich sequence-binding protein-1, STr subiculum transition area, Str. rad. stratum radiatum, str. luc. Stratum lucidum, Str. Ori. stratum oriens, Str. Pyr. stratum pyramidale, VDB vertical diagonal band, VGAT vesicular GABA transporter.

5.3 Discussion

I have analysed the anatomical and electrophysiological characteristics of a subtype of GABAergic septo-hippocampal neuron, which is active during SWRs. These neurons share molecular markers and theta-related firing parameters with canonical SWR inhibited GABAergic septal projection neurons (see Chapters 3 and 4). This demonstrates that a PV, HCN4 and SATB1 immunopositive profile correlates with a theta-frequency rhythmic firing pattern during hippocampal theta oscillation, but is not predictive of firing behaviour during SWRs. It was also demonstrated that SWR active neurons project to the hippocampus.

The septum is capable of synchronising cortical regions by modulating interneuron firing as has been demonstrated during theta oscillation (Hangya et al., 2009). During different network states, the timing and distribution of inhibition within the hippocampus differs, which relates to the release of GABA at different subcellular locations at different times by different interneuron types (Klausberger et al., 2003, Lapray et al., 2012, Tukker et al., 2013). It is hypothesised that canonical GABAergic medial septum neurons are inhibited during SWRs by a group of somatostatin-expressing projection neurons (Jinno and Kosaka, 2002, Gulyás et al., 2003, Jinno et al., 2007, Takács et al., 2008). This is the only GABAergic neuron type known to project to the medial septum and fire during SWRs. Ripple-dependent excitatory input, originating from the glutamatergic pyramidal neurons, has not been observed from any hippocampal or parahippocampal region to medial septal GABAergic neurons. Therefore, an unknown input, a non-canonical transduction of a known input, or an unknown hippocampal-independent SWR initiation event might exist.

The pyramidal neurons of the hippocampus, subiculum and entorhinal cortex are known glutamatergic populations, which are active during SWRs (Buzsáki et al., 1983, Chrobak and Buzsáki, 1996). The projections of these neurons have been extensively studied and have not been observed to innervate medial septal neurons (Kosel et al., 1982, Finch et al., 1983, Toth et al., 1993, Naber and Witter, 1998, Prasad and Chudasama, 2013) although see (Alonso and Köhler, 1982) who, using

retrograde tracing, described hippocampal and subicular pyramidal neurons that project to the medial septum, but the spread of their tracer to the lateral septum where pyramidal cells terminate could not be excluded. As illustrated in this chapter, SWR active neurons appear to be fewer than other canonically firing neurons in the medial septum. If they are localised to a particular subregion within the septum then retrograde tracing techniques may be ineffective in demonstrating an input to them by a small number of pyramidal neurons. Likewise hippocampal pyramidal neuron subpopulations have been shown to project differently within the brain (Graves et al., 2012). Whilst the majority of pyramidal neurons may project to the lateral septum (amongst other areas), it is possible that a small, as yet undefined population target the SWR active neurons of the medial septum causing the activation/increase in firing observed during SWR events. A specific innervation by pyramidal neurons to SWR active neurons may be relatively sparse in comparison to the lateral septum, which receive input from both hippocampal and subicular pyramidal neurons, and has not been observed with classical tracing methods (Finch et al., 1983, Alonso and Frotscher, 1989, Risold and Swanson, 1997). As demonstrated in this chapter using known and novel immunohistochemical markers of medial septum neurons, no markers are known which separate SWR active neurons from inhibited neurons. Therefore, without electrophysiological identification of the cells, it would not be possible to demonstrate by anatomical methods a potential pyramidal cell projection to SWR active neurons specifically.

Furthermore, bulk injection based tracing studies would not be able to resolve an input to the distal dendrites of medial septal neurons occurring on the border or within the lateral septum. Equally, injections of retrograde tracer within a relatively narrow structure like the medial septum (as seen in (Alonso and Köhler, 1982)) could spread into the lateral septum. Genetic labelling of neurons specifically within each area of the hippocampal formation could be used to address this question (Groh et al., 2010, Chung et al., 2013, Zhang et al., 2013), or full labelling of the axons of single pyramidal neurons in these areas might reveal as yet unknown connections (Zheng and Wilson,

2002, Mallet et al., 2012). A sparse, unidentified pyramidal cell projection provides a possible anatomical explanation of the firing patterns described in this chapter.

Intrinsic differences between SWR active neurons and canonical medial septal neurons may explain the differences in SWR-related firing patterns. Differences in synaptic integration may result in excitation rather than inhibition during SWR events. As discussed above, the only known SWR-related extrinsic input to GABAergic medial septal neurons is that from the somatostatin-expressing hippocampo-septal projection neurons (Jinno et al., 2007, Takács et al., 2008). It has been hypothesised that under certain conditions GABA can evoke depolarisation post-synaptically through activation of the GABA-A receptor. Specifically, at the axon initial segment of neocortical pyramidal neurons the reversal potential for GABA is more positive than the resting membrane potential *in vitro* (Szabadics et al., 2006, Molnár et al., 2008, Woodruff et al., 2009). Innervation to the axon initial segment of hippocampo-septal neurons by GABAergic medial septal neurons has been demonstrated (Takács et al., 2008), however it is not known if hippocampo-septal GABAergic neurons also innervated axon initial segment in the septum, as would be required for GABAergic excitation of SWR active neurons. A potential GABAergic excitation in the septum by hippocampo-septal innervation is consistent with the *in vivo* firing patterns of labelled neurons during both theta and SWR oscillations: hippocampo-septal (or "double projection neurons") have maximal firing around the trough of theta oscillation (recorded in CA1) and increased firing during SWRs (Jinno et al., 2007) as do SWR active septal neurons. Further, the surprising result that two of the SWR active neurons were phase locked to the ripple oscillation may also be explained by an excitatory input from hippocampo-septal neurons, which can also be phase locked to local ripples (Jinno et al., 2007). However this does rely on the depolarising action of GABA which is yet to be conclusively observed in adult synapses *in vivo*. Moreover, the *in vivo* spike timing of axo-axonic neurons also correlates with an inhibitory action of GABA on pyramidal neurons during physiological network activity (Viney et al., 2013).

Hippocampo-septal neurons may release somatostatin in addition to GABA. Peptide release occurs during high frequency firing of the presynaptic neuron (Whim and Lloyd, 1989) which may include SWRs. The action of somatostatin, a peptide transmitter, on single medial septal neurons was investigated pharmacologically *in vivo (Bassant* et al*., 2005)*. The somatostatin receptor sst2a is present in the membranes of GABAergic neurons within the medial septum as shown by immunohistochemistry. Using the juxtacellular method for recording, rhythmic PV-expressing neurons were shown to decrease firing frequency during local application of somatostatin and the sst2a agonist octreotide. The exact action potential correlates of somatostatin release onto medial septum have not been established to my knowledge, nor has an excitatory effect of somatostatin been reported in these neurons, thus it is unlikely that somatostatin signal transduction is responsible for SWR-dependent excitation of medial septum neurons.

An interesting possible explanation of the SWR active firing pattern of the neurons described here is that the firing is a cause, not a consequence of the SWR event. The current hypothesis is that SWRs are initiated in CA3 of the hippocampus and propagate to CA1 and other extra-hippocampal regions where SWRs also occur (Buzsáki et al., 1983, Ylinen et al., 1995, Csicsvari et al., 2000). For the SWR to be initiated by the septum, the firing of SWR active neurons is expected to occur before that of pyramidal cells in CA3. Peak activation of SWR active neurons was approximately 40 ms after the SWR recorded from the reference electrode in CA1 stratum pyramidale. This suggests that SWR active septal neurons fire maximally after the peak of the event in the hippocampus. However, the lack of an anatomically defined excitatory input could suggest a causative role for these neurons in SWR initiation. Axo-axonic neurons receive medial septal input (Viney et al., 2013). It has been postulated that the disinhibition of pyramidal cells during the SWR is a key prerequisite to allow pyramidal neurons to burst and SWRs to build up (Buzsáki, 1986). The input by SWR active neurons to axo-axonic and other GABAergic neurons, if not an initiating event, could provide disinhibition of pyramidal cells and encourage SWR maintenance. By providing inhibition to axo-axonic cells during the SWR, the medial septum contributes to the reduction of GABA release to pyramidal

neurons until the SWR excitation stops and/or an unknown terminating event occurs. Although the targets of a SWR active neurons were not exclusively axo-axonic cells (but see SWR inhibited neuron M76 in Chapter 4 which does innervate axo-axonic neurons), this does not rule out that: 1) other types of neurons require inhibition to initiate and/or maintain SWRs, 2) that axo-axonic neurons are also targeted synaptically by these neurons. It is also interesting that as a population, the peak firing of these neurons cluster around the trough of theta, counter-phased to that of the axo-axonic neurons, which may indicate that they are providing inhibition to axo-axonic neurons during the trough and dictating the firing phase during theta oscillation (Toth et al., 1997, Viney et al., 2013)

These findings have interesting implications for the hippocampus in behaving animals. As stated previously, the septo-hippocampal pathway is usually interpreted in the context of theta oscillation alone; that is, for contributing to the animal's behaviour during exploration and paradoxical sleep. Here I demonstrate an active role during SWR for a small population of septo-hippocampal neurons; events that occur during slow wave sleep, quiet wakefulness and consummatory behaviours (Buzsáki, 1986). In awake animals, SWR active neurons have not been published to my knowledge. Using tetrodes Dragoi et al. (1999) recorded the SWR firing behaviour of medial and lateral septum neurons and found that all but one of the medial septal neurons were inhibited or did not change their firing pattern during SWRs (Dragoi et al., 1999). This may indicate that the SWR active firing pattern is an artefact of anaesthesia; however they only recorded a small sample (25 neurons in 7 animals) so may not have sampled these rarer neurons. Under anaesthesia however, SWR active neurons have been observed *in vivo* (Varga et al., 2008). Of 37 neurons analysed in this study, 12 met the criteria used (>50 % increase in firing compared to the 250 ms peri-ripple period). It is noteworthy however that only 9 were found to be inhibited; this is very different to the proportions of neurons I observed, when much more frequently neurons were inhibited than active.

There is loss of GABAergic (and cholinergic) neurons in the basal forebrain during Alzheimer's disease and Alzheimer's disease models (Whitehouse et al., 1982, Villette et al., 2010, Loreth et al., 2012). It has been established that this loss correlates with deficits in memory formation and consolidation in humans and rodents (Yiu et al., 2011, Moss Mb, 1986, Moulin et al., 2004, Blanchard et al., 2008). The specific effects that septal lesions have on SWRs, and how this relates to the deficits in memory consolidation seen in rodent models and humans has not been investigated to my knowledge (Moss Mb, 1986, Hart et al., 1988, Moulin et al., 2004, Blanchard et al., 2008, Freir et al., 2011, Wang et al., 2012, Borlikova et al., 2013). If the septum had an initiating or maintenance role for SWRs dependent on SWR active neurons, then it may provide a novel target in the treatment of memory deficits. Inactivation of the GABAergic and PV-expressing components of the medial septum via optogenetic methods has been used to investigate theta oscillation and memory acquisition but not the SWR oscillations and memory consolidation and may play a vital role in dissecting the role of the septal projection neurons in SWR-dependent behaviour.

Previous publications have emphasised the SWR-dependent inhibition of GABAergic septo-hippocampal neurons. However a small population of septal rhythmic neurons are active during these events (Varga et al., 2008), and as I have shown project to the hippocampus and other brain regions. Long-range GABAergic neurotransmission during SWRs is a powerful mechanism for modulating information processing within the hippocampal formation. The divergent projections suggest a role in facilitating coherence in SWRs between multiple structures, probably via the inhibition of interneurons.

This chapter has provided evidence that the septo-hippocampal pathway is not only theta oscillation, but plays a role during SWR events in multiple brain regions, and hence memory consolidation.

Chapter 6 - Diverse firing patterns of medial septal neurons

Any sufficiently advanced technology is indistinguishable from magic

Arthur C Clarke

6.1 Introduction

A fundamental tenet of neuroscience for over a century has been the attempt to identify and classify different cell types within the nervous system. The methods used have evolved in complexity: from the subjective identification of morphological characteristics visualised by the Golgi impregnation method (Cajal, 1899), to electrophysiological parameters (Halabisky et al., 2006), and/or single cell mRNA data (Sotty et al., 2003).

The definition of cell types has been useful to understanding neuronal circuits in both health and disease. The cell types of the hippocampus have been extensively defined; the hippocampus is composed of numerous principle cell types and at least 21 cell types (Somogyi, 2010) although it is likely to be larger as further subtypes are defined. Broadly there are two categories of cell, glutamatergic principal neurons such as pyramidal, granule and mossy cells and GABAergic interneurons. This is a useful distinction based on many parameters such as spike width, neurotransmitter, axonal target, presence of dendritic spines, synaptic inputs and molecular profile. These parameters correlate with functional differences relating to behaviour. It is known that the firing patterns of some pyramidal neurons encode place-related information (O'Keefe and Dostrovsky, 1971, Lapray et al., 2012), whereas interneuron firing patterns are much less modulated by place, relating more to pyramidal cell oscillation generation and spike timing (Middleton et al., 2008, Hangya et al., 2010, Losonczy et al., 2010). This correlation between features helps to infer features based on limited measured parameters e.g. a stratum pyramidale neuron which expresses NOS will also express NPY, have a wide action potential wave form, be slow firing, and is an ivy neuron (Fuentealba et al., 2008a). However, different neuron types can be similar in some features, e.g. the molecular profiles of PV-expressing basket and axo-axonic neurons, but differ in other features, such as firing patterns, anatomical parameters, and functions within a circuit (Lasztóczi et al., 2011, Massi et al., 2012). Characterisation of neurons usually relies on more than just a single type of parameter.

Neurons of the medial septum are have been characterised only to a limited extent. There are three recognised neuronal classes currently acknowledged within the medial septum, based entirely on the neurotransmitter used by each; i.e. cholinergic, GABAergic and glutamatergic (Lewis et al., 1967, Manns et al., 2001, Sotty et al., 2003). Several immunohistochemical and genetic markers have also been used to define mostly non-overlapping populations e.g. ChAT, PV, NOS, CR; these may or may not overlap completely with the neurotransmitter used by the cells (Kiss et al., 1990, Sugaya and McKinney, 1994, Kiss et al., 1997b, Zaborszky et al., 2005, Wei et al., 2012).

In vivo recording of medial septal neurons has demonstrated firing pattern features which segregate populations of neurons. Septo-hippocampal GABAergic neurons, some of which express PV, have a rhythmic firing pattern phase-locked to the hippocampal theta oscillation (Borhegyi et al., 2004, Simon et al., 2006). This differs from the firing of cholinergic neurons which, whilst phase-locked to hippocampal theta, are not rhythmic but slow firing in both anaesthetised and drug-free rats (Simon et al., 2006). Cholinergic neurons can be divided by the expression of GABAB and CB1-receptors, those that lack these receptors project to the hippocampus (Nyíri et al., 2005). A minority of cholinergic neurons are also immunopositive for NOS although the functional correlates of this have not been investigated (Sugaya and McKinney, 1994). Slow firing, putative cholinergic neurons may functionally segregate in awake, behaving animals (Garrido-Sanabria et al., 2007). So called pro-arousal neurons can be differentiated from other slow firing neurons by *in vivo* electrophysiological parameters alone i.e. auditory stimulus-induced increase in firing, increased firing during REM state, and increased firing in “small-amplitude irregular activity” in the hippocampal LFP. Using only electrophysiological parameters, cell types could be clustered reliably. This diversity has not been correlated with any molecular markers for identification by histological and genetic means. Furthermore, pro-arousal slow-firing neurons are more strongly phase locked to the septal LFP than the hippocampal LFP.

Like the cholinergic neurons, diversity within the GABAergic population has been found in both immunohistochemical and electrophysiological parameters. Parvalbumin and HCN1 expression in GABAergic neurons correlates with a theta-frequency rhythmic firing pattern (often referred to as "pace-maker" septal neurons, although see Introduction). The neuronal population which express HCN1 fire action potentials preferentially during one of two phases of the hippocampal theta oscillation, either during the ascending phase or the peak of the theta LFP in the pyramidal layer in urethane anaesthetised rats (Varga et al., 2008). The GABAergic neuronal population which do not express HCN1, although firing in a phase locked manner, as a population, have no consistent firing phase. Whilst each HCN1-negative neuron will fire consistently during a single preferred phase, this may be at any point during the theta cycle (Varga et al., 2008, Hangya et al., 2009).

During another hippocampal network state, the sharp-wave ripple oscillation, rhythmic GABAergic neurons have been observed to have one of three firing patterns: the majority reduce their firing frequency and are inhibited during these epochs, a smaller number do not change their firing frequency, and the rest increase their firing frequency and are activated (Dragoi et al., 1999, Borhegyi et al., 2004, Varga et al., 2008). No other differences have thus far been reported between these groups either electrophysiologically or immunohistochemically.

Without intact connectivity, such as in an *in vitro* system, the above firing features are no longer observed, however diversity between cells is present. The major classification of medial septum neurons *in vitro* has utilised the differences in firing response to a depolarising current delivered from a whole-cell recording configuration, resulting in four classes of firing pattern: slow-, fast-, burst-, and cluster- firing (Sotty et al., 2003). It is not known how these classes relate to the firing patterns of neurons recorded *in vivo*, but some inferences can be made based on immunohistochemical comparisons. Fast spiking neurons have been shown to express PV (Morris et al., 1999) and project to the hippocampus, and have transcripts for GAD67 and a prominent Ih current which correlates with the HCN channel (Sotty et al., 2003, Morris et al., 2004); these are

likely theta rhythmic PV-, HCN1-expressing septo-hippocampal neurons (but see Huh et al. (2010)). Similarly, some slow-firing neurons *in vitro* have been shown to express transcripts for ChAT and project to the hippocampus (Sotty et al., 2003).

A confounding factor in the classification of medial septal neurons *in vitro* is the presence of VGluT expression found in cells. Amongst the fast-, burst-, and cluster- firing neurons which express GAD67 and ChAT, all types have also been found to express mRNAs for VGluT1/2 further subdividing these neurons. Some neurons also expressed both ChAT and GAD67 transcripts (Sotty et al., 2003). Purely VGluT1/2-expressing neurons, without either ChAT or GAD67, co-expression exhibit fast, slow- and/or cluster- firing pattern (Sotty et al., 2003, Huh et al., 2010). This suggests that within the previously categorised slow-firing group some of these neurons will be glutamatergic. No glutamatergic neuronal recordings have been reported *in vivo*, so their firing pattern is currently unknown. Co-expression of GABAergic and cholinergic markers has not been tested immunohistochemically within the medial septum (Kiss et al., 1990).

The aim of my study is to investigate and define the diversity of firing patterns of medial septum neurons recorded *in vivo* under anaesthesia, using both theta and sharp-wave ripple oscillation related activity. I will then discuss how this diversity relates to the anatomical features of the recorded neurons after labelling by the juxtacellular method.

6.2 Results

From a total of 73 experiments targeting the septum in urethane-anaesthetised rats, 190 septal neurons were extracellularly recorded and could be at least partially analysed in at least one network state. From these neurons 51 septal neurons met recording quality criteria for inclusion in unsupervised cluster analysis (Table 6.1; see Methods). Neurons displayed diverse firing patterns (Figure 6.1 A). The majority being typical theta rhythmic putative medial septum neurons (37/51; 15 labelled); fewer displayed, to my knowledge, an unidentified firing pattern; here termed “delta-coupled” (n = 6/51; 1 labelled); and the remaining 8/51 (4 labelled) were lateral septum neurons.

Sampling of neurons in this study was not unbiased and therefore the proportion of different neuron types within the septum may not be represented by the proportions found here. Primarily theta rhythmic neurons were of interest which meant neurons of other types were not recorded when they were encountered as the electrode was advanced. Likewise, a higher proportion of theta rhythmic neurons were recorded when encountered which produces an unrepresentatively high sample proportion. Later in this study, I made a biased search for SWR active neurons over other theta rhythmic types; therefore the percentage of theta rhythmic neurons which are SWR active may not be generalizable from this data set.

Initial groupings were based on semi-quantitative differences in firing patterns and anatomical analysis. Theta rhythmic neurons displayed high percentage of active theta cycles in combination with a high mean theta vector length. Delta-coupled neurons displayed a preference for the septal 1-3 Hz oscillation over the hippocampal theta oscillation, as demonstrated by a greater mean delta vector length than theta vector length. Lateral septum neurons were recorded at depths expected to be within the lateral septum (~5000 - 5400 µm), typically did not display rhythmic activity (low number of active theta cycles), and fired complex bursts.

Table 6.1 – Firing properties of all 51 neurons including all parameters which are used to calculate clustering parameters

Type	Cell	Mean theta phase (deg)	Mean vector length (theta)	Mean vector length (delta)	Percentage of active theta cycles	Mean action potentials per cycle	Firing frequency during theta (Hz)	Firing frequency peri-SWR (Hz)	Firing frequency intra-SWR (Hz)	Number of theta cycles analysed	Number of SWR events analysed	Labelled
SWR Active	**M82f**	49.82	0.55	0.13	99.1	6	23	5.5	23.4	919	27	Y
SWR Active	**M75a**	144.06	0.58	0.04	93.1	3.5	12.8	3.9	7.1	29	33	Y
SWR Active	**M79a**	14.78	0.68	0.07	99.6	5.4	24	8.8	17.8	1547	60	
SWR Active	**M40d**	33.2	0.52	0.05	95.5	2.2	8.6	4	11.8	425	12	
SWR Active	**M77a**	269.925	0.73	0.03	99.8	10	49.5	15.7	36.5	3252	59	
SWR Active	**M31h**	303.53	0.53	0.03	99	12.4	46.9	39	65.2	306	31	
SWR Active	**M40f**	16.2	0.64	0.09	98.7	5.2	20	20.6	43.9	789	57	Y
SWR Active	**M65b**	56.19	0.67	0.04	96.5	2.7	11.7	8.5	16.3	1543	34	Y
SWR Active	**M41d**	70.96	0.46	0.08	95.5	7.9	31.8	14.1	30.6	44	22	
SWR Active	**M74c**	318.297	0.76	0.12	99.1	7.3	28.9	10.6	24	1241	49	
SWR Active	**M31b**	38.55	0.43	0.03	90.6	3.3	11.4	4.3	35.3	1443	45	
SWR Active	**M60d**	207.28	0.65	0.06	96.8	3.8	14.2	8.9	13.7	31	47	
SWR Active	**M80d**	129.93	0.68	0.09	94.4	3.5	13.4	5.3	27.7	71	68	Y
SWR Inhibited	**M80b**	112.693	0.49	0.08	98	5.9	24	10.3	7.7	1691	94	
SWR Inhibited	**M60a**	262.5	0.73	0.11	71.8	1.7	5	3.9	0.8	629	43	Y
SWR Inhibited	**M37f**	330.31	0.53	0.02	94.8	3.4	11.3	11.9	2.3	325	30	
SWR Inhibited	**M31g**	267.38	0.62	0.09	94.9	3.3	11.7	9.9	0	78	15	

SWR Inhibited	**M21c**	270.56	0.4	0.02	98.3	4.9	19.8	18.3	1.9	881	14	Y
SWR Inhibited	**M22a**	263.4	0.61	0.04	92.4	4.3	17.5	20.4	2.1	1824	8	Y
SWR Inhibited	**M37h**	171.96	0.38	0.1	99.6	15.3	55.5	38.7	14.9	497	57	Y
SWR Inhibited	**M82e**	169.444	0.22	0.03	97.7	11.3	44.8	47.7	3.8	128	21	
SWR Inhibited	**M37e**	64.61	0.7	0.04	90.5	4.7	14.8	10.8	4.1	463	45	
SWR Inhibited	**M30e**	305.6	0.37	0.02	99.5	4.7	19.4	18.9	3.8	2361	25	
SWR Inhibited	**M41e**	220.73	0.67	0.03	94.6	7.1	25.6	21.9	0.2	1046	52	Y
SWR Inhibited	**M77b**	267.216	0.18	0.01	99.7	10	42.5	12.4	2	386	116	
SWR Inhibited	**M22c**	288.5	0.82	0.06	98.9	3.9	17.7	17.8	3.9	355	18	
SWR Inhibited	**M74b**	224.48	0.68	0.03	99.6	5.3	20.7	35	21.7	1163	17	
SWR Inhibited	**M77c**	295.96	0.73	0.01	99.7	5.6	26.1	18.6	2.9	5368	57	Y
SWR Inhibited	**M76a**	264.817	0.49	0.05	98.4	5	20.9	25.6	4.4	2547	35	Y
SWR Inhibited	**M82a**	327.48	0.58	0.05	89.7	2.3	8	15.4	1.2	1524	35	
SWR No change	**M67a**	39.39	0.64	0.08	98.6	3.2	12.6	7.9	10	489	29	Y
SWR No change	**M82b**	283.23	0.66	0.01	97.4	2.4	9.1	16.2	14.1	1294	35	
SWR No change	**M37b**	96.8	0.57	0.15	96.8	4.1	13.7	4.5	1.1	124	20	
SWR No change	**M66b**	275.99	0.33	0.08	72.4	3	8.4	10	7.5	2129	20	
SWR No change	**M40g**	38.8	0.59	0.17	96.2	3.7	13.1	7.8	6	213	49	Y
SWR No change	**M40b**	294.2	0.62	0.05	99.6	9.5	37	38.7	35	1140	53	
SWR No change	**M73a**	278.505	0.56	0.04	95.7	2.6	10.2	2	0	6382	13	Y
Lateral septum Active	**M66c**	35.76	0.28	0.08	56.8	1.6	3.4	2.7	32.38	923	58	
Lateral septum Active	**M67b**	80.02	0.34	0.18	19.2	1.33	1	0.8	2.35	1082	85	Y

Lateral septum Active	**D53e**	50.6	0.52	0.12	52.4	1.5	3.3	2.8	12.5	927	29	Y
Lateral septum Active	**M72e**	11.6	0.09	0.22	52.3	1.4	3.07	2.5	11.3	911	103	Y
Lateral septum	**M64c**	119.3	0.35	0.15	4.8	1.1	0.2	0.09	0	2579	10	Y
Lateral septum	**M31f**	238.4	0.42	0.08	33.8	1.6	2.2	3	3.7	983	55	
Lateral septum	**M71c**	126.2	0.64	0.07	2.93	1.5	0.18	0.2	0	3886	13	
Lateral septum	**M34b**	351.82	0.38	0.24	62.8	3	7.5	2.8	0	1068	13	
Delta coupled	**M34a**	269.7	0.07	0.45	84.9	2.6	8.7	10.4	13.3	378	6	
Delta coupled	**M35f**	23.7	0.05	0.16	32	1	1.2	1	1.4	1808	9	
Delta coupled	**M38e**	318.8	0.04	0.5	46.8	2.2	4.2	2	1.1	814	25	Y
Delta coupled	**M40h**	189.8	0.13	0.18	97.6	4.4	16	13.9	13.1	1198	61	
Delta coupled	**M41b**	303.8	0.06	0.51	23	1.3	1.1	0.7	2	1165	11	
Delta coupled	**M42b**	276.5	0.2	0.2	46.8	1.8	3.1	0.1	0	1375	5	

The firing frequency of theta rhythmic, lateral septum, and delta-coupled neurons differed during theta epochs (theta rhythmic: 21.2 ± 2.1 Hz, n = 37; lateral septum: 2.6 ± 0.84 Hz, n = 8; delta-coupled: 5.7 ± 2.3 Hz, n = 6; $p < 0.001$; one-way ANOVA). A *post-hoc* Tukey HSD test demonstrated that theta rhythmic neurons fired at a significantly higher frequency during theta epochs than either other group ($p < 0.01$); however delta-coupled and lateral septum neurons did not differ from each other ($p > 0.05$; Figure 6.1 B1). Mean vector length, which is used as a measurement of coupling strength, was used to compare theta rhythmic, delta-coupled, and lateral septum groups with respect to theta oscillations recorded in the CA1 region of the hippocampus; coupling strength differed between all groups (mean vector lengths of: theta rhythmic: 0.6 ± 0.02, n = 37; lateral septum: 0.4 ± 0.06, n = 8; delta-coupled: 0.1 ± 0.03, n = 6 respectively; $p < 0.001$; one-way ANOVA). Similarly, the mean vector lengths for coupling to septal delta oscillations (1 - 3 Hz) differed between all groups (theta rhythmic: 0.06 ± 0.01, n = 37; lateral septum: 0.14 ± 0.02, n = 8; delta-coupled: 0.3 ± 0.07, n = 6 respectively; $p < 0.001$; one-way ANOVA; Figure 6.1 B2). Each group also differed by percentage of active theta cycles during theta epochs (theta rhythmic: 95.5 ± 1.0 %, n = 37; lateral septum: 55.2 ± 12.1 %, n = 8; delta-coupled: 35.6 ± 8.5 %, n = 6; $p <0.001$; one-way ANOVA; Figure 6.1 B3). The SWR index, which I use as a measure of the differences between firing rate outside of and inside of the SWR period, did not differ between the groups (theta rhythmic: -0.3 ± 0.1, n = 37; lateral septum: -0.1 ± 0.2, n = 8; delta-coupled: -0.1 ± 0.3, n = 6; $p > 0.05$; one-way ANOVA; Figure 6.1 B4).

The preferred phase of all neurons was not uniformly distributed across the theta cycle (Rayleigh's test; $p < 0.05$; n = 51). Theta rhythmic neurons (n = 37; 72.5%) showed a bimodal distribution with peaks at ~270 and ~40° (descending phase and ascending phase respectively) although a small proportion of neurons (n = 9; 17.6 %) had preferred phases outside these two peaks (Figure 6.1 C1).

Interestingly, within the theta rhythmic group, a correlation was found between theta phase and both the SWR index and delta-theta index (circular-linear correlation; $r = 0.57$; $p < 0.01$; and r =

0.46; $p < 0.05$ respectively; $n = 37$; Figure 6.1 C1). In the lateral septum neuronal group, a correlation was found between theta phase and the percentage of active theta cycles (circular-linear correlation; $r = 0.96$; $p < 0.05$; $n = 8$; Figure 6.1 C2).

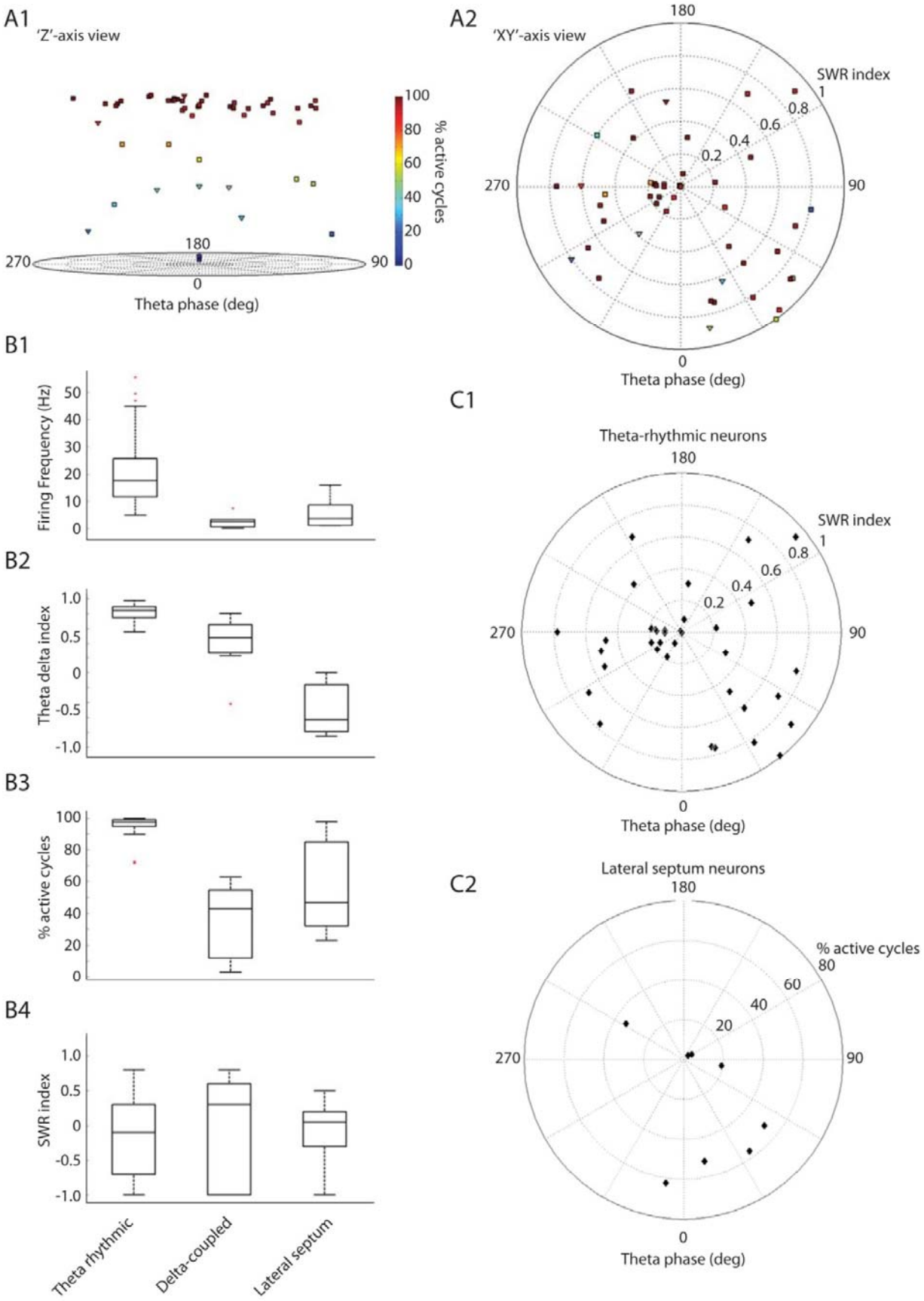
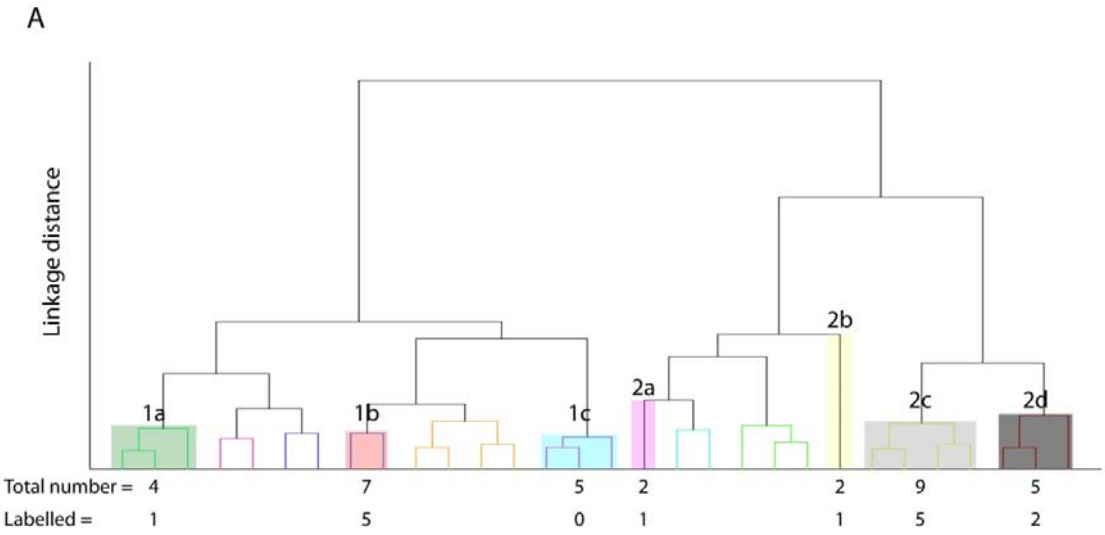
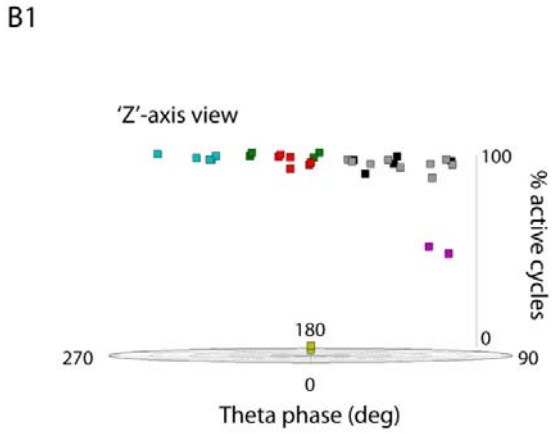

A1
'Z'-axis view
100
80
60
40
20
0
% active cycles
180
270
90
0
Theta phase (deg)
A2
'XY'-axis view
180
SWR index
1
0.8
0.6
0.4
0.2
270
90
0
Theta phase (deg)
B1
Firing Frequency (Hz)
50
40
30
20
10
0
B2
Theta delta index
1.0
0.5
0
-0.5
-1.0
B3
% active cycles
100
80
60
40
20
0
B4
SWR index
1.0
0.5
0
-0.5
-1.0
Theta rhythmic
Delta-coupled
Lateral septum
C1
Theta-rhythmic neurons
180
SWR index
1
0.8
0.6
0.4
0.2
270
90
0
Theta phase (deg)
C2
Lateral septum neurons
180
% active cycles
80
60
40
20
270
90
0
Theta phase (deg)

Figure 6.1 – Electrophysiological parameters of *in vivo* recorded septal neurons. **A1)** 'Z'-axis view of 4-dimensional plot of all neurons included (n = 51). Z-axis and colour denote percentage of active cycles during theta oscillation. Shape shows the theta delta index: >0 = square; <0 = triangle. **A2)** 'XY'-axis view of 4D plot of all neurons included. Phase is the preferred mean phase of theta oscillation for each neuron; radial axis is the SWR index (normalised to 0-1). Colours/symbols are the same as in A1. **B)** Box and whisker plots of firing parameters and distribution of neurons of different types. Midline of each box is the median value, box denotes 95% distribution; whiskers indicate minimum and maximum value. Red points are outliers. Parameters are: **B1)** firing frequency during theta oscillation; **B2)** theta delta mean vector length index; (theta-delta)/(theta+delta). **B3)** Percentage of theta cycles with action potentials; B4) SWR index; (intra Hz-peri Hz)/(intra Hz+peri Hz). **C1-C2)** Circular-linear correlations were found in theta rhythmic neurons' preferred theta phase (degrees) and SWR index (radial); lateral septum neurons' mean theta phase (degrees) and the percentage of active theta cycles (radial). Note the radial axis of C2 differs from A2 and C1 and displays percentage of active cycles rather than SWR index.

6.2.1 Hierarchical clustering

Using unsupervised hierarchical clustering I have investigated the diversity of septal neurons based on electrophysiological parameters. Both the L-method and silhouette optimisation method suggest similar numbers of clusters: 12 and 10 respectively. Therefore I chose a cut off of 11 for the final clustering analysis. From the 51 neurons included, 11 clusters were formed in two major branches (Figure 6.2 A). Overall clustering quality was not strong, with a mean silhouette value for all clusters of 0.35. This was evident with a number of clusters containing mixed types of neurons, i.e. theta rhythmic and non-theta rhythmic neurons. Lateral septum and delta-coupled neurons were reliably clustered separately from theta rhythmic neurons (14/14 neurons tested). Lateral septum neurons could not be distinguished from delta-coupled neurons in this study; two clusters were composed of both types (2 delta-coupled neurons, two lateral septum neurons, mean silhouette value = 0.08; 1 delta-coupled neuron and 4 lateral septum neurons, mean silhouette value = 0.24). Using the electrophysiologically measured parameters from multiple brain network states I was able to cluster theta rhythmic neurons from lateral septum and delta-coupled neurons but could not differentiate lateral septum neuron from delta-coupled.


A
Linkage distance
1a
1b
1c
2a
2b
2c
2d
Total number = 4 7 5 2 2 9 5
Labelled = 1 5 0 1 1 5 2


B1
'Z'-axis view
100
% active cycles
0
180
270
90
0
Theta phase (deg)

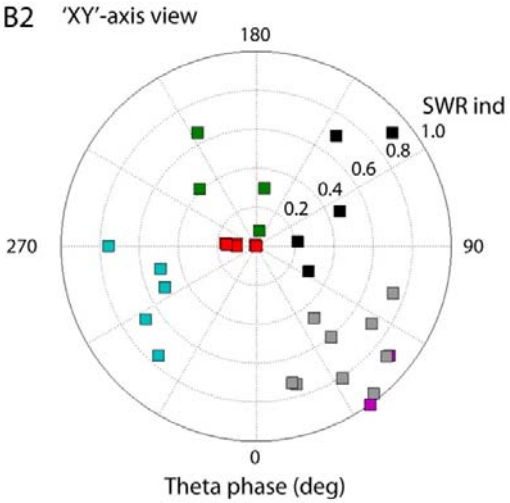

B2
'XY'-axis view
180
SWR ind
1.0
0.8
0.6
0.4
0.2
270
90
0
Theta phase (deg)

Figure 6.2 – Unsupervised hierarchical clustering of septal neurons (n = 51). **A)** Dendrogram displaying linkage distances between clusters. Individual clusters are colour coded, and those which display robustness are highlighted with boxes, the colours corresponding to member neurons found in B and C. Numbers underneath are total number of neurons within the cluster and number of labelled neurons. **B)** Multi-dimensional polar plot showing robustly clustered neurons within the clustering feature space (34 neurons; 15 labelled). **B1)** 'Z'- axis view of 4-dimension plot of robustly clustered neurons. Percentage of active cycles (Z-axis) and cluster (colour). Lateral septum neurons in clusters 2a and 2b (purple and yellow respectively) are segregated from theta rhythmic neurons by percentage of active cycle **B2)** 'XY'-axis view of robustly clustered neurons. Preferred theta phase (degrees) and SWR index (radial) for robustly clustered neurons (colour code). Theta-delta index is not shown for clarity.

Seven robust clusters were found (sum of silhouette >1.0) containing 34 neurons. Of the 37 initial theta rhythmic neurons, 30 were robustly clustered into 5 clusters: 1a, 1b, 1c, 2c, and 2d (Figure 6.2 B; Table 2). The remaining 4 neurons form clusters 2a, and 2b, and were lateral septum neurons. Clusters 2a and 2b had a significantly lower percentage of active cycles than the clusters containing theta rhythmic neurons (29.2 ± 14.7 %, n = 4; 96.9 ± 0.5 %, n = 30; $p < 0.001$; Student's t-test). They did not differ by theta-delta index (0.6 ± 0.1, n = 4; 0.8 ± 0.02, n = 30; $p > 0.05$; Student's t-test). Whilst theta delta index significantly differed between all groups (one-way ANOVA; $p < 0.05$) post-hoc Tukey HSD test demonstrate that no two groups differ ($p > 0.05$). Of note, a subset of lateral septum neurons could be robustly clustered from theta rhythmic neurons by differences in theta related activity, namely the difference in percentage of active cycles. These may have a high (cluster 2a; neurons active during SWRs) or low (cluster 2b; neurons not active during SWRs) SWR index.

The theta rhythmic neurons had preferred phases spanning the entire theta cycle (Figure 6.2 B), however the descending phase (~280 - 330°) and early-ascending phase (0 - 90°) contained the majority of theta rhythmic neurons (11 and 10 neurons respectively). Preferred phases ranging from 90 - 240° contain the remaining 9 neurons (Figure 6.2 C). Robustly clustered theta rhythmic neurons display diverse theta phase preference.

Theta rhythmic neurons are further separated by SWR index (Figure 6.2 B). Neurons which make up the group with preferred mean phase ~ 45° (Figure 6.2 C) are within a single cluster (2c; grey) in all but one case. These neurons display a high SWR index (0.36 ± 0.1, n = 9) with only a single neuron occupying this theta phase range displaying a low SWR value (64.1°; -0.45); it is a member of cluster 2d. All theta rhythmic neurons which were initially included and fired at this phase were robustly clustered. For theta rhythmic medial septum neurons, a preferred mean theta phase which is within the range of 0 - 90° is predictive of a high SWR index.

During the descending theta phase (~30 – 280°) two robust clusters: 1b (Figure 6.2 B2; red) and 1c (cyan) have preferred theta phases, however they differ in their SWR index (Student's t-test; -0.86

± 0.05, n = 7; 0.18 ± 0.1, n = 5; $p < 0.05$). In the initial group of 51 neurons: 14 (including cluster 1b) fire during this range and have low SWR indices, and 5 have high SWR indices (cluster 1c). There is a correlation in these neurons between firing frequency during theta epochs and SWR index (Pearson correlation; $r = 0.54$; $p < 0.05$; $n = 19$). This correlation was not seen when all theta rhythmic neurons of all mean phases were included, suggesting it is specific to neurons firing during this theta phase (Pearson correlation; $r = 0.04$; $p > 0.05$; $n = 37$), and in combination with the clustering analysis, may suggest distinct populations of neurons with a common mean theta phase range. To investigate if this correlation was formed by two groups I tested the firing frequencies of the group of neurons with a relatively high SWR index (n = 6) against the neurons with a relatively low SWR index (n = 13). I found that they did not differ significantly in theta firing frequency (One-way ANOVA; $p > 0.05$; $n = 19$).

In many brain regions electrophysiological parameters correlate with anatomical features. Many of the neurons which are robustly clustered are also juxtacellularly labelled as described in previous chapters. Of the large SWR inhibited group (1b; red), neurons M76a (see chapters 3 and 4) and M21c are labelled sufficiently as to allow comparison. Whereas M76a innervates putative axo-axonic and PV-expressing neurons of the dorsal CA3 and dentate gyrus, M21c has observable axon projecting to the ventral hippocampus suggesting that whilst these neurons have common electrophysiological parameters they may differ in their target areas. Electrophysiological parameters used in this study may not be predictive of axonal target in robustly clustered SWR inhibited neurons.

In contrast to the above, the SWR active neurons are present in 4 clusters (1a, green; 1c, cyan, and 2c, grey and 2d, black). Interestingly, cluster 2c (grey) contains neurons M82f and M65b (see Chapter 5) which are both established CA3-projecting medial septal neurons. These neurons have main axons which travel dorsally and caudally towards the hippocampus within the fimbria. In contrast cluster 2d (black) contains neurons M75a and M80d (see Chapter 5) which have different

axonal characteristics. These neurons do not have a projection axon within the fimbria; their axon is found in the dorsal fornix. Whilst M80d has been proven to innervate the hippocampus, as well as being to my knowledge the first example of a septo-subicular neuron, it has a visible main axon as far as the deep cerebral white matter and may project to the cortex. As the number of cells with known projections is limited, more examples are required to establish/determine whether the electrophysiological parameters they display are predictive of their axonal target.

Table 6.2 – Clustering parameters used in the hierarchical clustering for all robustly clustered neurons. Cluster colours correspond to Figure 6.2.

Cell	Mean theta phase (deg)	SWR index	Theta Delta index	Percentage of active theta cycles	Cluster name	Silhouette value	Cluster Silhouette mean	Cluster Silhouette sum	Labelled
M60d	207.28	0.21	0.83	96.80	1a	0.32			
M82e	169.44	-0.85	0.76	97.70	1a	0.37			
M74b	224.48	-0.23	0.92	99.60	1a	0.08			
M37h	171.96	-0.44	0.58	99.60	1a	0.45	0.30	1.21	y
M22a	263.40	-0.81	0.88	92.40	1b	0.58			y
M77b	267.22	-0.72	0.89	99.70	1b	0.51			
M31g	267.38	-1.00	0.75	94.90	1b	0.54			
M73a	278.51	-1.00	0.87	95.70	1b	0.47			y
M41e	220.73	-0.98	0.91	94.60	1b	0.23			y
M21c	270.56	-0.81	0.90	98.30	1b	0.55			y
M76a	264.82	-0.71	0.81	98.40	1b	0.49	0.48	3.36	y
M77a	269.93	0.40	0.92	99.80	1c	0.46			
M82b	283.23	-0.07	0.97	97.40	1c	0.28			
M40b	294.20	-0.05	0.85	99.60	1c	0.38			
M31h	303.53	0.25	0.89	99.00	1c	0.58			
M74c	318.30	0.39	0.73	99.10	1c	0.41	0.42	2.12	
M66c	35.76	0.85	0.56	56.80	2a	0.76			
D53e	50.60	0.63	0.63	52.40	2a	0.75	0.75	1.50	y
M64c	119.30	-1.00	0.40	4.80	2b	0.84			y
M71c	126.20	-1.00	0.80	2.93	2b	0.85	0.84	1.68	
M82f	49.82	0.62	0.62	99.10	2c	0.35			y
M65b	56.19	0.31	0.89	96.50	2c	0.53			y
M40g	38.80	-0.13	0.55	96.20	2c	0.33			y
M31b	38.55	0.78	0.87	90.60	2c	0.13			
M41d	70.96	0.37	0.70	95.50	2c	0.36			
M40d	33.20	0.49	0.82	95.50	2c	0.55			
M79a	14.78	0.34	0.81	99.60	2c	0.55			
M67a	39.39	0.12	0.78	98.60	2c	0.54			y
M40f	16.20	0.36	0.75	98.70	2c	0.56	0.43	3.90	y
M80b	112.69	-0.14	0.72	98.00	2d	0.43			
M75a	144.06	0.29	0.87	93.10	2d	0.37			y
M37e	64.61	-0.45	0.89	90.50	2d	0.05			
M37b	96.80	-0.61	0.58	96.80	2d	0.39			
M80d	129.93	0.68	0.77	94.40	2d	0.18	0.28	1.42	y

SWR index (Intra SWR frequency - Peri SWR frequency)/(Intra SWR frequency + Peri SWR frequency)

Theta delta index (theta MVL - delta MVL)/(theta MVL + delta MVL)

6.3 Discussion

I have used unsupervised hierarchical clustering and statistical comparison to investigate the diversity of electrophysiological parameters of septal neurons. Using both theta- and SWR- related parameters I have expanded the previously known diversity of rhythmic neurons within the septum. This supported that septal neuron firing patterns may represent a more diverse population than previously demonstrated. The preffered theta phase may be at least partially predictive of SWR response. I have successfully distinguished rhythmic medial septal neurons from other distinct cell types using electrophysiological parameters.

Previous investigations into the diversity of putative GABAergic septo-hippocampal neurons during theta oscillation demonstrated a bimodal distribution of neurons with the majority of neurons firing at one of two preferred theta phases: the trough and the late ascending/peak phase (Borhegyi et al., 2004). The neurons in this chapter also demonstrate a clear preference to one of two phases however the relative phase of theta differs from the published data. They are approximately the same in terms of degrees separation in the theta cycle (135° compared to the published 152°). The reason for the differences may relate to methodological differences. Whilst both studies use a reference in the pyramidal layer of dorsal CA1, the exact placement relative to the medio-lateral and rostro-caudal axis is important in producing phase data which is comparable between studies. Phase is not uniform across the whole hippocampal pyramidal layer (Lubenov and Siapas, 2009). The Borhegyi et al. (2004) study does define the reference position as dorsal CA1, stratum pyramidale, but nothing more specific than that which would allow comparison with my study. Another possible variable is the apparent sampling differences of septal neurons. The authors in the above study would not record the first theta rhythmic neurons encountered and thus are likely to have sampled from a deeper group of neurons (personal communication Zsolt Borhegyi). This may be indicated by the anatomical differences between the neurons presented in this published study and here; ventrally extending axons were rarely seen in neurons labelled in this thesis even

in cases where neurons were labelled well enough to characterise the hippocampal targets. In the few cases that I found a ventral axon, neurons were located ventrally in the septum, potentially within the vertical limb of the diagonal band. These cells likely represent a different group of a type similar to those of the more dorsal medial septum septo-hippocampal neurons recorded by myself. I hypothesise that the bimodal distribution seen in the study by Borhegyi et al., (2004) is comparable to that found in my study but shifted by approximately a quarter of a theta cycle, and that phase differences may be due to differing reference positions.

Using both theta- and SWR- related parameters I have found further diversity not previously published. It is known that some medial septum theta rhythmic neurons increase their firing frequency during SWR recorded from the hippocampus *in vivo* (Dragoi et al., 1999, Borhegyi et al., 2004, Varga et al., 2008). To my knowledge it has not been investigated how these neurons fire during theta oscillation compared to canonical SWR-inhibited neurons. Using SWR index, a measure of the change in firing frequency between peri- and intra- SWR periods, I found a correlation with preferred theta phase. This correlation was only found with theta rhythmic neurons suggesting that neurons with high or low SWR index are not uniformly distributed throughout the theta cycle. Indeed the clustering analysis demonstrates distinct clusters which share a preferred theta phase and similar SWR index. The majority of neurons with a low SWR index, neurons which are inhibited, were in two clusters with a preferred theta phase around the descending phase. Neurons with a mid or high SWR index, neurons which did not change their firing frequency or increased it, were much more diverse, clustering into three groups of differing preferred theta phases. All but one of the neurons which had a preferred theta phase during the ascending phase had a high SWR index.

This has interesting implications for the model proposed by (Borhegyi et al., 2004) in which two opposing phased groups act upon each other to generate an oscillation as well as target distinct interneurons within the hippocampus. I have been able to address a number of the hypothesis made in that study. Firstly, many SWR active neurons have extensive local axons (see Chapter 5).

In the Borhegyi et al. model mutual inhibition drives theta frequency burst firing. The ascending phase neurons (trough phase in Borhegyi model) all have high SWR indices. I propose that inhibition of descending phase (peak in Borhegyi model) medial septum neurons during SWR is at least partially dependent on local medial septal SWR active neurons which fire during the opposing theta phase. I have not been able to test this directly. The descending phase group may reciprocally innervate the ascending phase SWR active neurons, generating theta frequency bursting, but they will be inhibited during SWRs.

Conversely, interconnected inhibitory neurons may fire at the same time with submillisecond synchrony (Hu et al., 2011). Synchrony with inhibition is demonstrated by the interconnected PV-expressing basket cells network within the hippocampus (Bartos et al., 2002). Here it acts to further synchronise groups of the same neurons. The model of mutual inhibition of counter phased septo-hippocampal neurons and the idea of synchrony via inhibition are not mutually exclusive. Both could occur within the septo-hippocampal intra-septal network to produce rhythmicity. Mutual inhibition between opposing groups could act to produce rhythmic firing, whilst between neurons in the same group reinforce firing at the same phase by GABA-dependent synchronous firing. The mechanism which transduces GABAergic inhibition into either an out-of-phase or a synchronous firing is to my knowledge unknown but may relate to the subcellular location of the synapses, such as the relationship between different interneuron types and a pyramidal neuron (Somogyi, 2010). Paired recording of septo-hippocampal neurons may provide evidence for this dual action of GABAergic input.

Secondly, the Borhegyi model makes predictions about the targets of these two theta phase groups: the descending theta rhythmic neurons will innervate dendritic-innervating interneurons within the hippocampus; the ascending phase group will innervate peri-somatically-innervating neurons. I have been able to partially test this hypothesis. Certainly neurons which occupy the same theta phase (and same robust cluster in this study) may innervate non-overlapping hippocampal

regions. For example two neurons which fire during the descending phase and are members of cluster 1b, M21c and M76a, innervate the ventral hippocampus CA3 and dorsal dentate gyrus / CA3 respectively. Interneurons of the same type fire action potentials at different times when they are located in different hippocampal area, such as dorsal CA1 or intermediate CA1 (Forro et al., 2013), even when the relative theta phase is not different. I would hypothesise that septal theta rhythmic neurons which innervate the same interneuron type at different regions would also have a similar phase shift to that of the theta oscillation and interneuron; neurons M76a and M21c differ by only 6 degrees which is less than would be expected if they innervated the same interneuron type. This data demonstrates that neurons with very similar firing parameters display differences in axonal location.

I have shown novel diversity within the theta rhythmic neurons, which fire during the descending phase. The majority of neurons were canonical SWR inhibited neurons but a cluster was found which fired during the same phase but had a higher SWR index (i.e. was SWR active). Within the hippocampal network, differences in SWR response correlate with differences in axonal target, even if the theta phase may not differ, such as PV-expressing bistratified and oriens-lacunosum moleculare cells (Klausberger and Somogyi, 2008). It is likely that these two groups of descending phase preferring theta rhythmic septal neurons are distinct cell types and provide theta and SWR-dependent input to distinct hippocampal targets.

These novel distinctions of rhythmic putative septo-hippocampal neurons supports the idea that the septal output is not purely theta oscillation related and that SWR input as well as SWR-dependent GABA release from these neurons is a key part of the intra- and extra-septal network and its functions. Whilst SWR-inhibited neurons are more numerous, SWR active neurons appear to be more diverse in electrophysiological parameters such as theta phase. Sharp-wave ripple-dependent firing is an important and defining feature of septo-hippocampal neurons and should be included in any further analysis of these cells.

Theta rhythmic neurons can be reliably distinguished from lateral septal and delta-coupled neurons by a significantly higher theta delta index and percentage of active theta cycles. Only one previous study has shown single neuron coupling to the septal oscillation *in vivo* (Zhang et al., 2011). Here, I demonstrate that both lateral septum and delta-coupled neurons are significantly modulated to the septal local LFP; making them distinct from theta rhythmic neurons. The existence of a neuron type that is significantly phase locked to the local, but not the hippocampal LFP, as is the case for some delta-coupled cells, is highly suggestive that these oscillations are distinct. Whilst they may be related and/or interacting, the presence of delta-couple neurons suggests that the septum is capable of generating its own oscillatory LFP and that this may have some influence on the pacing of neurons in the hippocampus. How this oscillation is generated and which currents contribute to it requires further investigation. It has been demonstrated that in freely moving rats, a slow oscillation is present in the septum during certain behavioural states, as well as coherent theta oscillation – to the dorsal hippocampal theta oscillation – during other behaviours (Nerad and McNaughton, 2006). The presence of delta-coupled neurons phase-locked to a septal LFP oscillation suggests that these neurons may contribute to the currents generating that oscillation. The co-modulation of some neurons, such as some lateral septum neurons, may indicate that this oscillation plays a modulatory role on the output of the hippocampus within the septum. Theta rhythmic neurons do not appear to be modulated by the delta oscillation. To better understand the generation and correlates of the septal delta oscillation, and its relevance to septal neuron firing patterns, current source density throughout the septum and surrounding areas will help identify where and what is responsible for this oscillation. Although not as laminar as the hippocampus, the septum displays clear layers of cell types and bands of input (Kiss et al., 1997a, Wei et al., 2012) which could produce a voltage oscillation.

Lateral septum neurons are a major recipient population of hippocampal and subicular pyramidal synaptic excitation (Alonso and Frotscher, 1989, Garcia and Jaffard, 1992). Lateral septum neurons have been shown to increase their firing during SWR recorded in the hippocampus (Dragoi et al.,

1999). In this chapter I have identified both SWR-active and inhibited lateral septal neurons, which form two distinct clusters. The diversity of SWR responses could reflect a difference in hippocampal excitatory input and cell type or predict a SWR-dependent GABAergic inhibition.

The increase in the diversity of septal neurons, especially as that diversity comes from non-theta oscillation related parameters means that the function of the medial septum is also likely to be more complex than providing rhythmogenesis drive and an arousal signal to the hippocampus. Future models of mutual inhibition by GABAergic neurons of the hippocampus and medial septum must be expanded to include the SWR responses.

Further conclusions will require the investigation of intra-septal connectivity. Knowledge of immunohistochemical markers to distinguish cell types, as in the hippocampus (Somogyi, 2010), would be a necessary for this advancement (see Chapter 3). Confirmation of firing diversity in unanaesthetised animals (Dragoi et al., 1999, Simon et al., 2006) and the functional significance of these neurons in memory formation, consolidation and retrieval will be important future goals.

Chapter 7 - Discussion

I would feel more optimistic about bright future for man if he spent less time proving that he can outwit Nature and more time tasting her sweetness and respecting her seniority.

E. B. White

I have investigated the septo-hippocampal pathway by anatomical and electrophysiological methods *in vivo*, to define single septo-hippocampal neurons and their putative synaptic targets within the hippocampus. This study demonstrates a number of previously unknown features of the septal projection to the hippocampus, both in terms of the connectivity and the firing patterns of septo-hippocampal neurons.

7.1 The glutamatergic septo-hippocampal projection is sparse and unlikely to be a major excitatory projection to CA3 pyramidal neurons

The glutamatergic component of the septo-hippocampal projection has recently been characterised by genetic means and retrograde tracing (Sotty et al., 2003, Henderson et al., 2010, Huh et al., 2010). A study using the whole septo-hippocampal preparation – which contains a complete septo-hippocampal projection – demonstrated that this excitatory projection depolarises pyramidal neurons in the CA3 region (Huh et al., 2010). This has led to the hypothesis that the glutamatergic projection neurons regulate the excitability of CA3 pyramidal neurons by monosynaptic excitation in a theta phase-locked manner. The VGluT2-immunopositive projection I identified in this study consisted of few axons and appeared to be minor in synapse number or density, compared to other glutamatergic inputs. A prominent glutamatergic projection to CA3 pyramidal neurons in rats comes from the entorhinal layer II pyramidal neurons and forms part of the perforant pathway (Tamamaki and Nojyo, 1993, Deller et al., 1996). This input is massive and produces a large current sink in the stratum lacunosum-moleculare which correlates with the position of the synapses between the entorhinal synaptic input and the distal dendritic tufts of pyramidal neurons (Buzsáki et al., 1986, Leung et al., 1995). The septal glutamatergic projection is very small by comparison and is unlikely to have an effect similar to the entorhinal input.

A well-defined modulatory projection from the septum is by cholinergic neurons to the hippocampus. In this study, I did not identify cholinergic neurons, in part due to the emphasis on theta rhythmic putative GABAergic neurons. Cholinergic neurons are reported to be very slow firing

(1 - 2 Hz) making them difficult to detect compared to faster firing GABAergic neurons (Simon et al., 2006). With the emphasis on theta rhythmic firing patterns, I would often not find other neurons before I had encountered a theta rhythmic neuron, which was my landmark of being within the medial septum. Cholinergic neurons, as a population, are located in a layer immediately outside of PV-expressing medial septal neurons (Zaborszky et al., 2005, Wei et al., 2012), and were less likely sampled than GABAergic cells.

Acetylcholine is a known modulator of the excitability of pyramidal neurons, granule cells and interneurons (Dalkara et al., 1986, Pitler and Alger, 1992, Brunner and Misgeld, 1994). Like the entorhinal input, this pathway is large and dense, occurring throughout the whole hippocampus (Fisone et al., 1987, Matthews et al., 1987). Ablation of the cholinergic pathway dramatically alters the coordinated activity of septo-hippocampal neurons (Apartis et al., 1998), produces a significant decrease in the hippocampal theta oscillatory power (Lee et al., 1994, Bassant et al., 1995, Yoder and Pang, 2005) and deficits in hippocampal-dependent learning (Cai et al., 2012, Hamlin et al., 2013).

As is common to all anterograde tracing experiments, the completeness of an observed projection relies on the injection occurring at the site which contains the somata of the cell population to be studied. In transgenic mice, the VGluT2-expressing neurons are found in the lateral portion of the medial septum (Henderson et al., 2010). Injections performed in this study were either at single sites, or multiple sites varying in depth, with the electrode always advanced with a medio-lateral angle. Septal cell populations often form an “onion-skin” like formation with different cell types forming bands in the dorso-ventral plane, which are thin in the medio-lateral plane (Wei et al., 2012). It is possible that due to the location of injection sites in this study, the site which contains the majority of the glutamatergic septo-hippocampal neurons was not injected, producing a false scarcity of VGluT2-expressing axons. Throughout the whole hippocampus, VGluT2-immunoreactivity is sparse suggesting a minor septal component. The only regions of dense

labelling are the thalamic input zone from the nucleus reuniens thalami to stratum lacunosum-moleculare (Halasy et al., 2004) and supramammillary nucleus innervation of CA2.

Currently, the immunohistochemical identification of glutamatergic neurons in the septum relies on the testing of boutons for VGluT2 as no somatic markers are currently accepted. Although both glutamate itself and the excitatory amino acid transporter (EAAC1) have been used (Colom et al., 2005, Sun et al., 2014), there is no characterisation of how these markers relate to neurons which use glutamate as a neurotransmitter. I attempted to replicate the results demonstrated with the antibody used by (Colom et al., 2005) without success.

Future investigation may use genetic means, such as a VGluT2-dependent Cre-expressing animal model and a reporter gene delivered by viral vector to investigate this pathway, or using opsins to perturb function of this pathway. An important step will be defining the post-synaptic targets and to characterise the distribution of this pathway within CA3. Recording the *in vivo* firing patterns during behaviour and establishing the synaptic targets of septal glutamatergic afferents within the hippocampus will help to elucidate the function of this pathway.

7.2 NOS-expressing neurons receive GABAergic septal input

Previous anatomical studies have demonstrated that many interneuron types receive synaptic input from the septal GABAergic population (Gulyas et al., 1990, Gulyás et al., 1991, Miettinen and Freund, 1992a, Miettinen and Freund, 1992b, Papp et al., 1999, Takács et al., 2008). More recently, novel immunohistochemical markers have been described which define interneuron types previously either unknown, or not definable with immunohistochemistry (Jinno and Kosaka, 2002b, Ferraguti et al., 2005, Fuentealba et al., 2008, Viney et al., 2013). Nitric oxide synthase-expressing neuronal populations, the ivy and neurogliaform interneurons, are present throughout the hippocampus. They are slow firing *in vivo* and phase locked to the theta oscillation (Fuentealba et al., 2008). The putative synaptic innervation of both ivy neurons and neurogliaform neurons that I

have found, by GABAergic septal axons may be causative in the observed theta-phased modulated firing patterns of both neuronal types *in vivo*.

The spike timing of NOS-expressing neurons, particularly the neurogliaform neurons may relate to modulation of incoming excitatory input from external regions (Capogna, 2010). In anaesthetised rats neurogliaform neurons fire around the peak of theta oscillation recorded in the pyramidal layer, coincident with the strongest perforant pathway inputs from the layer III entorhinal cortex (Mizuseki et al., 2009, Fuentealba et al., 2010, Burgalossi et al., 2011, Lapray et al., 2012). In contrast ivy cells fire around the trough of the pyramidal layer theta local field potential.

Neurogliaform neurons are innervated by the Schaffer collaterals, the glutamatergic inputs from CA3 pyramidal neurons (Price et al., 2005). Neurogliaform neurons probably coordinate the excitability of CA1 pyramidal neurons through the distal dendritic tufts in stratum lacunosum-moleculare. Neurogliaform synchrony is supported by the heavy interconnections by both chemical and electrical synapses (Price et al., 2005). Connectivity between the entorhinal cortex and hippocampus may be crucial for spatial representation and production of place cell firing in the hippocampus, mediated by grid and other spatially selective cells from the entorhinal cortices (O'Keefe and Burgess, 2005, Pilly and Grossberg, 2013); although see Castro and Aguiar (2014) and Bush et al. (2014). The integration by CA1 place neurons of entorhinal spatial information may be modulated by dendritic fast and slow inhibition by neurogliaform neurons (Price et al., 2005, Karayannis et al., 2010, Armstrong et al., 2012). In this study I demonstrate that neurogliaform cells receive septal GABAergic innervation. This may influence their spike timing. Nitric oxide synthase-expressing interneurons receive depolarising input from upstream regions which also innervate principal cells in the same regions (reviewed in Armstrong et al. (2012)). Perforant pathway / Schaffer collateral excitation causes disynaptic feedforward inhibition of the pyramidal neurons excited monosynaptically by these pathways, via the NOS-expressing interneurons “gating” and modulating the spike timing and excitability of the efferent neurons (Capogna, 2010).

Interestingly, GABAergic septal input is hypothesised to govern output and synchrony of both the CA3 region and therefore the output via the Schaffer collaterals (Goutagny et al., 2008, Takács et al., 2008, Viney et al., 2013), and entorhinal cortices and therefore the perforant pathway (Brandon et al., 2011, Koenig et al., 2011). Coordination of all inputs at a theta time scale may provide appropriate integration of signals to produce spatial coding. Both feedforward inhibition via NOS-expressing interneurons, and overall theta-phased inhibition of all components of this pathway may provide the temporal synchronicity required for this integration. It is unknown whether single septal neurons innervate multiple areas, e.g. both CA3 and entorhinal cortex, and are capable of coordinating activity between cortical regions. It is possible that single neurons innervate only one region and through synaptic connectivity within the septum coordinate multiple regions. One of the consequences of possible single region innervation is that modulatory inputs can alter theta related firing in specific regions. The possible innervation of multiple regions by single neurons does not allow for regulation of individual regions independently, but may produce greater synchronicity between all interconnected regions. Increased oscillatory synchronicity between regions is implicated in effective coding during behavioural tasks (Fujisawa and Buzsáki, 2011, Hipp et al., 2011, Buschman et al., 2012) and network correlate of this requires a better understanding of the pathways.

Ivy cells, the NOS-expressing cells associated with strata oriens, pyramidale and radiatum, fire action potentials phase locked to the trough of theta oscillation under both anaesthesia and drug-free conditions (Fuentealba et al., 2008, Lapray et al., 2012). Ivy neurons are one of the most phase locked interneuron types, even though they are slow firing. When the theta oscillation increases in frequency the ivy neurons fire at higher rates whilst maintaining their phase locking (Lapray et al., 2012). Medial septal GABAergic neurons are known to increase their firing frequency whilst still being phase locked and rhythmic during conditions which increase theta oscillatory frequency (Vinogradova et al., 1998, Tsanov et al., 2013). These positive correlations between firing frequencies and theta oscillation frequency raises the question of how higher frequency septal

GABAergic input might be compatible with higher firing rates of ivy neurons. I hypothesise that the action potentials occur at the same phase of theta but for shorter periods of absolute time. Likewise phase locked excitation to interneurons including ivy cells may also increase their firing frequencies during these times (Sargolini et al., 2006). These may speed up or decrease under different conditions, such as differences in running speed of the animal, but they fire at the same phase range during theta irrespective of the oscillatory frequency. In fact even when anaesthetised, the relative spike timing of different cell types may remain the same as in drug-free freely behaving conditions (Somogyi et al., 2014).

7.3 Parvalbumin-immunopositive, SATB1-immunonegative putative axo-axonic neurons receive GABAergic septo-hippocampal input

Recently, immunohistochemical differences were found between axo-axonic, and all other PV-expressing neurons in the hippocampus; axo-axonic neurons, unlike others, were immunonegative for the transcription factor SATB1 (Viney et al., 2013). Axo-axonic neurons have a firing pattern strongly phase modulated to the hippocampal theta oscillation *in vivo*, both under anaesthesia and in drug free conditions, and in both dorsal and intermediate hippocampus (Baude et al., 2007, Forro et al., 2013, Viney et al., 2013). This may be caused by the theta-phase modulated release of GABA from septo-hippocampal neurons at synapses with axo-axonic neurons. Large GABAergic septal terminals may produce large inhibitory post-synaptic currents, as size of the presynaptic machinery/structure correlates with the size of the post-synaptic current event (Kay et al., 2011). Compared to the size of interneuron boutons, septal boutons are significantly larger (Eyre et al., 2007). Rhythmic GABAergic inhibition of axo-axonic neurons during theta oscillation may be responsible for the strong theta-phase locked firing seen in axo-axonic neurons both under anaesthesia and drug-free conditions.

7.4 Expression of presynaptic mGluR8a within some medial septal terminals in the hippocampus and an input to trilaminar neurons

Trilaminar neurons are defined by M2R-immunoreactivity and I have provided evidence for a previous suggestion (Ferraguti et al., 2005) that they receive a specific mGluR8a-positive innervation from the septum. The role of septal input may be similar to that described for the NOS-expressing and axo-axonic neurons, i.e. to modulate the firing of this population to the theta oscillation. The presence of the group III metabotropic glutamate receptor mGluR8a in the septal boutons has implications for the function of the synapse between the putative GABAergic septal bouton and the trilaminar neuron. Group III mGluRs can be activated by low levels of glutamate and cause an inhibition of GABA release, a response mediated via N-type calcium channels (Kogo et al., 2004, Guo and Ikeda, 2005). I hypothesise a role for the mGluR8a-mediated uncoupling of the trilaminar neurons from the septal-dependent theta-phase pacing under conditions of high glutamate release, such as during phase precession of place cells. During periods of movement, pyramidal place cells fire bursts of action potentials, as the animal moves through physical locations in space (O'Keefe and Dostrovsky, 1971, O'Keefe and Nadel, 1978, Lapray et al., 2012). During these times, place cell action potential timing relative to the theta oscillation occurs earlier during subsequent theta cycles, a process known as phase precession (O'Keefe and Recce, 1993). Thus far, unidentified interneurons have also been observed during these periods to have a dynamic theta phase which phase precesses (Maurer et al., 2006, Ego-Stengel and Wilson, 2007). The current model of this phenomenon is that these interneurons, under the monosynaptic excitation of precessing place cells, are entrained (Maurer et al., 2006). The interneuron, which is usually thought to be under the theta phase control of the septum, fires outside of its usual theta phase. Firing probability of pyramidal neurons is highest during the time of maximal phase precession at the middle of the place field (O'Keefe and Dostrovsky, 1971). This increased glutamate release may activate presynaptic mGluR8a receptors on septal boutons, reducing rhythmic GABAergic release, uncoupling the interneuron from the septal rhythmic input and reducing theta-phase inhibition

during this time. Accordingly, interneuron phase precession may rely not only on the increasing excitation from pyramidal neurons, but also the decreasing inhibition from the septal boutons. I predict that trilaminar neurons will display phase precession and suggest that other interneurons, which may also display phase precession, such as O-LM interneurons may also receive theta phased septal innervation, which contains the mGluR8a receptor. Likewise, when the majority of pyramidal neurons are silent, these interneurons will fire at a fixed phase, solely dictated by the septal input. This could be tested by anterograde labelling of septal GABAergic terminals in PHAL injected tissue using immunohistochemistry. Further, using *in vivo* calcium imaging of septal terminals (such as in Kaifosh et al. (2013)) one could test the effect of mGluR8a on septal bouton firing using pharmacological tools. One would expect to see that during periods of locomotion where place cells are active, the boutons containing mGluR8a would decrease their calcium transients related to the physical location of the animal, whilst the majority (that do not contain mGluR8a) would not show this dynamism. Critical to this hypothesis is that interneuron types which are innervated by mGluR8a-expressing septal boutons phase precess, which will rely on the *in vivo* recording of behaviour-dependent firing patterns, and post hoc identification of neurons.

I have demonstrated the GABAergic synaptic input from the medial septum to four previously untested populations of hippocampal interneurons: the ivy, the neurogliaform, the axo-axonic and trilaminar neurons. This is consistent with the hypothesis that interneurons which display theta phase locked firing patterns do so because of rhythmic inhibition by septal afferents.

7.5 Novel immunohistochemical markers in theta rhythmic neurons did not correlate with difference in SWR-dependent firing patterns or axonal location

Molecular expression profiles have been correlated with differences in other cell-type properties such as axonal arbour, neurotransmitter, and spike timing within the hippocampus (Somogyi, 2010). Often immunohistochemical molecular markers, such as PV, NOS or CCK have been fundamental in identifying neuronal groups (Klausberger et al., 2005, Fuentealba et al., 2008,

Fuentealba et al., 2010, Lapray et al., 2012). Both PV and various HCN channel subunits have been demonstrated as markers of GABAergic septo-hippocampal neurons (Freund, 1989, Morris et al., 2004, Varga et al., 2008). Further diversity has been observed in firing patterns of these neurons, particularly in the mean phase at which medial septal neurons fire during the hippocampal theta oscillation (Borhegyi et al., 2004). In this study I aimed to investigate novel markers of these neurons by immunohistochemistry of neurons recorded and labelled *in vivo*. Several novel markers were tested for expression by both confirmed and putative septo-hippocampal neurons, however so far none of these markers correlated with a particular firing pattern or axonal distribution.

The ion channels HCN4, (as well as other HCN subunits such as 1 and 2) and Kv1.1 may contribute to the induction and maintenance of rhythmic activity in neurons. The delayed rectifier channel Kv1.1 (*KCNA1*) is widely expressed by neurons throughout the brain including the hippocampus (Tsaur et al., 1992). Within the hippocampus the loss of Kv1.1 causes hyperexcitability and epileptiform discharge, as well as epileptic seizures (Smart et al., 1998, Lopantsev et al., 2003). Hippocampal network states, such as SWR epochs are also aberrant in Kv1.1 null animals (Simeone et al., 2013). The Kv1.1 channel is involved in neuronal repolarisation, increasing the membrane potential threshold for action potential generation (Chi and Nicol, 2007, Goldberg et al., 2008) and bursting behaviour (Hsiao et al., 2009). Excitability in septo-hippocampal neurons, as with other neurons, is important in producing firing pattern behaviour appropriate for the relevant coding. Inhibition by septal neurons occurs during the same phase of the theta oscillation i.e. phase coding, which is fundamental to the hypothesis of theta rhythmic inhibition of interneurons and generation of the hippocampal theta. The inhibitory bursting of mutually inhibiting septal neurons which can increase and decrease with external stimuli, i.e. rate coding, also likely plays a crucial role in intraseptal inhibition and rhythmogenesis (Borhegyi et al., 2004). These two phenomena of septo-hippocampal function are intimately linked, and different septal cell types display differences in intrinsic currents such as K^+ currents (Garrido-Sanabria et al., 2011). If we take the mutual inhibition hypothesis as necessary for theta rhythmogenesis, and the signal between septal neurons is

inseparable from that which is sent to the hippocampus, then the intrinsic factors which effect bursting and action potential characteristics (rate code) are intimately linked by the network to the timing at which these neurons fire during theta oscillation (phase code). Expression of ion channels such as the Kv1.1, Kv3.1b (Henderson et al., 2010) and the HCN channels (discussed below), are intrinsic to the production of not only the rate of theta frequency, but also the timing of inhibition to interneurons.

The Ih current has been implicated in numerous cortical oscillations and behaviours including the hippocampal theta oscillation, spindle oscillations and cortical slow waves and rebound spiking (Lüthi et al., 1998, Lüthi and McCormick, 1998, Varga et al., 2008, Hu et al., 2009, Kanyshkova et al., 2009, Engbers et al., 2011). HCN channels, including HCN1, 2, and 4, have a well-documented role of promoting rhythmogenesis within medial septal neurons (Morris et al., 2004). The HCN antagonist ZD7288, when directly applied to medial septal neurons *in vivo*, reduces the intra-burst firing frequency of rhythmic neurons without reducing the coupling to the theta oscillation (Varga et al., 2008). This blockade of HCN channels reduces septo-hippocampal dependent memory (Xu et al., 2004, Cissé et al., 2008). Interestingly, hippocampal pyramidal neurons also express HCN channels and this contributes to a theta frequency resonance (Leung and Yu, 1998, Hu et al., 2002). This shared intrinsic frequency may help to maintain and propagate the theta oscillatory behaviour dependent on HCN currents.

7.6 Possible relevance of transcription factor SATB1 to connectivity

Transcription factors are one mechanism responsible for genomic regulation of cells. The factor SATB1 is required for proper differentiation, maturation, and connectivity of GABAergic interneurons within the cortex (Close et al., 2012, Denaxa et al., 2012), which suggest that SATB1 may have a role in the development of the synaptic relationship between cells in other loci which express it. The laminar distribution of boutons from septal neurons in this, and previous studies demonstrates non-uniformity, i.e. septal axons do not occupy all laminae of the hippocampus

uniformly (Nyakas et al., 1987). Septal neurons as a population may innervate their interneuron target with dense somatic basket-like structures, throughout the dendritic arbour, and at the axon initial segment (Takács et al., 2008). I have found that single septal neurons can and do innervate interneurons at multiple cellular locations, both at the dendrites and the soma, unlike hippocampal interneurons which tend to be more selective in the domains of their target. I have not investigated the axon initial segment as a target of septal GABAergic terminals (Takács et al., 2008), and some of the axons could have innervated the axon initial segments of interneurons.

The non-uniform distribution of septal inhibition to interneurons subcellular domains, as in the case of the same relationship between interneuron types and pyramidal neurons, is functionally significant. The prevalence of boutons on the dendritic domain is suggestive that dendritic inhibition is important in phasing theta oscillation by the rhythmic septal inhibitory input to interneurons. However, the distribution may be dependent on the targeted interneuron type and/or the septo-hippocampal neuron types involved in any given synaptic interaction. A better understanding of the integration of inhibitory signals by each interneurons type throughout their somatodendritic domain will be an advancement for explaining septo-hippocampal pace-making.

Although SATB1 may not have been differentially expressed within the septal neuronal population I observed, other transcription factors, and the gene products they regulate may provide a means for differentiating septo-hippocampal neurons, which display the axonal and firing pattern differences found in this study. Novel methods such as virally-mediated phosphorylated ribosome capture during behaviour (Knight et al., 2012) could aid in the discovery of markers which differentiate neurons projecting to different areas/regions.

7.7 Axonal location and distribution of septo-hippocampal neurons

The hippocampal theta oscillation is a travelling wave and therefore the phase is not uniform across the whole hippocampus at any given time (Lubenov and Siapas, 2009, Patel et al., 2012). I have found that each septo-hippocampal neuron influences the theta related firing patterns of

interneurons within a relatively small area of the total hippocampal volume. If we assume that the same neurons throughout the dorso-ventral extent of any given region, e.g. CA1, fire with the same firing phase relative to the local theta, they will fire sequentially as the travelling wave progresses from dorsal to ventral hippocampus. A shift in the mean theta phase firing of PV-expressing basket cells to later phases with more posterior positions has been demonstrated (Lapray et al., 2012, Fig6f). This is also seen when we compare dorsal and intermediate hippocampal interneurons of similar types (Forro et al., 2013). Interneurons of the same type fire at different theta phase depending on their septo-temporal location from a shared dorsal hippocampal reference location. This theta phase shift between dorsal and intermediate interneurons is explained by a coherent shift in the theta oscillation between these locations; theta waves in the intermediate hippocampus occurring consistently later than dorsally located theta waves by an average of 49°. The magnitude of the phase shift between dorsal and intermediate theta oscillation positively correlates with the distance temporal from the dorsal hippocampus (Forro et al., 2013). The small scale of each septal axon, along with its potentially specific targeting of interneuron types, means that only a small difference will be present between the preferred phase occurring in the most anterior and most posterior neurons innervated by a single axon. Not all septo-hippocampal neurons were so localised on the septo-temporal axis (e.g. D55c and M82f), but the most well characterised neurons were (e.g. M76a and M44). The observed small axonal fields of septal neurons support the hypothesis that interneurons of a similar preferred theta phase receive selective septal input, and that neurons which fire at different phases – even if they are the same interneuron types but in a different septo-temporal location – do not.

Likewise, the differences in phase demonstrated by interneurons within different regions, e.g. CA1, CA3, or dentate gyrus, receive appropriate phase information by specific septal neurons. Single septo-hippocampal neurons such as D55c and M76a had axon distributed in more than a single hippocampal region, even though the overall size of the axon was relatively small. Different regions of the dorsal hippocampus have phase shifted theta oscillation (Buzsáki et al., 1983). Interneurons

of a similar type fire at different times if they are located in different regions, even if they fire at a similar phase of the theta oscillation (Somogyi, 2010, Forro et al., 2013).

Septo-hippocampal neurons may show preferential targeting of specific interneuron types throughout their axonal arbour which correlates with their theta-related firing pattern, as has been previously hypothesised (Borhegyi et al., 2004). In the two examples where target interneuron type could be defined and mean theta phase of the septal neurons was known, septo-hippocampal neurons fired a quarter of a cycle, and half a cycle later respectively than the mean firing phase of the target interneuron under similar anaesthetised recording conditions (summarised in Somogyi et al. (2014)). Theta phase bursts of action potentials by septo-hippocampal neurons correlates with a decreased firing probability of their interneuron targets, suggesting an inhibitory role. However, monosynaptic spike timing between neurons connected with solely inhibitory synapses may be synchronised to within a millisecond (Hu et al., 2011) providing an alternative hypothesis for septo-hippocampal GABAergic theta pace-making. Certain interneuron types are maximally active during the theta cycle when pyramidal neurons are also maximally active such as the bistratified neurons (Klausberger et al., 2004). This alternative hypothesis is not supported by the observed theta phase data presented here and recorded under anaesthesia. The septo-hippocampal inhibition occurs counter phased to the maximal firing of the likely hippocampal targets.

If single septal neurons innervate similar interneurons in different regions of the hippocampus, how does the single phase information transmitted by a septal neuron relate to interneurons which fire at different times *in vivo*? From a comparison between anterograde tracing studies and single labelled septal neurons, it is likely that single interneurons are innervated by several septal neurons, i.e. there is summation of septal inputs to hippocampal interneurons. Rhythmic inputs of different phases to a single interneuron type might alter the mean theta phase of that type of neuron. Variations of the relative amounts inhibition by multiple, differently phased, septal

neurons could result in a complex inhibitory dynamic of interneuron targets. For example, the same type of interneuron in two different hippocampal areas may receive GABAergic input from different septal firing at different theta phases. Neurons in other region may have a mixture of inputs from differently phased septal neurons in a topographic manner. In addition, a septal neuron which primarily innervates neurons within the dentate gyrus may provide the majority of the input to a given cell type there, but provide a smaller, secondary input to interneurons in CA3 or CA1, such is the case with M76a – which primarily targeted the dentate gyrus and CA3 and had a smaller innervation of CA1. My work has provided information about the extent of septal input to distinct regions of the hippocampus but the extent of overlap between individual septal neurons remains unknown.

Calcium imaging of septal axons innervating single interneurons could be used to test if all septal axons converging on a single interneuron fire at the same theta phase or if all septal inputs to an interneuron are active during all behavioural states. This at present cannot be achieved because of the limitations of the temporal resolution of calcium dyes. Whilst septal boutons on the same axons display the same response to stimulus using this technique (Kaifosh et al., 2013), the kinetics of the calcium dye used, and relatively low sampling rate used to detect the signals, do not make it possible to establish the theta phase of firing. Discovering immunohistochemical markers that correlate with septal neurons firing with a particular theta phase, would allow for the post hoc identification of the phase of neurons labelled by retrograde transport of viral vectors injected into single interneurons (Marshel et al., 2010), or the retrograde labelling of all septal inputs to a genetically-defined population of interneurons (Sun et al., 2014). Investigation of the integration of inhibitory signals by interneuron types will be important to explain the relative effects of septal input to different subcellular domains of interneurons and their role in theta generation.

7.8 Limitations of confocal microscopy and synaptic markers

A major conclusion of this study is that single septo-hippocampal neurons have a specific and non-uniform distribution of interneuron targets. This relies on the reliable identification of both synapses and interneuron types by immunohistochemistry.

Optical microscopy has been used extensively in the identification and quantification of pre- and post- synaptic structures, as well as the quantification of inputs to specific cell types or structures (Alvarez et al., 1999, Bannatyne et al., 2009, Chen et al., 2011, Jackson et al., 2012, Fogarty et al., 2013, Viney et al., 2013). Electron microscopy is the "gold standard" for the localisation of synapses between structures, however this method does not easily allow for the testing of multiple immunohistochemical markers on the post synaptic structure needed for identifying the interneuron type. Fluorescent immunohistochemistry allowed for up to 7 immunoreactions on a single target neuron and the streptavidin-based visualisation of the juxtacellularly filled neuron. Multiple immunoreactions can be performed on electron microscopic tissue but it is usually done on serial sections of the same structure (e.g. Sandler and Smith (1991), and is much more difficult and time consuming than the equivalent reactions done for immunofluorescent identification, as well as being confined to the immediate structure of the synapse rather than the larger structures commonly found by immunofluorescence. Although the high levels of certainty over the presence of a synapse is valuable, the thorough testing of the target structure to the point of interneuron identification was of a higher priority during this study. The high number of boutons tested (>500 in total) would be outside the scope of an electron microscopic study.

The resolution of the confocal microscope in this study at optimal conditions is approximately 400 by 400 by 800 nm in x, y, and z respectively depending on the wavelength of light used. The size of a synaptic cleft is ~20-40 nm: at least 10 times smaller than the best resolvable distance by light microscopy. Further evidence is required that a synapse is present between two structures than just an unresolvable apposition between the axon and a potential postsynaptic structure; this is

provided by the localisation of a pre- or post- synaptic proteins in GABAergic synapses such as VGAT and/or gephyrin. The vesicular transporter VGAT and the post-synaptic GABAA receptor anchoring protein gephyrin have been found consistently throughout the brain in GABAergic synapses (McIntire et al., 1997, Fritschy et al., 2012, Tyagarajan and Fritschy, 2014). A key assumption of this methodology is the specificity of the antibodies to avoid false identification of synaptic contacts. As with all antibodies used throughout this study, the specificity and labelling quality were considered to be appropriate for this method.

A previous study on putative septo-hippocampal neurons, and their boutons within the septum attempted to address the reliability of the septal bouton, at the light microscopic level, and the occurrence of a synapse, at the electron microscopic level (Henderson et al., 2004). Although they only tested 8 boutons of 320 boutons seen at the light microscopic level, all 8 were confirmed to form synapses between pre- and post- synaptic identified neurons. Firstly, this should illustrate the difficulties in translating light to electron microscopy even for *in vitro* filled neurons and a single immunoreactive target, and it also suggests that basket-like structures seen in that study, and used in my study are in fact synaptic in nature. This is especially important when considering the majority of fully identified postsynaptic neurons, e.g. PV-expressing basket cells rather than only PV-expressing interneurons, which were innervated in this basket-like fashion.

7.9 Caveats of immunohistochemical identification of interneuron targets

The identification of interneuron types by immunohistochemistry is well established for the majority of known interneurons types using a combination of available markers (Somogyi, 2010), provided the expression of sufficient number of molecules can be tested on a single neuron. However, in this study it was not always possible to identify the soma of targeted interneurons, as the majority of the structures targeted synaptically by three characterised septal neurons were dendrites. Currently, there are fewer cell-type specific molecular markers for the testing of the origin of dendrites than the identity of somata; the nucleus and other somatic organelles such as

the Golgi apparatus express many proteins not present in distal dendrites. The innervation of dendrites by septal axons limits the identification of postsynaptic neurons. This leads to a bias in the identification of cytoplasmic, and strong and ubiquitous membrane markers that are present throughout neurons such as PV, calretinin, calbindin, M2 receptor and nitric oxide synthase. Molecules such as CCK, somatostatin, and SATB1 are mainly present in somatic domains or nerve terminals and although they define cell-types, cannot be observed in dendrites using immunohistochemistry. Unfortunately, because of the labour-intensive nature of immunohistochemistry on single juxtacellularly filled neurons, in most cases, I was unable to trace the targeted interneuron dendrites back to a soma for further characterisation. I made the assumption that neurons which were innervated at the dendrites are likely to be similar to those cells targeted at the soma, which are easier to identify due to the broad repertoire of molecules that are located in somata.

Certain populations of interneurons are marked by molecules not expressed uniformly in the cytoplasm, such as CCK which is found within somatic organelles. No protein markers are currently known which allow for the immunohistochemical visualisation of the dendrites in these populations. If a septal neuron labelled by the juxtacellular method innervated CCK neurons, for example, only somatic innervation would be identifiable as the majority of boutons were found to be in apposition to dendrites. This would manifest as a high number of unidentifiable boutons, which were not found in the neurons I characterised. This method of target identification is bias to identifying interneuron populations which are marked by proteins found in the cytoplasm and plasma membrane, such as the primary targets of the neurons which I observed.

I have attempted to address the hypothesis that single septal neurons innervate specific targets within the hippocampus in a non-uniform manner. I suggest that this is the case from the qualitative sampling of presumed and identified synaptic targets. Interneuron types are not distributed uniformly and in comparable numbers throughout the hippocampus, as interneuron density varies

in different strata and regions (Kosaka et al., 1987, Nomura et al., 1997b, a, Fuentealba et al., 2010). Very few studies have addressed the dendritic lengths and surface areas of different interneuron types throughout the hippocampus (see Bezaire and Soltesz (2013) for a review of unknown and assumed parameters). It is possible, but unlikely, that the apparent non-uniformity shown by the target selectivity of neurons in this study results from differences in cell-type surface area in the regions which the septal axon occupies. In all cases, bouton-bearing branches were documented close to, but not in apposition to, interneurons, which express markers other than those that were innervated. Furthermore, branches were observed to form multiple synaptic structures with the same neuron over large distances, on different dendritic branches, and not with large numbers of other close by dendrites, which even expressed the same protein markers.

Parvalbumin is expressed by several types of interneuron and may be the marker which labels the most interneurons within the hippocampus (Kosaka et al., 1987, Somogyi, 2010). Nitric oxide synthase however is also expressed by a large proportion of interneurons, as well as being the most frequent interneuron type found in strata radiatum, lacunosum-moleculare and pyramidale (Jinno and Kosaka, 2002b, Fuentealba et al., 2008). The septal neurons characterised here were only infrequently in synaptic contact with NOS-expressing neurons, even when bouton-bearing branches were found throughout strata radiatum and lacunosum-moleculare; the presumed density of NOS expressing interneuron soma and dendrites may be greater than those expressing PV in these regions. I was able to detect gephyrin and VGAT puncta in contacts involving PV unlabelled structures such as those containing NOS and CR ruling out that the result is due to a cell-type dependent methodological bias favouring PV neurons.

The accurate characterisation of interneurons by immunohistochemistry relies upon differences in protein composition between neuronal types. This has been characterised extensively in the CA1 region of the hippocampus, but less well in the CA3 region. The correlation between protein markers and *in vivo* firing patterns of dentate gyrus interneurons is relatively limited by

comparison; to my knowledge no *in vivo* firing patterns have been defined for single interneuron types within the dentate gyrus. The tested targets of septo-hippocampal neurons M76a were PV-positive, SATB1- negative interneurons throughout the dentate gyrus, CA1, and CA3. This molecular profile in CA1 and CA3 correlates with the axo-axonic cell-type, however preliminary data of *in vitro* filled dentate gyrus cells indicates that this may not be the case in this region (Janos Szabadics; personal communication). Thus, PV-expressing SATB1-negative neurons may not necessarily be axo-axonic neurons, but could also include PV-expressing basket cells. More detailed understanding of the cell-types present within the dentate gyrus, the molecular markers which differentiate each type, and the *in vivo* behaviour-dependent firing patterns of neurons is needed before I can make further conclusions about the possible role of M76a, which innervated PV-expressing, SATB1-negative neurons in both the dentate gyrus and CA1 and 3, in theta rhythmogenesis. Axo-axonic neurons within CA1 and CA3 are active at similar times relative to a shared reference time; they fire most around the peak of the CA1 theta oscillation (Klausberger et al., 2003, Viney et al., 2013). My results support the hypothesis that septal neurons fire out of phase with their interneuron targets and makes the prediction that PV-expressing, SATB1- negative dentate gyrus neurons fire at a similar phase to other neuronal cell types innervated by this single septal neuron, i.e. at the peak of CA1 stratum pyramidale theta oscillation.

7.10 Future quantification of single septo-hippocampal neurons

A number of methodological and empirical advances are required to quantify the conclusions suggested in this study. The current methodology for characterisation and identification of interneuron targets, does not allow for the statistical comparison between neurons. Each neuron was tested for markers based on the results of previous reactions, to increase the knowledge of which markers were present in a given target and to rule out other molecules. Many more boutons were tested for PV after it was found that the initially tested boutons were apposed to PV-positive structures. Relatively rare molecules, which are expressed by populations of neurons other than

PV-expressing cells, may have been tested on relatively few boutons or none. The small number of boutons visible in fluorescence of most neurons meant that I prioritised finding positive markers rather than ruling out markers that might be absent from targets. This biased sampling allowed for the cell-type identification of targets, but is unsuitable for quantitative comparisons.

For testing whether the innervation of interneurons is uniform or not, one would need to compare the axonal target distribution to a known distribution or estimate using a general linear model for example. For each neuron all markers would have to be tested on boutons using unbiased sampling. The limitation to this methodology is that even though quantitative statements can be made about distribution and uniformity, one would not identify interneuron types and be able to make biologically relevant comparisons about the network-state dependent firing patterns of the individual septal cells.

Neuron M44 was fully reconstructed in three dimensions and a quantification of axonal arbour and boutons was carried out. Again, for better comparison between neurons whilst also providing data more efficiently, a standardised protocol for section processing should be used. In my project the majority of sections that could be used for immunohistochemical identification of interneuron targets were processed by TBST, which provides the best tissue for immunohistochemistry, but reduces the quality of later permanent processing used for reconstruction. I would propose that every fourth section throughout the axonal arbour be processed specifically for quantification of relative proportions of axonal length and bouton number per layer. This would provide better quality material and more comparable data for each neuron. Again, this assumes that these properties are uniform across the axonal arbour of each septo-hippocampal neuron.

I have concluded that septo-hippocampal neurons may target specific interneuron targets within the hippocampus. To demonstrate this statistically, one would need to compare the demonstrated distribution of interneuron target by each septal neuron, to that of uniform distribution of interneurons found in the hippocampus. Currently, it is not known as to what proportion of surface

area each interneuron type provides to the total available targets in each layer. If PV interneurons provide 50 % of the total available interneuron surface area in stratum oriens then a non-selective neuron would be expected to have 50 % of boutons in apposition to PV-positive structures by chance. The apparent sparsity of the septo-hippocampal neurons may be better interpreted as the proportion of the preferred cell type/s which received innervation by each septal neuron; a VIP-expressing interneuron specific septo-hippocampal neuron targeting CA1 may appear very sparse in comparison to a NOS-expressing interneuron specific septo-hippocampal neuron even if both target a similar proportion of the target cell population.

7.11 Septo-hippocampal neurons during theta oscillation.

I have recorded medial septal neurons with theta frequency bursting pattern similar to those published previously. This is the most common firing pattern of medial septum neurons encountered and has been implicated in leading the hippocampal theta oscillation. Frequency changes in the firing of single septo-hippocampal neurons preceded changes occurring in the hippocampal local field potential theta oscillation (Hangya et al., 2009). Using the spike timing of single septo-hippocampal neurons and the known spike timing of populations of interneurons innervated by these neurons, I have suggested that septo-hippocampal neurons fire out of phase with their hippocampal targets. The theta-phased rhythmic inhibition provided by their septal input is likely to contribute to the phase-locked firing patterns of the interneurons.

Models of CA1 theta generation and function propose inputs arriving to pyramidal neurons which are temporally modulated at theta frequency (Buzsáki, 2002, Hasselmo et al., 2002, Burgess and O'Keefe, 2011). The phase locking of interneurons plays a large role in the currents that contribute to not only theta oscillation but to gamma and ripple band oscillations too (Tukker et al., 2007, Cutsuridis and Hasselmo, 2012, Hájos et al., 2013, Lasztóczi and Klausberger, 2014, Somogyi et al., 2014). Changes to the firing patterns of interneurons could therefore be causative in the oscillations that are observed within the hippocampus. The septo-hippocampal GABAergic projection can

rhythmically reduce interneuron firing and disinhibit pyramidal cells (Toth et al., 1997). Single septo-hippocampal neurons inhibiting specific interneuron targets, which innervate restricted pyramidal cell domains, hence disinhibit specific pyramidal cell subcellular domains. A change in the firing patterns of septal neurons, the resultant inhibition of specific interneurons and disinhibition of pyramidal neuron domains, could alter the hippocampal theta oscillation. The distribution of interneuron-dependent inhibition, dictated by the septum, modulates excitatory inputs to distinct pyramidal cell domains (Leao et al., 2012). External excitatory inputs are also theta modulated (Jones and Wilson, 2005, Mizuseki et al., 2009, Kim et al., 2012). Other regions projecting to CA1, such as CA3 and the entorhinal cortex, also receive septal input (Nyakas et al., 1987, Gaykema et al., 1990, Rowland et al., 2013). The CA3-projecting septal neuron M44 is one example of a septal neuron which has input to an area which projects to CA1.

The entorhinal cortex that provides glutamatergic input to pyramidal neurons in the hippocampus and receives subicular input, also receives a septo-cortical projection (Gaykema et al., 1990). I was not able to visualise theta rhythmic septo-entorhinal axon although on two occasions neurons projected very long distances further posterior than the hippocampus and subiculum, potentially heading to the entorhinal cortex. The distinguishing features in firing patterns of septo-cortical (subicular and entorhinal) compared to septo-hippocampal projecting neurons is unknown.

The innervation of multiple brain areas by single septal neurons could represent a component of the connectivity supporting oscillatory coherence and functional coupling seen during behaviour and network states between different regions, including during hippocampal theta and SWR oscillations (Kim et al., 2012, Taxidis et al., 2013). Specific oscillatory synchrony over large-scale networks has been demonstrated in humans to correlate with performance in a perceptual task, highlighting the importance of understanding oscillations (Hipp et al., 2011). By its projection to the dentate gyrus, CA3, and the CA1, neuron M76a represents a septo-hippocampal neurons which is capable of modulating network behaviour throughout the whole trisynaptic loop of the

hippocampus. However, the axonal arbour was not uniformly distributed between these areas, most boutons were in the dentate gyrus. Likewise, M80d forms synapses with unidentified neurons in CA1 and one of the immediate downstream structures to CA1 pyramidal neurons, the subiculum. Synaptic plasticity, such as long term potentiation and depression, which are prominent hippocampal network, are dependent on the spike timing of pre- and post- synaptic neurons in connected areas (Froemke and Dan, 2002, Wittenberg and Wang, 2006, Jacob et al., 2007, Brandalise and Gerber, 2014). The coordination of cell firing by network oscillations is hypothesised to be necessary for memory processing and learning of hippocampus-dependent tasks (Buzsáki and Draguhn, 2004, Axmacher et al., 2006). Septal neurons that provide rhythmic inhibition to multiple related regions, which can include the medial septum itself, ensure that multiple areas receive a temporal framework for theta time scale synchronisation of neurons. The precise mechanism may involve the septum dependent redistribution of disinhibition of pyramidal neuron domains hypothesised to occur in the hippocampus, which may also occur in other related regions (Somogyi et al., 2014). Although data are available mostly for the dorsal CA1 circuit, as similar network patterns, such as theta and SWR oscillations are found in the intermediate CA1, CA3, subiculum and entorhinal cortices, similar cellular mechanisms may also apply (Chrobak and Buzsáki, 1996, Chrobak and Buzsáki, 1998, Kim et al., 2012, Forro et al., 2013). Interestingly, another region which receives very large dense input from the hippocampus is the lateral septum; lateral septal neurons display place fields, receive plastic synapses from hippocampal pyramidal cells, are theta phase locked, fire bursts during SWRs, but this region does not display the network state dependent oscillations seen in the hippocampo-entorhinal axis (Alonso and Frotscher, 1989, Garcia and Jaffard, 1992, Dragoi et al., 1999, Takamura et al., 2006). There is no published medial septal input to lateral septum, and I never observed a labelled medial septal theta rhythmic neuron innervating the lateral septum (Risold and Swanson, 1997).

7.12 Septo-hippocampal neurons during SWR

During SWR events recorded in dorsal CA1 stratum pyramidale, the majority of rhythmic septal neurons decreased their firing frequency consistent with previous studies. However, a smaller group did not change their firing frequency and this has also been observed previously (Dragoi et al., 1999, Borhegyi et al., 2004, Varga et al., 2008). The decrease in firing frequency may be important in reducing inhibition to interneurons which have an increase in firing frequency during these times such as PV-expressing basket cells and bistratified cells (Klausberger et al., 2004, Tukker et al., 2007, Lapray et al., 2012). SWR-inhibited neurons rarely stopped firing completely. GABAergic input during SWRs, when the interneuron targets might increase their firing frequency, could have numerous functions including the phasing of interneuron firing to the ripple oscillation. This has been hypothesised for bistratified cells which fire ripple oscillatory phased bursts of action potentials during SWRs and the effect on pyramidal cell spike timing (Klausberger et al., 2004). Septal action potentials, unlike bistratified cells, are rarely phase locked to the ripple oscillation making ripple phase spike modulation of the interneurons by the septal cell unlikely. Ripples are generated in small areas of the hippocampus (Patel et al., 2013) and the lack of observed phase locking of septal neurons could be artificial due to the reference being outside of the relevant hippocampal region, for example. Another possibility is that action potentials occurring during SWRs are acting as a feedback to inhibit interneuron hyperexcitability and/or extraneous firing during the large scale excitation that emerges during SWRs (Hájos et al., 2013). Action potentials only occur in a proportion of the SWRs for each inhibited neuron. These active SWRs may represent a quantitatively different group of events which surpass a threshold and produce action potential spiking in usually SWR inhibited neurons.

The proposed mechanism by which medial septal neurons are inhibited during SWRs is by increased GABA release from hippocampo-septal neurons which increase their firing frequency during SWRs (Jinno et al., 2007). This mono-synaptic fast inhibition is supported by the maximal decrease in firing frequency in septal neurons immediately after the peak of the detected SWR epochs. Optogenetic

control of retrogradely labelled hippocampo-septal neurons could give insight into the importance of this pathway, both by stimulation and by real-time detection of ripple epochs and silencing of these neurons *in vivo*. Some hippocampo-septal neurons target interneurons within the hippocampus (Gulyás et al., 2003). To avoid more complex circuit effects from these experiments, light stimulation of the septum itself would be optimal.

A less frequently encountered group of rhythmic septal neurons were found to be active during SWRs recorded from CA1 (Viney et al., 2013). Hippocampal pyramidal cells, which are active during SWRs, have not been demonstrated to project to the medial septum. Hippocampal pyramidal neurons project to the lateral septum (Alonso and Frotscher, 1989, Jakab and Leranth, 1990). Ripple-related increase in firing is known to occur in pyramidal neurons and GABAergic-projection neurons. Only the GABAergic projection neurons are known to innervate the medial septum (Toth et al., 1993, Jinno et al., 2007).

Under some circumstances *in vitro*, GABAergic interneurons produce excitation due to the shift of the reversal potential of chloride towards positive values (Szabadics et al., 2006, Woodruff et al., 2009). The lack of normal chloride transport in the axon initial segment may produce a higher intracellular chloride concentration compared to that of the extracellular space due to a lack of KCC2, which usually maintains a relatively low extracellular Cl^- concentration. In this situation, when GABA receptors are activated, chloride may leave the neuron, producing a positive and depolarising current (Szabadics et al., 2006), depending on the membrane potential. Thus far no depolarising effect has been observed when GABA is applied to septal neurons *in vitro*; GABA agonists produce an inhibitory effect (Frye et al., 1994, Soldo et al., 1994, Hsiao et al., 1998, Henderson and Jones, 2005). *In vivo*, GABA or other GABA agonist application silences the medial septum. The functional result of GABA-A receptor activation in the septum *in vivo* is the abolition of the theta oscillation and reduced performance in memory tasks, suggesting that overall the

effect of GABA on the septo-hippocampal projection is inhibition (Allen and Crawford, 1984, Chrobak et al., 1989, Brioni et al., 1990, Brandon et al., 2011, Tsanov et al., 2013).

The synaptic release of neuropeptide transmitters is thought to require high firing rates (Whim and Lloyd, 1989). Most hippocampo-septal neurons express the neuropeptide somatostatin, and septo-hippocampal neurons express the receptor sst2a (Jinno and Kosaka, 2002a, Bassant et al., 2005). However, the conditions under which the peptide is released to septal neurons are unknown. Somatostatin could represent an excitatory input to septal neurons during SWRs. Sharp-wave ripple events, during which projection neurons have an increased firing frequency, may be sufficient to release somatostatin synaptically. However, the effect of exogenously applied somatostatin on septal neurons recorded *in vivo* has been found to be inhibitory, potentially via the sst2a receptor, on septal neurons, and produce a reduction in hippocampal theta power (Bassant et al., 2005). Therefore, it is unlikely that somatostatin release during SWRs by hippocampo-septal projection neurons is a source of excitation that might explain the increased firing frequency observed in some rhythmic septo-hippocampal neurons during SWR epochs.

Sharp-wave ripple active septal neurons may represent a previously unknown initiation event in the generation of SWRs, currently assumed to begin in CA3 by recurrent pyramidal neuron excitation (Buzsáki et al., 1983). Some septal neurons which are active during SWRs, project to CA3 and may produce a disinhibition of the pyramidal cells thus evoking SWRs. Axo-axonic neurons decrease their firing during and shortly after the SWR events in both CA1 and CA3 (Klausberger et al., 2003, Viney et al., 2013). It is hypothesised that this inhibition, and consequent disinhibition of the pyramidal neuron axon initial segments, is necessary for local SWRs (Viney et al., 2013). Septal neurons do provide GABAergic input to axo-axonic neurons as discussed earlier. GABAergic inhibition may occur out of phase to the maximal firing probability of the interneuron types they target as observed in the neurons of this study. The SWR active septal neurons of this study have mean firing phases which centre around the trough of theta, out of phase with CA1 and CA3 (and

a single CA2) axo-axonic neurons (Viney et al., 2013), suggesting that axo-axonic cells could be a target for SWR active septal neurons.

The peak increase in firing frequency observed in SWR active septal neurons occurred after peak of the SWR events recorded in CA1, which itself occurs after the CA3 SWRs recorded concurrently (Csicsvari et al., 2000). The role of SWR active neurons is unlikely to be that of initiation but may maintain and/or propagate the SWRs through interneuron inhibition in the hippocampus. The septum is well placed to receive and integrate signals from a wide range of ascending and descending inputs and my observations of confirmed septo-hippocampal GABAergic neurons suggest an active role of the medial septum during the SWR events.

Further work is required for the immunohistochemical identification of SWR active neurons within the larger group of septo-hippocampal neurons. The optogenetic manipulation of this population, e.g. the silencing of these neurons with halorhodopsin during the SWR event would define how the action of SWR active septal neurons affects the hippocampal network state. *Post hoc* identification by immunohistochemistry would also allow the investigation of the internal circuitry of the septum; SWR-dependent inhibition of canonical inhibited neurons may be provided internally by the active GABAergic neurons. Single cell retrograde synaptic tracing from these neurons may also demonstrate where the excitatory input originates from. Numerous excitatory inputs to the septum have demonstrated theta-frequency rhythmic firing which may contribute to the firing of septo-hippocampal neuron; to my knowledge none of these cell types in these regions have been investigated during hippocampal SWRs.

7.13 Clustering of septal neurons

To better understand the septal cells, I performed an unsupervised hierarchical clustering and demonstrated the robust clustering of at least three types of rhythmic septal neuron based on the mean theta phase of firing and the SWR response. These being: SWR inhibited neurons which fire maximally at the descending theta phase, SWR active neurons which fire maximally at the

descending theta phase, or SWR active neurons which fire maximally at the ascending phase of theta. The relationship of these parameters has not been investigated to my knowledge previously.

The grouping of medial septal GABAergic cells is at least partially compatible with a previously proposed model. Descending theta phased, SWR inhibited neurons, and ascending theta phased, SWR active neurons may provide two mutually inhibiting neuronal populations. During theta epochs, each population would rhythmically inhibit the other; during SWRs, the active neurons would provide additional inhibition to canonical ripple-inhibited neurons. The third group of rhythmic neurons, descending theta phased and SWR active neurons, may also provide counter-phase inhibition to the ascending phased SWR active neuron group. Inhibition during SWRs may act to modulate inputs arriving to these neurons rather than suppressing the firing of the SWR active neurons that they might innervate. Peri-somatic and dendritic inhibition, such as that provided to hippocampal pyramidal neurons during SWRs by PV-expressing basket cells and bistratified cells, respectively, may act to "fine-tune" the spike timing of the neuron to a particular ripple phase (Klausberger et al., 2004). Therefore all SWR active septal neurons may be phase locked to the ripple oscillations in the hippocampal regions which they innervate, although this is often not the region where the hippocampal LFP recoding electrode was placed. However, non-phase locked spikes may function differently to that which is phase-locked. Phase-locked inhibition my function to modulate spike timing of hippocampal and septal neurons, but non-phase locked inhibition may function to inhibit and suppress firing of neurons innervated synaptically throughout the whole SWR event.

Clustering analysis has allowed the identification and definition of novel groups of rhythmic septo-hippocampal neurons based on firing pattern measures, which are readily applicable to medial septal neurons recorded in freely behaving animals; a condition currently being pursued in our group. Without more knowledge of the axonal arbour of each type of rhythmic septal neuron the definitive description of septo-hippocampal relationships cannot be defined at the single cell level.

Currently, only the single neuron juxtacellular recording and labelling method applied *in vivo* is capable of providing both electrophysiological and anatomical data of this nature. Recent advances in *in vivo* electroporation and other means for gene transfer have shown promise and may supersede the juxtacellular neurobiotin labelling method for this purpose (Kitamura et al., 2008, Oyama et al., 2013). Neurons are recorded during network states by extracellular glass electrodes as with juxtacellular recording. Instead of the prolonged injection of square pulses modulated by hand to label the neuron as in the juxtacellular protocol (Pinault, 1996), the electroporation method uses a single large current injection protocol delivering a plasmid. The method has been established using a vector containing a translatable fluorescent protein but any reporter or protein could be used. Genetic labelling has the potential to improve the visualisation of single neurons and has already been used, without *in vivo* recording of spike trains, to investigate long-range projections and connectivity by viral delivery (Marshel et al., 2010, Fujiyama et al., 2011, Levinthal and Strick, 2012).

A major rate-limiting step in the investigation of the diversity of septo-hippocampal neurons and their target was the labelling of the axons. Axons were frequently labelled over several millimetres, however thin branches were too faint to observe. With genetic labelling, strong and uniform labelling can be produced throughout the whole neuron. Visualisation of the axon by CLARITY could drastically reduce the time taken for assessment, reconstruction and immunohistochemical identification of the synaptic targets of septal neurons (Chung et al., 2013, Zhang et al., 2014). This has yet to be coupled with extracellular recording and labelling of single neurons. Due to the widespread background resulting from endogenous biotin and produced by streptavdin-based visualisation, as used in this study, this method is unlikely to be compatible with CLARITY. Genetic visualisation of single cells produces very high signal-to-noise ratio and is likely to be used in the future. With improved anatomical analysis, parameters relating to axonal location and hippocampal targets may be used to resolve even better defined clusters from these neurons.

Concluding remarks

In this thesis I have explored the relationship between the firing patterns and the axonal patterns of neurons of the medial septum, specifically those which form the GABAergic theta rhythmic projection to the hippocampus. My results complement previous work detailing the firing patterns of hippocampal interneurons *in vivo*, both under anaesthesia and recently, in awake animals. I have provided the first evidence to support the hypothesis that theta rhythmic GABAergic septo-hippocampal neurons described by others target specific interneuron types, and that this may relate to the theta phase firing of the target cells. Septo-hippocampal neurons fire out of phase with interneurons that they innervate and this spike timing may provide the temporal bias and dictate the theta frequency of the network. The diversity of septo-hippocampal neurons is greater than previously described; they fire differentially relating to SWR epochs. I propose that it is no longer appropriate to refer to rhythmic neurons in the medial septum as "septo-hippocampal", because this term does not apply to all such neurons and does not cover the complexity of the network. Above all, I hope that my results help to stimulate interest in this pathway and lead to further investigation so that some of the questions that I have asked can be answered.

References

Acsady L, Halasy K, Freund TF (1993) Calretinin is present in non-pyramidal cells of the rat hippocampus. III. Their inputs from the median raphe and medial septal nuclei. Neuroscience 52:829-841.

Adamantidis AR, Zhang F, Aravanis AM, Deisseroth K, de Lecea L (2007) Neural substrates of awakening probed with optogenetic control of hypocretin neurons. Nature 450:420-424.

Aguilar-Melero P, Ferrin G, Muntane J (2012) Effects of nitric oxide synthase-3 overexpression on post-translational modifications and cell survival in HepG2 cells. Journal of Proteomics 75(3): 740-755.

Airaksinen MS, Eilers J, Garaschuk O, Thoenen H, Konnerth A, Meyer M (1997) Ataxia and altered dendritic calcium signaling in mice carrying a targeted null mutation of the calbindin D28k gene. Proceedings of the National Academy of Sciences 94(4): 1488-1493.

Allen CN, Crawford IL (1984) GABAergic agents on the medial septal nucleus affect hippocampal theta rhythm and acetylcholine utilization. Brain Research 322:261-267.

Alonso A, Köhler C (1982) Evidence for separate projections of hippocampal pyramidal and non-pyramidal neurons to different parts of the septum in the rat brain. Neuroscience Letters 31:209-214.

Alonso JR, Frotscher M (1989) Hippocampo-septal fibers terminate on identified spiny neurons in the lateral septum: A combined Golgi/electron-microscopic and degeneration study in the rat. Cell and Tissue Research 258:243-246.

Alreja M (1996) Excitatory actions of serotonin on GABAergic neurons of the medial septum and diagonal band of Broca. Synapse (New York, NY) 22:15-27.

Alreja M, Liu W (1996) Noradrenaline induces IPSCs in rat medial septal/diagonal band neurons: involvement of septohippocampal GABAergic neurons. The Journal of Physiology 494:201-215.

Alvarez FJ, Dewey DE, McMillin P, Fyffe REW (1999) Distribution of cholinergic contacts on Renshaw cells in the rat spinal cord: a light microscopic study. The Journal of Physiology 515:787-797.

Antonopoulos J, Latsari M, Dori I, Chiotelli M, Parnavelas JG, Dinopoulos A (2004) Noradrenergic innervation of the developing and mature septal area of the rat. The Journal of Comparative Neurology 476:80-90.

Apartis E, Poindessous-Jazat FR, Lamour YA, Bassant MH (1998) Loss of Rhythmically Bursting Neurons in Rat Medial Septum Following Selective Lesion of Septohippocampal Cholinergic System. Journal of Neurophysiology 79:1633-1642.

Aponte Y, Bischofberger J, Jonas P (2008) Efficient Ca2+ buffering in fast-spiking basket cells of rat hippocampus. The Journal of Physiology 586:2061-2075.

Armstrong C, Krook-Magnuson E, Soltesz I (2012) Neurogliaform and Ivy cells: a major class of nNOS expressing GABAergic neurons. Frontiers in Neural Circuits 6.

Axmacher N, Mormann F, Fernández G, Elger CE, Fell J (2006) Memory formation by neuronal synchronization. Brain Research Reviews 52:170-182.

Babiloni C, Frisoni GB, Pievani M, Vecchio F, Lizio R, Buttiglione M, Geroldi C, Fracassi C, Eusebi F, Ferri R, Rossini PM (2009) Hippocampal volume and cortical sources of EEG alpha rhythms in mild cognitive impairment and Alzheimer disease. NeuroImage 44:123-135.

Bannatyne BA, Liu TT, Hammar I, Stecina K, Jankowska E, Maxwell DJ (2009) Excitatory and inhibitory intermediate zone interneurons in pathways from feline group I and II afferents: differences in axonal projections and input. The Journal of Physiology 587:379-399.

Bartos M, Vida I, Frotscher M, Meyer A, Monyer H, Geiger JRP, Jonas P (2002) Fast synaptic inhibition promotes synchronized gamma oscillations in hippocampal interneuron networks. Proceedings of the National Academy of Sciences 99:13222-13227.

Bassant MH, Apartis E, Jazat-Poindessous FR, Wiley RG, Lamour YA, Lamour YA (1995) Selective Immunolesion of the Basal Forebrain Cholinergic Neurons: Effects on Hippocampal Activity During Sleep and Wakefulness in the Rat. Neurodegeneration 4:61-70.

Bassant M-H, Simon A, Poindessous-Jazat F, Csaba Z, Epelbaum J, Dournaud P (2005) Medial Septal GABAergic Neurons Express the Somatostatin sst2A Receptor: Functional Consequences on Unit Firing and Hippocampal Theta. J Neurosci 25:2032-2041.

Baude A, Bleasdale C, Dalezios Y, Somogyi P, Klausberger T (2007) Immunoreactivity for the GABAA Receptor α1 Subunit, Somatostatin and Connexin36 Distinguishes Axoaxonic, Basket, and Bistratified Interneurons of the Rat Hippocampus. Cerebral Cortex 17:2094-2107.

Behr J, Wozny C, Fidzinski P, Schmitz D (2009) Synaptic plasticity in the subiculum. Progress in Neurobiology 89:334-342.

Belbin O, Carrasquillo M, Crump M, Culley O, Hunter T, Ma L, Bisceglio G, Zou F, Allen M, Dickson D, Graff-Radford N, Petersen R, Morgan K, Younkin S (2011) Investigation of 15 of the top candidate genes for late-onset Alzheimer's disease. Human Genetics 129:273-282.

Bell LA, Bell KA, McQuiston AR (2013) Synaptic muscarinic response types in hippocampal CA1 interneurons depend on different levels of presynaptic activity and different muscarinic receptor subtypes. Neuropharmacology 73:160-173.

Berens P (2009) CircStat: A MATLAB Toolbox for Circular Statistics. Journal of Statistical Software 31.

Bergado JA, Frey S, López J, Almaguer-Melian W, Frey JU (2007) Cholinergic afferents to the locus coeruleus and noradrenergic afferents to the medial septum mediate LTP-reinforcement in the dentate gyrus by stimulation of the amygdala. Neurobiology of Learning and Memory 88:331-341.

Berridge CW, Foote SL (1996) Enhancement of Behavioral and Electroencephalographic Indices of Waking following Stimulation of Noradrenergic β-Receptors within the Medial Septal Region of the Basal Forebrain. The Journal of Neuroscience 16:6999-7009.

Bezaire MJ, Soltesz I (2013) Quantitative assessment of CA1 local circuits: Knowledge base for interneuron-pyramidal cell connectivity. Hippocampus 23:751-785.

Bischop DP, Orduz D, Lambot L, Schiffmann SN, Gall D (2012) Control of neuronal excitability by calcium binding proteins : a new mathematical model for striatal fast-spiking interneurons. Frontiers in Molecular Neuroscience 5.

Blanchard J, Martel G, Guillou JL, Noguès X, Micheau J (2008) Impairment of spatial memory consolidation in APP751SL mice results in cue-guided response. Neurobiology of Aging 29:1011-1021.

Bliss TVP, Lømo T (1973) Long-lasting potentiation of synaptic transmission in the dentate area of the anaesthetized rabbit following stimulation of the perforant path. The Journal of Physiology 232:331-356.

Bokor H, Csáki Á, Kocsis K, Kiss J (2002) Cellular architecture of the nucleus reuniens thalami and its putative aspartatergic/glutamatergic projection to the hippocampus and medial septum in the rat. European Journal of Neuroscience 16:1227-1239.

Borhegyi Z, Varga V, Szilagyi N, Fabo D, Freund TF (2004) Phase segregation of medial septal GABAergic neurons during hippocampal theta activity. J Neurosci 24:8470-8479.

Borlikova GG, Trejo M, Mably AJ, Mc Donald JM, Sala Frigerio C, Regan CM, Murphy KJ, Masliah E, Walsh DM (2013) Alzheimer brain-derived amyloid β-protein impairs synaptic remodeling and memory consolidation. Neurobiology of Aging 34:1315-1327.

Brandalise F, Gerber U (2014) Mossy fiber-evoked subthreshold responses induce timing-dependent plasticity at hippocampal CA3 recurrent synapses. Proceedings of the National Academy of Sciences 111:4303-4308.

Brandon MP, Bogaard AR, Libby CP, Connerney MA, Gupta K, Hasselmo ME (2011) Reduction of Theta Rhythm Dissociates Grid Cell Spatial Periodicity from Directional Tuning. Science 332:595-599.

Brioni JD, Decker MW, Gamboa LP, Izquierdo I, McGaugh JL (1990) Muscimol injections in the medial septum impair spatial learning. Brain Research 522:227-234.

Britanova O, Akapov S, Lukyanov S, Gruss P, Tarabykin V (2005) Novel transcription factor Satb2 interacts with matrix attachment region DNA elements in a tissue-specific manner and demonstrates cell-type-dependent expression in the developing mouse CNS. European Journal of Neuroscience 21(3): 658-668.

Britanova O, de Juan Romero C, Cheung A, Kwan KY, Schwark M, Gyorgy A, Vogel T, Akapov S, Mitkovski M, Agoston D, Sestan N, Molnar Z, Tarabykin V (2008) Satb2 Is a Postmitotic Determinant for Upper-Layer Neuron Specification in the Neocortex. Neuron 57(3): 378-392.

Brunner H, Misgeld U (1994) Muscarinic amplification of fast excitation in hilar neurones and inhibition in granule cells in the guinea-pig hippocampus. The Journal of Physiology 480:513-526.

Buck N, Cali S, Behr J (2006) Enhancement of long-term potentiation at CA1-subiculum synapses in MK-801-treated rats. Neuroscience Letters 392:5-9.

Burgalossi A, Herfst L, von Heimendahl M, Förste H, Haskic K, Schmidt M, Brecht M (2011) Microcircuits of Functionally Identified Neurons in the Rat Medial Entorhinal Cortex. Neuron 70:773-786.

Burgess N, O'Keefe J (2011) Models of place and grid cell firing and theta rhythmicity. Current Opinion in Neurobiology 21:734-744.

Buschman Timothy J, Denovellis Eric L, Diogo C, Bullock D, Miller Earl K (2012) Synchronous Oscillatory Neural Ensembles for Rules in the Prefrontal Cortex. Neuron 76:838-846.

Bush D, Barry C, Burgess N (2014) What do grid cells contribute to place cell firing? Trends in neurosciences 37:136-145.

Buzsáki G (1986) Hippocampal sharp waves: Their origin and significance. Brain Research 398:242-252.

Buzsáki G (2002) Theta Oscillations in the Hippocampus. Neuron 33:325-340.

Buzsáki G, Czopf J, Kondákor I, Kellényi L (1986) Laminar distribution of hippocampal rhythmic slow activity (RSA) in the behaving rat: Current-source density analysis, effects of urethane and atropine. Brain Research 365:125-137.

Buzsáki G, Draguhn A (2004) Neuronal Oscillations in Cortical Networks. Science 304:1926-1929.

Buzsaki G, Horvath Z, Urioste R, Hetke J, Wise K (1992) High-frequency network oscillation in the hippocampus. Science 256:1025-1027.

Buzsáki G, Lai-Wo S L, Vanderwolf CH (1983) Cellular bases of hippocampal EEG in the behaving rat. Brain Research Reviews 6:139-171.

Cai L, Gibbs RB, Johnson DA (2012) Recognition of novel objects and their location in rats with selective cholinergic lesion of the medial septum. Neuroscience Letters 506:261-265.

Cajal SRy (1899) Comparative study of the sensory areas of human cortex.

Capogna M (2010) Neurogliaform cells and other interneurons of stratum lacunosum moleculare gate entorhinal-hippocampal dialogue. The Journal of Physiology.

Carr Margaret F, Karlsson Mattias P, Frank Loren M (2012) Transient Slow Gamma Synchrony Underlies Hippocampal Memory Replay. Neuron 75:700-713.

Carter ME, Adamantidis A, Ohtsu H, Deisseroth K, de Lecea L (2009) Sleep Homeostasis Modulates Hypocretin-Mediated Sleep-to-Wake Transitions. The Journal of Neuroscience 29:10939-10949.

Carvalho Pimentel H, Santos J, Macêdo-Lima M, Almeida F, Santos M, Molowny A, Ponsoda X, Lopez-Garcia C, Marchioro M (2011) Structural organization of the cerebral cortex of the neotropical lizard Tropidurus hispidus. Cell and Tissue Research 343:319-330.

Castro L, Aguiar P (2014) A feedforward model for the formation of a grid field where spatial information is provided solely from place cells. Biol Cybern 108:133-143.

Cervera-Ferri A, Guerrero-Martínez J, Bataller-Mompeán M, Taberner-Cortes A, Martínez-Ricós J, Ruiz-Torner A, Teruel-Martí V (2011) Theta synchronization between the

hippocampus and the nucleus incertus in urethane-anesthetized rats. Experimental Brain Research 211:177-192.

Cervera-Ferri A, Rahmani Y, Martínez-Bellver S, Teruel-Martí V, Martínez-Ricós J (2012) Glutamatergic projection from the nucleus incertus to the septohippocampal system. Neuroscience Letters 517:71-76.

Chen AI, Nguyen CN, Copenhagen DR, Badurek S, Minichiello L, Ranscht B, Reichardt LF (2011) TrkB (Tropomyosin-Related Kinase B) Controls the Assembly and Maintenance of GABAergic Synapses in the Cerebellar Cortex. The Journal of Neuroscience 31:2769-2780.

Chen X, Levkowitz G, Tzahar E, Karunagaren D, Lavi S, Ben-Baruch N, Leitner O, Ratzkin BJ, Bacus SS, Yarden Y (1996) An Immunological Approach Reveals Biological Differences between the Two NDF/Heregulin Receptors, ErbB-3 and ErbB-4. Journal of Biological Chemistry 271(13): 7620-7629.

Chi XX, Nicol GD (2007) Manipulation of the Potassium Channel Kv1.1 and Its Effect on Neuronal Excitability in Rat Sensory Neurons. Journal of Neurophysiology 98:2683-2692.

Chrobak JJ, Buzsáki G (1996) High-Frequency Oscillations in the Output Networks of the Hippocampal–Entorhinal Axis of the Freely Behaving Rat. The Journal of Neuroscience 16:3056-3066.

Chrobak JJ, Buzsáki G (1998) Operational Dynamics in the Hippocampal-entorhinal Axis. Neuroscience & Biobehavioral Reviews 22:303-310.

Chrobak JJ, Lörincz A, Buzsáki G (2000) Physiological patterns in the hippocampo-entorhinal cortex system. Hippocampus 10:457-465.

Chrobak JJ, Stackman RW, Walsh TJ (1989) Intraseptal administration of muscimol produces dose-dependent memory impairments in the rat. Behavioral and Neural Biology 52:357-369.

Chung K, Wallace J, Kim S-Y, Kalyanasundaram S, Andalman AS, Davidson TJ, Mirzabekov JJ, Zalocusky KA, Mattis J, Denisin AK, Pak S, Bernstein H, Ramakrishnan C, Grosenick L, Gradinaru V, Deisseroth K (2013) Structural and molecular interrogation of intact biological systems. Nature 497:332-337.

Cissé RS, Krebs-Kraft DL, Parent MB (2008) Septal infusions of the hyperpolarization-activated cyclic nucleotide-gated channel (HCN-channel) blocker ZD7288 impair spontaneous alternation but not inhibitory avoidance. Behavioral neuroscience 122:549-556.

Clarke DJ (1985) Cholinergic innervation of the rat dentate gyrus: an immunocytochemical and electron microscopical study. Brain Research 360:349-354.

Close J, Xu H, De Marco García N, Batista-Brito R, Rossignol E, Rudy B, Fishell G (2012) Satb1 Is an Activity-Modulated Transcription Factor Required for the Terminal Differentiation and Connectivity of Medial Ganglionic Eminence-Derived Cortical Interneurons. The Journal of Neuroscience 32:17690-17705.

Colom LV, Castaneda MT, Reyna T, Hernandez S, Garrido-sanabria E (2005) Characterization of medial septal glutamatergic neurons and their projection to the hippocampus. Synapse 58:151-164.

Craig S, Commins S (2005) Interaction between paired-pulse facilitation and long-term potentiation in the projection from hippocampal area CA1 to the entorhinal cortex. Neuroscience Research 53:140-146.

Crooks R, Jackson J, Bland BH (2012) Dissociable pathways facilitate theta and non-theta states in the median raphe—Septohippocampal circuit. Hippocampus 22:1567-1576.

Csicsvari J, Hirase H, Mamiya A, Buzsáki G (2000) Ensemble Patterns of Hippocampal CA3-CA1 Neurons during Sharp Wave–Associated Population Events. Neuron 28:585-594.

Cui Z, Gerfen CR, Young WS (2013) Hypothalamic and other connections with dorsal CA2 area of the mouse hippocampus. Journal of Comparative Neurology 521:1844-1866.

Cutsuridis V, Hasselmo M (2012) GABAergic contributions to gating, timing, and phase precession of hippocampal neuronal activity during theta oscillations. Hippocampus n/a-n/a.

Cutsuridis V, Taxidis J (2013) Deciphering the Role of CA1 Inhibitory Circuits in Sharp Wave-Ripple Complexes. Frontiers in Systems Neuroscience 7.

Dalkara T, Krnjević K, Ropert N, Yim CY (1986) Chemical modulation of ephaptic activation of CA3 hippocampal pyramids. Neuroscience 17:361-370.

Danik M, Cassoly E, Manseau F, Sotty F, Mouginot D, Williams S (2005) Frequent coexpression of the vesicular glutamate transporter 1 and 2 genes, as well as coexpression with genes for choline acetyltransferase or glutamic acid decarboxylase in neurons of rat brain. Journal of Neuroscience Research 81:506-521.

Deller T, Adelmann G, Nitsch R, Frotscher M (1996) The alvear pathway of the rat hippocampus. Cell Tissue Res 286:293-303.

Denaxa M, Kalaitzidou M, Garefalaki A, Achimastou A, Lasrado R, Maes T, Pachnis V (2012) Maturation-Promoting Activity of SATB1 in MGE-Derived Cortical Interneurons. Cell Reports 2:1351-1362.

Deuchars J, Thomson AM (1996) CA1 pyramid-pyramid connections in rat hippocampus *in vitro*: Dual intracellular recordings with biocytin filling. Neuroscience 74:1009-1018.

Dickson CT, Trepel C, Bland BH (1994) Extrinsic modulation of theta field activity in the entorhinal cortex of the anesthetized rat. Hippocampus 4:37-51.

Dodson PD, Pastoll H, Nolan MF (2011) Dorsal-ventral organization of theta-like activity intrinsic to entorhinal stellate neurons is mediated by differences in stochastic current fluctuations. The Journal of Physiology.

Dolleman-Van der Weel MJ, Lopes da Silva FH, Witter MP (1997) Nucleus Reuniens Thalami Modulates Activity in Hippocampal Field CA1 through Excitatory and Inhibitory Mechanisms. The Journal of Neuroscience 17:5640-5650.

Dolleman-Van der Weel MJ, Witter MP (2000) Nucleus reuniens thalami innervates γ aminobutyric acid positive cells in hippocampal field CA1 of the rat. Neuroscience Letters 278:145-148.

Doutrelant O, Poulain P, Carette B (1993) Comparative distribution of calbindin and Met-enkephalin immunoreactivities in the guinea-pig lateral septum, with reference to electrophysiologically characterized neurons in the mediolateral part. Brain Research 615:335-341.

Dragoi G, Carpi D, Recce M, Csicsvari J, Buzsaki G (1999) Interactions between hippocampus and medial septum during sharp waves and theta oscillation in the behaving rat. J Neurosci 19:6191-6199.

Dragoi G, Tonegawa S (2011) Preplay of future place cell sequences by hippocampal cellular assemblies. Nature 469:397-401.

Dragoi G, Tonegawa S (2013) Distinct preplay of multiple novel spatial experiences in the rat. Proceedings of the National Academy of Sciences 110:9100-9105.

DuBois DW, Damborsky JC, Fincher AS, Frye GD, Winzer-Serhan UH (2013) Varenicline and nicotine enhance GABAergic synaptic transmission in rat CA1 hippocampal and medial septum/diagonal band neurons. Life Sciences 92:337-344.

Ego-Stengel V, Wilson MA (2007) Spatial selectivity and theta phase precession in CA1 interneurons. Hippocampus 17:161-174.

Ego-Stengel V, Wilson MA (2010) Disruption of ripple-associated hippocampal activity during rest impairs spatial learning in the rat. Hippocampus 20:1-10.

Eichenbaum H, Wiener S, Shapiro M, Cohen N (1989) The organization of spatial coding in the hippocampus: a study of neural ensemble activity. The Journal of Neuroscience 9:2764-2775.

Ekstrom AD, Kahana MJ, Caplan JB, Fields TA, Isham EA, Newman EL, Fried I (2003) Cellular networks underlying human spatial navigation. Nature 425:184-188.

Ellender TJ, Nissen W, Colgin LL, Mann EO, Paulsen O (2010) Priming of Hippocampal Population Bursts by Individual Perisomatic-Targeting Interneurons. The Journal of Neuroscience 30:5979-5991.

Engbers JDT, Anderson D, Tadayonnejad R, Mehaffey WH, Molineux ML, Turner RW (2011) Distinct roles for IT and IH in controlling the frequency and timing of rebound spike responses. The Journal of Physiology 589:5391-5413.

Eyre MD, Freund TF, Gulyas AI (2007) Quantitative ultrastructural differences between local and medial septal GABAergic axon terminals in the rat hippocampus. Neuroscience 149:537-548.

Faris PD, Sainsbury RS (1990) The role of the pontis oralis in the generation of RSA activity in the hippocampus of the guinea pig. Physiology & Behavior 47:1193-1199.

Fenske S, Krause SC, Hassan SIH, Becirovic E, Auer F, Bernard R, Kupatt C, Lange P, Ziegler T, Wotjak CT, Zhang H, Hammelmann V, Paparizos C, Biel M, Wahl-Schott CA (2013) Sick Sinus Syndrome in HCN1-Deficient Mice. Circulation 128(24): 2585-2594.

Ferraguti F, Klausberger T, Cobden P, Baude A, Roberts JDB, Szucs P, Kinoshita A, Shigemoto R, Somogyi P, Dalezios Y (2005) Metabotropic Glutamate Receptor 8-Expressing Nerve Terminals Target Subsets of GABAergic Neurons in the Hippocampus. The Journal of Neuroscience 25:10520-10536.

Fidzinski P, Shor O, Behr J (2008) Target-cell-specific bidirectional synaptic plasticity at hippocampal output synapses. European Journal of Neuroscience 27:1111-1118.

Finch DM, Nowlin NL, Babb TL (1983) Demonstration of axonal projections of neurons in the rat hippocampus and subiculum by intracellular injection of HRP. Brain Research 271:201-216.

Fisone G, Wu CF, Consolo S, Nordström O, Brynne N, Bartfai T, Melander T, Hökfelt T (1987) Galanin inhibits acetylcholine release in the ventral hippocampus of the rat: histochemical, autoradiographic, *in vivo*, and *in vitro* studies. Proceedings of the National Academy of Sciences 84:7339-7343.

Fogarty MJ, Hammond LA, Kanjhan R, Bellingham MC, Noakes PG (2013) A method for the three-dimensional reconstruction of Neurobiotin™-filled neurons and the location of their synaptic inputs. Frontiers in Neural Circuits 7.

Fonseca LC, Tedrus GMAS, Prandi LR, Almeida AM, Furlanetto DS (2011) Alzheimer's disease: relationship between cognitive aspects and power and coherence EEG measures. Arquivos de Neuro-Psiquiatria 69:875-881.

Forro T, Valenti O, Lasztoczi B, Klausberger T (2013) Temporal Organization of GABAergic Interneurons in the Intermediate CA1 Hippocampus During Network Oscillations. Cerebral Cortex.

Förstermann U, Gorsky LD, Pollock JS, Schmidt HHHW, Heller M, Murad F (1990) Regional distribution of EDRF/NO-synthesizing enzyme(s) in rat brain. Biochemical and Biophysical Research Communications 168:727-732.

Foster DJ, Wilson MA (2006) Reverse replay of behavioural sequences in hippocampal place cells during the awake state. Nature 440:680-683.

Freir DB, Fedriani R, Scully D, Smith IM, Selkoe DJ, Walsh DM, Regan CM (2011) Aβ oligomers inhibit synapse remodelling necessary for memory consolidation. Neurobiology of Aging 32:2211-2218.

Freund TF (1989) GABAergic septohippocampal neurons contain parvalbumin. Brain Research 478:375-381.

Freund TF, Antal M (1988) GABA-containing neurons in the septum control inhibitory interneurons in the hippocampus. Nature 336:170-173.

Fritschy J-M, Panzanelli P, Tyagarajan S (2012) Molecular and functional heterogeneity of GABAergic synapses. Cell Mol Life Sci 69:2485-2499.

Froemke RC, Dan Y (2002) Spike-timing-dependent synaptic modification induced by natural spike trains. Nature 416:433-438.

Frotscher M, Léránth C (1985) Cholinergic innervation of the rat hippocampus as revealed by choline acetyltransferase immunocytochemistry: A combined light and electron microscopic study. The Journal of Comparative Neurology 239:237-246.

Frye GD, Fincher AS, Grover CA, Griffith WH (1994) Interaction of ethanol and allosteric modulators with GABAA-activated currents in adult medial septum/diagonal band neurons. Brain Research 635:283-292.

Fuentealba P, Begum R, Jinno S, Marton LF, Csicsvari J, Thomson A, Somogyi P, Klausberger T (2008) Ivy cells: a population of nitric oxide-producing, slow-spiking GABAergic neurons and their involvement in hippocampal network activity. Neuron 57:917-929.

Fuentealba P, Klausberger T, Karayannis T, Suen WY, Huck J, Tomioka R, Rockland K, Capogna M, Studer M, Morales M, Somogyi P (2010) Expression of COUP-TFII nuclear receptor in restricted GABAergic neuronal populations in the adult rat hippocampus. J Neurosci 30:1595-1609.

Fuentealba P, Tomioka R, Dalezios Y, Márton LF, Studer M, Rockland K, Klausberger T, Somogyi P (2008) Rhythmically active enkephalin-expressing GABAergic cells in the CA1 area of the hippocampus project to the subiculum and preferentially innervate interneurons. J Neurosci 28:10017-10022.

Fujisawa S, Buzsáki G (2011) A 4 Hz Oscillation Adaptively Synchronizes Prefrontal, VTA, and Hippocampal Activities. Neuron 72:153-165.

Fujiyama F, Sohn J, Nakano T, Furuta T, Nakamura KC, Matsuda W, Kaneko T (2011) Exclusive and common targets of neostriatofugal projections of rat striosome neurons: a single neuron-tracing study using a viral vector. European Journal of Neuroscience 33:668-677.

Fukudome Y, Ohno-Shosaku T, Matsui M, Omori Y, Fukaya M, Tsubokawa H, Taketo MM, Watanabe M, Manabe T, Kano M (2004). Two distinct classes of muscarinic action on hippocampal inhibitory synapses: M2-mediated direct suppression and M1/M3-mediated indirect suppression through endocannabinoid signalling. European Journal of Neuroscience 19(10): 2682-2692.

Fuller P, Sherman D, Pedersen NP, Saper CB, Lu J (2011) Reassessment of the structural basis of the ascending arousal system. The Journal of Comparative Neurology 519:933-956.

Garcia R, Jaffard R (1992) The hippocampo-septal projection in mice: long-term potentiation in the lateral septum. NeuroReport 3:193-196.

Garcia R, Jaffard R (1993) A comparative study of age-related changes in inhibitory processes and long-term potentiation in the lateral septum of mice. Brain Research 620:229-236.

García-Hernández A, Bland BH, Facelli JC, Colom LV (2010) Septo-hippocampal networks in chronic epilepsy. Experimental Neurology 222:86-92.

Garrido-Sanabria ER, Perez MG, Banuelos C, Reyna T, Hernandez S, Castaneda MT, Colom LV (2007) Electrophysiological and morphological heterogeneity of slow firing neurons in medial septal/diagonal band complex as revealed by cluster analysis. Neuroscience 146:931-945.

Garrido-Sanabria ER, Perez-Cordova MG, Colom LV (2011) Differential expression of voltage-gated K+ currents in medial septum/diagonal band complex neurons exhibiting distinct firing phenotypes. Neuroscience Research 70:361-369.

Gautron L, Rutkowski JM, Burton MD, Wei W, Wan Y, Elmquist JK (2013). Neuronal and nonneuronal cholinergic structures in the mouse gastrointestinal tract and spleen. Journal of Comparative Neurology 521(16): 3741-3767.

Gaykema RPA, Luiten PGM, Nyakas C, Traber J (1990) Cortical projection patterns of the medial septum-diagonal band complex. The Journal of Comparative Neurology 293:103-124.

Gerashchenko D, Wisor JP, Burns D, Reh RK, Shiromani PJ, Sakurai T, de la Iglesia HO, Kilduff TS (2008) Identification of a population of sleep-active cerebral cortex neurons. Proceedings of the National Academy of Sciences 105:10227-10232.

Gerfen CR, Sawchenko PE (1984) An anterograde neuroanatomical tracing method that shows the detailed morphology of neurons, their axons and terminals: Immunohistochemical localization of an axonally transported plant lectin,Phaseolus vulgaris leucoagglutinin (PHA-L). Brain Research 290:219-238.

Girardeau G, Benchenane K, Wiener SI, Buzsaki G, Zugaro MB (2009) Selective suppression of hippocampal ripples impairs spatial memory. Nat Neurosci 12:1222-1223.

Goldberg EM, Clark BD, Zagha E, Nahmani M, Erisir A, Rudy B (2008) K+ Channels at the Axon Initial Segment Dampen Near-Threshold Excitability of Neocortical Fast-Spiking GABAergic Interneurons. Neuron 58:387-400.

Gong Y, Xu L, Wang H, Guo F, Sun X, Gao S (2013) Involvements of the lateral hypothalamic area in gastric motility and its regulation by the lateral septum. General and Comparative Endocrinology 194:275-285.

Goutagny R, Jackson J, Williams S (2009) Self-generated theta oscillations in the hippocampus. Nat Neurosci 12:1491-1493.

Goutagny R, Manseau F, Jackson J, Danik M, Williams S (2008) *In vitro* activation of the medial septum—Diagonal band complex generates atropine-sensitive and atropine-resistant hippocampal theta rhythm: An investigation using a complete septohippocampal preparation. Hippocampus 18:531-535.

Graves Austin R, Moore Shannon J, Bloss Erik B, Mensh Brett D, Kath William L, Spruston N (2012) Hippocampal Pyramidal Neurons Comprise Two Distinct Cell Types that Are Countermodulated by Metabotropic Receptors. Neuron 76:776-789.

Green JD, Arduini AA (1954) HIPPOCAMPAL ELECTRICAL ACTIVITY IN AROUSAL. Journal of Neurophysiology 17:533-557.

Groh A, Meyer HS, Schmidt EF, Heintz N, Sakmann B, Krieger P (2010) Cell-Type Specific Properties of Pyramidal Neurons in Neocortex Underlying a Layout that Is Modifiable Depending on the Cortical Area. Cerebral Cortex 20:826-836.

Gulyas AI, Gorcs TJ, Freund TF (1990) Innervation of different peptide-containing neurons in the hippocampus by GABAergic septal afferents. Neuroscience 37:31-44.

Gulyás AI, Hájos N, Katona I, Freund TF (2003) Interneurons are the local targets of hippocampal inhibitory cells which project to the medial septum. European Journal of Neuroscience 17:1861-1872.

Gulyás AI, Seress L, Tóth K, Acsády L, Antal M, Freund TF (1991) Septal GABAergic neurons innervate inhibitory interneurons in the hippocampus of the macaque monkey. Neuroscience 41:381-390.

Guo J, Ikeda SR (2005) Coupling of Metabotropic Glutamate Receptor 8 to N-Type Ca2+ Channels in Rat Sympathetic Neurons. Molecular Pharmacology 67:1840-1851.

Gupta AS, van der Meer MAA, Touretzky DS, Redish AD (2012) Segmentation of spatial experience by hippocampal theta sequences. Nat Neurosci advance online publication.

Hafting T, Fyhn M, Molden S, Moser M-B, Moser EI (2005) Microstructure of a spatial map in the entorhinal cortex. Nature 436:801-806.

Hagan JJ, Verheijck EE, Spigt MH, Ruigt GSF (1992) Behavioural and electrophysiological studies of entorhinal cortex lesions in the rat. Physiology & Behavior 51:255-266.

Hajos M, Hoffmann WE, Robinson DD, Yu JH, Hajos-Korcsok E (2003) Norepinephrine but not Serotonin Reuptake Inhibitors Enhance Theta and Gamma Activity of the Septo-Hippocampal System. Neuropsychopharmacology 28:857-864.

Hájos N, Karlócai MR, Németh B, Ulbert I, Monyer H, Szabó G, Erdélyi F, Freund TF, Gulyás AI (2013) Input-Output Features of Anatomically Identified CA3 Neurons during Hippocampal Sharp Wave/Ripple Oscillation *In vitro*. The Journal of Neuroscience 33:11677-11691.

Hájos N, Papp EC, Acsády L, Levey AI, Freund TF (1997) Distinct interneuron types express m2 muscarinic receptor immunoreactivity on their dendrites or axon terminals in the hippocampus. Neuroscience 82:355-376.

Halabisky B, Shen F, Huguenard JR, Prince DA (2006) Electrophysiological Classification of Somatostatin-Positive Interneurons in Mouse Sensorimotor Cortex. Journal of Neurophysiology 96:834-845.

Halasy K, Hajszan T, Kovács ÉG, Lam T-T, Leranth C (2004) Distribution and origin of vesicular glutamate transporter 2-immunoreactive fibers in the rat hippocampus. Hippocampus 14:908-918.

Halliwell JV, Adams PR (1982) Voltage-clamp analysis of muscarinic excitation in hippocampal neurons. Brain Research 250:71-92.

Hamlin AS, Windels F, Boskovic Z, Sah P, Coulson EJ (2013) Lesions of the Basal Forebrain Cholinergic System in Mice Disrupt Idiothetic Navigation. PLoS ONE 8:e53472.

Hangya B, Borhegyi Z, Szilagyi N, Freund TF, Varga V (2009) GABAergic neurons of the medial septum lead the hippocampal network during theta activity. J Neurosci 29:8094-8102.

Hangya B, Li Y, Muller RU, Czurkó A (2010) Complementary spatial firing in place cell–interneuron pairs. The Journal of Physiology 588:4165-4175.

Harnett Mark T, Xu N-L, Magee Jeffrey C, Williams Stephen R (2013) Potassium Channels Control the Interaction between Active Dendritic Integration Compartments in Layer 5 Cortical Pyramidal Neurons. Neuron 79:516-529.

Harris-White ME, Zanotti SA, Frautschy SA, Charles AC (1998) Spiral Intercellular Calcium Waves in Hippocampal Slice Cultures. Journal of Neurophysiology 79:1045-1052.

Hart RP, Kwentus JA, Harkins SW, Taylor JR (1988) Rate of forgetting in mild Alzheimer's-type dementia. Brain and Cognition 7:31-38.

Hasselmo ME, Bodelón C, Wyble BP (2002) A Proposed Function for Hippocampal Theta Rhythm: Separate Phases of Encoding and Retrieval Enhance Reversal of Prior Learning. Neural Computation 14:793-817.

Hasuo H, Matsuoka T, Akasu T (2002) Activation of Presynaptic 5-Hydroxytryptamine 2A Receptors Facilitates Excitatory Synaptic Transmission via Protein Kinase C in the Dorsolateral Septal Nucleus. The Journal of Neuroscience 22:7509-7517.

Henderson Z, Fiddler G, Saha S, Boros A, Halasy K (2004) A parvalbumin-containing, axosomatic synaptic network in the rat medial septum: relevance to rhythmogenesis*. European Journal of Neuroscience 19:2753-2768.

Henderson Z, Jones GA (2005) GABAB receptors in the medial septum/diagonal band slice from 16–25 day rat. Neuroscience 132:789-800.

Henderson Z, Lu CB, Janzso G, Matto N, McKinley CE, Yanagawa Y, Halasy K (2010) Distribution and role of Kv3.1b in neurons in the medial septum diagonal band complex. Neuroscience 166:952-969.

Henke H, Lang W (1983) Cholinergic enzymes in neocortex, hippocampus and basal forebrain of non-neurological and senile dementia of alzheimer-type patients. Brain Research 267:281-291.

Herreras O, Makarov V, Fernández-Ruiz A (2012) Sustained increase of spontaneous input and spike transfer in the CA3-CA1 pathway following long term potentiation *in vivo*. Frontiers in Neural Circuits 6.

Herzog E, Takamori S, Jahn R, Brose N, Wojcik SM (2006) Synaptic and vesicular co-localization of the glutamate transporters VGLUT1 and VGLUT2 in the mouse hippocampus. Journal of Neurochemistry 99(3): 1011-1018.

Hipp JF, Engel AK, Siegel M (2011) Oscillatory Synchronization in Large-Scale Cortical Networks Predicts Perception. Neuron 69:387-396.

Hjorth-Simonsen A (1972) Projection of the lateral part of the entorhinal area to the hippocampus and fascia dentata. The Journal of Comparative Neurology 146:219-231.

Hjorth-Simonsen A, Jeune B (1972) Origin and termination of the hippocampal perforant path in the rat studied by silver impregnation. The Journal of Comparative Neurology 144:215-231.

Hsiao C-F, Kaur G, Vong A, Bawa H, Chandler SH (2009) Participation of Kv1 Channels in Control of Membrane Excitability and Burst Generation in Mesencephalic V Neurons. Journal of Neurophysiology 101:1407-1418.

Hsiao S-H, Mahoney JC, West JR, Frye GD (1998) Development of GABAA receptors on medial septum/diagonal band (MS/DB) neurons after postnatal ethanol exposure. Brain Research 810:100-113.

Hu H, Ma Y, Agmon A (2011) Submillisecond Firing Synchrony between Different Subtypes of Cortical Interneurons Connected Chemically But Not Electrically. The Journal of Neuroscience 31:3351-3361.

Hu H, Vervaeke K, Graham LJ, Storm JF (2009) Complementary Theta Resonance Filtering by Two Spatially Segregated Mechanisms in CA1 Hippocampal Pyramidal Neurons. The Journal of Neuroscience 29:14472-14483.

Hu H, Vervaeke K, Storm JF (2002) Two forms of electrical resonance at theta frequencies, generated by M-current, h-current and persistent Na+ current in rat hippocampal pyramidal cells. The Journal of Physiology 545:783-805.

Huang X, Xu W, Liang J, Takagaki K, Gao X, Wu J-y (2010) Spiral Wave Dynamics in Neocortex. Neuron 68:978-990.

Huang Y, Zhang L, Song N-N, Hu Z-L, Chen J-Y, Ding Y-Q (2011) Distribution of Satb1 in the central nervous system of adult mice. Neuroscience Research 71(1): 12-21.

Hughes DI, Boyle KA, Kinnon CM, Bilsland C, Quayle JA, Callister RJ, Graham BA (2013) HCN4 subunit expression in fast-spiking interneurons of the rat spinal cord and hippocampus. Neuroscience 237(0): 7-18.

Huh CYL, Goutagny R, Williams S (2010) Glutamatergic Neurons of the Mouse Medial Septum and Diagonal Band of Broca Synaptically Drive Hippocampal Pyramidal Cells: Relevance for Hippocampal Theta Rhythm. J Neurosci 30:15951-15961.

Iannetti P, Papetti L, Nicita F, Castronovo A, Ursitti F, Parisi P, Spalice A, Verrotti A (2011) Developmental anomalies of the medial septal area: possible implication for limbic epileptogenesis. Childs Nerv Syst 27:765-770.

Ishizuka N, Weber J, Amaral DG (1990) Organization of intrahippocampal projections originating from CA3 pyramidal cells in the rat. The Journal of Comparative Neurology 295:580-623.

Jackson J, Chugh D, Nilsson P, Wood J, Carlström K, Lindvall O, Ekdahl CT (2012) Altered Synaptic Properties During Integration of Adult-Born Hippocampal Neurons Following a Seizure Insult. PLoS ONE 7:e35557.

Jacob V, Brasier DJ, Erchova I, Feldman D, Shulz DE (2007) Spike Timing-Dependent Synaptic Depression in the *In vivo* Barrel Cortex of the Rat. The Journal of Neuroscience 27:1271-1284.

Jaffard R, Vouimba RM, Marighetto A, Garcia R (1996) Long-term potentiation and long-term depression in the lateral septum in spatial working and reference memory. Journal of Physiology-Paris 90:339-341.

Jakab RL, Leranth C (1990) Somatospiny neurons in the rat lateral septal area are synaptic targets of hippocamposeptal fibers: A combined EM/Golgi and degejeration study. Synapse 6:10-22.

Jinno S, Klausberger T, Marton LF, Dalezios Y, Roberts JDB, Fuentealba P, Bushong EA, Henze D, Buzsáki G, Somogyi P (2007) Neuronal diversity in GABAergic long-range projections from the hippocampus. J Neurosci 27:8790-8804.

Jinno S, Kosaka T (2002a) Immunocytochemical characterization of hippocamposeptal projecting GABAergic nonprincipal neurons in the mouse brain: a retrograde labeling study. Brain Research 945:219-231.

Jinno S, Kosaka T (2002b) Patterns of expression of calcium binding proteins and neuronal nitric oxide synthase in different populations of hippocampal GABAergic neurons in mice. The Journal of Comparative Neurology 449:1-25.

Jones GA, Norris SK, Henderson Z (1999) Conduction velocities and membrane properties of different classes of rat septohippocampal neurons recorded *in vitro*. The Journal of Physiology 517:867-877.

Jones MW, Wilson MA (2005) Phase precession of medial prefrontal cortical activity relative to the hippocampal theta rhythm. Hippocampus 15:867-873.

Jyoti A, Plano A, Riedel G, Platt B (2010) EEG, Activity, and Sleep Architecture in a Transgenic AβPP_{swe}/PSEN1_{A246E} Alzheimer's Disease Mouse. Journal of Alzheimer's Disease 22:873-887.

Kagi U, Berchtold MW, Heizmann CW (1987) Ca2+-binding parvalbumin in rat testis. Characterization, localization, and expression during development. Journal of Biological Chemistry 262(15): 7314-7320.

Kaifosh P, Lovett-Barron M, Turi GF, Reardon TR, Losonczy A (2013) Septo-hippocampal GABAergic signaling across multiple modalities in awake mice. Nat Neurosci advance online publication.

Kanyshkova T, Pawlowski M, Meuth P, Dubé C, Bender RA, Brewster AL, Baumann A, Baram TZ, Pape H-C, Budde T (2009) Postnatal Expression Pattern of HCN Channel Isoforms in Thalamic Neurons: Relationship to Maturation of Thalamocortical Oscillations. The Journal of Neuroscience 29:8847-8857.

Karayannis T, Elfant D, Huerta-Ocampo I, Teki S, Scott RS, Rusakov DA, Jones MV, Capogna M (2010) Slow GABA Transient and Receptor Desensitization Shape Synaptic Responses Evoked by Hippocampal Neurogliaform Cells. The Journal of Neuroscience 30:9898-9909.

Kay L, Humphreys L, Eickholt BJ, Burrone J (2011) Neuronal activity drives matching of pre- and postsynaptic function during synapse maturation. Nat Neurosci 14:688-690.

Kim J-S, Lee S-H, Park G, Kim S, Bae S-M, Kim D-W, Im C-H (2012) Clinical Implications of Quantitative Electroencephalography and Current Source Density in Patients with Alzheimer's Disease. Brain Topography 25:461-474.

Kim SM, Ganguli S, Frank LM (2012) Spatial Information Outflow from the Hippocampal Circuit: Distributed Spatial Coding and Phase Precession in the Subiculum. The Journal of Neuroscience 32:11539-11558.

Kinoshita A, Ohishi H, Neki A, Nomura S, Shigemoto R, Takada M, Nakanishi S, Mizuno N (1996) Presynaptic localization of a metabotropic glutamate receptor, mGluR8, in the rhinencephalic areas: a light and electron microscope study in the rat. Neuroscience Letters 207(1): 61-64.

Kirk IJ, McNaughton N (1993) Mapping the differential effects of procaine on frequency and amplitude of reticularly elicited hippocampal rhythmical slow activity. Hippocampus 3:517-525.

Kiss J, Borhegyi Z, Csaky A, Szeiffert G, Leranth C (1997) Parvalbumin-containing cells of the angular portion of the vertical limb terminate on calbindin-immunoreactive neurons located at the border between the lateral and medial septum of the rat. Experimental Brain Research 113:48-56.

Kiss J, Maglóczky Z, Somogyi J, Freund TF (1997) Distribution of calretinin-containing neurons relative to other neurochemically-identified cell types in the medial septum of the rat. Neuroscience 78:399-410.

Kiss J, Patel AJ, Baimbridge KG, Freund TF (1990) Topographical localization of neurons containing parvalbumin and choline acetyltransferase in the medial septum-diagonal band region of the rat. Neuroscience 36:61-72.

Kitamura K, Judkewitz B, Kano M, Denk W, Hausser M (2008) Targeted patch-clamp recordings and single-cell electroporation of unlabeled neurons *in vivo*. Nat Meth 5:61-67.

Kitchigina VF, Kudina TA, Kutyreva EV, Vinogradova OS (1999) Neuronal activity of the septal pacemaker of theta rhythm under the influence of stimulation and blockade of the median raphe nucleus in the awake rabbit. Neuroscience 94:453-463.

Klausberger T, Magill PJ, Marton LF, Roberts JDB, Cobden PM, Buzsaki G, Somogyi P (2003) Brain-state- and cell-type-specific firing of hippocampal interneurons *in vivo*. Nature 421:844-848.

Klausberger T, Marton LF, Baude A, Roberts JDB, Magill PJ, Somogyi P (2004) Spike timing of dendrite-targeting bistratified cells during hippocampal network oscillations *in vivo*. Nat Neurosci 7:41-47.

Klausberger T, Marton LF, O'Neill J, Huck JHJ, Dalezios Y, Fuentealba P, Suen WY, Papp E, Kaneko T, Watanabe M, Csicsvari J, Somogyi P (2005) Complementary Roles of Cholecystokinin- and Parvalbumin-Expressing GABAergic Neurons in Hippocampal Network Oscillations. J Neurosci 25:9782-9793.

Klausberger T, Somogyi P (2008) Neuronal Diversity and Temporal Dynamics: The Unity of Hippocampal Circuit Operations. Science 321:53-57.

Knapp JA, Morris NP, Henderson Z, Matthews RT (2000) Electrophysiological characteristics of non-bursting, glutamate decarboxylase messenger RNA-positive neurons of the medial septum/diagonal band nuclei of guinea-pig and rat. Neuroscience 98:661-668.

Knight Zachary A, Tan K, Birsoy K, Schmidt S, Garrison Jennifer L, Wysocki Robert W, Emiliano A, Ekstrand Mats I, Friedman Jeffrey M (2012) Molecular Profiling of Activated Neurons by Phosphorylated Ribosome Capture. Cell 151:1126-1137.

Kocsis B, Varga V, Dahan L, Sik A (2006) Serotonergic neuron diversity: Identification of raphe neurons with discharges time-locked to the hippocampal theta rhythm. Proc Nat Acad Sci USA 103:1059-1064.

Kocsis B, Vertes R (1994) Characterization of neurons of the supramammillary nucleus and mammillary body that discharge rhythmically with the hippocampal theta rhythm in the rat. The Journal of Neuroscience 14:7040-7052.

Koenig J, Linder AN, Leutgeb JK, Leutgeb S (2011) The Spatial Periodicity of Grid Cells Is Not Sustained During Reduced Theta Oscillations. Science 332:592-595.

Kogo N, Dalezios Y, Capogna M, Ferraguti F, Shigemoto R, Somogyi P (2004) Depression of GABAergic input to identified hippocampal neurons by group III metabotropic glutamate receptors in the rat. European Journal of Neuroscience 19:2727-2740.

Kollack-Walker S, Newman SW (1995) Mating and agonistic behavior produce different patterns of Fos immunolabeling in the male Syrian hamster brain. Neuroscience 66:721-736.

Kosaka T, Katsumaru H, Hama K, Wu J-Y, Heizmann CW (1987) GABAergic neurons containing the Ca2+-binding protein parvalbumin in the rat hippocampus and dentate gyrus. Brain Research 419:119-130.

Kosel KC, Van Hoesen GW, Rosene DL (1982) Non-hippocampal cortical projections from the entorhinal cortex in the rat and rhesus monkey. Brain Research 244:201-213.

Kramis R, Vanderwolf CH, Bland BH (1975) Two types of hippocampal rhythmical slow activity in both the rabbit and the rat: Relations to behavior and effects of atropine, diethyl ether, urethane, and pentobarbital. Experimental Neurology 49:58-85.

Kubota Y, Shigematsu N, Karube F, Sekigawa A, Kato S, Yamaguchi N, Hirai Y, Morishima M, Kawaguchi Y (2011) Selective Coexpression of Multiple Chemical Markers Defines Discrete Populations of Neocortical GABAergic Neurons. Cerebral Cortex 21(8): 1803-1817.

Kuenzel WJ, Medina L, Csillag A, Perkel DJ, Reiner A (2011) The avian subpallium: New insights into structural and functional subdivisions occupying the lateral subpallial wall and their embryological origins. Brain Research 1424:67-101.

Kuhl DE, Minoshima S, Fessler JA, Ficaro EP, Wieland DM, Koeppe RA, Frey KA, Foster NL (1996) *In vivo* mapping of cholinergic terminals in normal aging, Alzheimer's disease, and Parkinson's disease. Annals of Neurology 40:399-410.

Kuhse J, Kalbouneh H, Schlicksupp A, Mukusch S, Nawrotzki R, Kirsch J (2012) Phosphorylation of Gephyrin in Hippocampal Neurons by Cyclin-dependent Kinase CDK5 at Ser-270 Is Dependent on Collybistin. Journal of Biological Chemistry 287(37): 30952-30966.

Lai-Wo Stan L (1985) Spectral analysis of hippocampal EEG in the freely moving rat: Effects of centrally active drugs and relations to evoked potentials. Electroencephalography and Clinical Neurophysiology 60:65-77.

Lambert J-C, Ibrahim-Verbaas CA, Harold D, Naj AC, Sims R, Bellenguez C, Jun G, DeStefano AL, Bis JC, Beecham GW, Grenier-Boley B, Russo G, Thornton-Wells TA, Jones N, Smith AV, Chouraki V, Thomas C, Ikram MA, Zelenika D, Vardarajan BN, Kamatani Y, Lin C-F, Gerrish A, Schmidt H, Kunkle B, Dunstan ML, Ruiz A, Bihoreau M-T, Choi S-H, Reitz C, Pasquier F, Hollingworth P, Ramirez A, Hanon O, Fitzpatrick AL, Buxbaum JD, Campion D, Crane PK, Baldwin C, Becker T, Gudnason V, Cruchaga C, Craig D, Amin N, Berr C, Lopez OL, De Jager PL, Deramecourt V, Johnston JA, Evans D, Lovestone S, Letenneur L, Moron FJ, Rubinsztein DC, Eiriksdottir G, Sleegers K, Goate AM, Fievet N, Huentelman MJ, Gill M, Brown K, Kamboh MI, Keller L, Barberger-Gateau P, McGuinness B, Larson EB, Green R, Myers AJ, Dufouil C, Todd S, Wallon D, Love S, Rogaeva E, Gallacher J, St George-Hyslop P, Clarimon J, Lleo A, Bayer A, Tsuang DW, Yu L, Tsolaki M, Bossu P, Spalletta G, Proitsi P, Collinge J, Sorbi S, Sanchez-Garcia F, Fox NC, Hardy J, Naranjo MCD, Bosco P, Clarke R, Brayne C, Galimberti D, Mancuso M, Matthews F, European Alzheimer's Disease I, Genetic, Environmental Risk in Alzheimer's D, Alzheimer's Disease Genetic C, Cohorts for H, Aging Research in Genomic E, Moebus S, Mecocci P, Del Zompo M, Maier W, Hampel H, Pilotto A, Bullido M, Panza F, Caffarra P, Nacmias B, Gilbert JR, Mayhaus M, Lannfelt L, Hakonarson H, Pichler S, Carrasquillo MM, Ingelsson M, Beekly D, Alvarez V, Zou F, Valladares O, Younkin SG, Coto E, Hamilton-Nelson KL, Gu W, Razquin C, Pastor P, Mateo I, Owen MJ, Faber KM, Jonsson PV, Combarros O, O'Donovan MC, Cantwell LB, Soininen H, Blacker D, Mead S, Mosley Jr TH, Bennett DA, Harris TB, Fratiglioni L, Holmes C, de Bruijn RFAG, Passmore P, Montine TJ, Bettens K, Rotter JI, Brice A, Morgan K, Foroud TM, Kukull WA, Hannequin D, Powell JF, Nalls MA, Ritchie K, Lunetta KL, Kauwe JSK, Boerwinkle E, Riemenschneider M, Boada M, Hiltunen M, Martin ER, Schmidt R, Rujescu D, Wang L-S, Dartigues J-F, Mayeux R, Tzourio C, Hofman A, Nothen MM, Graff C, Psaty BM, Jones L, Haines JL, Holmans PA, Lathrop M, Pericak-Vance MA, Launer LJ, Farrer LA, van Duijn CM, Van Broeckhoven C, Moskvina V, Seshadri S, Williams J, Schellenberg GD, Amouyel P (2013) Meta-analysis of 74,046 individuals identifies 11 new susceptibility loci for Alzheimer's disease. Nat Genet advance online publication.

Lamprea MR, Garcia AMB, Morato S (2010) Effects of reversible inactivation of the medial septum on rat exploratory behavior in the elevated plus-maze using a test–retest paradigm. Behavioural Brain Research 210:67-73.

Lapray D, Lasztoczi B, Lagler M, Viney TJ, Katona L, Valenti O, Hartwich K, Borhegyi Z, Somogyi P, Klausberger T (2012) Behavior-dependent specialization of identified hippocampal interneurons. Nat Neurosci 15:1265-1271.

Lasztóczi B, Klausberger T (2014) Layer-Specific GABAergic Control of Distinct Gamma Oscillations in the CA1 Hippocampus. Neuron 81:1126-1139.

Lasztóczi B, Tukker JJ, Somogyi P, Klausberger T (2011) Terminal Field and Firing Selectivity of Cholecystokinin-Expressing Interneurons in the Hippocampal CA3 Area. The Journal of Neuroscience 31:18073-18093.

Leao RN, Mikulovic S, Leao KE, Munguba H, Gezelius H, Enjin A, Patra K, Eriksson A, Loew LM, Tort ABL, Kullander K (2012) OLM interneurons differentially modulate CA3 and entorhinal inputs to hippocampal CA1 neurons. Nat Neurosci 15:1524-1530.

Lecourtier L, de Vasconcelos AP, Leroux E, Cosquer B, Geiger K, Lithfous S, Cassel J-C (2011) Septohippocampal pathways contribute to system consolidation of a spatial memory: Sequential implication of gabaergic and cholinergic neurons. Hippocampus 21:1277-1289.

Lee AK, Wilson MA (2002) Memory of Sequential Experience in the Hippocampus during Slow Wave Sleep. Neuron 36:1183-1194.

Lee MG, Chrobak JJ, Sik A, Wiley RG, Buzsáki G (1994) Hippocampal theta activity following selective lesion of the septal cholinergic systeM. Neuroscience 62:1033-1047.

Lee S, Kruglikov I, Huang ZJ, Fishell G, Rudy B (2013) A disinhibitory circuit mediates motor integration in the somatosensory cortex. Nat Neurosci 16:1662-1670.

Leigh PN, Connick JH, Stone TW (1990) Distribution of NADPH-diaphorase positive cells in the rat brain. Comparative Biochemistry and Physiology Part C: Comparative Pharmacology 97:259-264.

Leranth C, Carpi D, Buzsaki G, Kiss J (1999) The entorhino-septo-supramammillary nucleus connection in the rat: morphological basis of a feedback mechanism regulating hippocampal theta rhythm. Neuroscience 88:701-718.

Leranth C, Deller T, Buzsáki G (1992) Intraseptal connections redefined: lack of a lateral septum to medial septum path. Brain Research 583:1-11.

Leranth C, Kiss J (1996) A Population of Supramammillary Area Calretinin Neurons Terminating on Medial Septal Area Cholinergic and Lateral Septal Area Calbindin-Containing Cells Are Aspartate/Glutamatergic. The Journal of Neuroscience 16:7699-7710.

Leranth C, Vertes RP (1999) Median raphe serotonergic innervation of medial septum/diagonal band of Broca (MSDB) parvalbumin-containing neurons: Possible involvement of the MSDB in the desynchronization of the hippocampal EEG. The Journal of Comparative Neurology 410:586-598.

Leung LS, Roth L, Canning KJ (1995) Entorhinal inputs to hippocampal CA1 and dentate gyrus in the rat: a current-source-density study. Journal of Neurophysiology 73:2392-2403.

Leung LS, Yu H-W (1998) Theta-Frequency Resonance in Hippocampal CA1 Neurons *In vitro* Demonstrated by Sinusoidal Current Injection. Journal of Neurophysiology 79:1592-1596.

Levinthal DJ, Strick PL (2012) The Motor Cortex Communicates with the Kidney. The Journal of Neuroscience 32:6726-6731.

Lewis PR, Shute CCD, Silver A (1967) Confirmation from choline acetylase analyses of a massive cholinergic innervation to the rat hippocampus. The Journal of Physiology 191:215-224.

Lopantsev V, Tempel BL, Schwartzkroin PA (2003) Hyperexcitability of CA3 Pyramidal Cells in Mice Lacking the Potassium Channel Subunit Kv1.1. Epilepsia 44:1506-1512.

Loreth D, Ozmen L, Revel FG, Knoflach F, Wetzel P, Frotscher M, Metzger F, Kretz O (2012) Selective degeneration of septal and hippocampal GABAergic neurons in a mouse model of amyloidosis and tauopathy. Neurobiology of Disease 47:1-12.

Lorincz A and Nusser Z (2008) Cell-Type-Dependent Molecular Composition of the Axon Initial Segment. The Journal of Neuroscience 28(53): 14329-14340.

Losonczy A, Zemelman BV, Vaziri A, Magee JC (2010) Network mechanisms of theta related neuronal activity in hippocampal CA1 pyramidal neurons. Nat Neurosci 13:967-972.

Louie K, Wilson MA (2001) Temporally Structured Replay of Awake Hippocampal Ensemble Activity during Rapid Eye Movement Sleep. Neuron 29:145-156.

Lovett-Barron M, Turi GF, Kaifosh P, Lee PH, Bolze F, Sun X-H, Nicoud J-F, Zemelman BV, Sternson SM, Losonczy A (2012) Regulation of neuronal input transformations by tunable dendritic inhibition. Nat Neurosci 15:423-430.

Lubenov EV, Siapas AG (2009) Hippocampal theta oscillations are travelling waves. Nature 459:534-539.

Lübke J, Deller T, Frotscher M (1997) Septal innervation of mossy cells in the hilus of the rat dentate gyrus: an anterograde tracing and intracellular labeling study. Experimental Brain Research 114:423-432.

Luiten PGM, Gaykema RPA, Traber J, Spencer Jr DG (1987) Cortical projection patterns of magnocellular basal nucleus subdivisions as revealed by anterogradely transportedPhaseolus vulgaris leucoagglutinin. Brain Research 413:229-250.

Lüthi A, Bal T, McCormick DA (1998) Periodicity of Thalamic Spindle Waves Is Abolished by ZD7288,a Blocker of I h. Journal of Neurophysiology 79:3284-3289.

Lüthi A, McCormick DA (1998) Periodicity of Thalamic Synchronized Oscillations: the Role of Ca2+-Mediated Upregulation of Ih. Neuron 20:553-563.

Lüttgen M, Ove Ögren S, Meister B (2004) Chemical identity of 5-HT2A receptor immunoreactive neurons of the rat septal complex and dorsal hippocampus. Brain Research 1010:156-165.

Ma S, Blasiak A, Olucha-Bordonau FE, Verberne AJM, Gundlach AL (2013) Heterogeneous Responses of Nucleus Incertus Neurons to Corticotropin-Releasing Factor and Coherent Activity with Hippocampal Theta Rhythm in the Rat. The Journal of Physiology.

Ma S, Olucha-Bordonau FE, Hossain MA, Lin F, Kuei C, Liu C, Wade JD, Sutton SW, Nuñez A, Gundlach AL (2009) Modulation of hippocampal theta oscillations and spatial memory by relaxin-3 neurons of the nucleus incertus. Learning & Memory 16:730-742.

Madison D, Lancaster B, Nicoll R (1987) Voltage clamp analysis of cholinergic action in the hippocampus. The Journal of Neuroscience 7:733-741.

Maier N, Morris G, Schuchmann S, Korotkova T, Ponomarenko A, Böhm C, Wozny C, Schmitz D (2012) Cannabinoids disrupt hippocampal sharp wave-ripples via inhibition of glutamate release. Hippocampus 22:1350-1362.

Maison SF, Liu X-P, Vetter DE, Eatock RA, Nathanson NM, Wess J, Liberman MC (2010) Muscarinic Signaling in the Cochlea: Presynaptic and Postsynaptic Effects on Efferent Feedback and Afferent Excitability. The Journal of Neuroscience 30(19): 6751-6762.

Malkov A, Popova I (2011) Functional changes in the septal GABAergic system of animals with a model of temporal lobe epilepsy. General Physiology and Biophysics 30:310-320.

Mallet N, Micklem Benjamin R, Henny P, Brown Matthew T, Williams C, Bolam JP, Nakamura Kouichi C, Magill Peter J (2012) Dichotomous Organization of the External Globus Pallidus. Neuron 74:1075-1086.

Manns ID, Mainville L, Jones BE (2001) Evidence for glutamate, in addition to acetylcholine and GABA, neurotransmitter synthesis in basal forebrain neurons projecting to the entorhinal cortex. Neuroscience 107:249-263.

Marshel JH, Mori T, Nielsen KJ, Callaway EM (2010) Targeting Single Neuronal Networks for Gene Expression and Cell Labeling *In vivo*. Neuron 67:562-574.

Massi L, Lagler M, Hartwich K, Borhegyi Z, Somogyi P, Klausberger T (2012) Temporal Dynamics of Parvalbumin-Expressing Axo-axonic and Basket Cells in the Rat Medial Prefrontal Cortex *In vivo*. The Journal of Neuroscience 32:16496-16502.

Matsukawa M, Ogawa M, Nakadate K, Maeshima T, Ichitani Y, Kawai N, Okado N (1997) Serotonin and acetylcholine are crucial to maintain hippocampal synapses and memory acquisition in rats. Neuroscience Letters 230:13-16.

Matthews DA, Salvaterra PM, Crawford GD, Houser CR, Vaughn JE (1987) An immunocytochemical study of choline acetyltransferase- containing neurons and axon terminals in normal and partially deafferented hippocampal formation. Brain Research 402:30-43.

Maurer AP, Cowen SL, Burke SN, Barnes CA, McNaughton BL (2006) Phase Precession in Hippocampal Interneurons Showing Strong Functional Coupling to Individual Pyramidal Cells. The Journal of Neuroscience 26:13485-13492.

McIntire SL, Reimer RJ, Schuske K, Edwards RH, Jorgensen EM (1997) Identification and characterization of the vesicular GABA transporter. Nature 389:870-876.

McNaughton N, Logan B, Panickar KS, Kirk IJ, Pan W-X, Brown NT, Heenan A (1995) Contribution of synapses in the medial supramammillary nucleus to the frequency of hippocampal theta rhythm in freely moving rats. Hippocampus 5:534-545.

McNaughton N, Ruan M, Woodnorth M-A (2006) Restoring theta-like rhythmicity in rats restores initial learning in the Morris water maze. Hippocampus 16:1102-1110.

Mellgren SI, Srebro B (1973) Changes in acetylcholinesterase and distribution of degenerating fibres in the hippocampal region after septal lesions in the rat. Brain Research 52:19-36.

Middleton S, Jalics J, Kispersky T, LeBeau FEN, Roopun AK, Kopell NJ, Whittington MA, Cunningham MO (2008) NMDA receptor-dependent switching between different gamma rhythm-generating microcircuits in entorhinal cortex. Proceedings of the National Academy of Sciences 105:18572-18577.

Miettinen R, Freund TF (1992a) Convergence and segregation of septal and median raphe inputs onto different subsets of hippocampal inhibitory interneurons. Brain Research 594:263-272.

Miettinen R, Freund TF (1992b) Neuropeptide Y-containing interneurons in the hippocampus receive synaptic input from median raphe and GABAergic septal afferents. Neuropeptides 22:185-193.

Miura Y, Ito T, Kadokawa T (1987) Effects of Intraseptally Injected Dopamine and Noradrenaline on Hippocampal Synchronized Theta Wave Activity in Rats. The Japanese Journal of Pharmacology 44:471-479.

Miyazaki T, Fukaya T, Shimizu H, Watanabe M (2003) Subtype switching of vesicular glutamate transporters at parallel fibre–Purkinje cell synapses in developing mouse cerebellum. European Journal of Neuroscience 17(12): 2563-2572.

Mizuseki K, Royer S, Diba K, Buzsáki G (2012) Activity dynamics and behavioral correlates of CA3 and CA1 hippocampal pyramidal neurons. Hippocampus 22:1659-1680.

Mizuseki K, Sirota A, Pastalkova E, Buzsáki G (2009) Theta Oscillations Provide Temporal Windows for Local Circuit Computation in the Entorhinal-Hippocampal Loop. Neuron 64:267-280.

Molnár G, Oláh S, Komlósi G, Füle M, Szabadics J, Varga C, Barzó P, Tamás G (2008) Complex Events Initiated by Individual Spikes in the Human Cerebral Cortex. PLoS Biol 6:e222.

Montagnese CM, Zachar G, Bálint E, Csillag A (2008) Afferent connections of septal nuclei of the domestic chick (Gallus domesticus): A retrograde pathway tracing study. The Journal of Comparative Neurology 511:109-150.

Montgomery SM, Betancur MI, BuzsÃ¡ki Gr (2009) Behavior-Dependent Coordination of Multiple Theta Dipoles in the Hippocampus. The Journal of Neuroscience 29:1381-1394.

Morales GJ, Ramcharan EJ, Sundararaman N, Morgera SD, Vertes RP (2007) Analysis of the Actions of Nucleus Reuniens and the Entorhinal Cortex on EEG and Evoked Population Behavior of the Hippocampus. In: Engineering in Medicine and Biology Society, 2007 EMBS 2007 29th Annual International Conference of the IEEE, pp 2480-2484.

Moretti DV, Miniussi C, Frisoni GB, Geroldi C, Zanetti O, Binetti G, Rossini PM (2007) Hippocampal atrophy and EEG markers in subjects with mild cognitive impairment. Clinical Neurophysiology 118:2716-2729.

Morris NP, Fyffe REW, Robertson B (2004) Characterisation of hyperpolarization-activated currents (Ih) in the medial septum/diagonal band complex in the mouse. Brain Research 1006:74-86.

Morris NP, Harris SJ, Henderson Z (1999) Parvalbumin-immunoreactive, fast-spiking neurons in the medial septum/diagonal band complex of the rat: intracellular recordings *in vitro*. Neuroscience 92:589-600.

Moss Mb AMSBNPM (1986) DIfferential patterns of memory loss among patients with alzheimer's disease, huntington's disease, and alcoholic korsakoff's syndrome. Archives of Neurology 43:239-246.

Moulin CJA, James N, Freeman JE, Jones RW (2004) Deficient Acquisition and Consolidation: Intertrial Free Recall Performance in Alzheimer's Disease and Mild Cognitive Impairment. Journal of Clinical and Experimental Neuropsychology 26:1-10.

Naber PA, Witter MP (1998) Subicular efferents are organized mostly as parallel projections: A double-labeling, retrograde-tracing study in the rat. The Journal of Comparative Neurology 393:284-297.

Nachkebiya NG, Nachkebiya AY, Oniani LT (1987) Role of septal and entorhinal inputs in the generation of hippocampal electrical activity in the cat sleep-wake cycle. Neurophysiology 19:458-465.

Nakamura M, Sato K, Fukaya M, Araishi K, Aiba A (2004) Signaling complex formation of phospholipase Cβ4 with metabotropic glutamate receptor type 1α and 1,4,5-trisphosphate receptor at the perisynapse and endoplasmic reticulum in the mouse brain. European Journal of Neuroscience 20(11): 2929-2944.

Neddens J, Fish KN, Tricoire L, Vullhorst D, Shamir A, Chung W, Lewis DA, McBain CJ, Buonanno A (2011) Conserved Interneuron-Specific ErbB4 Expression in Frontal Cortex of Rodents, Monkeys, and Humans: Implications for Schizophrenia. Biological Psychiatry 70(7): 636-645.

Nerad L, McNaughton N (2006) The septal EEG suggests a distributed organization of the pacemaker of hippocampal theta in the rat. European Journal of Neuroscience 24:155-166.

Nielsen JV, Blom JB, Noraberg J, Jensen NA (2010) Zbtb20-Induced CA1 Pyramidal Neuron Development and Area Enlargement in the Cerebral Midline Cortex of Mice. Cerebral Cortex 20(8): 1904-1914.

Nimmrich V, Maier N, Schmitz D, Draguhn A (2005) Induced sharp wave-ripple complexes in the absence of synaptic inhibition in mouse hippocampal slices. The Journal of Physiology 563:663-670.

Nokia MS, Mikkonen JE, Penttonen M, Wikgren J (2012) Disrupting neural activity related to awake-state sharp wave-ripple complexes prevents hippocampal learning. Frontiers in Behavioral Neuroscience 6.

Nomura T, Fukuda T, Aika Y, Heizmann CW, Emson PC, Kobayashi T, Kosaka T (1997a) Distribution of nonprincipal neurons in the rat hippocampus, with special reference to their dorsoventral difference. Brain Research 751:64-80.

Nomura T, Fukuda T, Aika Y, Heizmann CW, Emson PC, Kobayashi T, Kosaka T (1997b) Laminar distribution of non-principal neurons in the rat hippocampus, with special reference to their compositional difference among layers. Brain Research 764:197-204.

Nuñez A, Cervera-Ferri A, Olucha-Bordonau F, Ruiz-Torner A, Teruel V (2006) Nucleus incertus contribution to hippocampal theta rhythm generation. European Journal of Neuroscience 23:2731-2738.

Nyakas C, Luiten PGM, Spencer DG, Traber J (1987) Detailed projection patterns of septal and diagonal band efferents to the hippocampus in the rat with emphasis on innervation of CA1 and dentate gyrus. Brain Research Bulletin 18:533-545.

Nyíri G, Szabadits E, Cserép C, Mackie K, Shigemoto R, Freund TF (2005) GABAB and CB1 cannabinoid receptor expression identifies two types of septal cholinergic neurons. European Journal of Neuroscience 21:3034-3042.

O'Keefe J, Burgess N (2005) Dual phase and rate coding in hippocampal place cells: Theoretical significance and relationship to entorhinal grid cells. Hippocampus 15:853-866.

O'Keefe J, Dostrovsky J (1971) The hippocampus as a spatial map. Preliminary evidence from unit activity in the freely-moving rat. Brain Research 34:171-175.

O'Keefe J, Nadel L (eds.) (1978) The hippocampus as a cognitive map. Oxford: Clarendon.

O'Keefe J, Recce ML (1993) Phase relationship between hippocampal place units and the EEG theta rhythm. Hippocampus 3:317-330.

Olucha-Bordonau FE, Otero-García M, Sánchez-Pérez AM, Núñez Á, Ma S, Gundlach AL (2012) Distribution and targets of the relaxin-3 innervation of the septal area in the rat. The Journal of Comparative Neurology 520:1903-1939.

O'Neill J, Senior T, Csicsvari J (2006) Place-Selective Firing of CA1 Pyramidal Cells during Sharp Wave/Ripple Network Patterns in Exploratory Behavior. Neuron 49:143-155.

Onténiente B, Simon H, Taghzouti K, Geffard M, Le Moal M, Calas A (1987) Dopamine-GABA interactions in the nucleus accumbens and lateral septum of the rat. Brain Research 421:391-396.

Orzeł-Gryglewska J, Kuśmierczak M, Majkutewicz I, Jurkowlaniec E (2012) Induction of hippocampal theta rhythm by electrical stimulation of the ventral tegmental area and its loss after septum inactivation. Brain Research 1436:51-67.

Oyama K, Ohara S, Sato S, Karube F, Fujiyama F, Isomura Y, Mushiake H, Iijima T, Tsutsui K-I (2013) Long-lasting single-neuron labeling by *in vivo* electroporation without microscopic guidance. Journal of Neuroscience Methods 218:139-147.

Papp EC, Hájos N, Acsády L, Freund TF (1999) Medial septal and median raphe innervation of vasoactive intestinal polypeptide-containing interneurons in the hippocampus. Neuroscience 90:369-382.

Patel J, Fujisawa S, Berényi A, Royer S, Buzsáki G (2012) Traveling Theta Waves along the Entire Septotemporal Axis of the Hippocampus. Neuron 75:410-417.

Patel J, Schomburg EW, Berényi A, Fujisawa S, Buzsáki G (2013) Local Generation and Propagation of Ripples along the Septotemporal Axis of the Hippocampus. The Journal of Neuroscience 33:17029-17041.

Perry EK, Perry RH, Blessed G, Tomlinson BE (1978) CHANGES IN BRAIN CHOLINESTERASES IN SENILE DEMENTIA OF ALZHEIMER TYPE. Neuropathology and Applied Neurobiology 4:273-277.

Petsche H, Stumpf C, Gogolak G (1962) The significance of the rabbit's septum as a relay station between the midbrain and the hippocampus I. The control of hippocampus arousal activity by the septum cells. Electroencephalography and Clinical Neurophysiology 14:202-211.

Pilly PK, Grossberg S (2013) How reduction of theta rhythm by medial septum inactivation may covary with disruption of entorhinal grid cell responses due to reduced cholinergic transmission. Frontiers in Neural Circuits 7.

Pilly PK, Grossberg S (2013) Spiking Neurons in a Hierarchical Self-Organizing Map Model Can Learn to Develop Spatial and Temporal Properties of Entorhinal Grid Cells and Hippocampal Place Cells. PLoS ONE 8:e60599.

Pinault D (1996) A novel single-cell staining procedure performed *in vivo* under electrophysiological control: morpho-functional features of juxtacellularly labeled thalamic cells and other central neurons with biocytin or Neurobiotin. Journal of Neuroscience Methods 65:113-136.

Pitler TA, Alger BE (1992) Cholinergic excitation of GABAergic interneurons in the rat hippocampal slice. The Journal of Physiology 450:127-142.

Prasad JA, Chudasama Y (2013) Viral Tracing Identifies Parallel Disynaptic Pathways to the Hippocampus. The Journal of Neuroscience 33:8494-8503.

Price CJ, Cauli B, Kovacs ER, Kulik A, Lambolez B, Shigemoto R, Capogna M (2005) Neurogliaform Neurons Form a Novel Inhibitory Network in the Hippocampal CA1 Area. The Journal of Neuroscience 25:6775-6786.

Qin J, Suh JM, Kim B-J, Yun C-T, Tanaka T, Kodama T, Tsai M-J, Tsai SY (2007) The expression pattern of nuclear receptors during cerebellar development. Developmental Dynamics 236(3): 810-820.

Quilichini Pascale P, Le Van Quyen M, Ivanov A, Turner Dennis A, Carabalona A, Gozlan H, Esclapez M, Bernard C (2012) Hub GABA Neurons Mediate Gamma-Frequency Oscillations at Ictal-like Event Onset in the Immature Hippocampus. Neuron 74:57-64.

Risold PY, Swanson LW (1997) Chemoarchitecture of the rat lateral septal nucleus. Brain Research Reviews 24:91-113.

Risold PY, Swanson LW (1997) Connections of the rat lateral septal complex. Brain Research Reviews 24:115-195.

Robertson RT, Baratta J, Yu J, LaFerla FM (2009) Amyloid-β expression in retrosplenial cortex of triple transgenic mice: relationship to cholinergic axonal afferents from medial septum. Neuroscience 164:1334-1346.

Rodriguez-Diaz R, Dando R, Jacques-Silva MC, Fachado A, Molina J, Abdulreda MH, Ricordi C, Roper SD, Berggren P-O, Caicedo A (2011) Alpha cells secrete acetylcholine as a non-neuronal paracrine signal priming beta cell function in humans. Nat Med 17(7): 888-892.

ROSSOR MN, GARRETT NJ, JOHNSON AL, MOUNTJOY CQ, ROTH M, IVERSEN LL (1982) A POST-MORTEM STUDY OF THE CHOLINERGIC AND GABA SYSTEMS IN SENILE DEMENTIA. Brain 105:313-330.

Rousseeuw PJ (1987). Silhouettes: A graphical aid to the interpretation and validation of cluster analysis. Journal of Computational and Applied Mathematics 20(0): 53-65.

Rowland DC, Weible AP, Wickersham IR, Wu H, Mayford M, Witter MP, Kentros CG (2013) Transgenically Targeted Rabies Virus Demonstrates a Major Monosynaptic Projection from Hippocampal Area CA2 to Medial Entorhinal Layer II Neurons. The Journal of Neuroscience 33:14889-14898.

Royer S, Zemelman BV, Losonczy A, Kim J, Chance F, Magee JC, Buzsaki G (2012) Control of timing, rate and bursts of hippocampal place cells by dendritic and somatic inhibition. Nat Neurosci 15:769-775.

Rubio SE, Vega-Flores G, Martínez A, Bosch C, Pérez-Mediavilla A, del Río J, Gruart A, Delgado-García JM, Soriano E, Pascual M (2012) Accelerated aging of the GABAergic septohippocampal pathway and decreased hippocampal rhythms in a mouse model of Alzheimer's disease. The FASEB Journal.

Rye DB, Wainer BH, Mesulam MM, Mufson EJ, Saper CB (1984) Cortical projections arising from the basal forebrain: A study of cholinergic and noncholinergic components employing combined retrograde tracing and immunohistochemical localization of choline acetyltransferase. Neuroscience 13:627-643.

Salvador S and Chan P (2004) Determining the number of clusters/segments in hierarchical clustering/segmentation algorithms. Tools with Artificial Intelligence, 2004. ICTAI 2004. 16th IEEE International Conference on.

Sandler R, Smith AD (1991) Coexistence of GABA and glutamate in mossy fiber terminals of the primate hippocampus: An ultrastructural study. The Journal of Comparative Neurology 303:177-192.

Sargolini F, Fyhn M, Hafting T, McNaughton BL, Witter MP, Moser M-B, Moser EI (2006) Conjunctive Representation of Position, Direction, and Velocity in Entorhinal Cortex. Science 312:758-762.

Sartor GC, Aston-Jones GS (2012) A Septal-Hypothalamic Pathway Drives Orexin Neurons, Which Is Necessary for Conditioned Cocaine Preference. The Journal of Neuroscience 32:4623-4631.

Schiffmann SN, Cheron G, Lohof A, de Alcantara P, Meyer M, Parmentier M, Schurmans S (1999) Impaired motor coordination and Purkinje cell excitability in mice lacking calretinin. Proceedings of the National Academy of Sciences 96(9): 5257-5262.

Schwaller B, Dick J, Dhoot G, Carroll S, Vrbova G, Nicotera P, Pette D, Wyss A, Bluethmann H, Hunziker W, Celio MR (1999) Prolonged contraction-relaxation cycle of fast-twitch muscles in parvalbumin knockout mice. American Journal of Physiology - Cell Physiology 276(2): C395-C403.

Simeone TA, Simeone KA, Samson KK, Kim DY, Rho JM (2013) Loss of the Kv1.1 potassium channel promotes pathologic sharp waves and high frequency oscillations in *in vitro* hippocampal slices. Neurobiology of Disease 54:68-81.

Simon AP, Poindessous-Jazat F, Dutar P, Epelbaum J, Bassant MH (2006) Firing properties of anatomically identified neurons in the medial septum of anesthetized and unanesthetized restrained rats. J Neurosci 26:9038-9046.

Smart SL, Lopantsev V, Zhang CL, Robbins CA, Wang H, Chiu SY, Schwartzkroin PA, Messing A, Tempel BL (1998) Deletion of the KV1.1 Potassium Channel Causes Epilepsy in Mice. Neuron 20:809-819.

Soldo BL, Proctor WR, Dunwiddie TV (1994) Ethanol differentially modulates GABAA receptor-mediated chloride currents in hippocampal, cortical, and septal neurons in rat brain slices. Synapse 18:94-103.

Somogyi P (2010) Hippocampus: Intrinsic Organisation. Handbook of Brain Microcircuits 148-164.

Somogyi P, Katona L, Klausberger T, Lasztóczi B, Viney TJ (2014) Temporal redistribution of inhibition over neuronal subcellular domains underlies state-dependent rhythmic change of excitability in the hippocampus. Philosophical Transactions of the Royal Society B: Biological Sciences 369.

Somogyi P, Klausberger T (2005) Defined types of cortical interneurone structure space and spike timing in the hippocampus. J Physiol 562:9-26.

Sosanya NM, Huang PPC, Cacheaux LP, Chen CJ, Nguyen K, Perrone-Bizzozero NI, Raab-Graham KF (2013) Degradation of high affinity HuD targets releases Kv1.1 mRNA from miR-129 repression by mTORC1. The Journal of Cell Biology 202(1): 53-69.

Sotomayor-Zárate R, Renard GM, Araya KA, Carreño P, Fuentealba JA, Andrés ME, Gysling K (2013) Long-term loss of dopamine release mediated by CRF-1 receptors in the rat lateral septum after repeated cocaine administration. Behavioural Brain Research 250:206-210.

Sotty F, Danik M, Manseau F, Laplante F, Quirion R, Williams S (2003) Distinct electrophysiological properties of glutamatergic, cholinergic and GABAergic rat septohippocampal neurons: novel implications for hippocampal rhythmicity. J Physiol(Lond) 551:927-943.

Stillitano F, Lonardo G, Giunti G, Del Lungo M, Coppini R, Spinelli L, Poggesi C, Mugelli A, Cerbai E (2013) Chronic Atrial Fibrillation Alters the Functional Properties of If in the Human Atrium. Journal of Cardiovascular Electrophysiology 24(12): 1391-1400.

Sugaya K, McKinney M (1994) Nitric oxide synthase gene expression in cholinergic neurons in the rat brain examined by combined immunocytochemistry and in situ hybridization histochemistry. Molecular Brain Research 23:111-125.

Sugita S, Ho A, Sudorf TC (2002) NECABs: a family of neuronal Ca2+-binding proteins with an unusual domain structure and a restricted expression pattern. Neuroscience **112**(1): 51-63.

Sugisaki E, Fukushima Y, Tsukada M, Aihara T (2011) Cholinergic modulation on spike timing-dependent plasticity in hippocampal CA1 network. Neuroscience 192:91-101.

Sun Y, Nguyen AQ, Nguyen JP, Le L, Saur D, Choi J, Callaway Edward M, Xu X (2014) Cell-Type-Specific Circuit Connectivity of Hippocampal CA1 Revealed through Cre-Dependent Rabies Tracing. Cell Reports.

Szabadics J, Varga C, Molnár G, Oláh S, Barzó P, Tamás G (2006) Excitatory Effect of GABAergic Axo-Axonic Cells in Cortical Microcircuits. Science 311:233-235.

Takács VT, Freund TF, Gulyás AI (2008) Types and synaptic connections of hippocampal inhibitory neurons reciprocally connected with the medial septum. European Journal of Neuroscience 28:148-164.

Takagi H, Setou M, Ito S, Yao I (2012) SCRAPPER Regulates the Thresholds of Long-Term Potentiation/Depression, the Bidirectional Synaptic Plasticity in Hippocampal CA3-CA1 Synapses. Neural Plasticity 2012:7.

Takamori S, Riedel D, Jahn R (2000) Immunoisolation of GABA-Specific Synaptic Vesicles Defines a Functionally Distinct Subset of Synaptic Vesicles. The Journal of Neuroscience 20(13): 4904-4911.

Takamura Y, Tamura R, Zhou TL, Kobayashi T, Tran AH, Eifuku S, Ono T (2006) Spatial firing properties of lateral septal neurons. Hippocampus 16:635-644.

Tamamaki N, Nojyo Y (1993) Projection of the entorhinal layer II neurons in the rat as revealed by intracellular pressure-injection of neurobiotin. Hippocampus 3:471-480.

Tanaka J, Nakagawa S, Kushiya E, Yamasaki M, Fukaya M, Iwanaga T, Simon MI, Sakimura K (2000) Gq protein α subunits Gαq and Gα11 are localized at postsynaptic extra-junctional membrane of cerebellar Purkinje cells and hippocampal pyramidal cells. European Journal of Neuroscience 12(3): 781-792.

Taxidis J, Mizuseki K, Mason R, Owen MR (2013) Influence of Slow Oscillation on Hippocampal Activity and Ripples Through Cortico-Hippocampal Synaptic Interactions, Analyzed by a Cortical-CA3-CA1 Network Model. Frontiers in Computational Neuroscience 7.

Teruel-Martí V, Cervera-Ferri A, Nuñez A, Valverde-Navarro AA, Olucha-Bordonau FE, Ruiz-Torner A (2008) Anatomical evidence for a ponto-septal pathway via the nucleus incertus in the rat. Brain Research 1218:87-96.

Thinschmidt JS, Kinney GG, Kocsis B (1995) The supramammillary nucleus: Is it necessary for the mediation of hippocampal theta rhythm? Neuroscience 67:301-312.

Toth K, Borhegyi Z, Freund T (1993) Postsynaptic targets of GABAergic hippocampal neurons in the medial septum-diagonal band of broca complex. J Neurosci 13:3712-3724.

Toth K, Freund TF, Miles R (1997) Disinhibition of rat hippocampal pyramidal cells by GABAergic afferents from the septum. The Journal of Physiology 500:463-474.

Trent NL, Menard JL (2013) Lateral septal infusions of the neuropeptide Y Y2 receptor agonist, NPY13–36 differentially affect different defensive behaviors in male, Long Evans rats. Physiology & Behavior 110–111:20-29.

Tretter V, Ehya N, Fuchs K, Sieghart W (1997) Stoichiometry and Assembly of a Recombinant GABAA Receptor Subtype. The Journal of Neuroscience 17(8): 2728-2737.

Tsanov M, Chah E, Reilly R, O'Mara SM (2013) Respiratory cycle entrainment of septal neurons mediates the fast coupling of sniffing rate and hippocampal theta rhythm. European Journal of Neuroscience n/a-n/a.

Tsaur M-L, Sheng M, Lowenstein DH, Jan YN, Jan LY (1992) Differential expression of K+ channel mRNAs in the rat brain and down-regulation in the hippocampus following seizures. Neuron 8:1055-1067.

Tsunematsu T, Kilduff TS, Boyden ES, Takahashi S, Tominaga M, Yamanaka A (2011) Acute Optogenetic Silencing of Orexin/Hypocretin Neurons Induces Slow-Wave Sleep in Mice. The Journal of Neuroscience 31:10529-10539.

Tukker JJ, Fuentealba P, Hartwich K, Somogyi P, Klausberger T (2007) Cell Type-Specific Tuning of Hippocampal Interneuron Firing during Gamma Oscillations *In vivo*. The Journal of Neuroscience 27:8184-8189.

Tukker JJ, Lasztóczi B, Katona L, Roberts JDB, Pissadaki EK, Dalezios Y, Márton L, Zhang L, Klausberger T, Somogyi P (2013) Distinct Dendritic Arborization and *In vivo* Firing Patterns of Parvalbumin-Expressing Basket Cells in the Hippocampal Area CA3. The Journal of Neuroscience 33:6809-6825.

Tyagarajan SK, Fritschy J-M (2014) Gephyrin: a master regulator of neuronal function? Nat Rev Neurosci 15:141-156.

Varga C, Golshani P, Soltesz I (2012) Frequency-invariant temporal ordering of interneuronal discharges during hippocampal oscillations in awake mice. Proceedings of the National Academy of Sciences 109:E2726–E2734.

Varga V, Hangya B, Kranitz K, Ludanyi A, Zemankovics R, Katona I, Shigemoto R, Freund TF, Borhegyi Z (2008) The presence of pacemaker HCN channels identifies theta rhythmic GABAergic neurons in the medial septum. J Physiol 586:3893-3915.

Varga V, Losonczy A, Zemelman BV, Borhegyi Z, Nyiri G, Domonkos A, Hangya B, Holderith N, Magee JC, Freund TF (2009) Fast Synaptic Subcortical Control of Hippocampal Circuits. Science 326:449-453.

Vertes RP (1992) PHA-L analysis of projections from the supramammillary nucleus in the rat. The Journal of Comparative Neurology 326:595-622.

Vertes RP, McKenna JT (2000) Collateral projections from the supramammillary nucleus to the medial septum and hippocampus. Synapse 38:281-293.

Villette V, Poindessous-Jazat F, Simon A, Lena C, Roullot E, Bellessort B, Epelbaum J, Dutar P, Stephan A (2010) Decreased Rhythmic GABAergic Septal Activity and Memory-Associated {theta} Oscillations after Hippocampal Amyloid-{beta} Pathology in the Rat. J Neurosci 30:10991-11003.

Viney TJ, Lasztoczi B, Katona L, Crump MG, Tukker JJ, Klausberger T, Somogyi P (2013) Network state-dependent inhibition of identified hippocampal CA3 axo-axonic cells *in vivo*. Nat Neurosci 16:1802-1811.

Vinogradova OS, Kitchigina VF, Zenchenko CI (1998) Pacemaker neurons of the forebrain medical septal area and theta rhythm of the hippocampus. Membrane & cell biology 11:715-725.

Vullhorst D, Neddens J, Karavanova I, Tricoire L, Petralia RS, McBain CJ, Buonanno A (2009) Selective Expression of ErbB4 in Interneurons, But Not Pyramidal Cells, of the Rodent Hippocampus. The Journal of Neuroscience 29(39): 12255-12264.

Wang D-Y, Han X-J, Li S-F, Liu D-Q, Yan C-G, Zuo X-N, Zhu C-Z, He Y, Kiviniemi V, Zang Y-F (2012) Effects of Apolipoprotein E Genotype on the Off-Line Memory Consolidation. PLoS ONE 7:e51617.

Wang F-H, Appelkvist P, Klason T, Gissberg O, Bogstedt A, Eliason K, Martinsson S, Briem S, Andersson A, Visser SAG, Ivarsson M, Lindberg M, Agerman K, Sandin J (2012) Decreased axonal transport rates in the Tg2576 APP transgenic mouse: improvement with the gamma-secretase inhibitor MRK-560 as detected by manganese-enhanced MRI. European Journal of Neuroscience no-no.

Wang J, Ikonen S, Gurevicius K, van Groen T, Tanila H (2002) Alteration of cortical EEG in mice carrying mutated human APP transgene. Brain Research 943:181-190.

Ward JH (1963). Hierarchical Grouping to Optimize an Objective Function. Journal of the American Statistical Association 58(301): 236-244.

Wei B, Huang Z, He S, Sun C, You Y, Liu F, Yang Z (2012) The onion skin-like organization of the septum arises from multiple embryonic origins to form multiple adult neuronal fates. Neuroscience.

Wen D, Peng C, Ou-yang G-x, Henderson Z, Li X-l, Lu C-b (2013) Effects of nicotine stimulation on spikes, theta frequency oscillations, and spike-theta oscillation relationship in rat medial septum diagonal band Broca slices. Acta Pharmacol Sin.

West MO, Christian E, Robinson JH, Deadwyler SA (1981) Dentate granule cell discharge during conditioning. Experimental Brain Research 44:287-294.

Whim MD, Lloyd PE (1989) Frequency-dependent release of peptide cotransmitters from identified cholinergic motor neurons in Aplysia. Proceedings of the National Academy of Sciences 86:9034-9038.

Whitehouse P, Price D, Struble R, Clark A, Coyle J, Delon M (1982) Alzheimer's disease and senile dementia: loss of neurons in the basal forebrain. Science 215:1237-1239.

Wierzynski CM, Lubenov EV, Gu M, Siapas AG (2009) State-Dependent Spike-Timing Relationships between Hippocampal and Prefrontal Circuits during Sleep. Neuron 61:587-596.

Wilson M, McNaughton B (1994) Reactivation of hippocampal ensemble memories during sleep. Science 265:676-679.

Wittenberg GM, Wang SS-H (2006) Malleability of Spike-Timing-Dependent Plasticity at the CA3–CA1 Synapse. The Journal of Neuroscience 26:6610-6617.

Wong H, Sternini C, Lloyd K, De Giorgio R, Walsh JH (1996) Monoclonal antibody to VIP: production, characterization, immunoneutralizing activity, and usefulness in cytochemical staining. Hybridoma 15(2): 133-139.

Woodruff A, Xu Q, Anderson SA, Yuste R (2009) Depolarizing effect of neocortical chandelier neurons. Frontiers in Neural Circuits 3.

Woolf NJ, Eckenstein F, Butcher LL (1984) Cholinergic systems in the rat brain: I. Projections to the limbic telencephalon. Brain Research Bulletin 13:751-784.

Wouterlood FG, Saldana E, Witter MP (1990) Projection from the nucleus reuniens thalami to the hippocampal region: Light and electron microscopic tracing study in the rat with the anterograde tracer Phaseolus vulgaris-leucoagglutinin. The Journal of Comparative Neurology 296:179-203.

Wu M, Zaborszky L, Hajszan T, van den Pol AN, Alreja M (2004) Hypocretin/Orexin Innervation and Excitation of Identified Septohippocampal Cholinergic Neurons. The Journal of Neuroscience 24:3527-3536.

Wu M, Zhang Z, Leranth C, Xu C, van den Pol AN, Alreja M (2002) Hypocretin Increases Impulse Flow in the Septohippocampal GABAergic Pathway: Implications for Arousal via a Mechanism of Hippocampal Disinhibition. The Journal of Neuroscience 22:7754-7765.

Xu C, Datta S, Wu M, Alreja M (2004) Hippocampal theta rhythm is reduced by suppression of the H-current in septohippocampal GABAergic neurons. European Journal of Neuroscience 19:2299-2309.

Xu C, Michelsen KA, Wu M, Morozova E, Panula P, Alreja M (2004) Histamine innervation and activation of septohippocampal GABAergic neurones: involvement of local ACh release. The Journal of Physiology 561:657-670.

Yamada K, Fukaya M, Shimizu H, Sakimura K, Watanabe M (2001) NMDA receptor subunits GluRε1, GluRε3 and GluRζ1 are enriched at the mossy fibre–granule cell synapse in the adult mouse cerebellum. European Journal of Neuroscience 13(11): 2025-2036.

Yiu AP, Rashid AJ, Josselyn SA (2011) Increasing CREB Function in the CA1 Region of Dorsal Hippocampus Rescues the Spatial Memory Deficits in a Mouse Model of Alzheimer's Disease. Neuropsychopharmacology 36:2169-2186.

Yiu AP, Rashid AJ, Josselyn SA Increasing CREB Function in the CA1 Region of Dorsal Hippocampus Rescues the Spatial Memory Deficits in a Mouse Model of Alzheimer's Disease. Neuropsychopharmacology 36:2169-2186.

Ylinen A, Bragin A, Nadasdy Z, Jando G, Szabo I, Sik A, Buzsaki G (1995) Sharp wave-associated high-frequency oscillation (200 Hz) in the intact hippocampus: network and intracellular mechanisms. The Journal of Neuroscience 15:30-46.

Yoder RM, Pang KCH (2005) Involvement of GABAergic and cholinergic medial septal neurons in hippocampal theta rhythm. Hippocampus 15:381-392.

Yousefi B, Nasehi M, Khakpai F, Zarrindast MR (2012) Possible interaction of cholinergic and GABAergic systems between MS and CA1 upon memory acquisition in rats. Behavioural Brain Research 235:231-243.

Zaborszky L, Buhl DL, Pobalashingham S, Bjaalie JG, Nadasdy Z (2005) Three-dimensional chemoarchitecture of the basal forebrain: Spatially specific association of cholinergic and calcium binding protein-containing neurons. Neuroscience 136:697-713.

Zezula J, Fuchs K, Sieghart W (1991) Separation of alpha 1, alpha 2 and alpha 3 subunits of the GABAA-benzodiazepine receptor complex by immunoaffinity chromatography. Brain Research 563(1-2): 325-328.

Zhang H, Lin S-C, Nicolelis MAL (2010) Spatiotemporal Coupling between Hippocampal Acetylcholine Release and Theta Oscillations *In vivo*. J Neurosci 30:13431-13440.

Zhang H, Lin S-C, Nicolelis MAL (2011) A distinctive subpopulation of medial septal slow-firing neurons promote hippocampal activation and theta oscillations. Journal of Neurophysiology 106:2749-2763.

Zhang J, Yang LM, Pan XD, Lin N, Chen XC (2013) Increased Vesicular γ-GABA Transporter and Decreased Phosphorylation of Synapsin I in the Rostral Preoptic Area is Associated with Decreased Gonadotrophin-Releasing Hormone and c-Fos Coexpression in Middle-Aged Female Mice. Journal of Neuroendocrinology 25(8): 753-761.

Zhang M-D, Tortoriello G, Hsueh B, Tomer R, Ye L, Mitsios N, Borgius L, Grant G, Kiehn O, Watanabe M, Uhlén M, Mulder J, Deisseroth K, Harkany T, Hökfelt TGM (2014) Neuronal calcium-binding proteins 1/2 localize to dorsal root ganglia and excitatory spinal neurons and are regulated by nerve injury. Proceedings of the National Academy of Sciences 111:E1149-E1158.

Zhang S-J, Ye J, Miao C, Tsao A, Cerniauskas I, Ledergerber D, Moser M-B, Moser EI (2013) Optogenetic Dissection of Entorhinal-Hippocampal Functional Connectivity. Science 340.

Zhao C, Eisinger B, Gammie SC (2013) Characterization of GABAergic Neurons in the Mouse Lateral Septum: A Double Fluorescence In Situ Hybridization and Immunohistochemical Study Using Tyramide Signal Amplification. PLoS ONE 8:e73750.

Zheng T, Wilson CJ (2002) Corticostriatal Combinatorics: The Implications of Corticostriatal Axonal Arborizations. J Neurophysiol 87:1007-1017.